Origin of cosmic gamma rays

Diana M. Worrall

ORIGIN OF COSMIC GAMMA RAYS

by

Diana M. Worrall, B.Sc.

A thesis submitted to the
University of Durham for
the Degree of Doctor of Philosophy

August, 1977.

To my parents

A B S T R A C T

An attempt is made to distinguish origin locations and dominant production mechanisms of cosmic gamma rays. The study adds to information about the cosmic ray progenitors, primarily electrons and protons of 10^8 - 10^{10}eV.

The disc longitude distribution for energies above 100 MeV is unfolded to give the Galactic gamma ray emissivity for radial symmetry or uniform emission along spiral sections. The correlation is reasonable with models based on the molecular hydrogen distribution. Inconsistency with spiral arm positions is found.

The Galactic centre region, where gas density is high, is a probable example of a thick target region for gamma ray-producing cosmic rays. The emissivity under these conditions is calculated. To satisfy the proportion of the observed flux interpreted as coming from the Galactic centre region, a cosmic ray intensity greater than that locally is required. This supports a Galactic origin for the cosmic rays in question. The required injection rate is several hundreds of times the local value, and its relationship to magnetic field and gas density is examined.

Contributions to the high latitude flux from the Galaxy and discrete extragalactic sources are calculated. It is shown that a large part may result from inverse Compton scattering of electrons diffusing away from the Galactic disc. The diffusion is modelled on the basis of other astrophysical data. With the Galaxy as a guide, and relating gamma ray emission to other properties, the contributions from external normal and radio

galaxies are calculated. The total of all contributions is found to be a significant proportion of the observed flux, casting doubt on such cosmological models as are normalised to fit the entire measured spectrum in magnitude and shape. Radio galaxies may provide the bulk of the 1 - 10 MeV background if there is proportionality between their gamma ray and radio luminosities.

PREFACE

The work presented in this thesis was carried out during the period 1974-77 while the author was a research student under the supervision of Professor A.W. Wolfendale, F.R.S., in the Physics Department of the University of Durham.

Some of the work reported here was carried out in collaboration with Professor A.W. Wolfendale and Dr. A.W. Strong, but most of the research and all calculations are of the author.

Parts of the work are published as follows:

The Galactic gamma ray emissivity,
Strong, A.W. and Worrall, D.M., 1976, J. Phys. A., 9, 823.

Gamma rays from the Galactic centre,
Wolfendale, A.W. and Worrall, D.M., 1976, Nature, 263, 482.
Wolfendale, A.W. and Worrall, D.M., 1977, Proc. 12th Eslab Symp., Frascati, ESA SP-124.
Wolfendale, A.W. and Worrall, D.M., 1977, Astron. Astrophys. In the press.

Gamma ray background contribution from extragalactic sources,
Strong, A.W., Wolfendale, A.W. and Worrall, D.M., 1976, Mon. Not. R. astr. Soc., 175, 23p.
Strong, A.W., Wolfendale, A.W. and Worrall, D.M., 1976, J. Phys. A., 9, 1553.

Inverse Compton Galactic halo gamma ray flux,
Worrall, D.M. and Strong, A.W., 1977, Astron. Astrophys., 57, 229.

CONTENTS

CHAPTER ONE

INTRODUCTION

The first detection of cosmic gamma rays, about 15 years ago, added a new dimension to high energy astrophysics. Another tool, possessing many advantageous properties, became available for the study of the constituents of the Universe, and, in particular, the primary cosmic radiation.

Cosmic ray physics is itself a child of this Century. Its birth resulted from several workers observing that their ground-based ionization chambers exhibited residual conductivity when shielded from known radiation sources. This can now be explained as due to secondary particles produced by primary cosmic ray interactions in the atmosphere. In the last 60 years much has been learnt about the nature of cosmic rays, and their study has led to advances in several areas of physics. The electron component, which is about 1% of the cosmic ray energy density above the atmosphere, must originate in the Galaxy, since it would suffer attenuation on the microwave background radiation. However, the origin of the dominant primary nuclear component is still, to a large extent, an unsolved problem. Gamma ray astronomy now provides useful additional clues.

Primary cosmic rays of energy between about 10^8 and 10^{12}eV are responsible for producing detectable secondary cosmic gamma rays. Laboratory experiments now provide much information about the relevant interactions. For theoretical study, the advantages offered by cosmic gamma rays are, firstly, that they are uncharged and therefore, unlike primary cosmic rays, their propagation is unaffected by magnetic fields,

and secondly, absorption is negligible on a scale almost as large as the Universe.

Experimental gamma ray astronomy must be carried out close to the top of, and preferably above, the atmosphere. Detectors are required to measure a component several orders of magnitude below that of the primary nucleon cosmic ray flux. By the 1960s suitable techniques had been developed and since then progress has been rapid. The first positive identification of a cosmic gamma ray flux is probably to be credited to Arnold et al. (1962) and Metzger et al. (1964) from scintillators on board the Ranger 3 and 5 moonprobes. At about the same time the important role that gamma rays could play in theoretical work, and in particular the potential of gamma ray astronomy as a subject in its own right, was realised. Interest was greatly stimulated by the paper of Morrison (1958).

To date, three satellites solely devoted to gamma ray astronomy have been launched, and data are augmented by results from rockets, other spacecraft and many high altitude balloons. The first satellite, OSO-3, showed the Galactic disc to be a strong emitter of gamma rays and pioneered the way for the SAS-2 satellite, which provides the best present data for theoretical study. COS-B, the third satellite, is in operation, and interesting new information is gradually becoming available. Recently, observations of gamma ray lines have been reported from the Galactic centre and the radio galaxy Centaurus A, possibly marking the beginning of an exciting new branch of gamma ray astronomy.

For theoretical study there are two main disadvantages to present measurements. Firstly, since fluxes are low, the number of true events detected is small, and statistically significant comparisons with theoretical models are difficult to achieve. Secondly, the optimum angular resolution is no better than a few degrees.

The first obvious question to ask regarding the Galactic flux is, "How much is from discrete sources?" The Crab and Vela have been known as gamma ray emitters for some time, but recently, from incomplete sky coverage, COS-B has found 11 other sources not as yet identified with pulsars or supernova remnants (Hermsen et al., 1977). It is not yet established whether it is correct to subtract these sources when considering the diffuse Galactic component since at least some may be interstellar gas clouds, manifestations of the patchy nature of the gas. "Diffuse" Galactic radiation may indeed be a slight misnomer. By modelling to the Crab and Vela and using some observational upper limits from other sources, Strong et al. (1977) find that pulsars should not give a contribution of above 10% to Galactic observations.

The study of discrete Galactic sources is not within the realm of the present work. Attention is restricted to the diffuse Galactic component and the high latitude flux, some of which may be of extragalactic origin.

It is pertinent to consider two questions. Firstly, "How much can be discovered about the origin of the gamma rays,", and secondly, "What information can be gleamed about the cosmic ray progenitors?" The second question can be studied without a full solution to the first. For example, Ginzburg (1972) proposed a test for the Magellenic clouds. If no flux is seen, cosmic rays must be Galactic. Detection of a flux is ambiguous since either cosmic rays pervade all space or the clouds themselves are a source of particles. The test is not yet possible because predicted fluxes are about 10^{-7} cm^{-2} s^{-1}, approximately an order of magnitude below present detector thresholds. Dodds et al. (1975b) have put forward evidence for Galactic origin by showing that unless there is a decrease in cosmic ray intensity towards the Galactic anticentre, the predicted flux is in excess of the observations.

In this work, the primary aim is to attempt a partial answer to the first question. In general, the approach taken is to assess the contributions from likely origins and then compare with the data. The alternative, that of proposing models where parameters are chosen to fit the measurements, is not so helpful due to large uncertainties in the gamma ray observations. Where possible, results are applied to the question of cosmic ray origin.

In Chapter 2, local gamma ray emissivities are derived, partly using work of other authors. Neutral pion decay is found to be the dominant production mechanism. Locally, therefore, gamma rays monitor the nucleon cosmic ray component. That this is so elsewhere in the Galaxy has recently been put in doubt by energy spectral measurements from the COS-B satellite (Bennett et al. 1977b), which suggest a higher percentage contribution from bremsstrahlung elsewhere in the Galaxy. It is an interesting problem that samples of gamma ray flux from several widespread directions in the Galaxy all suggest an electron to proton ratio higher than that locally.

In Chapter 3, a method for unfolding the gamma ray longitude distribution to give the Galactic emissivity is described. Models of radial symmetry and uniform emission along spiral arms are adopted, the aim being to compare with gas distributions. The possibility of determining whether we require a cosmic ray gradient in the inner Galaxy of either electrons or nucleons, whichever are responsible for the gamma rays, is investigated.

In a region of high gas density it is likely that cosmic rays lose all their energy before escape. The equations for gamma ray production under these conditions are developed in Chapters 4 and 5. A likely such region is within about 300 pc of the Galactic centre where large amounts of molecular hydrogen have been observed. This direction is of particular

interest since there is a large peak in the SAS-2 flux. If this is attributed to the central gas, an ambient cosmic ray density higher than that locally is required, implying Galactic origin for the particles. An injection rate several hundreds of times the local value is required and its relationship to magnetic field and gas density is examined. The results take on more significance if it is shown that the gamma rays are mainly of neutral pion decay origin, but this is as yet uncertain.

In the remaining chapters, attention is paid to the high latitude component. There has been a tendancy in the past to propose models to fit the measured spectrum in magnitude and shape. The work here casts serious doubt on this approach since it is found that the flux from the Galaxy and the sum of discrete extragalactic sources is probably a large percentage of that observed. Chapter 6 tackles the determination of the contribution from a class of extragalactic objects where the emission of one member is known. In Chapters 7 and 8 a model for diffusion of electrons from the Galactic disc is given, and the gamma ray flux from inverse Compton interactions in the resultant "halo" calculated. In Chapter 9 the sum of all these contributions is compared with the observations, and is found to be a significant percentage.

CHAPTER TWO

PRODUCTION MECHANISMS FOR GALACTIC GAMMA RAYS

2.1 INTRODUCTION

The following three sections describe the important processes for gamma ray production at energies of about 100 MeV and above in the Galaxy. Their local emissivities (i.e. production rate per unit volume) are calculated and shown in figure 2.3. In section 2.5 their relative importance as production mechanisms at different positions in the Galaxy is discussed.

In the following, mass, momentum and energy are written in equivalent units. A normalised distribution function in X is represented by P(X)dX.

2.2 GAMMA RAYS FROM NEUTRAL PION DECAY

Gamma rays are produced by the decay of neutral pions, themselves created in collisions of cosmic ray nuclei with interstellar gas atoms. Since a neutral pion has a rest mass energy of about 140 MeV and decays into two gamma rays, it follows that the gamma ray production peaks at about 70 MeV.

A neutral pion decays into two gamma rays each of energy $M_\pi/2$ in its rest frame.

Let one gamma ray be emitted at Θ' to the axis of transformation in the pion rest frame. The laboratory frame energy is:

$$E_\gamma = \frac{M_\pi \gamma_\pi}{2}(1 + \beta_\pi \cos \Theta') \qquad (2.1)$$

Since the distribution in Θ' is isotropic:

$$P(\cos \Theta')\, d(\cos \Theta') = \frac{1}{2}\, d(\cos \Theta') \qquad (2.2)$$

from 2.1:

$$P(E_\gamma, E_\pi)\, dE_\gamma = \frac{dE_\gamma}{M_\pi \gamma_\pi \beta_\pi} \tag{2.3}$$

Therefore:

$$P(E_\gamma, E_\pi)\, dE_\gamma = \begin{cases} \dfrac{dE_\gamma}{(E_\pi^2 - M_\pi^2)^{\frac{1}{2}}} & \text{if } \dfrac{E_\pi}{2}(1-\beta_\pi) \leq E_\gamma \leq \dfrac{E_\pi}{2}(1+\beta_\pi) \\ 0 & \text{otherwise} \end{cases} \tag{2.4}$$

The number of gamma rays at position $\underline{r}$ produced with an energy between E_γ and $E_\gamma + dE_\gamma$ per unit volume per unit time (i.e. emissivity) from collisions between cosmic ray nuclei of type k and differential intensity $j_k(E_k, \underline{r})$ and gas nuclei of type j and density $n_j(\underline{r})$ is given by $q(E_\gamma, \underline{r})\, dE_\gamma$ such that:

$$q(E_\gamma, \underline{r}) = 4\pi \sum_{j,k} n_j(\underline{r}) \int dE_k\; j_k(E_k, \underline{r}) \int_{E_{\pi\,min}}^{\infty} 2 \frac{\sigma(E_\pi, E_k)}{(E_\pi^2 - M_\pi^2)^{\frac{1}{2}}}\, dE_\pi \tag{2.5}$$

where σ denotes the interaction cross section and using 2.1:

$$E_{\pi\,min} = E_\gamma + (M_\pi^2 / 4E_\gamma) \tag{2.6}$$

The differential intensity of γ-rays at the earth is given by:

$$j(E_\gamma) = \frac{1}{4\pi} \int_0^\infty q(E_\gamma, \underline{r})\, dr \tag{2.7}$$

The major contribution to equation 2.5 comes from cosmic ray protons interacting with interstellar hydrogen. The cross section for neutral pion production falls rapidly below proton energies of 400 MeV and the

bulk of production is from protons of between 1 and 3 GeV. The emissivity from these proton-proton collisions is increased by the effective mean mass per hydrogen atom to include contributions from protons interacting with the whole interstellar material. This factor is given as 1.36 by Allen (1973), whereas Trimble (1975) quotes values of 1.34, 1.46 and 1.71 for the solar atmosphere, the Orion nebular and planetary nebulae respectively. In this work, where appropriate, a value of 1.4 is taken in accordance with Dodds et al. (1976). A further factor of about 1.4 arises from inclusion of the cosmic ray alpha particle flux.

Equation 2.5 has been evaluated by several authors, but the most detailed calculations are those of Stecker (1970) and Cavallo and Gould (1971), and their results agree well. These authors base their values for cross section and multiplicity on measurements from accelerator experiments. Levy and Goldsmith (1972) adopt a theoretical multiplicity law based on Feynman scaling, but the results disagree with the other calculations and it was pointed out by Stecker (1973) that the scaling hypothesis, although probably valid for proton energies above 50 GeV, breaks down in the regime of interest.

In the present work the gamma ray spectrum of Stecker (1970) is adopted. His result for the local integral gamma ray production spectrum is shown in figure 2.3. The local gas density, $n_{H_\odot}$, is taken to be 1 H atom cm^{-3} (see section 3.3.3).

Stecker has found the local production of gamma rays of energy above 100 MeV to be:

$$q_\gamma(\ >100\ \text{MeV}) = 1.3\ 10^{-25}\ \text{H atom}^{-1}\ s^{-1}$$

The total yield of all gamma rays from neutral pion decay can be expressed:

$$Q_\gamma(\underline{r}) = 8\pi \sum_{j,k} \int n_j(\underline{r})\, \sigma_{\pi^o}(E_k)\, m_{\pi^o}(E_k)\, j(E_k, \underline{r})\, dE_k \qquad (2.8)$$

where $\sigma_{\pi^o}(E_k)\, m_{\pi^o}(E_k)$ denotes the product of total cross section and multiplicity. Stecker (1973) finds good agreement between his calculated total yield using equations 2.5 and 2.8 respectively.

Neutral pion production is a catastrophic energy loss process for the proton which typically retains about one half to two thirds of its energy after interaction.

2.3 GAMMA RAYS FROM ELECTRON BREMSSTRAHLUNG

Gamma rays are radiated by electrons decelerating in the fields of gas nuclei. Relevant cross sections are given by Heitler (1954) and Koch and Motz (1959). They are calculated using the Born approximation plus various screening effects.

Following Stecker (1971), the dependence of cross section on electron energy is weak and to a good approximation, for $E \geq E_\gamma$:

$$\sigma(E_\gamma, E)\, dE_\gamma = \frac{\langle M \rangle}{\langle X \rangle} \frac{dE_\gamma}{E_\gamma} \qquad (2.9)$$

where $\langle M \rangle$ is the average mass of the target atoms in grams, and $\langle X \rangle$ is the average radiation length for the gas (g cm^{-2}).

The differential emissivity is given by:

$$q(E_\gamma, \underline{r}) = 4\pi \int_{E_\gamma}^{\infty} n(\underline{r})\, j(E, \underline{r})\, \sigma(E_\gamma, E)\, dE \qquad (2.10)$$

where $n(\underline{r})$ is the gas density in H atoms per unit volume and $j(E, \underline{r})$ is the differential electron intensity.

As in the previous section we take $\langle M \rangle = 1.4\ M_H$ locally, where M_H is the mass of a hydrogen atom in grams. The appropriate value for $\langle M \rangle$ is probably higher towards the Galactic centre (see D'Odorico et al., 1976) with a likely maximum of $\langle M \rangle = 1.9\ M_H$. Following Stecker (1971), $\langle X \rangle = 65\ g\ cm^{-2}$ for the interstellar composition, and using the local value for $\langle M \rangle$ we find:

$$q(E_\gamma, \underline{r}) = 4.53\ 10^{-25}\ n(\underline{r}) \int_{E_\gamma}^{\infty} \frac{j(E, \underline{r})}{E_\gamma}\, dE \qquad (2.11)$$

It can be seen that a power law electron spectrum of differential slope $-\gamma$ will produce a bremsstrahlung γ-ray spectrum of the same differential slope. However, the local electron spectrum cannot be expressed in terms of a single power law over the whole energy range of interest which is from a few MeV to about ten thousand GeV. Direct measurement of the electron spectrum can be made above a few GeV, but below this the solar wind sweeps away particles and balloon flight observations are no longer true representations of the local interstellar intensity. Even to observations at periods of minimum solar activity a modulation correction must be applied.

Two methods have been employed to calculate the low energy interstellar electron intensity. The first involves fitting to the non-thermal radio emission (e.g. Goldstein et al., 1970, and Cummings et al., 1973). The second is based on comparing the observed positron

spectrum with that calculated on the assumption that the positrons are all of secondary origin (e.g. Daugherty et al., 1975). Both methods involve large uncertainties such that the interstellar electron intensity is known to no better than a factor of two or worse. It has been pointed out by Setti and Woltjer (1971) and others that, to reconcile the observed non-thermal radio emission with the low values for the interstellar magnetic field of (2-3) 10^{-6} gauss found from pulsar dispersion measures, an electron intensity up to ten times that generally accepted is required. It may well be that the measured local magnetic field is only characteristic of inter spiral arm regions, but nevertheless in the anticentre direction it is not expected to be high. Goldstein et al. (1970) employ a magnetic field of 5 10^{-6} gauss for a path length of 4 kpc towards the anticentre. The alternative approach of Daugherty et al. (1975) uses the calculation of the local positron spectrum of Ramaty (1974) which assumes energy independent escape for the positrons, something over which there is now considerable doubt (see Giler et al., 1977; Orth and Buffington, 1976, and references therein).

In this work the spectrum of Goldstein et al. is adopted with a steepening of slope above 10 GeV in accordance with Meyer (1975). It is expressed as follows:

$$j(E) = \begin{cases} 150\ E^{-1.8}\ m^{-2}\ s^{-1}\ sr^{-1}\ GeV^{-1} & E < 1\ GeV \\ 150\ E^{-2.5} & 1 < E < 10\ GeV \\ 299.3\ E^{-2.8} & 10\ GeV < E \end{cases} \qquad (2.12)$$

This spectrum is shown in figure 2.1. For comparison, the spectra used by Fichtel et al. (1976) and Dodds (1977) are given, which are taken

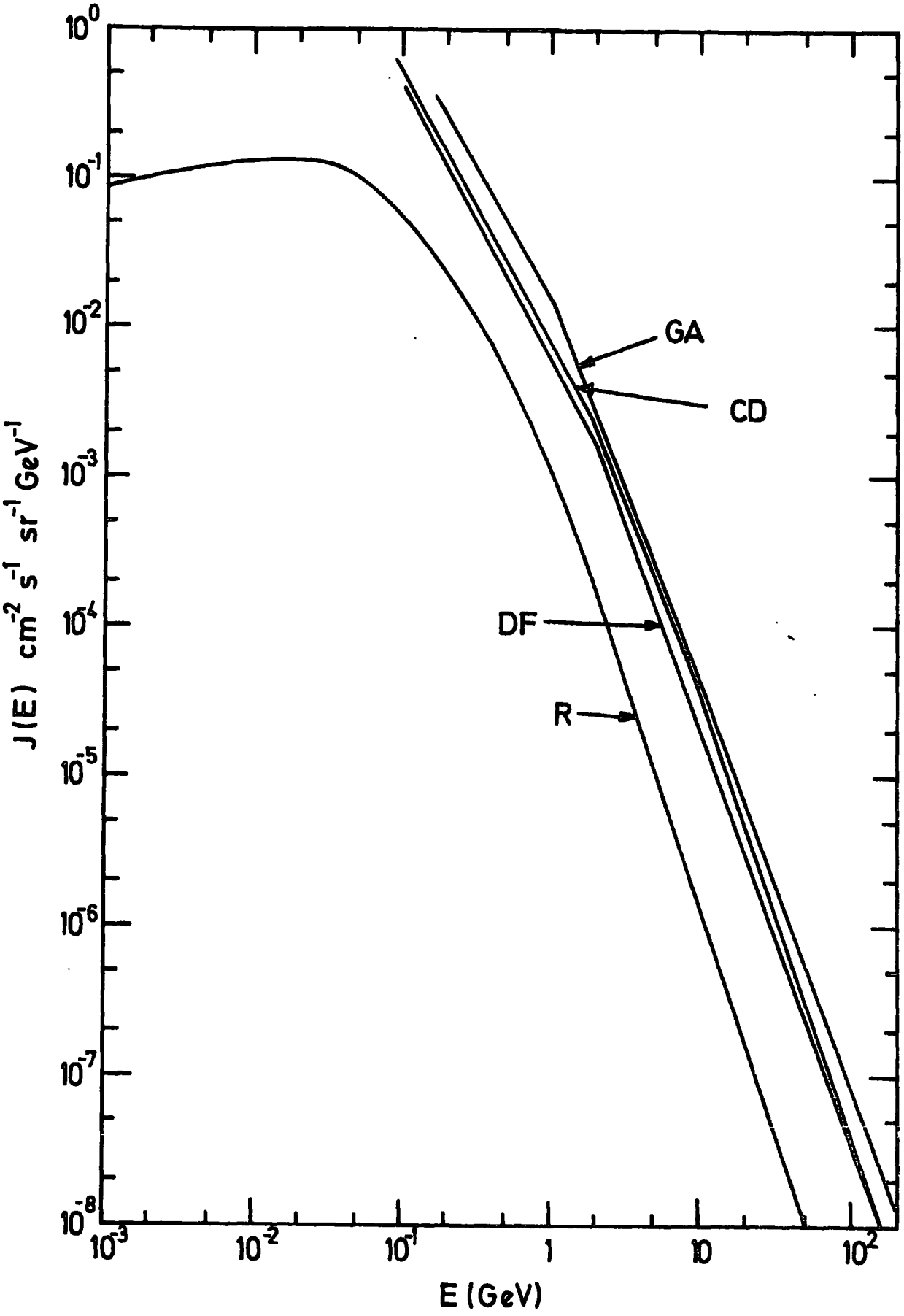

Figure 2.1 Local electron and positron intensities labelled as follows:
R: Positron spectrum calculated by Ramaty(1974).
GA: Goldstein et al.(1970) spectrum 'A', as used in these calculations.
CD: Spectrum of Cummings et al.(1973) as used by Dodds(1977).
DF: Spectrum of Daugherty et al.(1975) as used by Fichtel et al.(1976).

Table 2.1

The local bremsstrahlung production function for n_{H_o} = 1 H atom cm^{-3} found by various authors. The emissivity of gamma rays above 100 MeV is given.

REFERENCE	ELECTRON SPECTRUM USED	q(>100 MeV) cm^{-3} s^{-1}
Fichtel et al. (1976)	Daugherty et al. (1975)	$3.38\ 10^{-26}$
Dodds (1977)	Cummings et al. (1973)	$1.5\ 10^{-26}$
Stecker (1977a)		$2.5\ 10^{-26}$
Present Work	Goldstein et al. (1970)	$5.0\ 10^{-26}$

from Daugherty et al. (1975) and Cummings et al. (1973) respectively.

Equation 2.11 has been evaluated locally using 2.12, for a local gas density of 1 H atom cm^{-3}. The integration from E_γ to infinity was solved using Romberg integration in decades of energy until higher decades contributed an addition of less than one per cent of the total (about four decades were required). The integral of equation 2.11 over gamma ray energy for the local region has been evaluated also using Romberg integration and the result is shown in figure 2.3. For comparison, table 2.1 gives recent results of other authors for the local production above 100 MeV. The discrepancies due to the different electron intensities used is evident.

The present work is in agreement with that of Fichtel et al. (1976) when allowance is made for the different electron spectra used in the two calculations. The value of Dodds (1977) is a little low, but reflects the influence of high energy electrons, i.e. about four orders of magnitude higher than the gamma ray energy; (the electron spectrum used by Dodds has a power law proportional to E^{-3} above 2 GeV). The most detailed calculation with reference to the bremsstrahlung cross section is that of Fichtel et al., but it is clear that uncertainties of factors of two will prevail until the electron intensity is known more precisely.

2.4 GAMMA RAYS FROM INVERSE COMPTON SCATTERING

The inverse Compton process is that of a low energy photon of energy E scattering from a high energy electron, E_e, to produce a gamma ray of energy E_γ. Figure 2.2 defines the notation to be used in the laboratory frame and the rest frame of the electron.

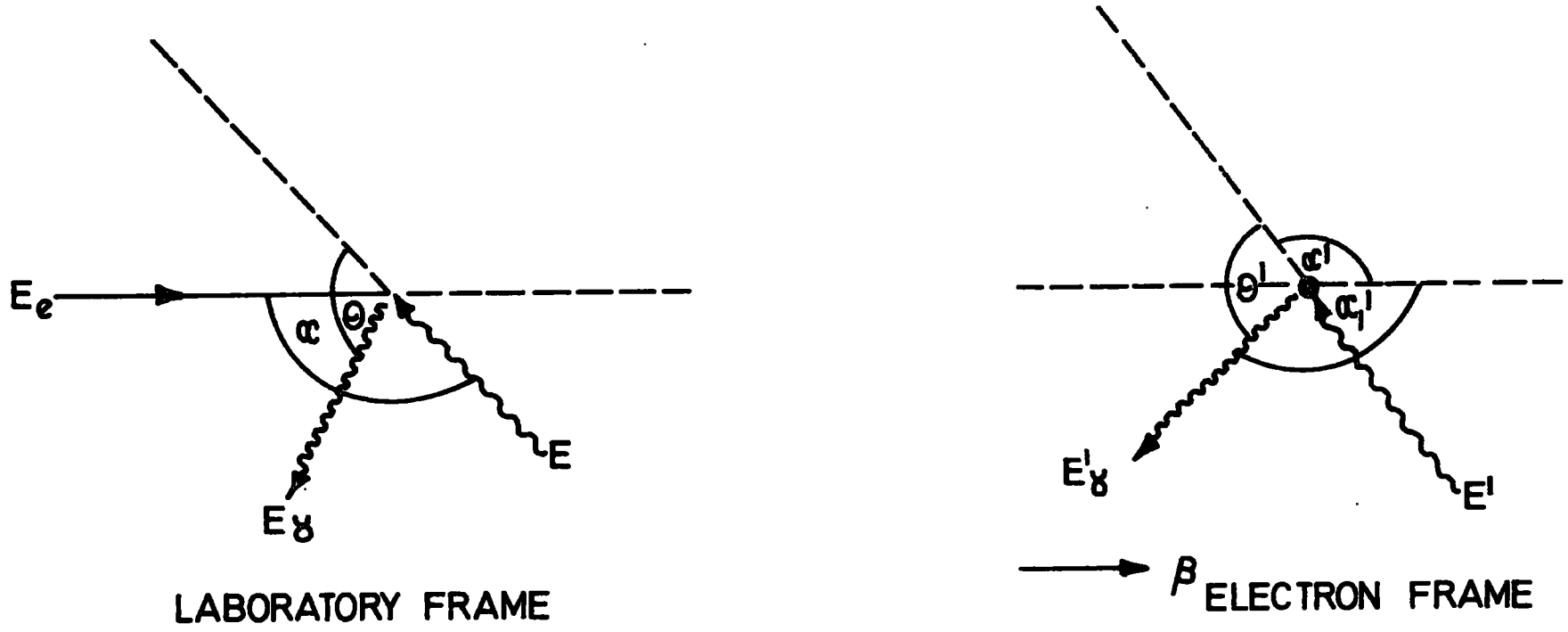

Figure 2.2 Notation for the theory of inverse Compton scattering.

From kinematics, in the electron rest frame:

$$\frac{E'_\gamma}{E'} = \frac{1}{1 + \frac{E'}{m_e}(1 - \cos\theta')} \tag{2.13}$$

where m_e is the electron rest mass.

Transforming E'_γ to the laboratory:

$$E_\gamma = \gamma E'_\gamma \quad (1 + \beta \cos\alpha'_1) \tag{2.14}$$

where γ is the Lorentz factor of the electron.

Since $\gamma >> 1$, the electron experiences the collisions with the low energy photons as head on, i.e.

$$\alpha' = 180^\circ$$

but, $$\alpha' + \theta' + \alpha'_1 = 360^\circ$$

therefore, $$\cos\alpha'_1 = -\cos\theta' \tag{2.15}$$

Substituting 2.15 and 2.14 into 2.13 and using $\beta = 1$ gives:

$$\frac{E_\gamma}{E'} = \frac{\gamma(1 - \cos\theta')}{1 + \frac{E'}{m_e}(1 - \cos\theta')} \tag{2.16}$$

Also we have

$$E' = \gamma E (1 - \cos\alpha) \tag{2.17}$$

The cross section for producing gamma rays of energy between E_γ and $E_\gamma + dE_\gamma$ by scattering from electrons of energy E_e is given by:

$$\frac{d\sigma}{dE_\gamma}(E_\gamma, E, E_e) = \int \frac{d\sigma}{dE_\gamma}(E_\gamma, E', E_e)\, P(E', E, E_e)\, dE' \,(1 - \cos\alpha) \tag{2.18}$$

Using 2.17, for an isotropic photon distribution we have:

$$P(E', E, E_e)\, dE' = \frac{dE'}{2\gamma E} \qquad 0 < E' < 2\gamma E \tag{2.19}$$

Therefore 2.18 becomes:

$$\frac{d\sigma}{dE_\gamma}(E_\gamma, E, E_e) = \int_0^{2\gamma E} \frac{d\sigma}{dE_\gamma}(E_\gamma, E', E_e)\, \frac{E'}{2\gamma^2 E^2}\, dE' \tag{2.20}$$

Inverse Compton scattering becomes inverse Thomson scattering in the limit:

$$\gamma E \ll m_e \tag{2.21}$$

In the Galaxy and intergalactic space this condition is satisfied. The justification for this is given after equation 2.30. The Thomson cross section is given by:

$$d\sigma(E_\gamma, E', E_e) = \frac{3}{8}\sigma_T\, (1 + \cos^2\theta')\, d(\cos\theta') \tag{2.22}$$

where σ_T is the Thomson cross section and has a value of $6.65\ 10^{-25}\ cm^2$.

From 2.16:

$$dE_\gamma = \frac{-E'\gamma}{\left[1 + \frac{E'}{m_e}(1 - \cos\theta')\right]^2}\, d(\cos\theta') \tag{2.23}$$

From 2.23, 2.22 and 2.16 we find:

$$\frac{d\sigma}{dE_\gamma}(E_\gamma, E', E_e) = \frac{3}{8}\sigma_T \left[1 + \left[1 - \frac{E_\gamma m_e}{E'(m_e\gamma - E_\gamma)}\right]^2\right] \left[1 + \frac{E_\gamma}{m_e\gamma - E_\gamma}\right]^2 \frac{1}{E'\gamma} \tag{2.24}$$

The upper limit to E' for a given E_e is $2\gamma E$ (from 2.17) and the lower limit is derived from 2.16 and is given by:

$$E'_{min} = \frac{E_\gamma m_e}{2(\gamma m_e - E_\gamma)} \tag{2.25}$$

Returning to an isotropic photon distribution, the solution of 2.20 using 2.24 and the approximation $E_\gamma \ll E_e$, gives:

$$\frac{d\sigma}{dX}(E_\gamma, E, E_e) = 3\sigma_T \left(1 + X - 2X^2 + 2X \ell nX\right) \tag{2.26}$$

where $X = \frac{E_\gamma}{4\gamma^2 E}$ and $\frac{1}{4\gamma^2} \leqslant X \leqslant 1$

Equation 2.26 is in agreement with other authors; see, for example, Ginzburg and Syrovatskii (1964) and Blumenthal and Gould (1970).

Writing, $f(X) = 1 + X - 2X^2 + 2X \ell nX$ gives:

$$\int_0^1 f(X)dX = \frac{1}{3} \tag{2.27}$$

$$\int_0^1 Xf(X)dX = \frac{1}{9} \tag{2.28}$$

Hence, as expected, the integration of 2.26 gives the Thomson cross section, σ_T.

Since,

$$\bar{X} = \frac{1}{3} \tag{2.29}$$

then for the mean value of E_γ from photons of mean energy $\bar{E}$, we find:

$$\bar{E}_\gamma = \frac{4}{3}\gamma^2 \bar{E} \tag{2.30}$$

We can now show that 2.21 is satisfied, i.e. the Thomson limit holds.

The photon fields on which inverse Compton (Thomson) scattering can occur are starlight ($\sim 6000^{\circ}K$), far infrared ($\sim 100\ \mu m$) and the isotropic $2.7^{\circ}K$ blackbody remnant radiation. The mean energy can be expressed:

$$\bar{E} = \frac{\int E\, n_{ph}(E)\, dE}{\int n_{ph}(E)\, dE} = \frac{w_{ph}}{n_{ph}} \qquad (2.31)$$

For a blackbody energy distribution:

$$\bar{E} = 2.7KT \qquad (2.32)$$

where T is the blackbody temperature of the photon field. For the $2.7^{\circ}K$ field, starlight and far infrared, we find mean energies of $6.3\ 10^{-4}$eV, 1.4 eV and $1.2\ 10^{-2}$eV respectively. For gamma rays of 100 MeV, using 2.30 we find:

Starlight:	$\gamma \sim 7.3\ 10^{3}$	$\gamma E \sim 1\ 10^{4}$
Far infrared:	$\gamma \sim 7.9\ 10^{4}$	$\gamma E \sim 9\ 10^{2}$
$2.7^{\circ}K$ blackbody:	$\gamma \sim 3.5\ 10^{5}$	$\gamma E \sim 2\ 10^{2}$

Thus, 2.21, i.e. the Thomson limit, is satisfied. A first order correction is only necessary for $E_{\gamma} > 10^{12}$eV (see Blumenthal and Gould, 1970).

The gamma ray emissivity is given by:

$$q(E_{\gamma}, \underline{r}) = 4\pi \int dE\, n_{ph}(E, \underline{r}) \int \sigma(E_{\gamma}, E, E_e)\, j(E_e, \underline{r})\, dE_e \qquad (2.33)$$

The solution has a very simple form if $n_{ph}(E, \underline{r}) = n_{ph}(E, \underline{r})\ \delta(E-\bar{E})$, in which case 2.33 becomes:

$$q(E_\gamma, \underline{r}) = 4\pi\, n_{ph}(\underline{r})\, \sigma_T\, j(E_e, \underline{r})\, \frac{dE_e}{dE_\gamma}\, \delta\left[E_e - \left(3\,\frac{E_\gamma m_e^2}{4E}\right)^{\frac{1}{2}}\right] \quad (2.34)$$

i.e., using 2.30:

$$q(E_\gamma, \underline{r}) = 2\pi\, n_{ph}(\underline{r})\, \sigma_T \left(\frac{3m_e^2}{4\bar{E}}\right)^{\frac{1}{2}} E_\gamma^{-\frac{1}{2}}\; j(E_e, \underline{r})\, \delta\left[E_e - \left(\frac{3E_\gamma m_e^2}{4E}\right)^{\frac{1}{2}}\right] \quad (2.35)$$

If the electron spectrum is a power law such that:

$$j(E_e, \underline{r})\, dE_e = A(\underline{r})\, E_e^{-\gamma} dE_e$$

then the differential gamma ray emissivity is a power law proportional to $E_\gamma^{-(\gamma+1)/2}$. 2.35 becomes:

$$q(E_\gamma, \underline{r}) = 2\pi\, n_{ph}(\underline{r})\, \sigma_T\, A(\underline{r}) \left(\frac{3m_e^2}{4\bar{E}}\right)^{-(\gamma-1)/2} E_\gamma^{-(\gamma+1)/2} \quad (2.36)$$

It is seen from 2.36 that:

$$q(E_\gamma, \underline{r}) \propto w_{ph}(r)\, \bar{E}^{(\gamma-3)/2} \quad (2.37)$$

Since the electron spectrum in the region of interest (>1 GeV) has a slope close to $\gamma = 3$, the sensitivity on electron energy is low and in general, use of the average value, $\bar{E}$, is a good approximation.

Ginzburg and Syrovatskii (1964) found the analytical solution to (2.32) where the photons have a blackbody distribution and the electron spectrum has a single power law. The solution is 2.36 multiplied by a function of the electron spectral slope $f(\gamma)$:

$$f(\gamma) = 4.74\,(1.05)^\gamma\, \frac{\gamma^2 + 4\gamma + 11}{(\gamma+1)(\gamma+3)^2(\gamma+5)}\, \Gamma\left(\frac{\gamma+5}{2}\right) \zeta\left(\frac{\gamma+5}{2}\right) \quad (2.38)$$

where $\Gamma(X)$ is the Euler gamma function and $\zeta(X)$ is the Riemann zeta

function. As expected from 2.37, the correction is small; e.g. $f(2) = 0.86$; $f(3) = 0.99$.

In general the electron spectrum is not of a single slope and the use of 2.38 is limited. Piccinotti and Bignami (1976) have derived the analytical expression for one break in the electron spectrum.

In this work, the delta function approximation for photon energy for each of the photon fields is taken. The energy density of the $2.7^{\circ}K$ field can be shown to be 0.25eV cm^{-3}; the energy density for starlight is taken as 0.44eV cm^{-3} (Allen, 1973); the energy density for the far infrared field is taken to be 0.49eV cm^{-3} (see section 8.3). Using the mean energies given above and the electron spectrum in 2.12, 2.34 has been solved. The integral local production spectrum has been found using Romberg integration by decade (as for the bremsstrahlung case) and the result is shown in figure 2.3. The values found by other authors for the production above 100 MeV are shown for comparison in table 2.2. The differences can be explained by the different electron intensities taken.

The importance of far infrared radiation in the Galaxy has only been appreciated of late. The calculations of Piccinotti and Bignami (1976) employ an energy density of 0.2eV cm^{-3} based on results from two rocket flights reported by Pipher (1973). In a more recent publication, since further infrared results have become available, these authors use a value of 0.4eV cm^{-3} (Bignami and Piccinotti, 1977). The value used in the present calculations (see discussion in section 8.3) causes the far infrared to dominate over the other inverse Compton contributions. From figure 2.3 it is seen that locally inverse Compton

Table 2.2

The local inverse Compton production function found by various authors. The emissivity of gamma rays above 100 MeV is given separately for the various photon fields. Only in the last two references has some account of far infrared radiation been taken.

Reference	Electron Spectrum Used	$q(>100$ MeV) $cm^{-3}\ s^{-1}$		
		$2.7^{o}K$	Starlight	Far Infrared
Fichtel et al. (1976)	Daugherty et al. (1975)	$2.0\ 10^{-27}$	$2.0\ 10^{-27}$	
Dodds (1977)	Cummings et al. (1973)	$8.5\ 10^{-28}$	$2.7\ 10^{-27}$	
Stecker (1977a)		$6.8\ 10^{-27}$	$1.7\ 10^{-27}$	
Piccinotti and Bignami (1976)	Daugherty et al. (1975)	$2.3\ 10^{-27}$	$1.3\ 10^{-27}$	$1.44\ 10^{-27}$ (Far infrared energy density 0.2eV cm^{-3}).
Present Work	Goldstein et al. (1970)	$5.0\ 10^{-27}$	$3.5\ 10^{-27}$	$7.3\ 10^{-27}$ (Far infrared energy density 0.49eV cm^{-3}).

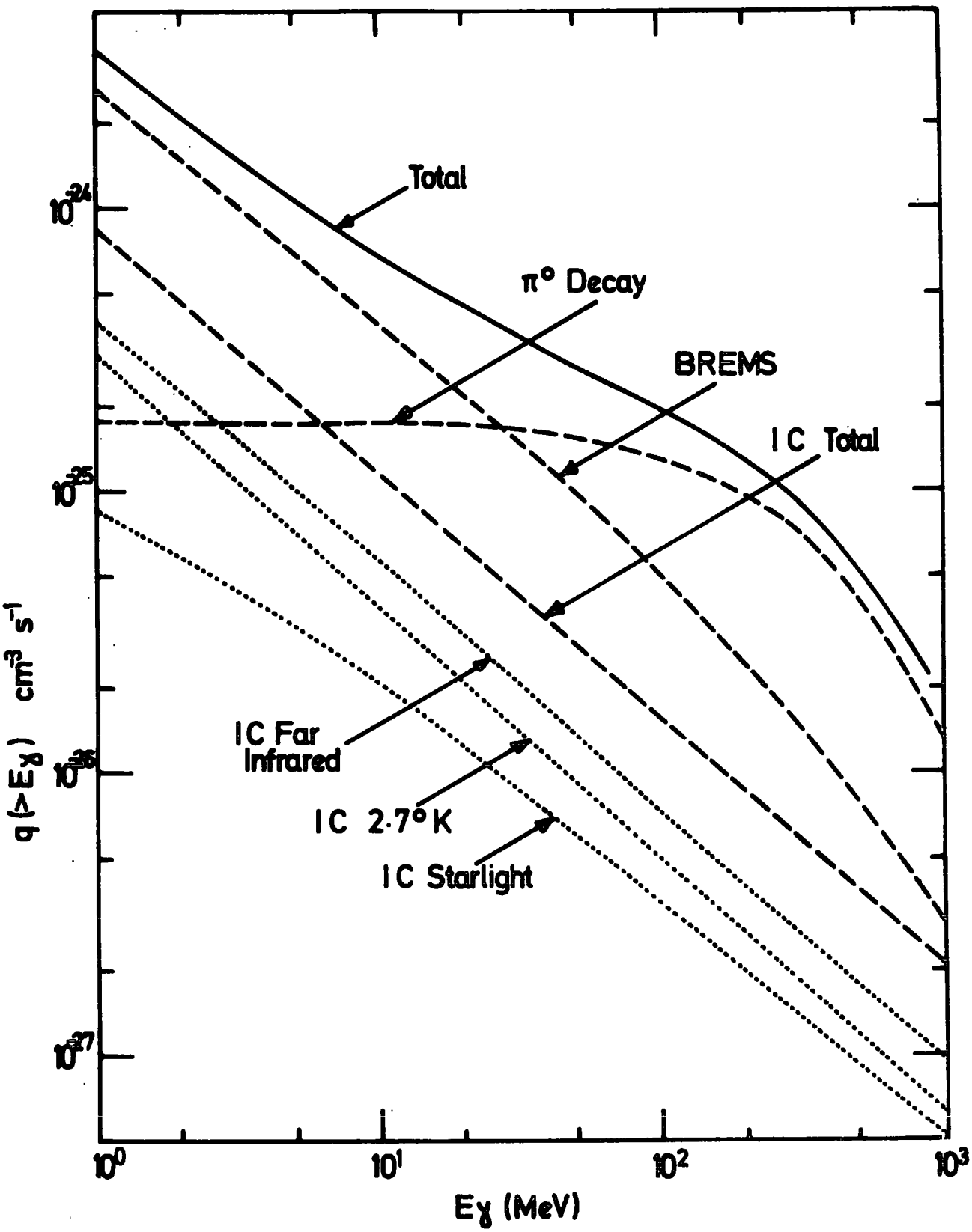

Figure 2.3 Local integral emissivities for n_H=1 H atom cm^{-3}. The neutral pion decay spectrum is taken from Stecker(1970) and the others are as calculated in the text. The inverse Compton contributions from the three photon fields are shown separately (dotted lines).

scattering is not a major source of cosmic gamma rays, providing only eight per cent of the total yield above 100 MeV.

2.5 RELATIVE IMPORTANCE OF THE PRODUCTION MECHANISMS WITH POSITION IN THE GALAXY

It is seen from figure 2.3 that locally for energies above 100 MeV the contribution to the gamma ray flux from neutral pion decay is dominant, with 26% and 8% of the total emissivity from bremsstrahlung and inverse Compton scattering respectively. Below 30 MeV bremsstralhung dominates (see Fichtel et al., 1976), but it must be emphasised that the uncertainty in the local primary electron intensity is about a factor of two or greater.

To find the variation of emissivity with position in the Galaxy the following variables (all position dependent) are defined:

$n_p(E, \underline{r})$ - cosmic ray proton number density.

$n_{ep}(E, \underline{r})$ - primary electron number density.

$n_{es}(E, \underline{r})$ - secondary electron number density.

$n_H(\underline{r})$ - interstellar matter density.

$w_{ph}(\underline{r})$ - energy density of dominant photon field.

For a given position, the dependence of the emissivity on these variables for each of the three gamma ray production mechanisms is:

$$q \text{ (neutral pion decay)} \propto n_p\, n_H \tag{2.39}$$

$$q \text{ (bremsstrahlung)} \propto (n_{ep} + n_{es})\, n_H \tag{2.40}$$
$$\uparrow_{\propto n_p\, n_H}$$

$$q \text{ (inverse Compton)} \propto (n_{ep} + n_{es})\, w_{ph} \tag{2.41}$$
$$\uparrow_{\propto n_p\, n_H}$$

It is probable that $n_p(\underline{r}) \propto n_{ep}(\underline{r})$ since there is no strong evidence at present to suggest otherwise.[1] A justification for the proportionality is given by Paul et al. (1974, 1976), based on the similarity between the gamma ray and 150 MHz radio synchrotron longitude and latitude Galactic profiles.

We now consider the possibility of one of the minor contributors (inverse Compton or bremsstrahlung) becoming dominant. Turning first to inverse Compton scattering, from 2.41 it is seen that the location of highest percentage contribution is that of maximum starlight and far infrared energy density, i.e. the Galactic centre. The flux in this direction has been calculated by several authors, but not without assumptions as to the variation of photon density with position. Dodds et al. (1975a) and Bignami and Piccinotti (1977) take the starlight energy density as increasing in proportion to the total mass density. Shukla and Paul (1976) have calculated the energy density as the integral over star sources with no Galactic absorption. They argue that "absorbed" radiation is just scattered and emitted at a redder wavelength causing a negligible change in total energy density. However, in this case their normalisation to the local starlight energy density of Allen (1973) is not valid. Bignami and Piccinotti are the only authors to include the far infrared photon field to which they assign a local energy density of 0.4eV cm^{-3} and a distribution closely following that of molecular hydrogen (Gordon and Burton, 1976). The calculations all agree that the contribution to the observed flux at about 100 MeV is small compared with the other two mechanisms. As a consequence of the higher matter density in the inner Galaxy, the

(1) The very recently reported gamma ray measurements (see Section A.5) now however suggest a steep Galactic gamma ray spectrum uncharacteristic of pion decay and implying that elsewhere in the Galaxy the primary electron to proton density ratio is higher than locally.

bremsstrahlung flux will dominate that from inverse Compton scattering even in the event of a much higher electron to proton density ratio causing the neutral pion decay flux to be overridden.

The bremsstrahlung contribution relative to that from neutral pion decay is increased with matter density due to the higher yield of secondary relative to primary electrons (see equations 2.39 and 2.40). However as the density of matter increases, the energy losses of electrons and protons become important. For a conservative Galactic containement time of 2.5 10^6 years, matter densities of only 10 atoms cm^{-3} and 20 atoms cm^{-3} will typically cause some energy loss for electrons and protons respectively before escape (see Chapter 4 and particularly figures 4.4, 4.5). The limiting case, considered in detail in Chapters 4 and 5, is that in which the proportion of secondary electrons is a maximum. This corresponds to a high enough density for total energy loss of all the particles. It is found that although the contribution to bremsstrahlung from secondary electrons is now about a factor of 2.5 greater than that from primary electrons for $n_p \propto n_{ep}$, pion decay still dominates at about 100 MeV. Fichtel et al. (1976) find that for the integral along the line of sight towards the Galactic centre, primary electron bremsstrahlung dominates over the secondary electron contribution.

In conclusion, unless the primary electron to proton density ratio is greatly increased in some location in the Galaxy, neutral pion decay is everywhere dominant over bremsstrahlung as a production mechanism for 100 MeV gamma rays. The line of sight contribution from inverse Compton scattering in the direction in which it is a maximum is still lower than from bremsstrahlung.

CHAPTER THREE

THE SPATIAL DISTRIBUTION OF GALACTIC GAMMA RAY EMISSIVITY ABOVE 100 MeV AND ASSESSMENT OF POSSIBLE PRODUCTION MODELS

3.1 INTRODUCTION

In this Chapter, the Galactic gamma ray observations are introduced. We consider to what extent they verify the conclusions of the previous Chapter about their production mechanisms. The observations of interstellar gas are reviewed, and a method for unfolding the gamma ray flux data to obtain the spatial emissivity of gamma rays is described. The possible spatial correlation of gamma ray emissivity with gas density is considered and an assessment made of current Galactic gamma ray production models.

3.2 THE GALACTIC GAMMA RAY ENERGY SPECTRUM

A summary of gamma ray experiments is to be found in Appendix A. Spectral information on the Galactic flux is very limited; a compilation of results towards the Galactic centre is shown in figure 3.1. The exact longitude and latitude range to which the various results apply differ and are given in tables A.3 and A.4. At the time of writing the best data are from the SAS-2 satellite (Fichtel et al., 1975), but soon results from the presently orbiting COS-B spacecraft will be available. Also shown in figure 3.1, for comparison with the observations, are the integral neutral pion production spectrum of Stecker (1970), and a power law of slope -0.8 (see figure 2.3), both normalised to be consistent with the SAS-2 data at 100 MeV. The power law is chosen to be consistent with the

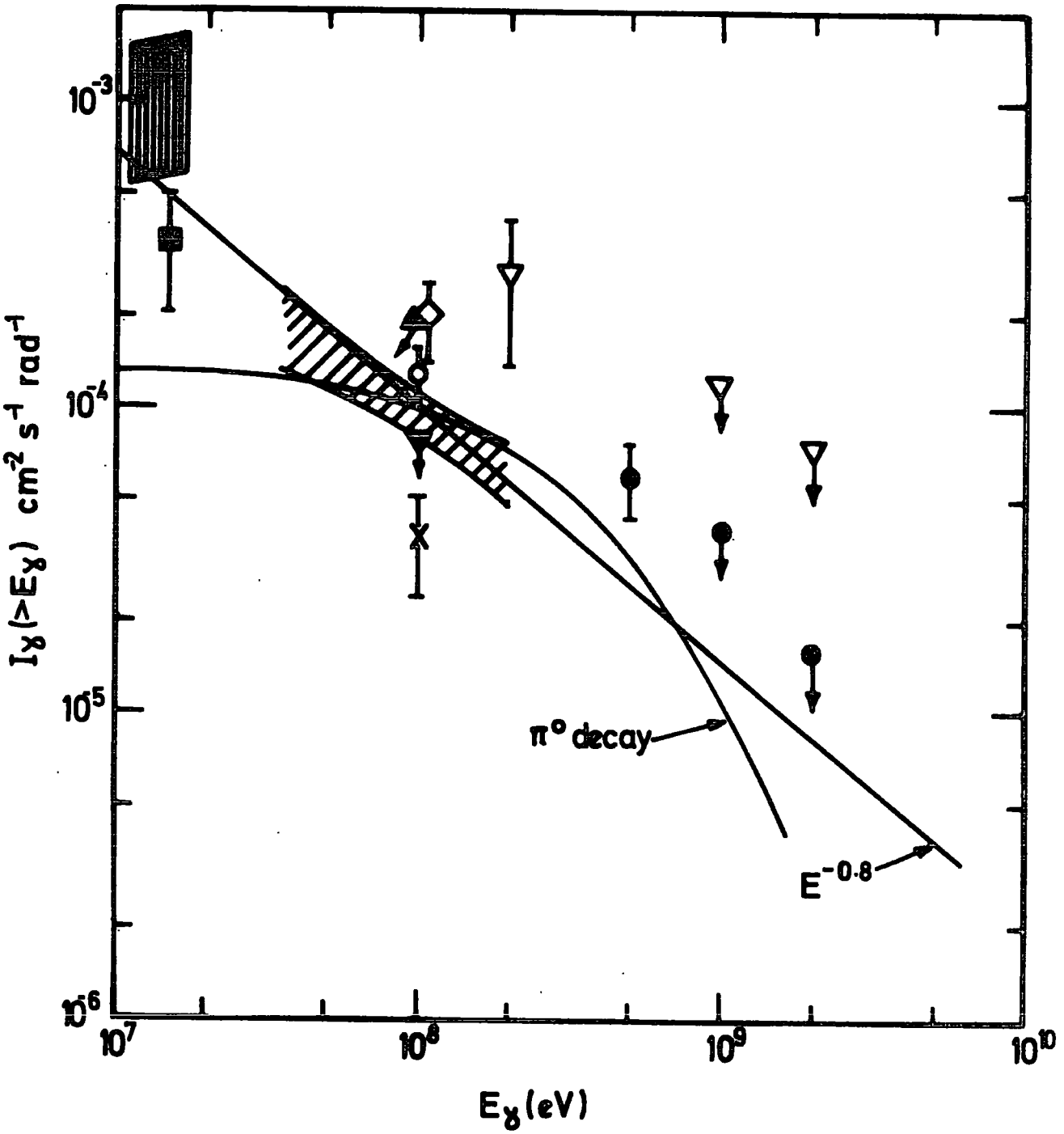

Figure 3.1 Integral plot of observations of gamma rays towards the Galactic centre. The longitude and latitude ranges to which individual results apply are found in tables A.3 and A.4. For comparison, the neutral pion production spectrum and power law of slope -0.8 are shown, both normalised at 10^8 eV. Fichtel et al.(1975), Sood et al.(1974), Kraushaar et al.(1972), Share et al.(1974b), Helmken and Hoffman(1973), Frye et al.(1974), Fichtel et al.(1972), Dahlbacka et al.(1973), Bennett et al.(1972), Browning et al.(1972a).

inverse Compton contribution, but bremsstrahlung will produce a slightly steeper slope at about 100 MeV. The SAS-2 data appear inconsistent with wholly neutral pion production, but accuracy is not high enough for the percentage of bremsstrahlung and inverse Compton production to be firmly deduced. The SAS-2 data are consistent with a zero neutral pion contribution, but this is not supported by the balloon measurements of Sood et al. (1974). It is seen from figure 3.1 that the balloon observations are very scattered. The critical region where more results are required is between 100 MeV and 500 MeV so that it can be determined how much of the characteristic pion production "shoulder" is present. Current observations do not contradict the conclusions of Chapter Two, but are insufficient to evaluate the precise contributions from the various mechanisms.

3.3 THE DISTRIBUTION OF INTERSTELLAR GAS

3.3.1. Relevance to Gamma Ray Observations

As discussed in Chapter Two, the production of Galactic gamma rays yields information on the product of cosmic ray intensity and gas density. Clearly, if the cosmic ray intensity is uniform and the gas and cosmic rays have similar scale heights, $\langle z \rangle$, the column density of gas in any direction would be proportional to the measured gamma ray flux in that direction. The constants of proportionality are determined using the locally observed cosmic ray spectrum. Such a comparison towards the anticentre, where the gas density is low and in the form of atomic hydrogen, has led Dodds et al. (1975b) to conclude that there must be a decrease of cosmic ray intensity at large galactocentric radii ($R > 15$ kpc). Towards the centre of the Galaxy the situation is

less clear. Here the majority of the gas appears to be in the form of molecular hydrogen, H_2. The observational errors are of the order of a factor of two (see below), and must be coupled with errors in the gamma ray observations. The tentative conclusions, however, suggest an increase in cosmic ray intensity towards the Galactic centre (see section 3.5).

Any model including non-uniform cosmic ray density requires a map of the spatial distribution of gas. In the following two subsections the extent to which this is now available is discussed. The two main constituents of the gas, neutral atomic hydrogen and molecular hydrogen, are considered separately. The distribution of heavier atoms and molecules is not discussed, but as mentioned in section 2.2 it is appropriate to multiply the mass in hydrogen by a factor of 1.4 to account for all species.

3.3.2. Neutral Atomic Hydrogen in the Galaxy

The 21 cm hyperfine transition line of neutral atomic hydrogen, HI, was discovered in the Galaxy in the early 1950's. Since then HI has been observed in every direction in the Galaxy. The highest resolution survey to date is that of Westerhout (1973).

The observations are of brightness temperature as a function of frequency. The frequencies, doppler shifted from the natural value of 1420.406 MHz, are converted to radial velocities with respect to the local standard of rest. The observations allow a determination of the Galactic rotation curve, i.e. the linear rotational velocity as a function of Galactocentric radius, R. The method involves measuring the terminal velocity along each longitude ℓ, which relates to $R = R_o \sin\ell$, where R_o is the distance between the Galactic centre and the Sun, (for

a description of the method see Burton, 1974). For $R > R_o$ the rotation curve is determined from fitting the total mass distribution with the curve for $R < R_o$ (see for example Innanen, 1973). Perturbations in the rotation curve are caused by density fluctuations in the Galactic mass distribution. Burton (1976a, b), discusses the many difficulties involved in unfolding the HI observations to give the spatial distribution.

Only if the HI is always optically thin will the measured brightness temperature, T_B, relate directly to the column density, N_{HI}, by:

$$N_{HI} \approx 1.823\ 10^{18} \int T_B(v)\ dv\ cm^{-2}$$

where v is velocity. The HI emission begins to saturate at longitudes $|\ell| < 20^o$ (Burton, 1976a). The correction factor manifests itself as almost a factor of two increase in the derived HI volume density for $R < R_o$. Results for the smoothed volume density as a function of R, for $R > 2$ kpc, are tabulated by Gordon and Burton (1976). Also given is the surface density distribution where the scale height distribution is that of Baker and Burton (1975). This height is found to be approximately 200 pc (FWHM) for $R < 9.5$ kpc, but increases at larger R.

Although data for smoothed radial distributions are presented in the literature, it is evident that there is an asymmetry between the two hemispheres of the Galaxy and spiral structure dominates. The irregularities in the terminal velocities point to the existence of spiral arms.

The density wave theory for spiral galaxies was formulated by Lin and Shu (1967), and Lin et al. (1969). This theory provides a Galactic map for the interpretation of HI velocity-longitude brightness temperature data. A recent review on the validity and applicability of the

density wave theory is given by Roberts (1976). In this thesis the map evolved by Simonson (1976) is used, which is based on a theoretical density wave model similar to that of Lin et al. (1969). Simonson generated longitude-velocity diagrams from the theoretical map and then perturbed the map to give a good fit to the observations. He found that the Scutum and Sagittarius arms lie at tangential points of longitudes 33° and 50° respectively. This is in agreement with Burton (1971) whose best fit spiral has a pitch angle which varies between 5° and 8°. Figure 3.5 shows the map of Simonson for the Scutum and Sagittarius arms with the addition of the 4 kpc ring given by Simonson and Mader (1973). The width of the arms is greater than on the diagram, perhaps as much as 1 kpc, and, although the density is not completely uniform throughout the arms, the positions of their tangential points are well defined. The spiral wave is thought to terminate at a radius of about 4 kpc (the inner Lindblad resonance), and the central region of the Galaxy must be treated separately.

High velocity dispersions close to the Galactic centre were first observed by Rougoor and Oort (1960). The brightest feature is the so called 3 or 4 kpc arm and there are other features closer to the centre. They exhibit finite velocities at longitudes close to zero and, therefore, the arms are not simply rotating about the Galactic centre. The fact that some of the features are out of the plane has been established by more recent surveys, see for example Kerr (1967), van der Kruit (1970), Wrixon and Sanders (1973), Sanders and Wrixon (1973), Cohen (1975), and Cohen and Davis (1976). It is still not distinguishable as to whether the features are the results of explosions at the Galactic centre (van der Kruit, 1971), or are non-expanding elliptical features such that the

observed velocities are only apparent expansions due to the orientation of the ellipses (Shane, 1972; Simonson and Mader, 1973).

3.3.3. Molecular Clouds in the Galaxy

Cold dark clouds have been found to exist in the interstellar medium. These are predominantly of H_2, which, in the cold compressed regions, forms on grain surfaces and is self-shielded against photo-dissociation (Solomon and Wickramasinghe, 1969; Hollenbach et al., 1971). The clouds have typical densities of 10^3-10^5 H atoms cm^{-3}, sizes of 1-10 pc and temperatures of 5-20°K.

Although nearby clouds have been studied for some time (see the review of Heiles, 1971), due to observational difficulties it is only in the last two years that it has been fully appreciated that molecular clouds could be the dominant contributor to the interstellar gas.

There are no H_2 emission lines in the radio or optical range and the first observations of the molecules were rocket measurements of the Lyman absorption bands in the ultraviolet spectra of reddened stars (Carruthers, 1970; Smith, 1973). Since then a wealth of data have resulted from the Copernicus satellite (Spitzer et al., 1973; Spitzer and Jenkins, 1975). Unfortunately, such observations are limited to within a radius of 1-2 kpc due to extinction by interstellar grains.

CO and NH_3 are seen in emission and act as tracers of H_2. NH_3 at 1.3 cm is a weak line, but observations have been reported for the Galactic centre direction by Kaifu et al. (1975). CO provides the best probe for clouds in the Galaxy and surveys have been presented by Scoville and Solomon (1975), Burton et al. (1975) and Gordon and Burton (1976). In addition, several observations of the Galactic centre have been made, but these are discussed separately in section 4.2. The

other tracers of molecular hydrogen are OH and H_2CO which have been observed in absorption against continuum sources near the Galactic centre. Unfortunately, the observed cloud spatial distribution is biased by that of the continuum sources.

The CO line normally observed is the $J = 1 \rightarrow 0$ transition at 2.6 mm and, due to the clumpy nature of the clouds, is well resolved in frequency. The transition $J = 2 \rightarrow 1$ at 1.3 mm has also been seen (e.g. Phillips et al., 1973), but the large scale surveys for the Galaxy are restricted to the 2.6 mm line. Unfortunately, there are difficulties involved with the conversion of CO brightness temperature to H_2 density because the ^{12}CO line, which is generally measured, is optically thick. Three observations of the rarer ^{13}CO isotope, which is optically thin, have been made by Scoville and Solomon (1975). A complete survey in ^{13}CO is desirable, but these observations take about twenty-five times as long as ^{12}CO measurements. The $^{13}CO/^{12}CO$ ratio measured by Scoville and Solomon ranges from $1/2$ to $1/6$ which, compared with the interstellar abundance value of $1/40$ (Wannier et al., 1976), provides good evidence that ^{12}CO is optically thick. If the ^{12}CO line were optically thin, then the column density would be proportional to the integrated brightness temperature along the line of sight (as for the 21 cm measurements of neutral atomic hydrogen). However, in the optically thick situation, the observed brightness temperature is a measure of the excitation temperature characterising the relative $J = 1$ and $J = 0$ level populations.

The approaches taken by Gordon and Burton on the one hand, and Scoville and Solomon on the other, to justify the conversion of their ^{12}CO results to the H_2 density, are very different. Gordon and Burton argue that the similar shape of the ^{12}CO and ^{13}CO lines indicates that

they are both optically thin. A model to explain this, based on multiple scattering of photons in regions of large velocity gradients, is given by Leung and Liszt (1976). The column density of CO is found from $\int T_v(^{12}CO)dv$ in the usual way and is multiplied by a factor of 40/3 to correct for the ratio of the measured and interstellar $^{13}CO/^{12}CO$ ratio. 10% of carbon is assumed to be in the form of ^{12}CO, leading to $n(CO)/n(H_2) = 6 \times 10^{-5}$.

Scoville et al. (1976) argue that the clouds are optically thick to ^{12}CO, but that each photon is absorbed and scattered approximately τ times before it escapes the clouds. Thus, the excitation temperature and optical depth are related. Detailed treatment (Scoville and Solomon, 1974), leads to: $T_B \propto n_{H_2}^{0.8}$. Support for the analysis of Scoville and Solomon arises from Plambeck et al. (1977) who compare the J = 2→1 and J = 1→0 spectra of CO in 8 clouds and explain the symmetry in the line profiles and intensities by large scale motions in the cloud, thus ruling out the small scale turbulence which is a feature of the Leung and Liszt model.

Excluding the Galactic centre, the smoothed radial distributions of volume density given by Scoville and Solomon (1975) and Gordon and Burton (1976), both show maxima at about 5.5 - 6 kpc. However, whereas Scoville and Solomon obtain 4 H atom cm^{-3} at the maximum, Gordon and Burton only obtain 2 H atom cm^{-3}. Despite this factor of two discrepancy, both sets of results agree that over 90% of the hydrogen in the inner Galaxy (in units of number of atoms) is in molecular form. Burton and Gordon (1977) find that 65% of the ^{12}CO is in the ring $4 < R < 8$ kpc whereas only 36% of the HI is in this region and there appears no evidence for important concentrations of CO into spiral arms.

The FWHM scale height of the gas is found to be (105 ± 15) pc (Scoville et al., 1976) and 118 pc (Burton and Gordon, 1976). These results agree and show that the molecular hydrogen is more confined to the plane than the atomic.

From the table of HI and H_2 densities of Gordon and Burton (1976), we find a total density at the radius of the Sun of 1.1 H atoms cm^{-3}, of which 65% is in the form of H_2. The total agrees with the value found from the Copernicus observations (Jenkins, 1976), but here the H_2 is only given as 20%. In this work the local density is generally taken as 1 H atom cm^{-3}.

It seems, therefore, that the Galactic gas is mainly in molecular form, although its present density is known to no better than a factor of two. It is possible that colder, as yet undetected, clouds are present, since Liszt et al. (1977) find CO in absorption towards the Galactic centre which they suggest is due to extremely cold clouds, somewhere along the line of sight, at about $3^{\circ}K$.

3.4 CALCULATION OF THE GALACTIC GAMMA RAY EMISSIVITY DISTRIBUTION

3.4.1. Introduction

The experiments designed to survey the Galaxy for gamma rays of about 100 MeV and above are those carried by the satellites OSO-3, SAS-2, and COS-B, (see Appendix A). Of these, the last is still in operation and complete results for the Galaxy have yet to be published. The OSO-3 experiment had poor angular resolution, but paved the way for SAS-2, the results from which will be used here.

The SAS-2 data have been published in the form of a distribution in Galactic longitude of gamma rays above 100 MeV integrated over ± 10° of Galactic latitude. Figure 3.2 shows the data in longitude bins of

5° published by Fichtel et al. (1975). Further analysis has provided a distribution in longitude bins of $2\frac{1}{2}^{\circ}$ published by Thompson et al. (1976), and shown here in figure 3.3. However, it should be remembered that the angular resolution of the experiment is about 3°. The positions of Galactic sources are indicated in figures 3.2 and 3.3. The breaks in the data around $\ell = 150^{\circ}$ and $\ell = 300^{\circ}$ are due to premature failure of a power supply. The dashed line shows the level of the high latitude flux. It has been estimated from six observations in directions away from the Galactic plane. The question of whether this flux is indeed isotropic and the likelyhood of it being of extragalactic origin are considered in later chapters. However, it is clear that the Galactic plane is a strong source of gamma rays rendering the high latitude flux small in comparison. The strong feature of the distributions, also found by the earlier OSO-3 experiment, is the broad enhancement within about $\pm 30^{\circ}$ of the Galactic centre.

There are two motives for unfolding the gamma ray flux distributions to give the spatial emissivity; firstly, to enable the total gamma ray yield from the Galactic disc to be determined, and secondly to allow comparison with gas features. The simplest model, that of radial symmetry, is taken to permit easy comparison with the radial gas distributions presented by Scoville and Solomon (1975) and Gordon and Burton (1976). Unfoldings of the SAS-2 data in its earlier published form (Kniffen et al., 1973) using this model, are given by Puget and Stecker (1974) and Strong (1975). The method used here for the unfolding is based on that of Strong (1975). The work is then extended for a model in which the emissivity is uniform along spiral arm sections.

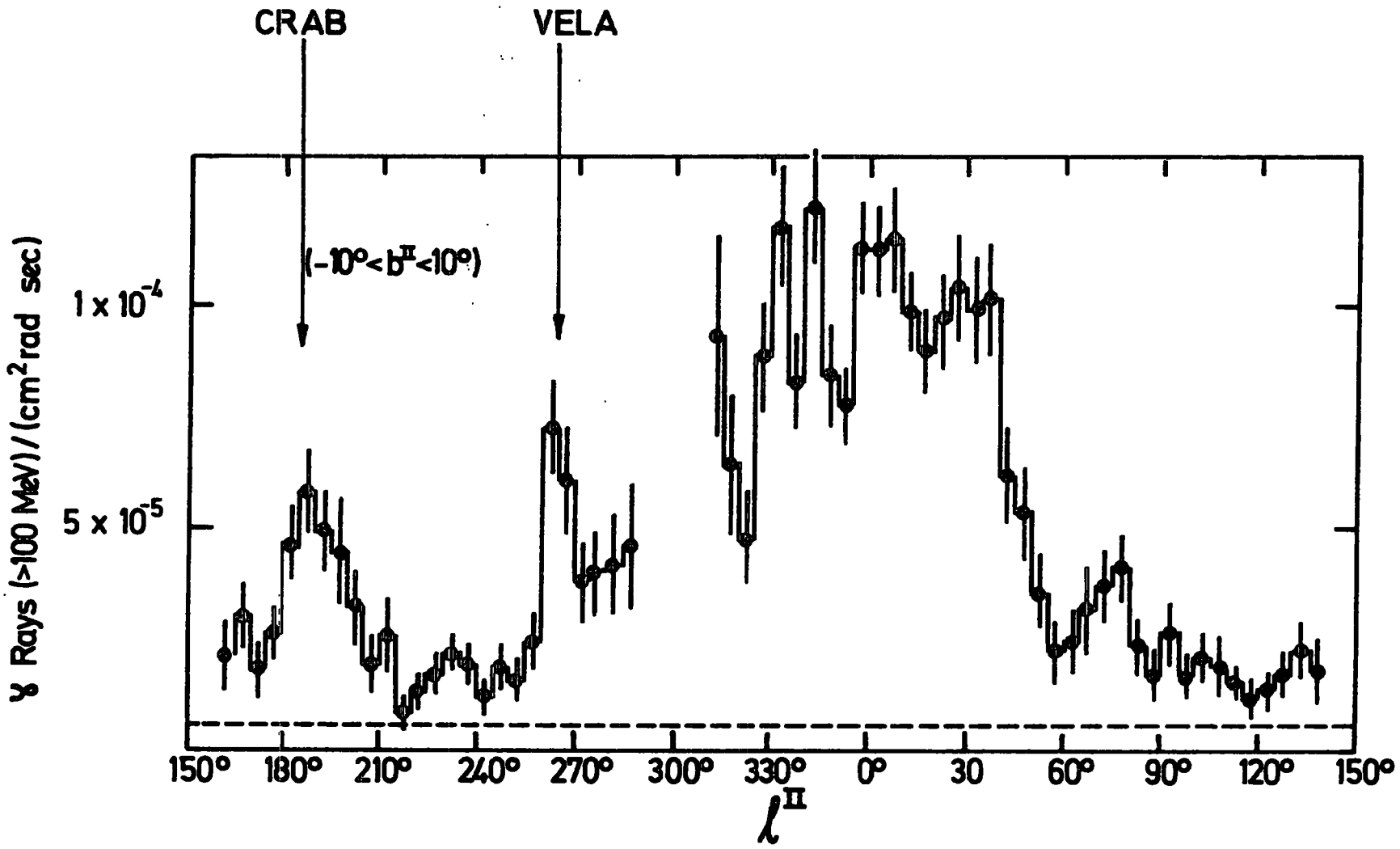

Figure 3.2 The SAS-2 Galactic longitude distribution (binwidth 5°) of gamma rays above 100 MeV, integrated over ±10° of latitude, from Fichtel et al.(1975). The positions of the Crab and Vela supernova remnants are shown.

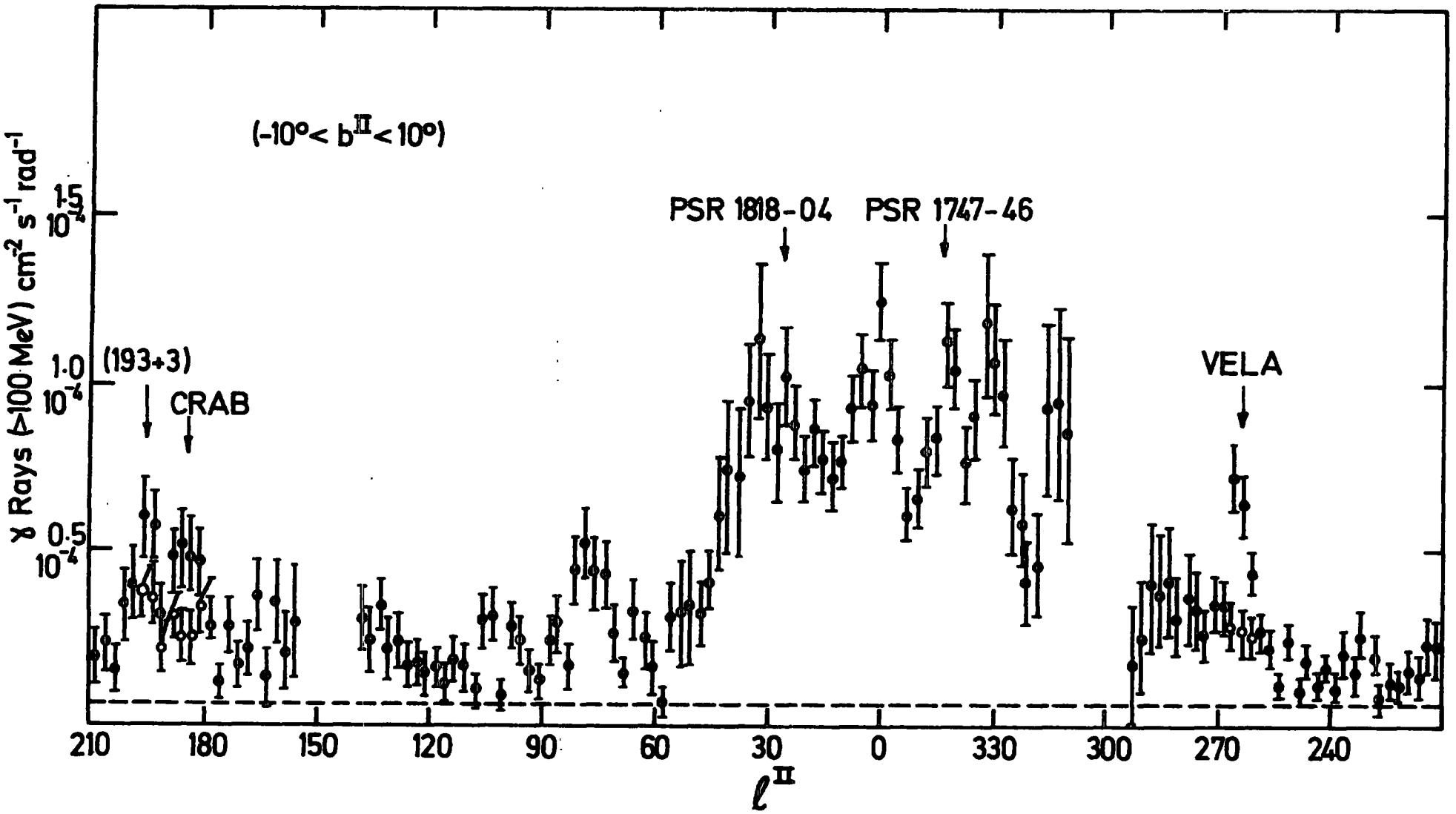

Figure 3.3 The SAS-2 Galactic longitude distribution (binwidth 2.5°) of gamma rays above 100 MeV, integrated over ±10° of latitude, from Thompson et al.(1976). The positions of reported sources are shown.

3.4.2. Method of Analysis

The analysis is restricted to the Northern Galactic Hemisphere because of the break in the SAS-2 data around $\ell = 300^{\circ}$. There are no known sources between longitudes 0° and 90° to be subtracted before unfolding. If $\Delta\ell$ is the longitude binwidth of the observations, the ith bin is defined as that between longitudes $(i-1)\Delta\ell$ and $i\Delta\ell$. The integral flux (per unit area per second per unit angle) of gamma rays of energy above 100 MeV in the ith bin, J_i (>100 MeV), integrated over $\pm 10^{\circ}$ of latitude, is given by:

$$J_i\ (>100\ \text{MeV}) = \frac{1}{\Delta\ell} \int_0^{\infty} \int_{-10^{\circ}}^{+10^{\circ}} \int_{(i-1)\Delta\ell}^{i\Delta\ell} \frac{q(r, \ell, b; >100\ \text{MeV})\ d\ell \cos b\ db\ dr}{4\pi} \qquad (3.1)$$

In 3.1, the line of sight distance r, the longitude ℓ and latitude b constitute a spherical coordinate system centred on the sun. The problem is to solve for the emissivity, q, as a function of cylindrical coordinates centred on the Galactic centre; R, Θ and z. A unique solution for q only exists for a specified functional dependence on Θ and z.

Firstly, concerning z, a "flat slab" of uniform thickness and constant emissivity with height has been chosen. The use of a more elaborate model is not justified by the data. A value for the half thickness, h, of 115 pc has been adopted. This value is appropriate to the disc thickness in HI, but is a little large for the molecular hydrogen (see section 3.3). However, the unfolded distribution is not very sensitive to h because the high gamma ray emission regions are found to be at distances great enough for the whole of the disc thickness to be included in the $|b| < 10^{\circ}$ opening angle.

The two models for the variation of q with Θ are described in (a) and (b) below.

(a) Radially Symmetric Emissivity

As shown in figure 3.4a, the disc is divided into constant emissivity rings such that the ith ring corresponds to the ith bin of data. The rings have inner and outer radii of $R_o \sin((i-1)\Delta\ell)$ and $R_o \sin(i\,\Delta\ell)$ respectively, where R_o is the Sun-Galactic centre distance. The emissivity in the Galactic plane is assumed to be constant for Galactocentric radii, R, satisfying $R_o \sin 80^\circ < R < 15$ kpc (the nth ring), and zero for $R > 15$ kpc.

We have:

$$J_i = \sum_{k=1}^{n} Q_{ik} W_k \qquad (3.2)$$

where W_k is the emissivity of the kth ring and Q_{ik} is its contribution to the flux observed in the ith bin. Using 3.1, the values for Q_{ik} are given by:

$$Q_{ik} = \frac{1}{\Delta\ell} \int_{r_{k3}(b,\ell)}^{r_{k2}(b,\ell)} \int_{-10^\circ}^{+10^\circ} \int_{(i-1)\Delta\ell}^{i\,\Delta\ell} \frac{d\ell \cos b \, db \, dr}{4\pi} \qquad (3.3)$$

where $r_{k1}(b,\ell)$ and $r_{k2}(b,\ell)$ are the intersection line of sight distances to the boundaries of the kth ring along the given b and ℓ.

3.3 can be rewritten:

$$Q_{ik} = \frac{1}{\Delta\ell\, 4\pi} \int_{(i-1)\Delta\ell}^{i\,\Delta\ell} J_k(\ell)\, d\ell \qquad (3.4)$$

Let X_{k1} and X_{k2} correspond to the distances of the far and near boundaries respectively the kth ring at $b = 0^\circ$ for a particular longi-

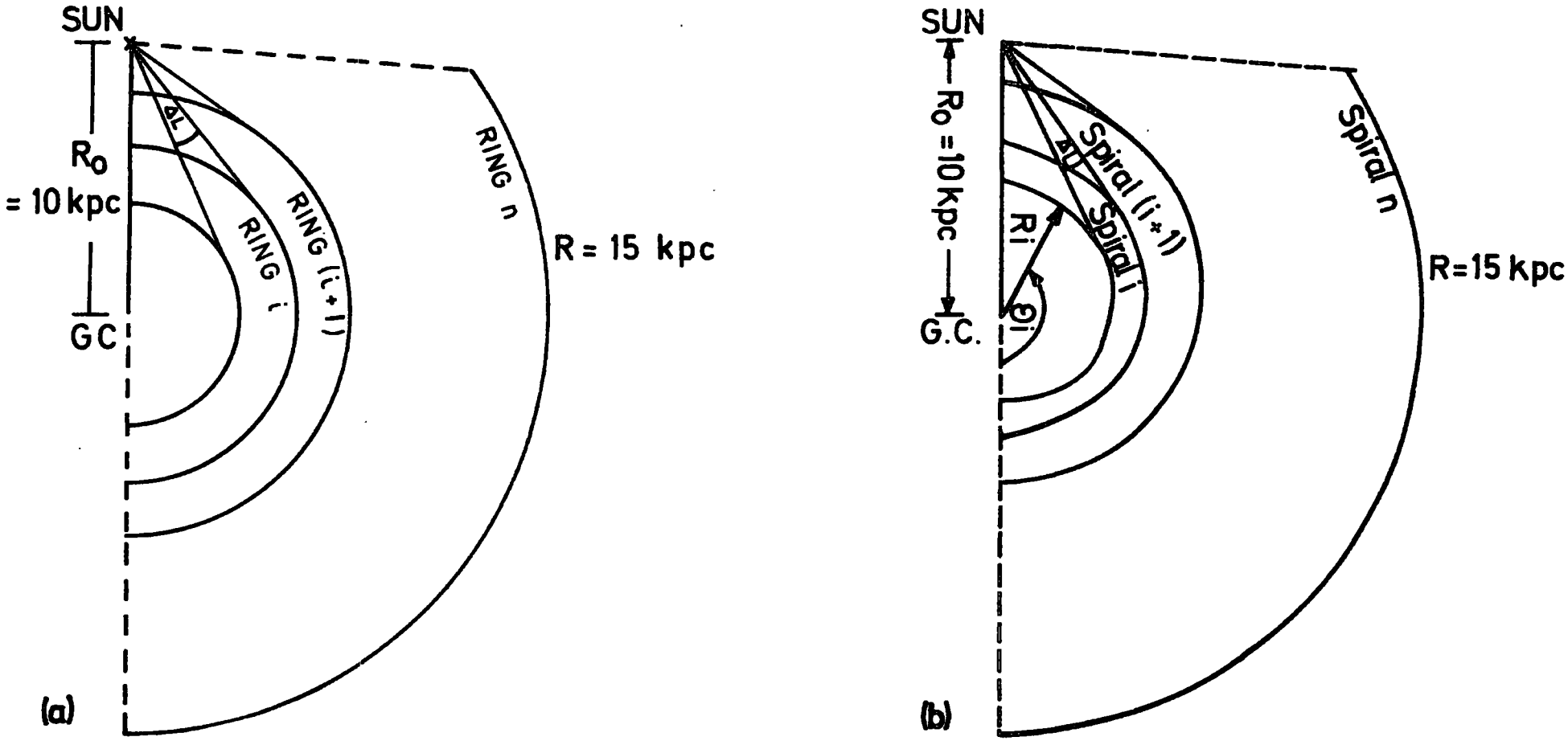

Figure 3.4 The geometry of the method for unfolding the distribution of gamma ray emissivity in the Galaxy for, (a) radially symmetric emissivity, and, (b) constant emissivity along 180° spiral sections.

tude direction. These values are easily calculated for a given ring and given direction. Using the following definitions:

$$\tan BA = \frac{h}{X_{k1}}$$

$$\tan BB = \frac{h}{X_{k2}}$$

and replacing $\int \cos b \, db$ by $\int db$ (a good approximation of less than 1% error since the maximum value of b is 10^{o}), we find:

(i) If $X_{k1} > h/\tan(\pi/18)$ and $X_{k2} > h/\tan(\pi/18)$,

$$J_k(\ell) = 2\left[h \ln\left(\tan\frac{BB}{2}\right) - h \ln\left(\tan\frac{BA}{2}\right) + X_{k1} \ln\left(\tan\left(\frac{\pi}{4} + \frac{BA}{2}\right)\right) - X_{k2} \ln\left(\tan\left(\frac{\pi}{4} + \frac{BB}{2}\right)\right)\right] \quad (3.5)$$

(ii) If $X_{k1} \leq h/\tan(\pi/18)$ and $X_{k2} \leq h/\tan(\pi/18)$

$$J_k(\ell) = 2[(X_{k1} - X_{k2}) \ln(\tan 10\pi/36)] \quad (3.6)$$

(iii) If $X_{k1} > h/\tan(\pi/18)$ and $X_{k2} \leq h/\tan(\pi/18)$

$$J_k(\ell) = 2\left[h \ln\left(\frac{\tan \pi/36}{\tan BA/2}\right) + X_{k1} \ln(\tan(\pi/4 + BA/2)) - X_{k2} \ln(\tan 10\pi/36)\right] \quad (3.7)$$

Equation 3.4 is evaluated using Simpsons integration. For each ring k and direction ℓ, the values for X_{k1} and X_{k2} are first evaluated and the appropriate expression from 3.5 - 3.7 chosen.

From 3.2 it can be seen that:

$$W_k = \frac{J_k - \sum_{j=k+1}^{n} W_j Q_{kj}}{Q_{kk}} \quad (3.8)$$

The emissivity of the outer ring, W_n, is first found, since:

$$W_n = J_n/Q_{nn} \tag{3.9}$$

This value for W_n is then used in 3.8 to find W_{n-1} and the procedure repeated to find all the values for W_k.

Rewriting 3.2 in matrix notation:

$$\tilde{J} = \tilde{Q}\tilde{W} \tag{3.10}$$

Therefore,

$$\tilde{W} = (\tilde{Q})^{-1}\,\tilde{J} \tag{3.11}$$

Since $\tilde{Q}$ is a matrix with all zero elements below the diagonal, the values for $\tilde{W}$ can be found without calculating all the elements of the inverse matrix (equations 3.8 and 3.9). However, the error on each W_k, expressed δW_k, is given by:

$$(\delta W_k)^2 = \sum_{i=k}^{n} (q_{ki}\ \delta J_i)^2 \tag{3.12}$$

where δJ_i is the error on J_i and q_{ki} are elements of the inverse matrix of Q, i.e.

$$\tilde{q} = \tilde{Q}^{-1} \tag{3.13}$$

3.12 can be written:

$$(\delta W_k)^2 = \left[\frac{\delta J_k}{Q_{kk}}\right]^2 + \sum_{i=k+1}^{n} (q_{ki}\ \delta J_i)^2 \tag{3.14}$$

We define,

$$x_{k+1} = \frac{1}{n-k} \sum_{i=k+1}^{n} \frac{Q_{ki}}{Q_{(k+1)i}} \tag{3.15}$$

Since neighbouring elements of Q_{ki} are very close in value (see next Chapter and figures 4.2 and 4.3), then a good approximation for J_k is given by:

$$J_k \approx (x_{k+1}\, J_{k+1}) + (Q_{kk}\, W_k) \tag{3.16}$$

Therefore equation 3.14 becomes:

$$\delta W_k = \frac{1}{Q_{kk}} \left[(\delta J_k)^2 + \left[\frac{\delta J_{k+1}}{n-k} \sum_{i=k+1}^{n} \frac{Q_{ki}}{Q_{(k+1)i}} \right]^2 \right]^{\frac{1}{2}} \tag{3.17}$$

This approximation allows the error on each W_k to be calculated without finding the inverse matrix, and is the method used in the present work.

(b) Constant Emissivity along 180° Spiral Sections

Ths disc is divided into 180° constant emissivity spiral sections (see figure 3.4b). The equations for the spiral arcs are of the form:

$$R = A_k\, e^{\Theta \tan(t)} \tag{3.18}$$

where the kth spiral arc is tangential to the longitude $k\,\Delta\ell$. However, following Burton (1971) the tilt angle, t, is itself a function of R such that:

$$\tan(t) = t_1 R + t_o \tag{3.19}$$

The values for t_1 and t_o are evaluated using the condition given by Burton that $t = 8^\circ$ at $R = 5$ kpc and $t = 5^\circ$ at $R = 10$ kpc, i.e. $t_o = 0.1936$ and $t_1 = -0.0106$.

The values of A_k for the n-1 spiral arcs, which are tangential to successive longitudes of spacing $\Delta\ell$ out to $\ell = 80^\circ$, are determined by geometry. The outer boundary of the nth section is the disc boundary of R = 15 kpc, and outside this the emissivity is assumed to be zero. Figure 3.5 shows the five spiral arcs corresponding to k = 3, 5, 7, 8, 10, superimposed on the map of Simonson (1976), (see the discussion in section 3.3.2). It is clear that this spiral is a good fit to the Sagittarius and Scutum spiral arms. Since the unfolding procedure commences at the maximum longitude and progresses inwards, the divergence of the Galactic structure from that of a spiral at radii less than about 4 kpc is not important.

The analysis is similar to that for the radially symmetric emissivity. However, a double iteration procedure is necessary in this case to find values for X_{k1} and X_{k2}. An intersection of the kth spiral with longitude ℓ occurs when:

$$R = \frac{R_o \sin\ell}{\sin(\Theta - \ell)} = A_k \, e^{\Theta(0.1936 - 0.0106\, R)} \qquad (3.20)$$

rewriting gives:

$$f(\Theta) = \ln\left[\frac{R_o \sin\ell}{A_k \sin(\Theta - \ell)}\right] - \left[0.1936\,\Theta - \frac{0.0106\, R_o\, \Theta \sin\ell}{\sin(\Theta - \ell)}\right] = 0 \qquad (3.21)$$

The two solutions for Θ in the region between 0° and 180° can be found using Newton Raphson iteration, in which the (n+1)th estimate for Θ is found from the nth using:

$$\Theta_{n+1} = \Theta_n - \frac{f(\Theta_n)}{f'(\Theta_n)} \qquad (3.22)$$

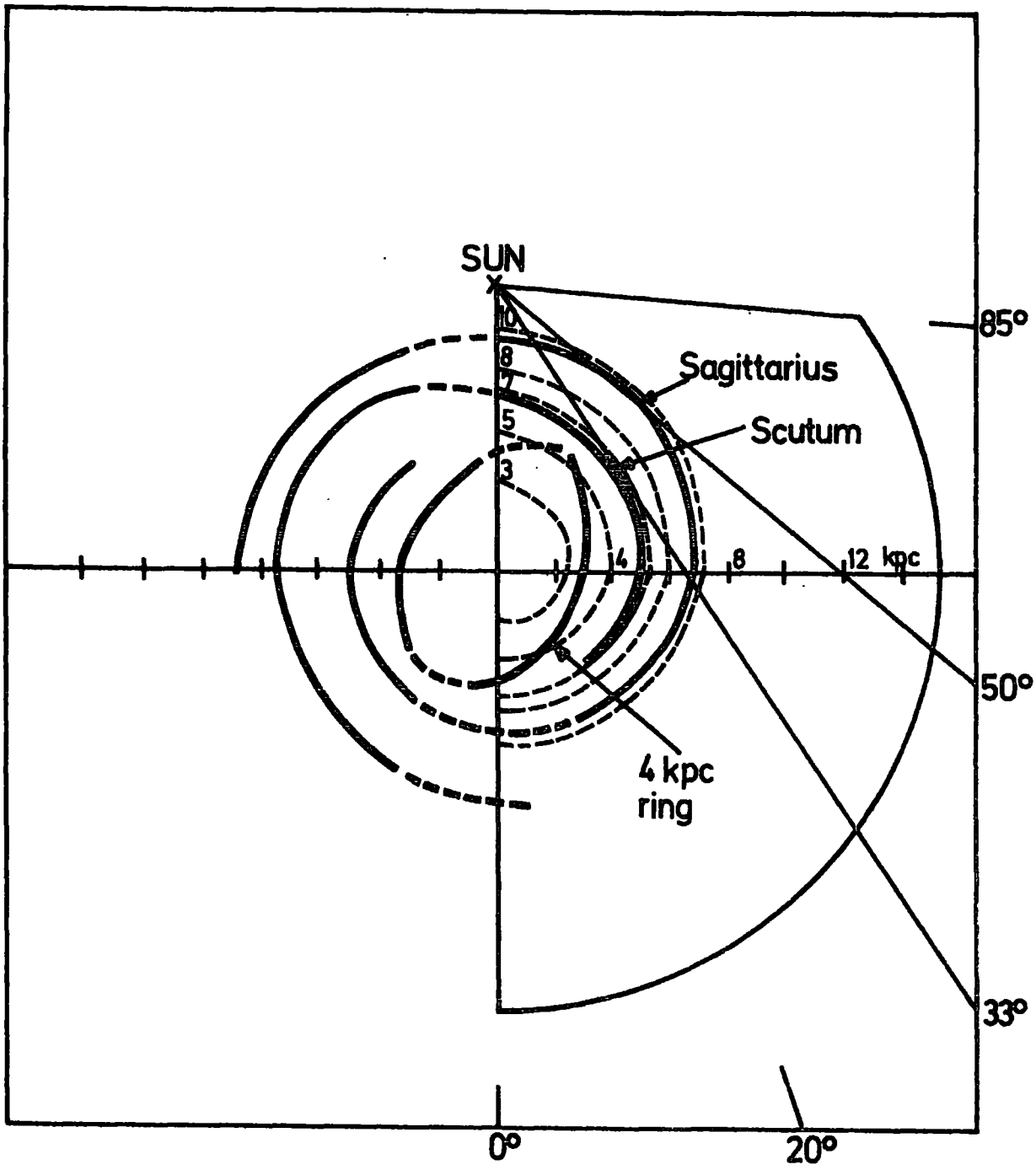

Figure 3.5 The map of Simonson(1976) for the Scutum and Sagittarius arms, with the 4kpc ring of Simonson and Mader(1973). For comparison, the dashed lines show five of the spiral arcs which are representative of the pattern used in the present work. These correspond to solutions of equation 3.18 for k=3,5,7,8 and 10.

The initial estimates of Θ_n are the two values which would be appropriate if the tilt angle were zero (i.e. radial symmetry).

For a value of Θ corresponding to spiral k and longitude ℓ , the appropriate X_k is given by:

$$X_k = \frac{\sin \Theta}{\sin \ell} \; A_k \; e^{\Theta(0.1936-(0.0106 \; X_k \sin \ell \; / \sin \Theta))} \qquad (3.23)$$

3.23 is solved for X_k also using Newton Raphson iteration. Equation 3.4 can now be evaluated as before, using 3.5 - 3.7, and the unfolding and error analysis are as in 3.8 and 3.17.

3.4.3. Results and Conclusions

The analysis has been firstly performed on the data shown in figure 3.2 with the isotropic background subtracted. Here $\Delta \ell = 5^o$ and n = 17.

The unfolded distributions shown in figures 3.6 and 3.7 indicate that the data are consistent with radial symmetry (otherwise negative values of W_i would be encountered). The relative emissivity, w, as plotted can be converted to volume emissivity, q_v, or surface emissivity, q_s, using:

$$q_v \; (>100 \text{ MeV}) = 9.4 \; 10^{-26} \; w \; cm^{-3} \; s^{-1}$$

$$q_s \; (>100 \text{ MeV}) = 6.5 \; 10^{-5} \; w \; cm^{-2} \; s^{-1}$$

The molecular hydrogen radial distribution of Scoville and Solomon (1975) is shown in figure 3.6, and the tabulated radial values for molecular plus atomic hydrogen of Gordon and Burton (1976) are given in figure 3.7. In both cases the gas has been scaled to correspond to gamma ray emissivity, assuming a uniform cosmic ray intensity. The

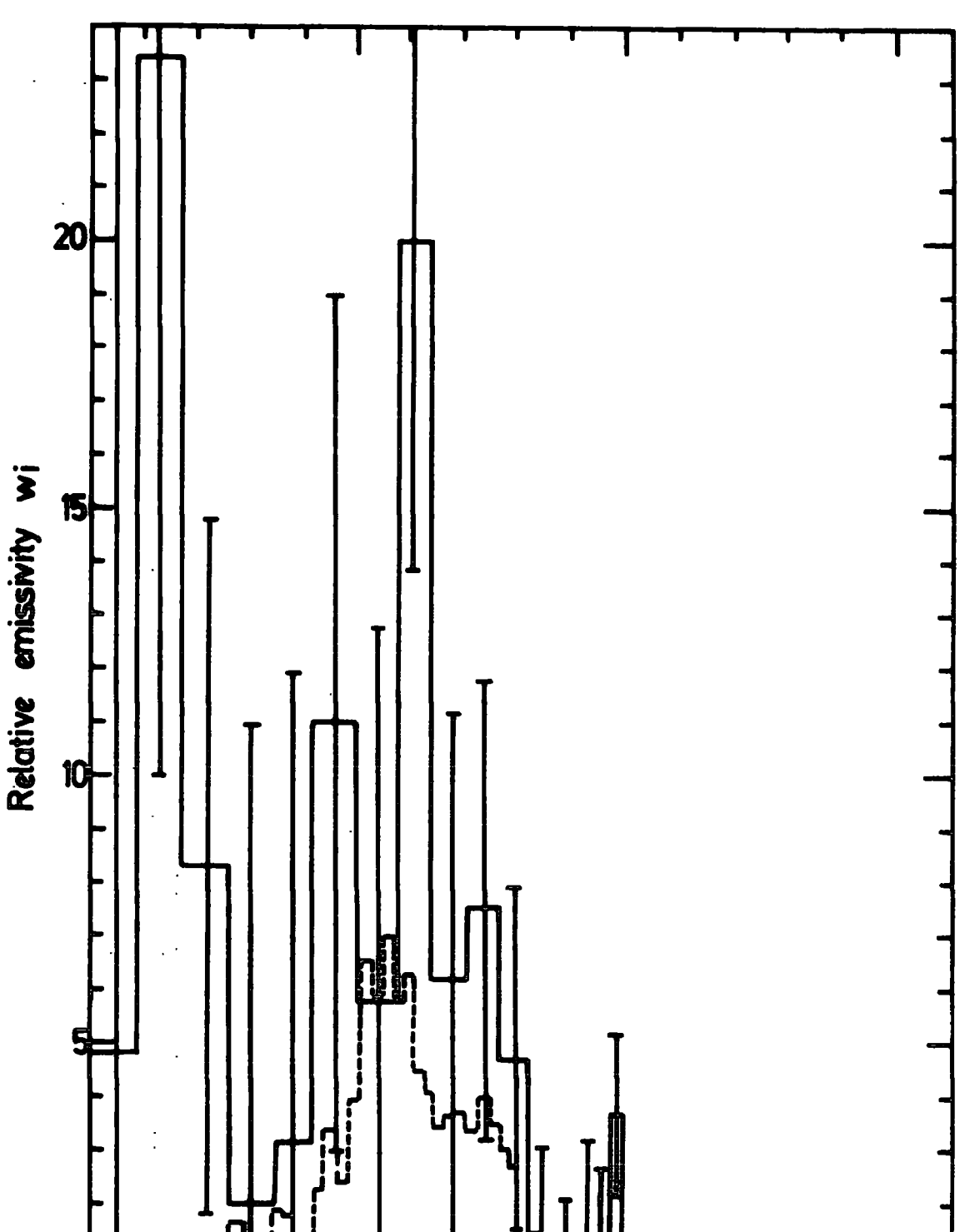

Figure 3.6 Result of unfolding the data of figure 3.2 for a radially symmetric emissivity model. The conversion factors for w_i to volume or surface emissivity are given in the text. The dashed line shows the molecular hydrogen radial distribution of Scoville and Solomon(1975), scaled to correspond to relative gamma ray emissivity for constant cosmic ray intensity throughout the Galaxy.

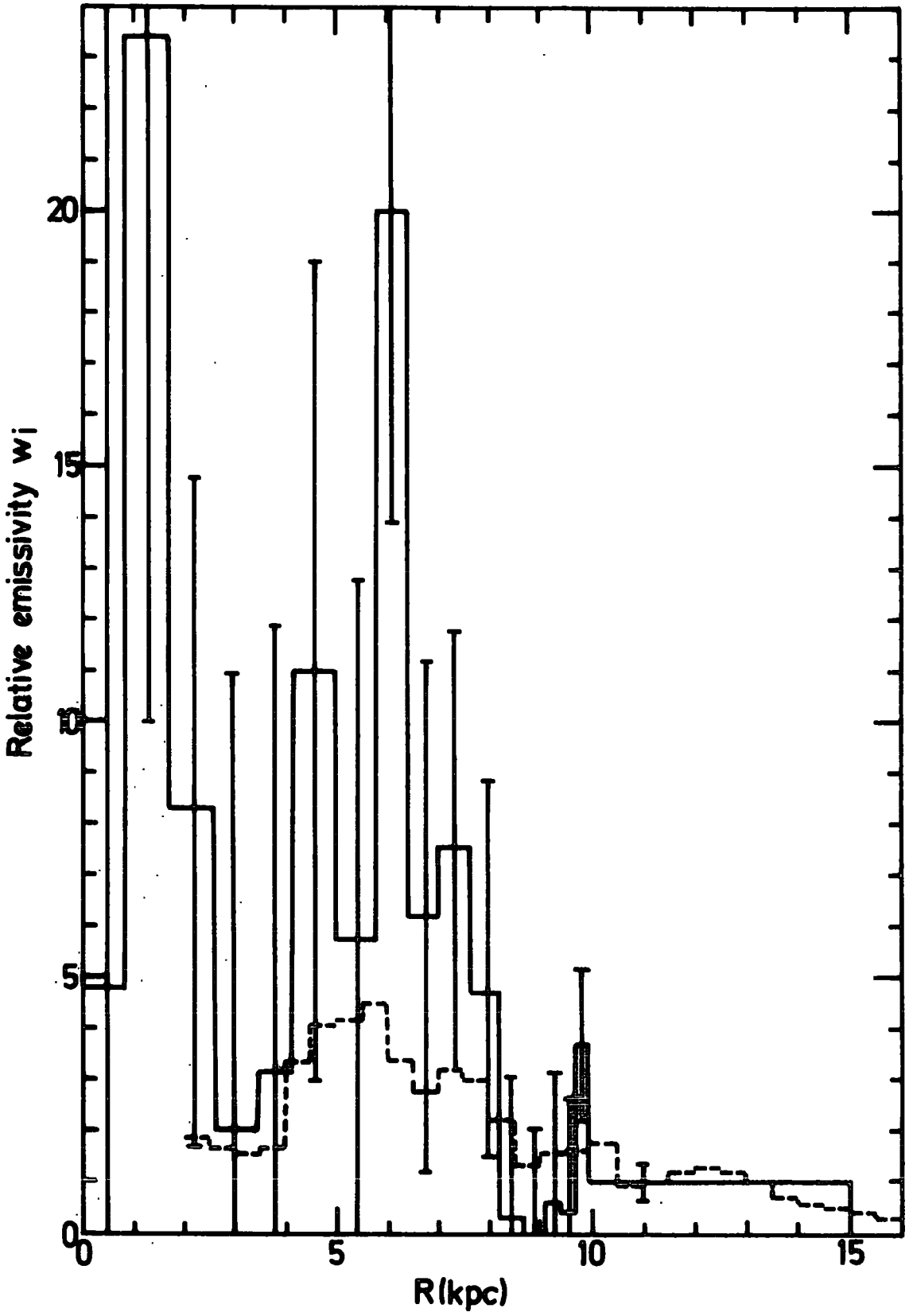

Figure 3.7 The gamma ray emissivity unfolding as in figure 3.6. The dashed line shows the H_2 plus HI radial distribution of Gordon and Burton(1976). The gas distribution has been scaled to correspond to relative gamma ray emissivity for constant cosmic ray intensity throughout the Galaxy.

gamma ray emissivity (>100 MeV) for the local cosmic ray spectrum has been taken as $1.5\ 10^{-25}$ H atom^{-1} s^{-1} (see figure 2.3 and discussion in Chapter 2).

It can be seen that apart from the Galactic centre where the errors in the unfolding become very large, the maximum emission occurs in bin 8, i.e. for R between 5.5 and 6.5 kpc. This correlates with the maximum in the molecular hydrogen radial distribution which is between 5 and 6 kpc. The approximate factor of two discrepancy between the gas density at the maximum found by Gordon and Burton (1976) and Scoville and Solomon (1975), already discussed in section 3.3, is apparent from comparison of figure 3.7 with figure 3.6. The factor by which the dashed lines in the two figures must be multiplied to give the gamma ray distribution, gives the cosmic ray intensity enhancement over the local value. It is of great importance to establish if this factor is greater or less than unity anywhere in the Galaxy, in which case a Universal cosmic ray origin (for energies close to 1 GeV) is ruled out. Because of the large errors on the gamma ray data, no firm conclusions can be reached concerning the region between radii of 4 kpc and 10 kpc except that it appears from figures 3.6 and 3.7 that an enhancement of cosmic rays is required to produce the gamma ray maximum at 6 kpc. However, this enhancement is only about a factor of 2 if the H_2 results of Scoville and Solomon are used, and slightly larger for those of Gordon and Burton. A factor this size is not really large enough for strong conclusions to be drawn, since it should be noted that the two published H_2 density distributions differ in magnitude by approximately the same factor.

From the radial unfolding in figures 3.6 and 3.7, the total emission of gamma rays above 100 MeV from the Galaxy is found to be $1.3\ 10^{42}\ s^{-1}$.

The data of figure 3.2 have been unfolded for constant emissivity along 180° spiral sections, and again consistency with the model is found. Since the results are very similar to those for radial symmetry, it is not possible to distinguish the models on this basis alone. In order to correct for any bias from nearby gas, the results shown in figure 3.8 are where the contribution from nearby (<1 kpc) gas as estimated by Puget et al. (1975, 1976) is first subtracted from the data. In fact it is found that the local contributions are reasonably uniform and so do not mask large scale structure. The conversion of w_i to volume or surface emissivity is as before. The direction for which the results are shown is $\Theta = 180^{\circ}$, i.e. the radius vector joining the Galactic centre and the sun. The positions of the Scutum and Sagittarius spiral arms are shown. (Their positions relative to the emissivity pattern are independent of Θ). It is apparent that the gamma ray enhancement does not correlate with the spiral arm positions and it can, therefore, be concluded that spiral structure does not fit the gamma ray distribution. This anti-correlation can be seen simply from the longitude gamma ray distribution but has not been given attention in the past. The general rise in gamma ray flux towards the Galactic centre has been the basis for many models which correlate with the gas density, and, before the discovery of molecular hydrogen in a large scale in the Galaxy, this gas was all atomic and was assumed to fit spiral structure. However, the correlation clearly cannot be excellent since inspection of figures 3.2 and 3.3 reveals that

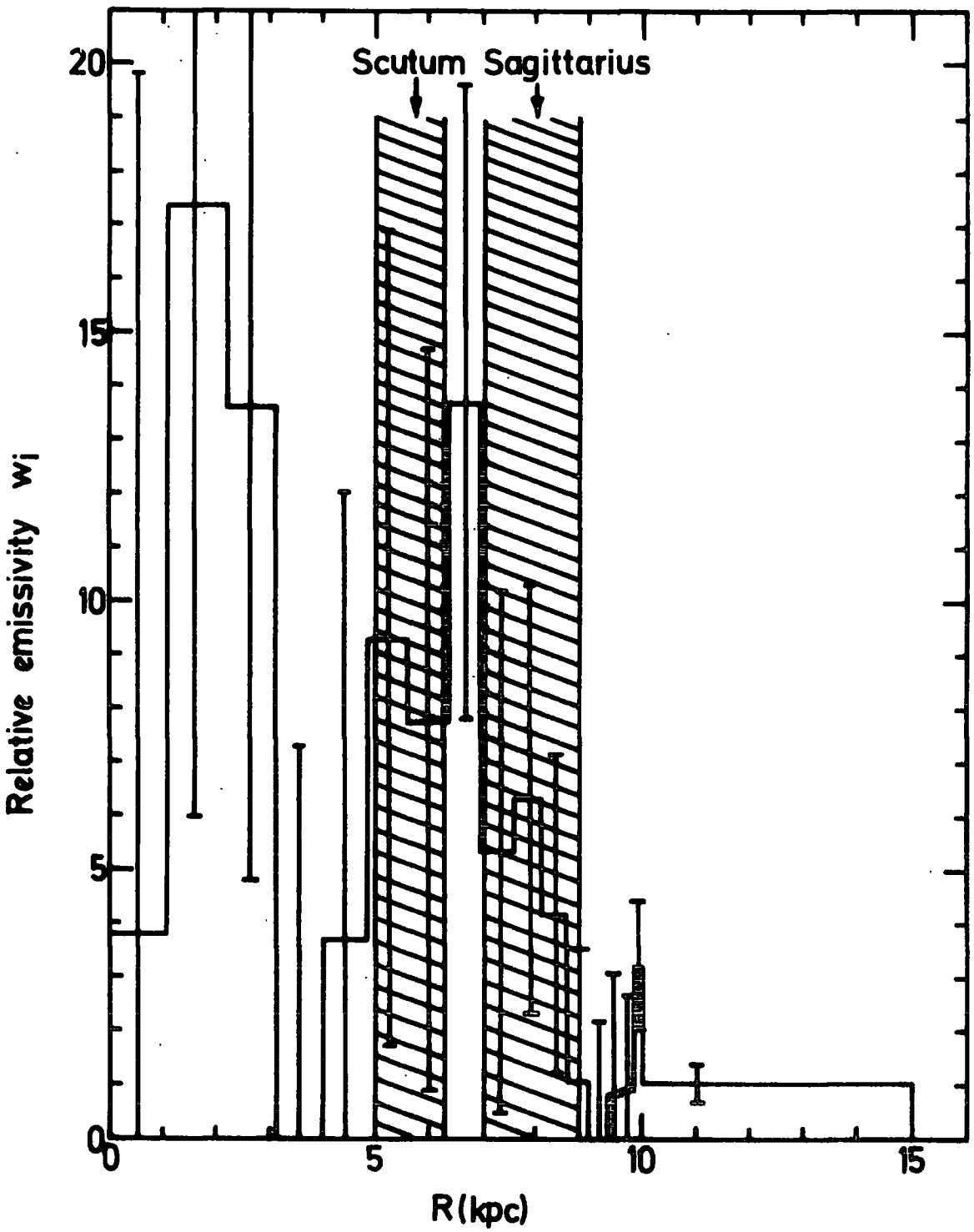

Figure 3.8 Result of unfolding the data of figure 3.2, for constant emissivity along 180° spiral sections, with the contribution from nearby (< 1 kpc) gas , as estimated by Puget et al.(1975,1976), first subtracted. The results are for the radius vector joining the Galactic centre and the Sun, and the positions of the Scutum and Sagittarius arms are shown.

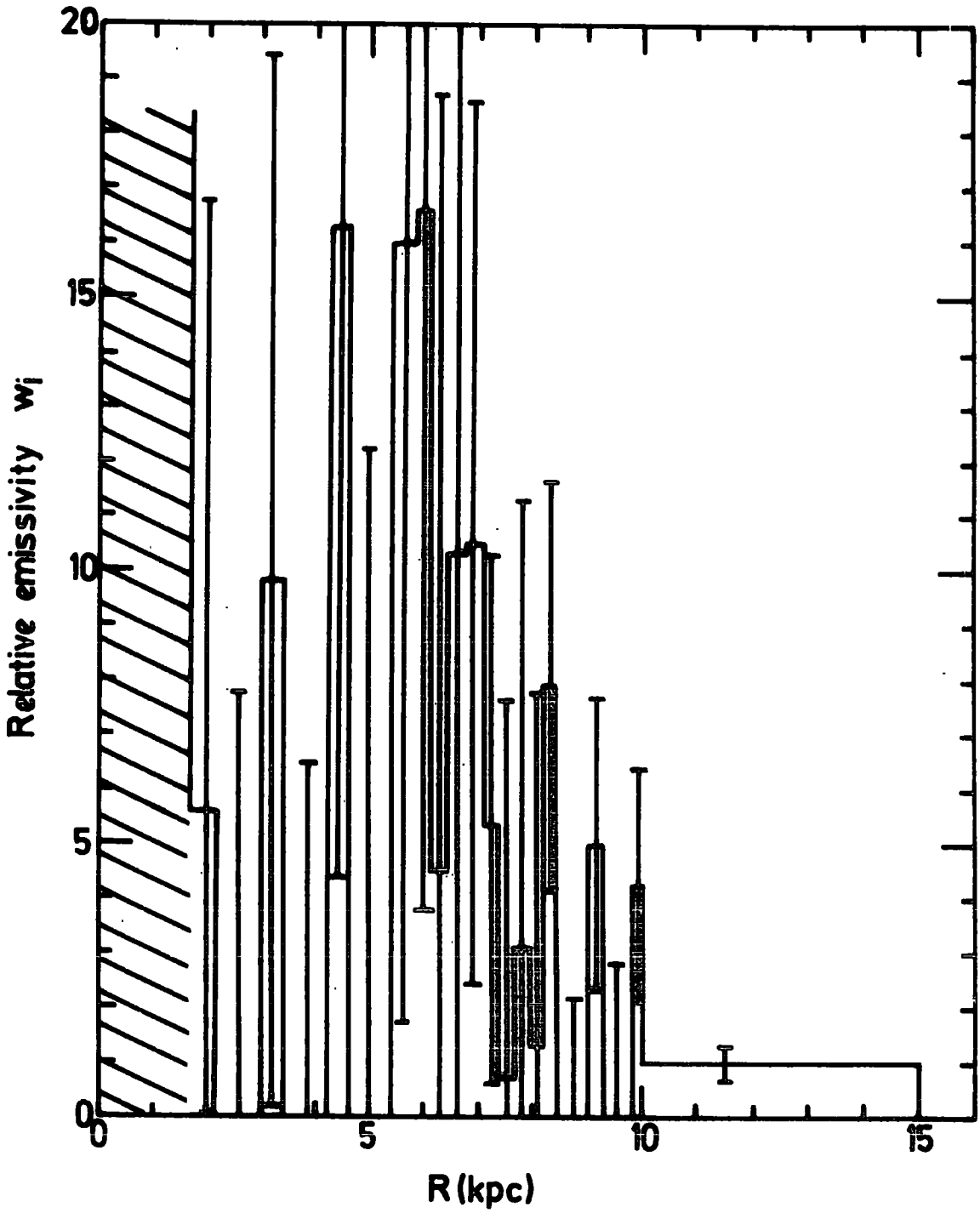

Figure 3.9 Result of unfolding the data of figure 3.3 for a radially symmetric emissivity model. Errors completely mask structure in the hatched region.

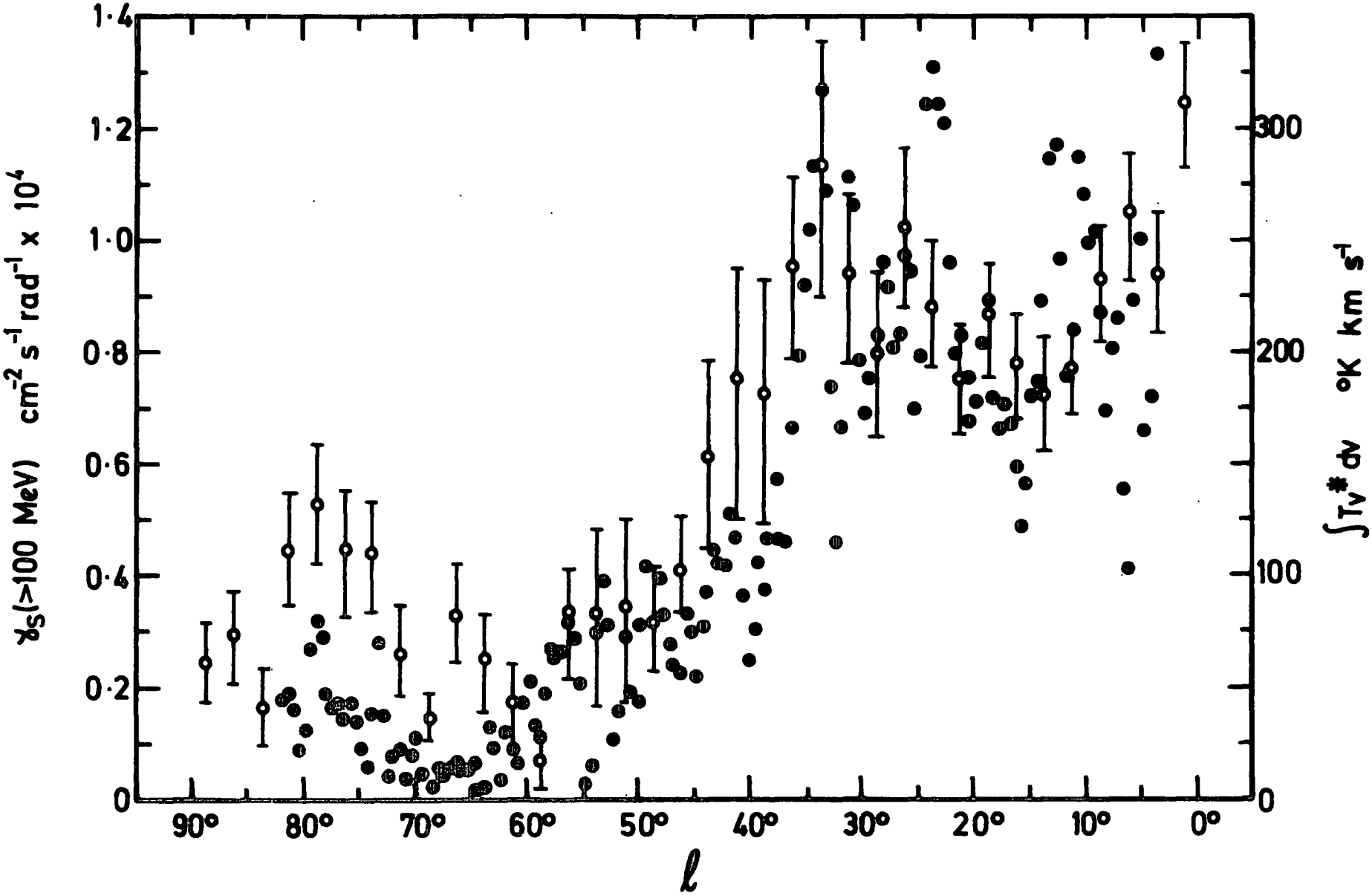

Figure 3.10 Comparison of the gamma ray observations of figure 3.3 (left hand scale and open circles) with the integrated line of sight CO data of Burton and Gordon(1977) (right hand scale and filled circles).

the rise in gamma ray flux occurs at about $\ell = 40^{\circ}$, whereas the Scutum and Sagittarius spiral arms are seen tangentially at longitudes of 33° and 50° respectively.

The data of figure 3.3 have also been unfolded. In this case, $\Delta\ell = 2\frac{1}{2}^{\circ}$ and n = 33. For completeness, the result for a radially symmetric model is shown in figure 3.9. However, it is clear that without smoothing over larger longitude bins the data are inconsistent with a radial unfolding. The relative emissivity can be converted to volume emissivity, q_v, or surface emissivity, q_s, using:

$$q_v \ (> 100 \text{ MeV}) = 1.13\ 10^{-25} \text{ w cm}^{-3} \text{ s}^{-1}$$

$$q_s \ (> 100 \text{ MeV}) = 8.0\ 10^{-5} \text{ w cm}^{-2} \text{ s}^{-1}$$

The longitude gamma ray data of figure 3.3 and the integrated line of sight CO emission given by Burton and Gordon (1977) are compared in figure 3.10. Both are seen to rise at a longitude close to 40°, which accounts for the good correlation of gas density with gamma ray emissivity shown in figures 3.6 and 3.7.

3.5 AN ASSESSMENT OF GALACTIC GAMMA RAY PRODUCTION MODELS

It has been shown in Chapter 2 that gamma rays above 100 MeV in the Galaxy are produced primarily in proportion to the product of cosmic ray and gas density. Before molecular hydrogen was first discovered on a large scale in the Galaxy (Scoville and Solomon, 1975), the gamma ray flux was in excess of that expected from a uniform cosmic ray density. Models such as those of Strong et al. (1973), Bignami and Fichtel (1974), and Dodds et al. (1975a), were therefore proposed. The significance of

molecular hydrogen as a possible cosmic ray target material was pointed out by Dodds et al. (1974) and Solomon and Stecker (1974), the former authors suggesting that the gas excess is possibly sufficient to account for the gamma ray results with a uniform cosmic ray flux. Since then, models to accommodate the extra gas have been proposed. A compilation of models, listing their important features, is given in table 3.1.

A reasonable overall fit to the gamma ray data is obtained for models in which the cosmic ray density, n_{CR}, is proportional to some power, α, of the gas density. There is disagreement between the values for α; Stecker et al. (1975) give $\alpha = 0.3$ and Kniffen et al. (1977), find $\alpha = 1$. The discrepancy can be accounted for by the fact that Stecker et al. have used the molecular hydrogen distribution of Scoville and Solomon (1975), whereas Kniffen et al. use the lower values given by Gordon and Burton (1976). Fuchs et al. (1976) use the distribution of Scoville and Solomon, together with some controversial arguments on hydrostatic equilibrium to obtain the z distribution, and find that a constant cosmic ray density in the inner Galaxy is consistent with the gamma ray observations.

Thus, so far, as expected from the discussion in section 3.4, and mainly because of uncertainties in the gas density, results as to whether or not there is a gradient of cosmic ray density in the inner Galaxy are inconclusive. The value of Galactic models such as are listed in table 3.1 is seriously limited.

The analyses of both Stecker et al. (1975) and Kniffen et al. (1977) employ the gas distribution as a function of R. Stecker et al. assume

Table 3.1

Compilation of models proposed to fit the Galactic gamma ray distribution. The cosmic ray density is denoted by n_{CR}, the gas density by n_H, the gamma ray emissivity by q_γ and the magnetic field strength by B.

REFERENCE	MODEL	
Strong et al. (1973)	$n_{CR} \propto B^2$ Magnetic field model of Thielheim and Langhoff (1968)	$q_\gamma \propto n_{CR}\, n_{HI}$
Bignami and Fichtel (1974)	$n_{CR} \propto n_{HI}$ Spiral Gas Distribution	$q_\gamma \propto n_{CR}\, n_{HI}$
Dodds et al. (1975a)	(a) $n_{CR} \propto$ Supernova density (b) $n_{CR} \propto$ total mass density.	$q_\gamma \propto n_{CR}\, n_{HI}$
Schlickeiser and Thielheim (1974a, b)	$q_\gamma \propto B^\beta$ for $\beta = 3\text{-}4$. Magnetic field model of Thielheim and Langhoff (1968)	
Paul et al. (1974, 1976)	$n_{CR} \propto n_H \propto B^2$ n_{CR} determined from radio synchrotron emissivity ($\propto n_{CR} B^2$) using spiral Galaxy model.	$q_\gamma \propto n_{CR}\, n_H$
Bignami et al. (1975)	$n_{CR} \propto n_{(HI + H_2)}$ where $n_{H_2} \propto n_{HI}$ Spiral gas distribution.	$q_\gamma \propto n_{CR}\, n_{(HI + H_2)}$
Stecker et al. (1975)	$n_{CR} \propto n_{(HI + H_2)}^{0.3}$ H_2 from Scoville and Solomon (1975). Radial gas distribution.	$q_\gamma \propto n_{CR}\, n_{(HI + H_2)}$
Fuchs et al. (1976)	n_{CR} constant in inner Galaxy but decreases towards anti-centre. No power law of n_{CR} on n_H gives good fit. H_2 from Scoville and Solomon (1975), using hydrostatic equilibrium arguments.	
Stecker (1975)	$n_{CR} \propto$ supernova density	$q_\gamma \propto n_{CR}\, n_{(HI + H_2)}$
Kniffen et al. (1977)	$n_{CR} \propto n_{(HI + H_2)}$ H_2 from Gordon and Burton (1976) Spiral Gas Distribution.	$q_\gamma \propto n_{CR}\, n_{(HI + H_2)}$

radial symmetry, whereas Kniffen et al. use a spiral form. Information on gas position is smoothed in such analyses.

In summary, from the work in this Chapter, the following two conclusions are arrived at:

(1) The gamma ray data and spiral structure are not well correlated. This is seen from inspection of the gamma ray observations at longitudes which are tangential to spiral arms. It is more evident from the gamma ray unfolding using spiral symmetry.

(2) At present no distinction can be made between uniform and varying cosmic ray density in the inner Galaxy ($R < R_o$) from the general longitude distribution. This is apparent from figures 3.6 and 3.7 and is supported by the conclusions of authors modelling the inner Galaxy.

CHAPTER FOUR

THE GALACTIC CENTRE: A THICK TARGET REGION FOR COSMIC RAYS

4.1 THE GAMMA RAY FLUX FROM THE GALACTIC CENTRE

4.1.1. The Observations

In the previous Chapter it was found that, on the basis of present knowledge of the large scale distribution of gamma rays and gas in the inner Galaxy, no firm conclusions can be reached regarding the possible intensity variation of the cosmic ray progenitors. In this Chapter we direct attention to a region which has attracted much study in X-ray, infra-red, millimeter and radio astronomy; the Galactic centre.

The SAS-2 experiment found an enhancement of gamma rays (above 100 MeV) within about 10° of the Galactic centre. The enhancement is evident from inspection of figure 3.3 where the longitude distribution is presented in the smallest bin size compatible with the angular resolution of the experiment. Detailed study of the Galactic centre by the COS-B experiment is still awaited although the provisional results published (Bennett et al., 1976) do not corroborate the existence of the enhancement.

The data of figure 3.3 within 30° of the Galactic centre have been replotted in figure 4.1. The FWHM of the central peak is about 6° although this includes some experimental broadening. The presence of broadening in the data of figure 3.3 is confirmed by the width of the peaks representing the Crab and Vela point sources.

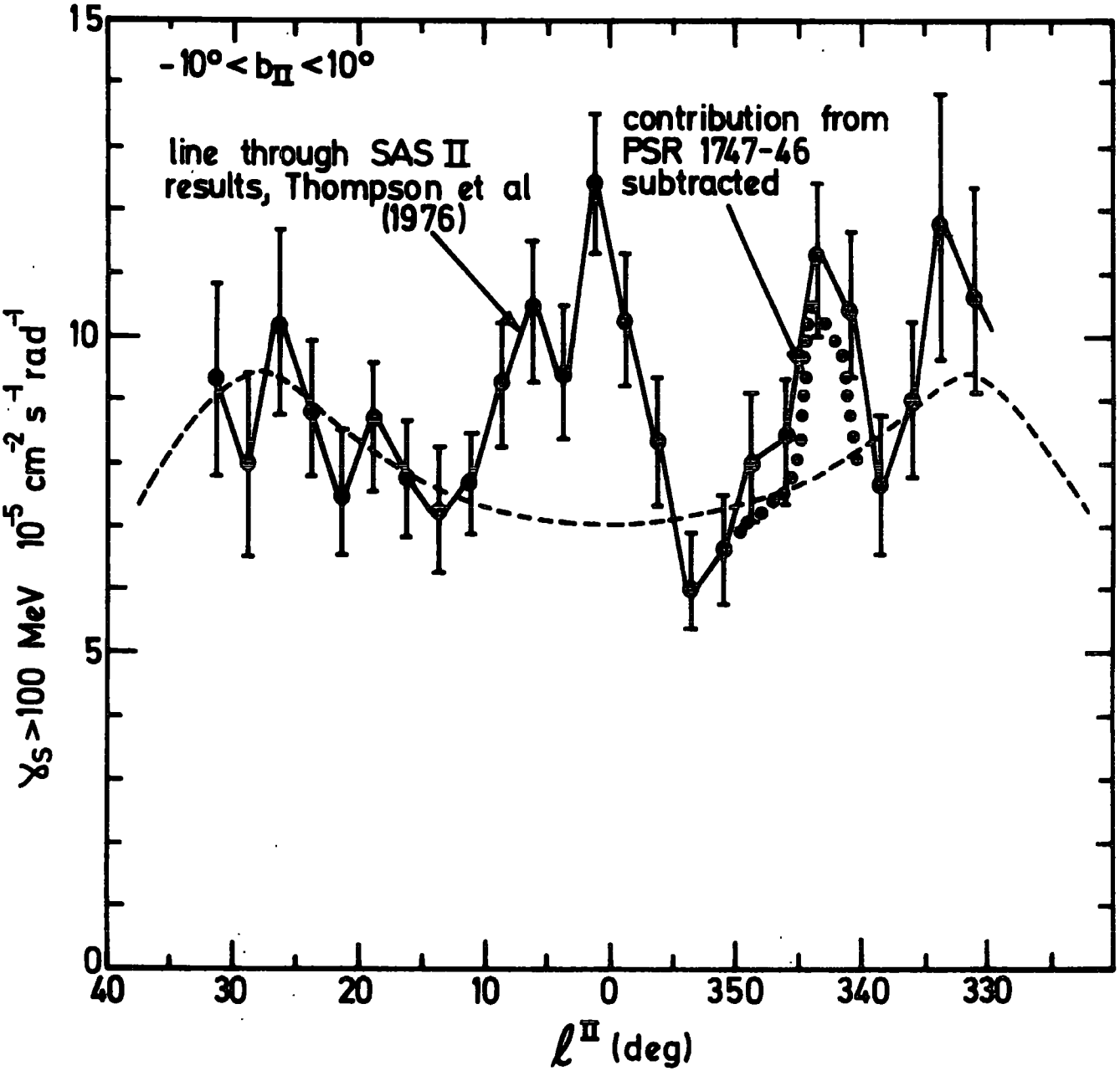

Figure 4.1. The flux of gamma rays above 100 MeV for longitudes close to the Galactic centre from Thompson et al.(1976). The dashed line is the estimate of the contribution for R >2.59 kpc.

4.1.2. The contribution from $R > 2.6$ kpc

The flux contributed by the region outside a certain radius from the Galactic centre is to be calculated and subtracted from the observations. One possible method would be to use the values found for W in Chapter 3 for $\Delta\ell = 2\frac{1}{2}^{\circ}$. The flux contribution to bin i for radii greater than $R_o \sin(m\,\Delta\ell)$, where m is some integer less than 33, is expressed:

$$J_i = \sum_{k=mm}^{33} Q_{ik} W_k \qquad \begin{matrix} mm = m + 1 \text{ if } i \leq m + 1 \\ mm = i \text{ if } i > m + 1 \end{matrix} \qquad (4.1)$$

The fit to the observations using this method is exact for bins with $i \geq m + 1$. However, the observed distribution of gamma rays is not symmetrical about the Galactic centre. The analysis in Chapter 3 is only for the Northern Galactic Hemisphere and a repetition for the Southern Hemisphere is not possible from the present observations due to the break at about 300° longitude. The non-symmetry of the data means that a treatment of the two hemispheres independently would cause a discontinuity in the ring emissivities at $\ell = 0^{\circ}$. Furthermore, it has been found that the present unfolding method is not applicable to the data in $2\frac{1}{2}^{\circ}$ bins of longitude. The small size of the bins causes structure to appear in the longitude distribution which is probably false considering the large errors and likelihood of overlap between neighbouring bins (the binwidth and experimental resolution are roughly equal). However, despite this, the central enhancement over the values close to $\ell = \pm 10^{\circ}$ is present in both figures 3.2 and 3.3 and appears a true feature.

To avoid bias to one particular Galactic Hemisphere in calculating the average for the foreground flux towards the Galactic centre, we adopt a model for the emissivity distribution. From those discussed in section 3.5 we chose that of Kniffen et al. (1977) in which the gas density follows that of Gordon and Burton (1976) and the cosmic ray and gas densities are proportional i.e. the gamma ray emissivity is proportional to the gas density squared.

For a bin size of $\Delta\ell = 5^{\circ}$, 4.1 can be written:

$$J_i = \sum_{k=mm}^{17} Q_{ik} W_k \qquad \begin{array}{l} mm = m + 1 \text{ if } i \leq m + 1 \\ mm = i \text{ if } i > m + 1 \end{array} \qquad (4.2)$$

As found in Chapter 3,

$$W_k = 9.4\ 10^{-26}\ w_k \qquad (4.3)$$

where w is the volume emissivity distribution normalised to unity in ring 17, i.e. $w_{17} = 1$. The elements of the matrix Q were calculated in the previous Chapter and are shown here in figures 4.2 and 4.3. These correspond to flat slabs of total thickness 230 pc and 117 pc to represent HI and H_2 respectively. As expected, comparing the two figures it is seen that the relative importance of rings of large i is greater in the case of the smaller slab thickness. Since in the present model the cosmic ray intensity is proportional to the gas density, the contributions from the HI and H_2 discs are not independent.

One disc size only can be used and that of the HI is taken. This is chosen because the gas in ring 17, which determines the normalisation of the distribution, is mainly atomic. Furthermore, the choice is

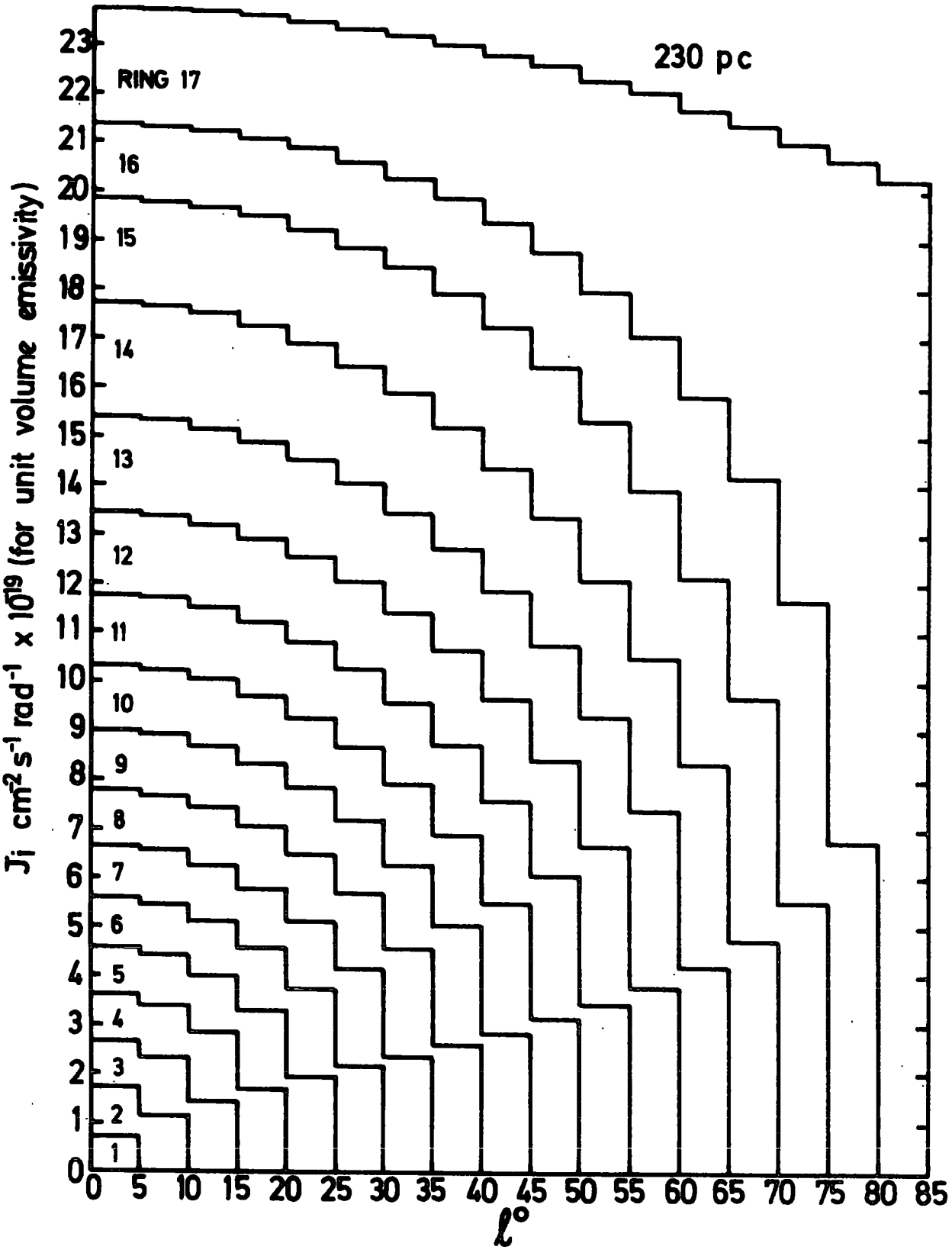

Figure 4.2 The flux contributions to each longitude bin, where each ring has unit emissivity, i.e., the matrix elements Q_{ik}. Results are for a disc thickness of 230 pc.

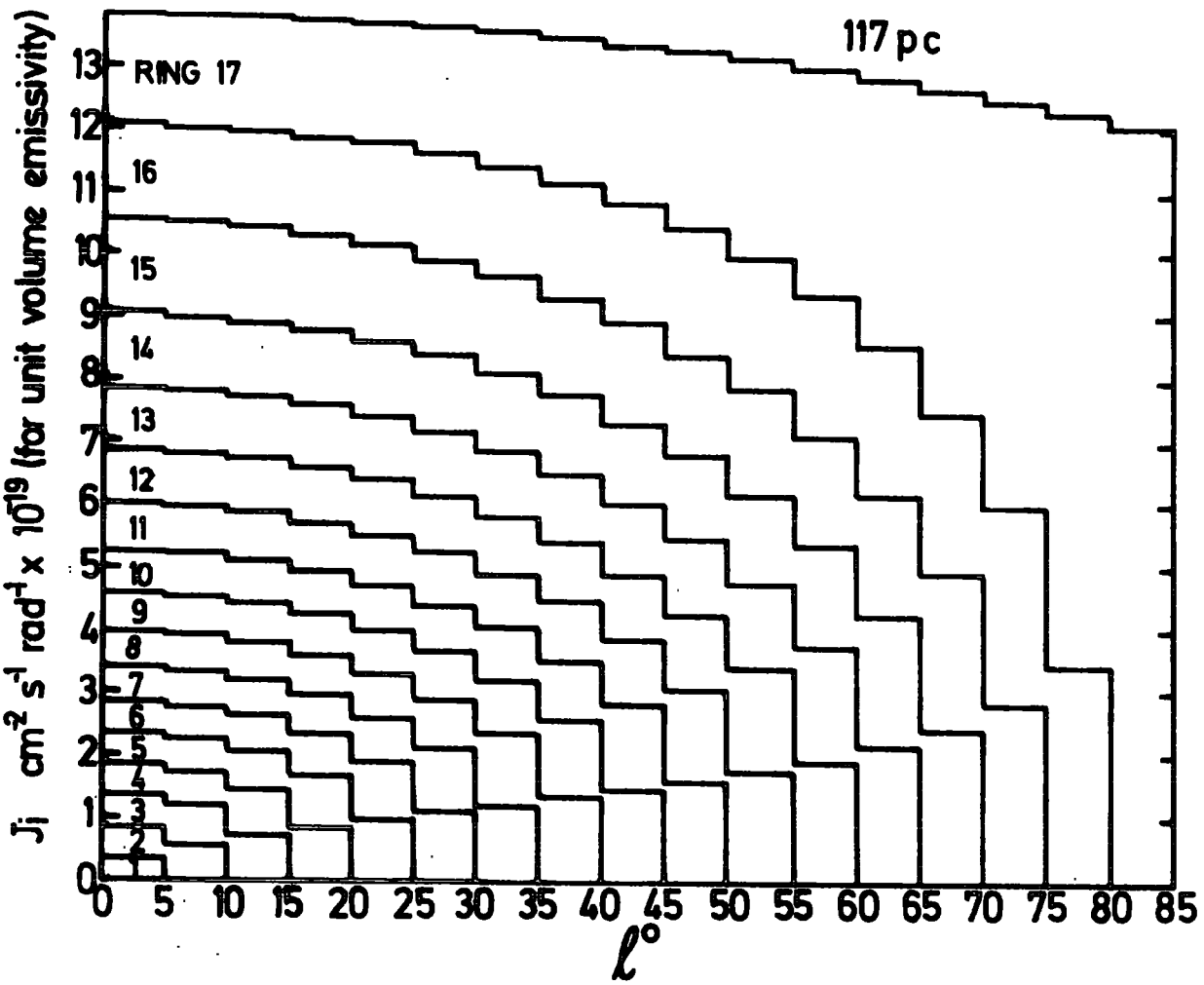

Figure 4.3 The flux contributions to each longitude bin, where each ring has unit emissivity, i.e., the matrix elements q_{ik}. Results are for a disc thickness of 117 pc.

Table 4.1

The variation of gamma ray emissivity, w, with radius, normalised to unity at the Sun, and based on proportionality to the square of the sum of surface densities of H_2 and HI. The gas densities are based on the values given by Gordon and Burton (1976).

Ring Number k	Radius Interval kpc	w_k
4	2.59 - 3.42	1.50
5	3.42 - 4.23	2.75
6	4.23 - 5	8.65
7	5 - 5.74	10.81
8	5.74 - 6.43	8.50
9	6.43 - 7.07	4.86
10	7.07 - 7.66	5.67
11	7.66 - 8.19	4.10
12	8.19 - 8.66	2.14
13	8.66 - 9.06	1.07
14	9.06 - 9.40	1.40
15	9.40 - 9.66	1.45
16	9.66 - 9.85	1.48
17	9.85 - 15	1

Table 4.2

The flux values, J_i, calculated from equation 4.2, where the relative emissivity values w_k are as in table 4.1 and values for Q_{ki} (the flux contribution of the kth ring to the ith bin) are shown in figure 4.2.

Bin Number i	Longitude Interval (degrees)	$\sum_{k=m}^{17} Q_{ik} w_k$ m = 4 if i < 4 m = i if i > 4	J_i $cm^{-2}\ s^{-1}\ rad^{-1}$
1	0-5, 355-360	$7.02\ 10^{20}$	$7.09\ 10^{-5}$
2	5-10, 350-355	$7.13\ 10^{20}$	$7.20\ 10^{-5}$
3	10-15, 345-350	$7.41\ 10^{20}$	$7.46\ 10^{-5}$
4	15-20, 340-345	$7.94\ 10^{20}$	$7.96\ 10^{-5}$
5	20-25, 335-340	$8.64\ 10^{20}$	$8.62\ 10^{-5}$
6	25-30, 330-335	$9.39\ 10^{20}$	$9.32\ 10^{-5}$
7	30-35, 325-330	$8.79\ 10^{20}$	$8.76\ 10^{-5}$
8	35-40, 320-325	$7.20\ 10^{20}$	$7.27\ 10^{-5}$

justified because the highest gamma ray emissivity occurs at Galactocentric radii small enough for the angular range of the experimental results to encompass all emission for either disc thickness.

Equation 4.2 is solved for m = 3, i.e. the flux includes contributions from all regions at Galactocentric radii greater than 2.59 kpc. The values for w_i are shown in table 4.1. In their derivation, proportionality to the square of the sum of HI plus H_2 surface density, as given by Gordon and Burton (1976), is assumed. The surface density rather than volume density is used because of the different scale heights of the two gas components. The ring boundaries here are different from those used by Gordon and Burton and the conversion is unfortunately approximate since the gas, particularly the molecular hydrogen, is patchy. Table 4.2 shows the corresponding values for J_i, where a contribution of 0.5×10^{-5} cm^{-2} s^{-1} rad^{-1} has been added to the values derived from 4.2 to account for the diffuse background flux. The results are shown in figure 4.1.

The flux originating within 2.6 kpc of the Galactic centre is found to be about 6.7×10^{-6} cm^{-2} s^{-1}.

4.2 GAS NEAR THE GALACTIC CENTRE: THE 300 pc RING

Within a few hundred parsecs of the Galactic centre the gas is predominantly molecular and forms dense clouds.

The molecular gas was first observed in absorption lines of OH (Robinson and McGee, 1970; McGee, 1970) and H_2CO (Scoville and Solomon, 1973 and references therein). The study of these data, together with the NH_3 emission measurements of Knowles and Cheung (1971), led Kaifu et al. (1972) to propose a model in which the gas forms an expanding ring. The

radius of the ring is 270 pc and it has rotation and expansion velocities of 50 km s^{-1} and 130 km s^{-1} respectively. A contracting ring inside at 140 pc, which could be the counter shock produced by the outgoing motion, was proposed to explain the positive velocity OH and H_2CO absorption. Scoville (1972), suggested a similar expanding ring model for the gas in which the radius is 220 pc and the rotation and expansion velocities are 50 km s^{-1} and 145 km s^{-1} respectively. The ring shows an asymmetry; it extends to 305 pc at positive longitudes and 218 pc at negative longitudes. Scoville requires all the HII regions, except the non-thermal core of Sgr A, to lie on the far side of the expanding ring. This is not consistent with their recombination line velocities.

The OH and H_2CO absorption measurements exclude gas lying beyond the continuum sources. These sources mainly lie close to the Galactic centre and their exact positions influence the measurements. Observations of emission lines provide more complete information.

The first Galactic centre survey of CO emission was that of Solomon et al. (1972). Only positive velocities were observed and sampling was only every 6' of longitude. More extensive measurements were recorded by Scoville et al. (1974). The mass within 600 pc of the centre was estimated as 10^7-10^8 $M_\odot$, which is very much greater than that in atomic hydrogen (see references given in section 3.3.3). The value is uncertain since no observations of ^{13}CO in this direction were made to enable the CO optical depth to be found. Scoville et al. (1974) suggest that in place of a rotating expanding ring, the gas forms a rotating expanding two-armed spiral. Further observations in CO of the Galactic nucleus are presented by Sanders and Wrixon (1974) and Liszt et al. (1975). The

most complete survey of the region in the NH_3 emission line is that of Kaifu et al. (1975).

A CO survey within 1^o of the centre has been recently reported by Liszt et al. (1977). The spatial resolution is 1' to 2'. These authors found that the features are well correlated with HI and therefore it is not necessary to invoke a model of expansion for the gas since the HI can be explained by pure rotation. More doubt is cast on the expansion models by Bania (1977) who finds a substantial amount of CO interior to 300 pc which would not be expected if the explosion were relatively recent and the "snow plough" effect operative. However, in conclusion, expansion is not excluded although the gas is certainly more patchy than suggested by the models of Kaifu et al. (1972) and Scoville (1972).

Bania (1977) also finds good correlation with the inner HI features of Cohen and Davies (1976). He estimates the H_2 mass to be higher than is given by Scoville et al. (1974), with an upper limit of 7.10^8 $M_\odot$ and a preferred value of $3.5\ 10^8$ $M_\odot$. However, he adopts the method used by Gordon and Burton (1976) for converting the CO results to H_2, about which there is controversy (see discussion in section 3.3.3). Scoville et al. (1976) maintain that the kinetic temperature of the clouds in the Galactic centre region is higher than elsewhere due to heating by infra-red sources, and therefore the actual mass is closer to the value they originally put forward in Scoville et al. (1974).

The longitude distribution of Bania (1977) for $-10^o < \ell < 10^o$ clearly shows that all the molecular gas within 2 kpc of the centre is concentrated inside a radius of about 350 pc.

The atomic hydrogen observations are discussed in section 3.3.2. The sum contribution to the mass from all the features close to the

Galactic centre is less than from molecular hydrogen. However, from the results given by Cohen and Davies (1976) the mass of atomic hydrogen inside a 2.5 kpc radius is as large as 2 10^7 $M_\odot$. The mass is distributed amongst features throughout the region, unlike the molecular hydrogen which shows high concentration within 300 pc.

In the following calculations of gamma ray emission from the Galactic centre it is assumed that the gas within 2.5 kpc is all concentrated in the smaller radius of 300 pc. A total mass of 5 10^7 $M_\odot$ is adopted, although effects due to the uncertainty of this value are considered. Adopting a z thickness for the gas of 70 pc (Kaifu et al., 1972), gives a volume of about 2 10^7 pc^3 interior to a 300 pc radius and a volume of about 10^7 pc^3 for rings with similar dimensions as those of Kaifu et al. (1972) and Scoville (1972). This implies a mean gas density of 220 atoms cm^{-3} or 110 atoms cm^{-3}, with or without ring confinement respectively. However it should be remembered that individual clouds have densities in the range 10^3-10^5 atoms cm^{-3} and therefore the gas distribution is extremely clumpy.

4.3 ENERGY LOSSES OF PRIMARY COSMIC RAYS IN HYDROGEN

4.3.1. Introduction

The gamma ray production functions for the local cosmic ray proton and electron intensities are shown in figure 2.3. Two factors will influence the spatial dependence of intensity of the primary cosmic rays. Firstly the origin of the particles and secondly the energy losses they undergo.

If the primary cosmic rays are of Galactic origin the spatial intensity is determined by the source distribution. This is definitely the

case for electrons due to the fact that a high extragalactic electron flux would quickly lose its energy by interaction with the 2.7^{o} K blackbody remnant radiation. The question of whether or not the protons of a few GeV in energy are of Galactic origin was considered in Chapter 3. Definite conclusions cannot be drawn as yet but the best evidence for Galactic origin comes from the study of the flux in the anticentre by Dodds et al. (1975b).

In general, the lifetime of cosmic rays in the Galactic disc is found to be a factor of ten or more shorter than their energy loss time. However, it is likely that there are regions in the disc where particles can be trapped for long enough for significant, or even total, energy loss to occur.

4.3.2. Proton energy losses

Protons undergo energy losses in hydrogen in the following ways:

Ionization

$$-\left(\frac{dE}{dt}\right)_i = 7.62\ 10^{-9}\ n_H \frac{\gamma}{(\gamma^2-1)^{\frac{1}{2}}} \left[22.2 + 4\ ln\left(\frac{E_T}{m_e c^2}\right) + 2\ ln\left(\frac{\gamma^2-1}{\gamma^2}\right) - \frac{2(\gamma^2-1)}{\gamma^2} \right] \text{eV s}^{-1} \qquad (4.4)$$

(p. 121, Ginzburg and Syrovatskii, 1964)

Strong Interaction

$$-\left(\frac{dE}{dt}\right)_s = 5\ 10^{-14}\ \frac{E_K\ n_H}{\lambda_a}\ \frac{(\gamma^2-1)^{\frac{1}{2}}}{\gamma}\ \text{eV s}^{-1} \qquad (4.5)$$

In the equations, γ is the Lorentz factor of the proton, n_H is the hydrogen density (H atom cm^{-3}), E_T and E_K are the proton total and kinetic

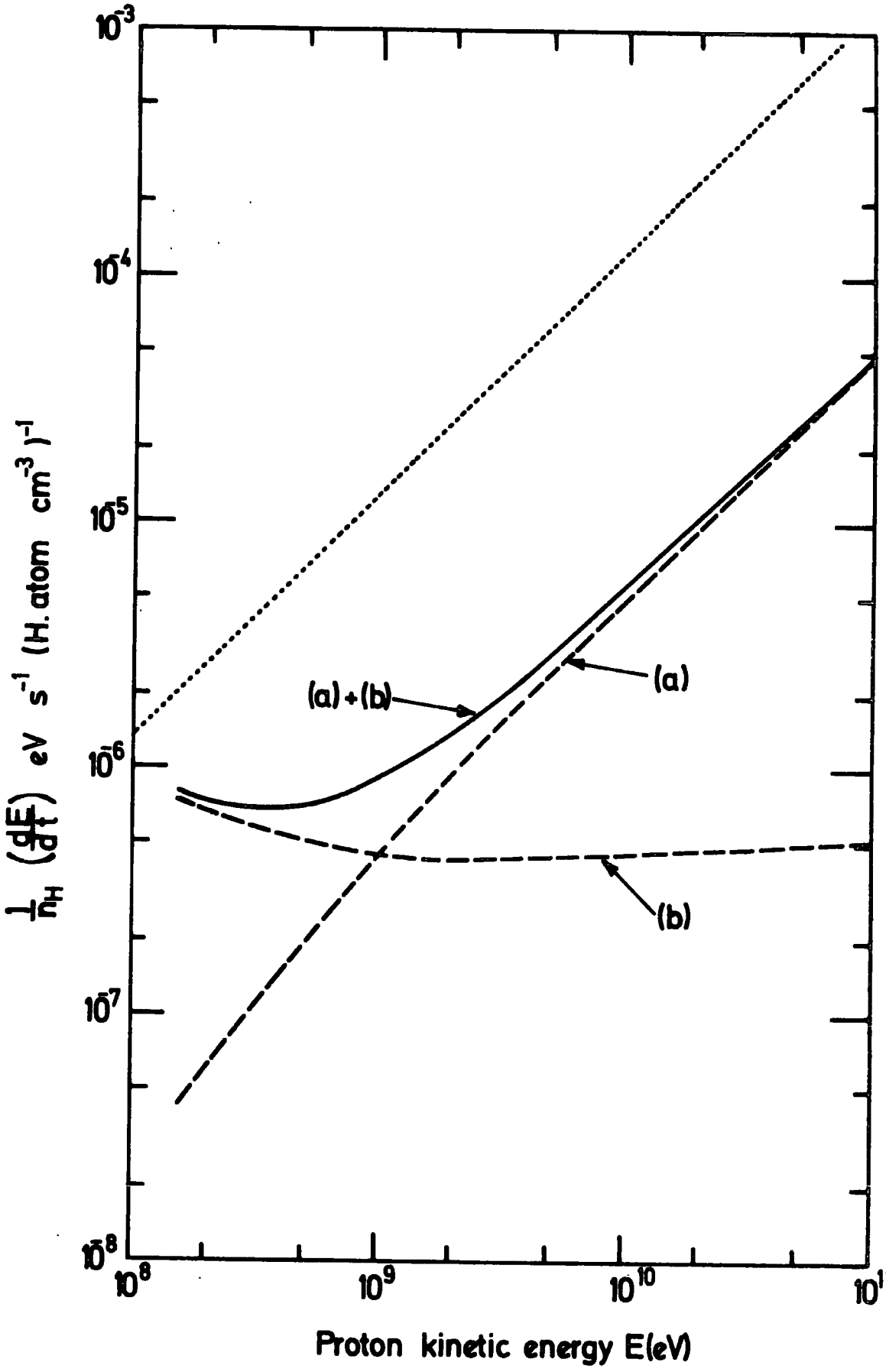

Figure 4.4 Proton energy loss rate per unit hydrogen density versus kinetic energy for, (a) strong interactions with λ_s=100 g cm^{-2}, (b) ionisation. The dotted line is for n_H=1 H atom cm^{-3} and a mean lifetime, E/(dE/dt), of 2.5 10^6 yr.

energies respectively (eV) and λ_a is the average grammage for attenuation by strong interaction. The ionization losses are continuous whereas in a strong interaction a proton loses about $^1/_3$ of its energy (see further discussion in section 4.5.1). The energy losses are shown in figure 4.4 for $\lambda_a = 100$ g cm^{-2}. It is seen that above a few GeV strong interaction losses dominate. A lower limit to the escape time of protons is 2.5 10^6 yr (see following section) and this is represented on figure 4.4 by a dotted line. From inspection of the figure it is seen that total energy loss occurs before escape if $n_H \gtrsim 20$ H atom cm^{-3}. The threshold is lower if the local escape time is greater.

4.3.3. Electron energy losses

Electrons lose energy by

Ionization

$$-\left(\frac{dE}{dt}\right)_i = 7.62\ 10^{-9}\ n_H\ (3\ \ln\left(\frac{E}{m_e c^2}\right) + 20.2) \quad \text{eV s}^{-1} \qquad (4.6)$$

(p. 73, Ginzburg, 1969).

Bremsstrahlung

$$-\left(\frac{dE}{dt}\right)_b = 5\ 10^{-14}\ \frac{E_K}{\lambda_b}\ n_H\ \frac{(\gamma^2-1)^{\frac{1}{2}}}{\gamma} \quad \text{eV s}^{-1} \qquad (4.7)$$

Inverse Compton scattering

$$-\left(\frac{dE}{dt}\right)_{IC} = 2.65\ 10^{-14}\ \gamma^2\ w_{ph} \quad \text{eV s}^{-1} \qquad (4.8)$$

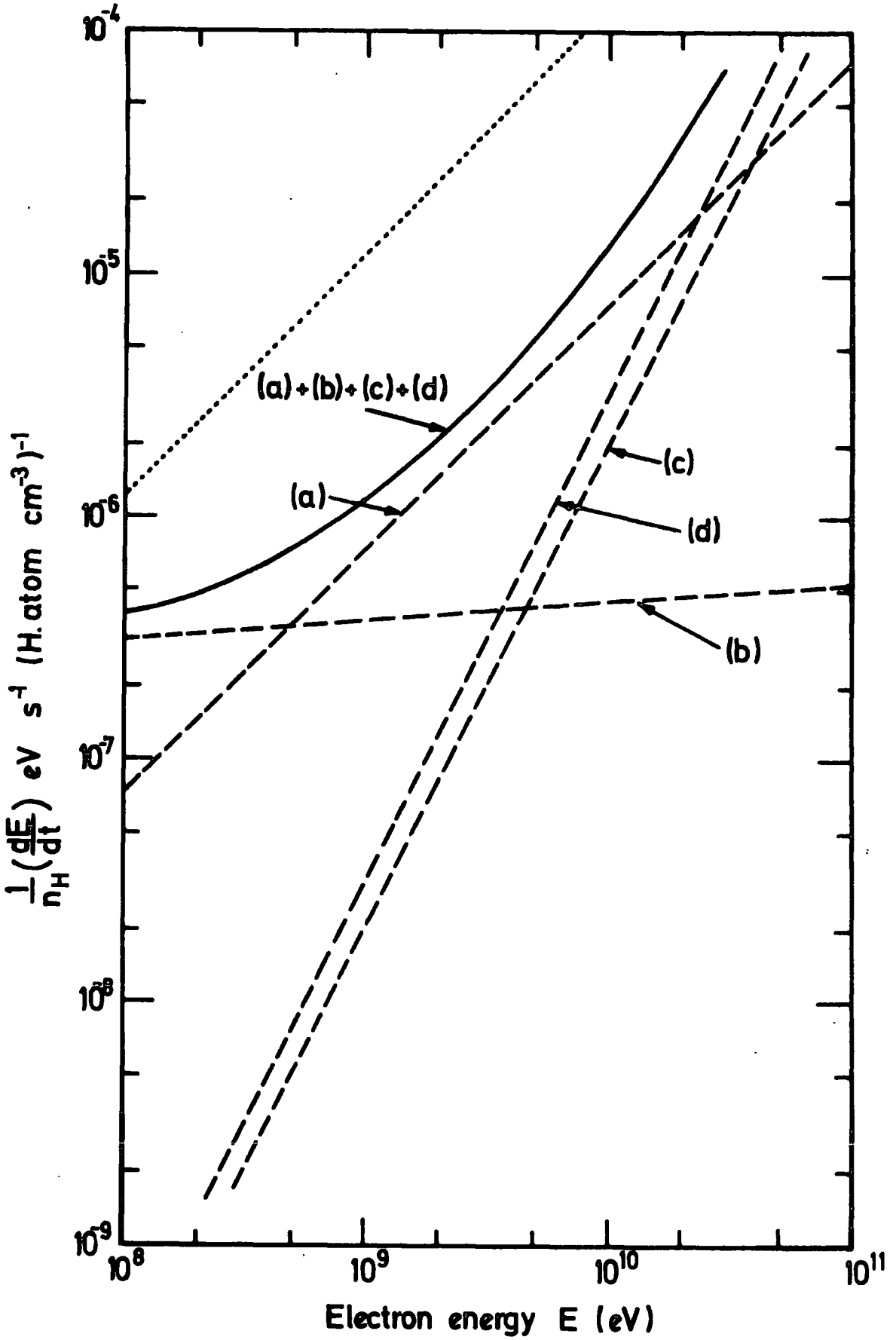

Figure 4.5 Electron energy loss rate per unit hydrogen density versus energy, using parameters given in the text, for, (a) bremsstrahlung, (b) ionisation, (c) inverse Compton scattering, (d) synchrotron emission. The dotted line is for n_H=1 H atom cm^{-3} and a mean lifetime, E/(dE/dt), of 2.5 10^6 yr.

Synchrotron emission

$$-\left(\frac{dE}{dt}\right)_{syn} = 9.89\ 10^{-4}\ \gamma^2\ H^2 \qquad \text{eV s}^{-1} \tag{4.9}$$

Inverse Compton scattering in the Galaxy will be predominantly on starlight and infra-red photons. In the Galactic centre region starlight dominates over infra-red (see discussion in section 5.1.2 and figure 1 of Bignami and Piccinotti, 1977). The mean photon energy is about 1.4 eV and the energy density is expressed as w_{ph} (eV cm^{-3}). H is the magnetic field (gauss) and λ_b is the radiation length for bremsstrahlung, taken in these calculations to be 66 g cm^{-2}. The energy lost by inverse Compton scattering and synchrotron emission relative to that via the other two mechanisms depends on the parameters w_{ph}, H and n_H. For illustration, values appropriate to the Galactic centre are chosen and the results shown in figure 4.5. The value for w_{ph} is 45 eV cm^{-3} (see section 5.1.2.). Assuming that the gas is confined to a ring (see section 4.2) the mean density, n_H, is about 220 H atom cm^{-3}. If $H^2 \propto n_H$ (e.g. Paul et al., 1976) we expect H = 44 μG. As for the proton case, the dotted line of figure 4.5 represents an escape time of 2.5 10^6 yr. The requirement is now that $n_H \gtrsim 10$ H atom cm^{-3} for total energy loss before escape, with a lower threshold if the escape time is greater than 2.5 10^6 yr.

4.3.4. Energy losses at the Galactic centre

The Galactic centre region possesses an average hydrogen density about a factor of ten higher than that needed for total energy loss before escape. As discussed in section 2.3, it is likely that towards the Galactic centre there is an increase in the percentage of heavier target nuclei. However, this is mainly in the form of helium and the energy loss

equations given above are applicable. Assuming Galactic origin for the primaries it is appropriate to relate the injection rate, rather than the ambient density, to the local value.

4.4 LIFETIMES AND SPECTRA OF LOCAL PRIMARY COSMIC RAY PROTONS AND ELECTRONS

The local interstellar electron intensity is discussed in section 2.3, where methods for correcting the observed spectrum for solar modulation are mentioned. The proton spectrum too suffers from solar modulation at the energies of interest for gamma ray production, i.e. below about 10 GeV.

Equations governing solar wind behaviour are reviewed by Fisk (1974). However the best choice of parameters for these models is still uncertain. Goldstein et al. (1970) calculate the unmodulated proton spectrum by requiring consistency with the electron modulation calculated using non-thermal radio measurements. They conclude that the interstellar proton spectrum is approximately a power law in total energy. This agrees with the results of Comstock et al. (1972) who searched for agreement with the measured ratios of ^{1}H, ^{2}H, ^{3}He and ^{4}He on the assumption that ^{1}H and ^{4}He are produced in the sources and ^{2}H and ^{3}He are produced by nuclear interactions of the cosmic rays during propagation. Their self consistent model is a power law in total energy and takes the form:

$$j(E) = 5.9\ 10^{8}\ (E_k + E_o)^{-2.6}\ m^{-2}\ s^{-1}\ sr^{-1}\ MeV^{-1} \qquad (4.10)$$

where E_o is the proton rest mass energy. This form is adopted in the calculations presented in this thesis.

The lifetime, τ, of the particles is related to their 'grammage', ($g\ cm^{-2}$), and the mean gas density via:

$$\tau = \lambda\ /(n_{H\odot}\ 1.58\ 10^{-6})\ yr \qquad (4.11)$$

The lifetime is determined by observing the quantity of ^{10}Be present in the cosmic rays. This is a radioactive substance with a half-life of about $1.5\ 10^6$ yr. The values to date show a spread of over a factor of ten. Garcia-Munoz et al. (1975) from their experiments on board the IMP-7 and IMP-8 satellites find consistency with virtually no ^{10}Be remaining and set a lifetime for the cosmic rays of greater than 10^7 yr, with a most probable value of $2\ 10^7$ yr. O'Dell et al. (1975) compare the observed elemental abundance ratio Be/B with the corresponding ratios calculated for the cases of ^{10}Be survival and decay respectively. They find a lifetime of 10^6-10^7 yr. Hagen et al. (1976) from a balloon flight find a survival of $(55 \pm 20)\%$ of the ^{10}Be which implies a lifetime of $5\ (+6, -3)\ 10^6$ yr.

The mean 'grammage' is determined from light element abundance ratios, and values for cosmic rays at a few GeV range between about 4 g cm^{-2} and 7 g cm^{-2} (see Orth and Buffington, 1976, and references therein). There is evidence of energy dependence of λ such that it falls by about a factor of two at 50 GeV/nucleon. There is disparity between these values for λ and those derived from comparison of the observed and calculated positron spectrum. The positron work yields slightly lower values for λ with evidence for a slight increase rather than decrease at the higher energies (Dilworth et al., 1974; Giler et al., 1977).

In conclusion, the lifetime in the disc of the local cosmic rays is probably between $2.5\ 10^6$ yr and $2\ 10^7$ yr. The lower limit is consistent with densities of the order of that locally, whereas the higher value requires that the cosmic rays spend time in a rarified medium.

4.5 CALCULATION OF THE GAMMA RAY EMISSIVITY FROM PROTON INTERACTIONS IN THICK TARGETS

4.5.1. Proton behaviour in strong interactions

From sections 4.2 and 4.3 it is seen that the mean density in the

Galactic centre region is considerably larger than that required for cosmic ray protons and electrons to lose all their energy before escape. For electrons, the energy loss rate depends on w_{ph}, H and n_H, and the values of these parameters determine the relative importance of the various mechanisms. Only two of the processes, bremsstrahlung and inverse Compton scattering, contribute to the gamma ray yield. For protons, the relative energy lost by the two mechanisms is constant, since both are only proportional to n_H. The gamma ray emissivity from neutral pion decay is therefore only dependent on the proton injection rate into the thick target region. In this section the emissivity is calculated. In the next Chapter the contribution from electron interactions is calculated, but results are for a specific region, i.e. the Galactic centre.

The scheme for the calculation of the emissivity from pion decay is shown in table 4.3. Assuming a local energy independent lifetime, τ, the local injection spectrum of protons, $J_\odot(E)$, is given by:

$$J_\odot(E) = j(E)/\tau \qquad (4.12)$$

where $j(E)$ takes the form given in equation 4.10. Elsewhere in the Galaxy the injection spectrum is assumed to have the same spectral shape but is scaled by a factor $f(\underline{r})$ such that:

$$J(E, \underline{r}) = f(\underline{r})\ j(E)/\tau \qquad (4.13)$$

Locally $f(\underline{r}) = 1$.

In the following, τ is expressed in terms of λ and $n_{H\odot}$ as given in equation 4.11.

In order to find the ambient proton spectrum, $n(E)$, we must first consider the behaviour of protons undergoing strong interaction losses.

Table 4.3

Scheme for calculation of the gamma ray emissivity from proton interactions in thick targets.

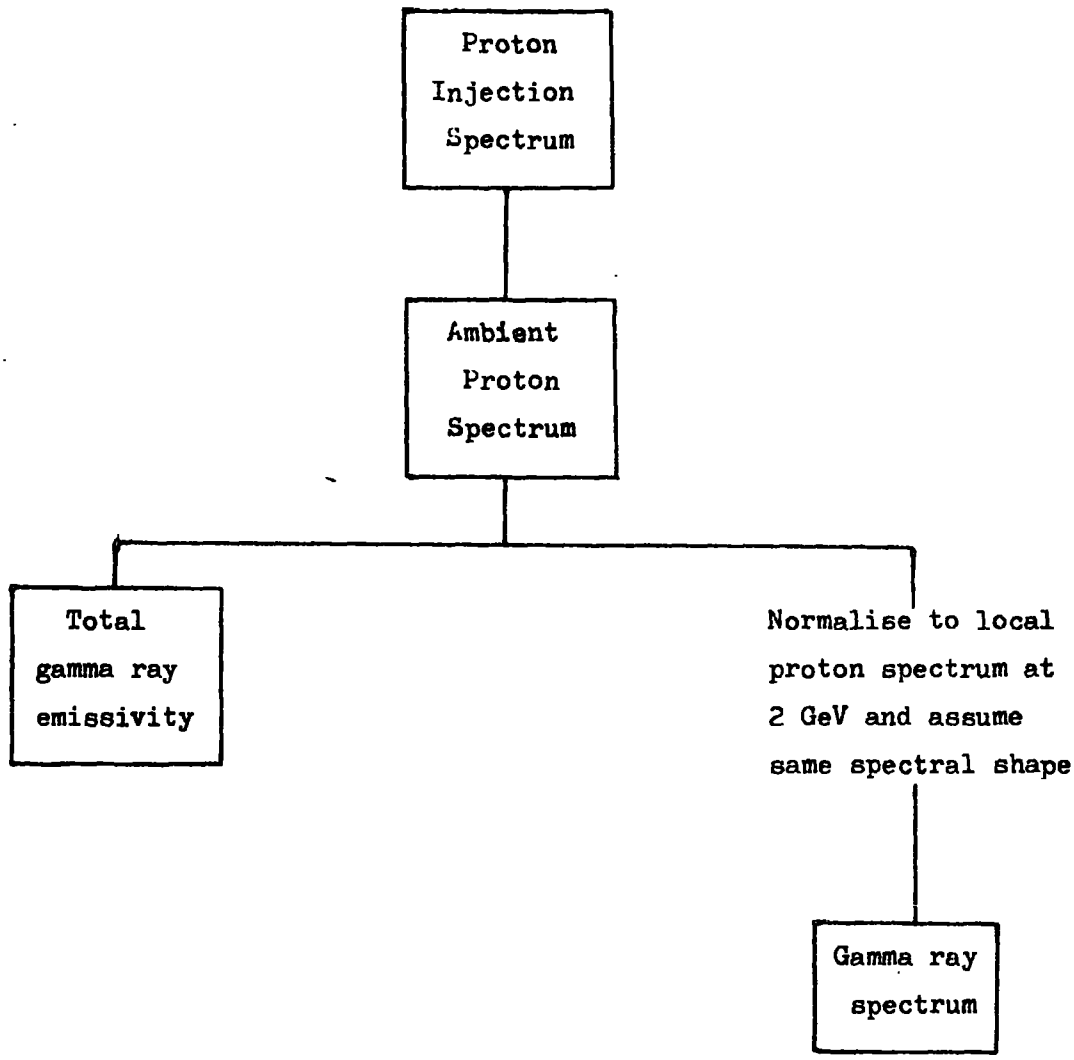

The energy range of interest is above 400 MeV. Below this energy the neutral pion cross section rapidly becomes zero. From the compilation of proton-proton cross sections of Bracci et al. (1973), it is seen that, between about 1 and 3 GeV, where the yield of pion decay gamma rays is a maximum, inelastic interactions dominate elastic. Therefore only the former are considered. In addition, elastic interactions cause redistribution rather than loss of energy, thus effecting only in a small way the total gamma ray emissivity. The interaction length for inelastic interactions is shown as a function of proton energy in figure 4.6.

Observations of the general inclusive proton spectrum from pp→pX are limited. The most common p-p experiments use a magnetic spectrometer detector consisting of bending magnets and scintillation counters. Often only the pions are measured after interaction. Bubble chambers give a measure of the energies of all the particles but statistics and precision are less good. Data have been studied from Blair et al. (1966), Allaby et al. (1970), Diddens and Schlupmann (1972) and Boggild et al. (1975). In all cases the incident proton energy is between 2 and 18 GeV. In general the data are incomplete in proton energy or angular range. For each set of measurements the mean value for the ratio of energy after to that before, K, has been found. Corrections are applied where data are incomplete. The most complete data, unfortunately at the rather high energy of 18.3 GeV, are tabulated in the compilation of Diddens and Schlupmann (1972). These give a value of K = 0.63. The values for the other energies are found to lie between 0.6 and 0.7.

At low energies, close to 1 GeV, the interactions are characterised by the creation of the Δ^+ 1.238 GeV resonance. A model using this is employed by Stecker (1970) in his calculation of the neutral pion decay

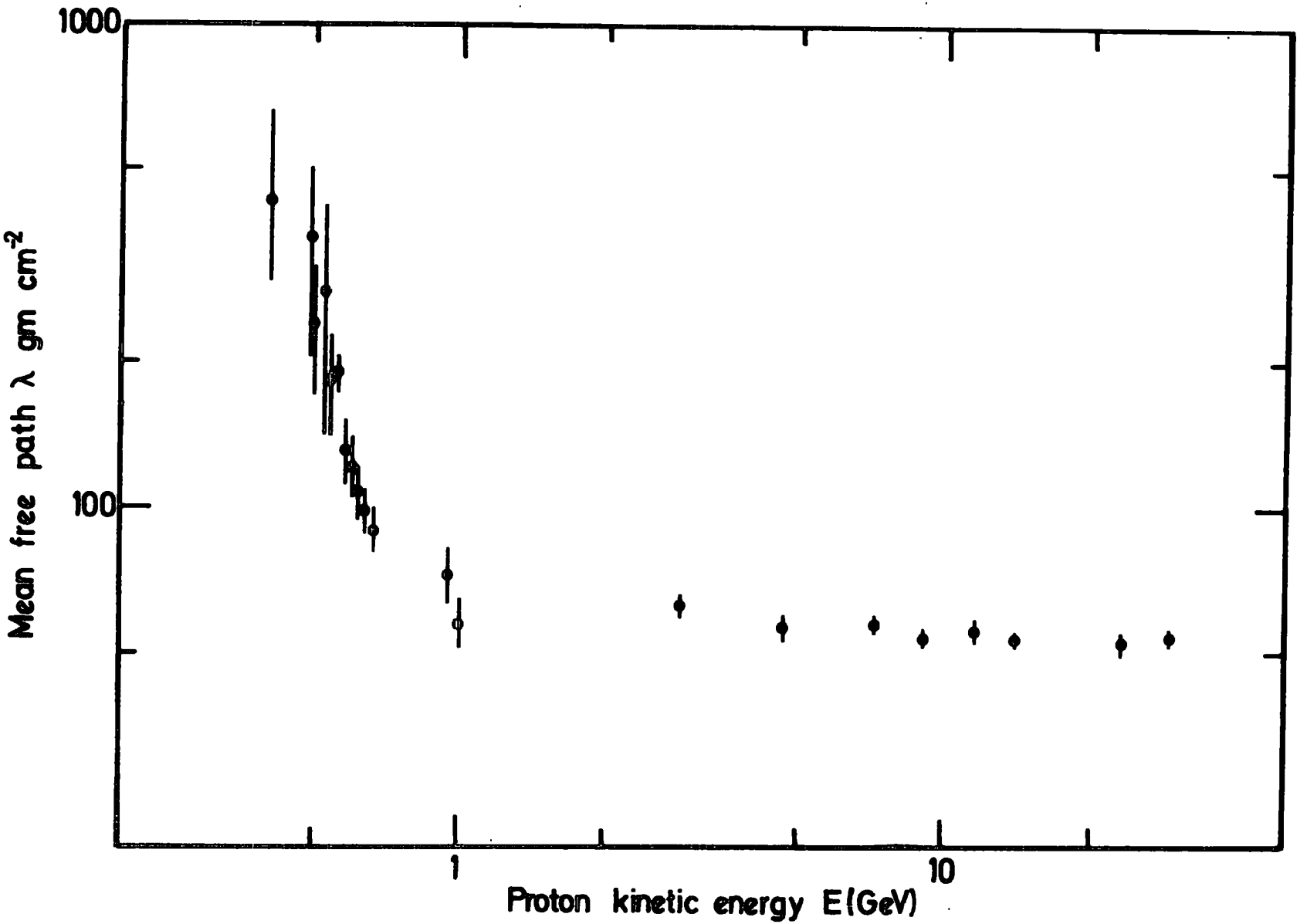

Figure 4.6 The interaction length for strong inelastic P-P interactions as a function of proton energy. The data are from the compilation of Bracci et al.(1973).

gamma ray spectrum. However the results of Blair et al. (1966) show that by 2 GeV, although the Δ^+ resonance peak can still be seen in the differential proton cross section data, the background is high. A simple calculation for K using the Δ^+ resonance has been performed where, following Stecker (1970), it is assumed that the isobar carries momentum directly forwards or backwards in the centre of mass frame after collision with equal probability. Let the proton and Δ^+ masses be written M_p and M_Δ respectively and the initial proton energy by E'. The Lorentz factor for transformation to the centre of mass frame is:

$$\gamma = E_*/(2M_p) \tag{4.14}$$

where E_* is the total centre of mass energy, given by:

$$E_* = (2 M_p^2 + 2E' M_p)^{\frac{1}{2}} \tag{4.15}$$

If the proton is carried forwards after interaction then its centre of mass energy, E_p, is given by:

$$E_p = (E_*^2 - M_\Delta^2 + M_p^2)/(2E_*) \tag{4.16}$$

The transformation to the laboratory frame gives the proton's energy after interaction as:

$$E = \gamma(E_p + (E_p^2 - M_p^2)^{\frac{1}{2}} (1 - 1/\gamma^2)^{\frac{1}{2}}) \tag{4.17}$$

If the Δ is carried forwards the calculation is similar but includes the decay of the Δ, isotropically in its centre of mass frame, to a proton and neutral pion. The average over decay angles for the proton after interaction can be found. The average for the cases of Δ^+ forward and proton forward is found to give a value of K = 0.6 at 1 GeV decreasing to

0.46 at 700 MeV. At 2 GeV the calculated value is 0.76 but here the model is probably not valid. Since there does not appear to be a particularly marked energy dependence of K, a value of $K = 0.65 \pm 0.05$ is adopted in the following.

4.5.2. Calculation of the ambient proton spectrum

Writing

$$r_i(E) = -\left(\frac{dE}{dt}\right)_i \quad , \quad r_s(E) = -\left(\frac{dE}{dt}\right)_s$$

we can express the relationship between the ambient proton spectrum, n(E), and the production spectrum, J(E), as:

$$J(E) = \frac{n(E)}{E} r_s(E) - \frac{n(E/K)}{E} r_s(E/K) + \frac{d}{dE}\left(-n(E)\, r_i(E)\right) \qquad (4.18)$$

where protons of energy E/K have energy E after interaction.

The solution to 4.18 is:

$$n(E) = \frac{1}{r_i(E)} \int_E^\infty dE' \left[J(E') + C(E')\right] \exp\left[-\int_E^{E'} \left[\, r_s(E'')/E\; r_i(E'') \,\right] dE''\right] \qquad (4.19)$$

where,

$$C(E') = \frac{n(E'/K)}{E'} r_s(E'/K) \qquad (4.20)$$

Since $E/K > E$, we can estimate a form for n(E/K) at high energies and use this to solve for n(E). The initial form adopted is:

$$n(E) = \int_E^\infty \frac{J(E')\, dE'}{r_s(E)} \qquad (4.21)$$

where $r_s(E)$ is given by equation 4.5. The value $\lambda_a = 80$ g cm^{-2} was chosen,

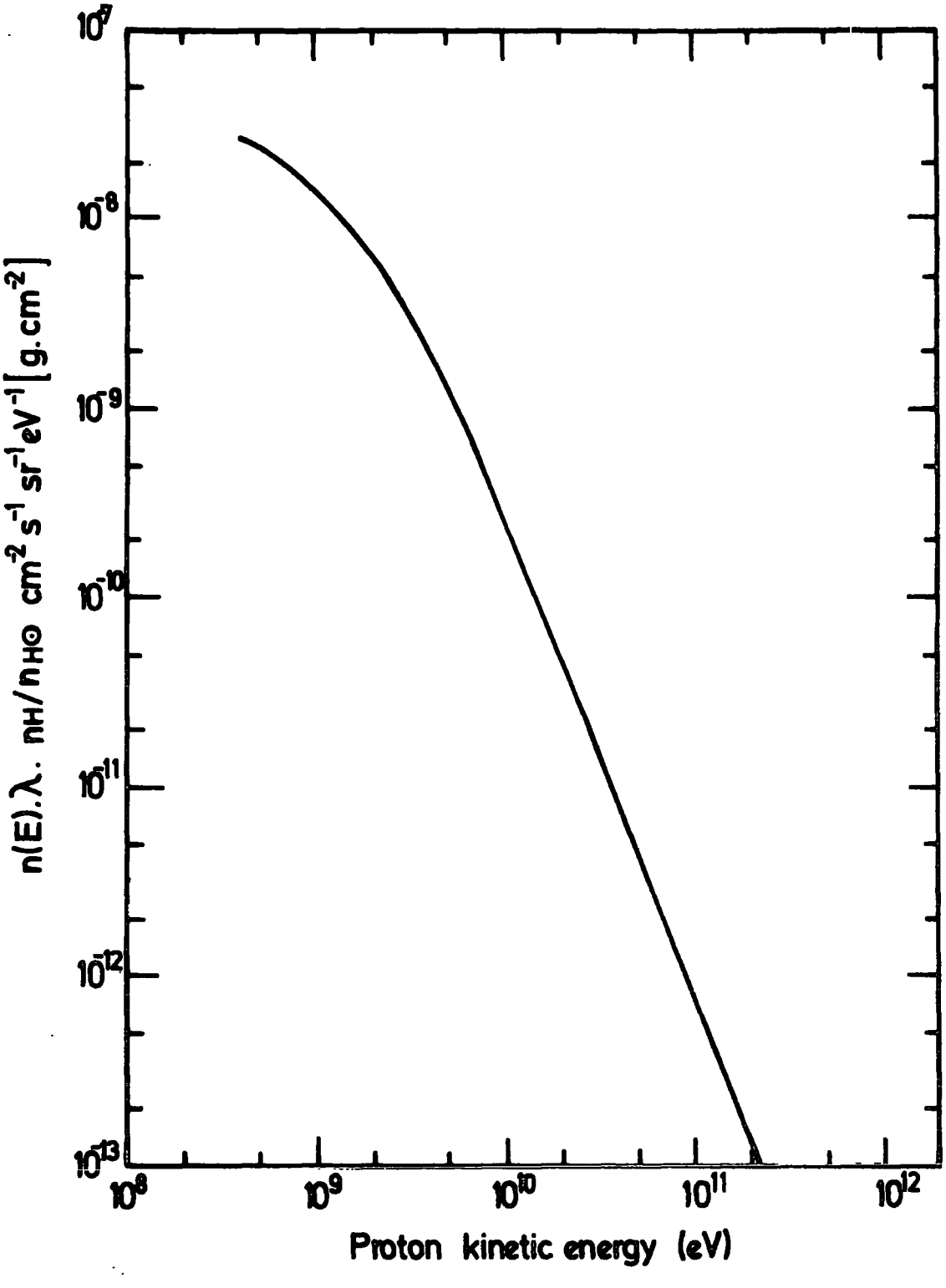

Figure 4.7 The ambient differential proton spectrum in a thick target, in terms of the density, n_H (atoms cm^{-3}), and two parameters governing the local proton injection rate; $n_{H\odot}$ (atoms cm^{-3}), and the local 'grammage', λ(g cm^{-2}). The result is for the local injection spectrum, i.e., f=1.

but by starting at a high energy (about 10^{15}eV) the solution was insensitive to this value. The form of r_s in equation 4.19 is also given by 4.5, but the attenuation length, λ_a, is replaced by the energy dependent interaction length as given in figure 4.6. These data are approximated by three power laws, and in terms of cross-section these are:

$$\sigma(E) = \begin{cases} 2.7\ 10^{-26}\ E^{0.036}\ cm^2 & E \geq 1\ GeV \\ 2.7\ 10^{-26}\ E^{0.945}\ cm^2 & 0.7 < E < 1\ GeV \\ 8\ \ 10^{-26}\ E^{3.86}\ cm^2 & 0.4 \leq E \leq 0.7\ GeV \\ 0 & E < 0.4\ GeV \end{cases} \qquad (4.22)$$

The expression for r_i is given by equation 4.4.

The solution of equation 4.19 is a function of n_{He} and λ due to the dependence of j(E) on these parameters (see equations 4.11 and 4.12). n(E) also depends on the density in the region where total energy loss is occurring, although this dependence cancels when the gamma ray emissivity is calculated. Figure 4.7 shows the solution of n(E) for $f(\underline{r}) = 1$, in terms of the parameters λ, n_H and n_{He}.

4.5.3. The gamma ray emissivity

The total integral emissivity of all gamma rays is calculated using equation 2.8. A factor of 1.44 is used to account for cosmic ray alpha particles. The product of total cross section and multiplicity takes the form given by Stecker (1973) which has been checked for consistency with the data of Bracci et al. (1973):

$$m_{\pi^0}(E)\,\sigma_{\pi^0}(E) = \begin{cases} 0 & E < 0.4\ GeV \\ 10^{-25}\ E^{7.64}\ cm^2 & 0.4 \leq E < 0.7\ GeV \\ 8.4\ 10^{-27}\ E^{0.53}\ cm^2 & E \geq 0.7\ GeV \end{cases} \qquad (4.23)$$

The total emissivity of gamma rays is found to be:

$$Q_\gamma(\underline{r}) = (1.1 \pm 0.2)\ 10^{-23}\ f(\underline{r})\ n_{He}/\lambda\ cm^{-3}\ s^{-1}$$

For comparison with SAS-2 observations, the proportion of the total emissivity which is above 100 MeV is required. Locally this proportion is 0.68 (Stecker, 1970) and, since n(E) (see figure 4.7) is not very different in shape from the local ambient spectrum, this same value is adopted here, giving:

$$q_\gamma(E_\gamma > 100\ MeV, \underline{r}) = (7.6 \pm 0.2)\ 10^{-24}\ f(\underline{r})\ n_{He}/\lambda\ cm^{-3}\ s^{-1}$$

For a local cosmic ray lifetime of $2.5\ 10^6$ yr (see section 4.4) this gives:

$$q_\gamma(E_\gamma > 100\ MeV, \underline{r}) = 1.9\ 10^{-24}\ f(\underline{r})\ cm^{-3}\ s^{-1}$$

Whereas for $\tau = 2\ 10^7$ yr we find:

$$q_\gamma(E_\gamma > 100\ MeV, \underline{r}) = 2.4\ 10^{-25}\ f(\underline{r})\ cm^{-3}\ s^{-1}$$

These results can be applied to any position in the Galaxy where matter is dense enough for total energy loss of the primary particles before escape. It must be assumed that the cosmic ray sources are within the dense region and the magnetic field configuration traps the particles. The gamma rays however experience no such trapping and can escape from the region without significant absorption. In the next Chapter the Galactic centre is considered in more detail. The gamma ray contribution emanating from secondary and primary electrons is calculated and the value for $f(\underline{r})$ is found.

CHAPTER FIVE

GAMMA RAYS FROM THE GALACTIC CENTRE

5.1 THE GAMMA RAY FLUX FROM ELECTRON INTERACTIONS IN THE 300 pc RING

5.1.1. The emissivity equations

The energy loss processes for electrons are given in section 4.3.3. Bremsstrahlung and inverse Compton losses produce gamma rays whereas synchrotron emission gives photons at radio wavelengths. In this section, for each of these processes, the equation for the gamma ray emissivity, $q(E_\gamma)$, due to total energy loss of an electron production spectrum, $J(E)$, is calculated.

Bremsstrahlung is considered first. It is treated as a continuous energy loss process. From equation 2.9 we have:

$$\sigma(E_\gamma, E)\, dE_\gamma \propto dE/E_\gamma \tag{5.1}$$

The contribution to the emissivity at E_γ from an electron of energy E losing energy dE, $q(E_\gamma, E, dE)$, is given by:

$$q(E_\gamma, E, dE)\, dE_\gamma = A(E)\, \frac{dE_\gamma}{E_\gamma} \tag{5.2}$$

where,

$$dE = \int_0^E q(E_\gamma, E, dE)\, E_\gamma\, dE_\gamma \tag{5.3}$$

Using 5.2 in 5.3:

$$A(E) = \frac{dE}{E} \tag{5.4}$$

Therefore,

$$q(E_\gamma, E)\, dE_\gamma = dE_\gamma \int_{E_\gamma}^{E} \frac{dE}{E_\gamma E} \tag{5.5}$$

Integrating over the total electron spectrum:

$$q(E_\gamma) = \frac{4\pi}{E_\gamma c} \int_{E_\gamma}^{\infty} J(E')\, dE' \int_{E_\gamma}^{E'} \frac{dE}{E} \tag{5.6}$$

Since four processes (see equations 4.6 - 4.9) contribute to the energy losses, 5.6 becomes:

$$q_b(E_\gamma) = \frac{4\pi}{E_\gamma c} \int_{E_\gamma}^{\infty} J(E')\, dE' \int_{E_\gamma}^{E'} \frac{\dot{E}_b}{E \sum \dot{E}}\, dE \tag{5.7}$$

Where $\sum \dot{E}$ is defined:

$$\sum \dot{E} = \dot{E}_i + \dot{E}_b + \dot{E}_{IC} + \dot{E}_{syn} \tag{5.8}$$

For both inverse Compton and synchrotron losses the average photon energy is proportional to the square of the electron energy:

$$\langle E_\gamma \rangle = bE^2 \tag{5.9}$$

For an electron of energy E losing dE:

$$dE = q(E_\gamma, E)\, E_\gamma\, dE_\gamma \tag{5.10}$$

Differentiating 5.9 and substituting into 5.10 gives:

$$q(E_\gamma, E) = \frac{1}{2E_\gamma \sqrt{bE_\gamma}} \tag{5.11}$$

Integrating over the electron spectrum:

$$q(E_\gamma) = \frac{4\pi}{c\, 2E_\gamma \sqrt{bE_\gamma}} \int_{\sqrt{E_\gamma/b}}^{\infty} j(E)\, dE \tag{5.12}$$

For inverse Compton interactions, if E_{ph} is the average energy of the low energy photon field and m denotes the electron mass, then from equation 2.30:

$$b_{IC} = \frac{4\ E_{ph}}{3\ m^2} \tag{5.13}$$

5.12 becomes:

$$q_{IC}(E_\gamma) = \frac{4\pi}{c2\ E_\gamma \sqrt{b_{IC}\ E_\gamma}} \int_{\sqrt{E_\gamma / b_{IC}}}^{\infty} J(E)\ \frac{\dot{E}_{IC}}{\sum \dot{E}}\ dE \tag{5.14}$$

In the case of synchrotron radiation the radio photon energy is expressed as E_ν. If E_γ and E_ν are in units of eV, a magnetic field of H gauss gives:

$$b_{syn} = 6.62\ 10^{-20}\ H \tag{5.15}$$

5.12 becomes:

$$q_{syn}(E_\nu) = \frac{4\pi}{c2E_\nu \sqrt{b_{syn}\ E_\nu}} \int_{\sqrt{E_\nu / b_{syn}}}^{\infty} J(E)\ \frac{\dot{E}_{syn}}{\sum \dot{E}}\ dE \tag{5.16}$$

5.1.2. <u>The contribution from bremsstrahlung and inverse Compton scattering</u>

In order to calculate 5.7 and 5.14, values for n_H, w_{ph} and H at the Galactic centre are required. Following section 4.2, the ring-confinement average density of 220 atoms cm^{-3} is adopted, and using the model of Paul et al. (1976), in which $H^2 \propto n_H$, the magnetic field is 44 μG. The choice of photon energy density is now discussed in more detail.

Innanen (1973) gives a star mass surface density at a Galactocentric radius of 300 pc which is approximately 92 times the local value. Assuming

the energy density is proportional to the mass of stars in the vicinity, and taking a local starlight energy density of 0.44 eV cm^{-3}, the value for the Galactic centre is 40 eV cm^{-3}. Sanders and Lowinger (1972) have studied the Galactic centre in more detail using 2.2 μm infrared measurements and relating these to total starlight luminosity by comparison with the nucleus of M31. They derive a relation for the total luminosity within a radius R pc:

$$L = 2\ 10^{6}\ R^{1.2}\ L_{\odot} \qquad (5.17)$$

The luminosity can be expressed in terms of the average energy density inside a sphere of surface area A:

$$L = \frac{1}{4}\ w c\ A \qquad (5.18)$$

In appropriate units (R pc and w eV cm^{-3}) this gives:

$$L = w\ 3.54\ 10^{2}\ R^{2}\ L_{\odot} \qquad (5.19)$$

From 5.17 and 5.19:

$$w = 5.6\ 10^{3}\ R^{-0.8}\ \text{eV cm}^{-3} \qquad (5.20)$$

Inside a radius of 300 pc we therefore have w = 59 eV cm^{-3}. This value is probably a slight overestimate for the dense cloud region since the starlight appears more concentrated towards the Galactic nucleus and there will be significant scattering into the far infrared in the clouds.

Galactic scans in the far infrared (at about 100 μm) show a clear enhancement within a few degrees of the centre. Hoffman et al. (1971)

find a total of $3.4\ 10^8\ L_\odot$, from a region $4^\circ \times 2^\circ$ about the centre, in the band 75 - 125μm. Assuming this is coming from a sphere of radius approximately 350 pc, and using 5.19, we find:

$$w_{IR} = 8 \text{ eV cm}^{-3}$$

Soifer and Houck (1973) find an infrared luminosity of $2\ 10^8\ L_\odot$ for the same region, yielding:

$$w_{IR} = 5 \text{ eV cm}^{-3}$$

It is therefore apparent that although there is a high intensity of infrared radiation it is dominated by the starlight energy density. In the present work the photon field is assumed to have a mean energy, E_{ph}, of 1.4 eV and a mean energy density, w_{ph}, of 45 eV cm^{-3}.

For primary electrons at the Galactic centre:

$$J(E) = f_e\ j(E)/\tau \qquad (5.21)$$

where j(E) is given by 2.12 and τ can be expressed in terms of λ and n_{He} as in 4.11. f_e is the factor by which the local injection rate of electrons is multiplied to get that at the Galactic centre. The bremsstrahlung and inverse Compton differential gamma ray emissivities can be calculated directly from equations 5.7 and 5.14 and the results are shown in figure 5.1, (labelled (c) and (e) respectively). A power law extrapolation in kinetic energy of the spectrum j(E) is assumed below 10^7eV where direct observations are not possible, which leads to corresponding uncertainty in the bremsstrahlung spectrum below this energy. Figure 5.2 shows the integral emissivities. All integrals were

calculated using a Romberg routine in decade steps until further contributions became negligible.

The emissivity of gamma rays above 100 MeV from primary electron bremsstrahlung is:

$$q_{p,b}\ (>100\ \text{MeV}) = f_e\ 9.64\ 10^{-25}\ n_{He}/\lambda\ \text{cm}^{-3}\ \text{s}^{-1}$$

For a local cosmic ray lifetime of $2.5\ 10^6$ yr this gives:

$$q_{p,b}\ (>100\ \text{MeV}) = f_e\ 2.4\ 10^{-25}\ \text{cm}^{-3}\ \text{s}^{-1}$$

whereas for $\tau = 2\ 10^7$ yr:

$$q_{p,b}\ (>100\ \text{MeV}) = f_e 3\ 10^{-26}\ \text{cm}^{-3}\ \text{s}^{-1}$$

The corresponding contribution from primary electrons undergoing inverse Compton scattering is:

$$q_{p,IC}\ (>100\ \text{MeV}) = f_e\ 7\ 10^{-26}\ n_{He}/\lambda\ \text{cm}^{-3}\ \text{s}^{-1}$$

For $\tau = 2.5\ 10^6$ yr,

$$q_{p,IC} = (>100\ \text{MeV}) = f_e\ 1.7\ 10^{-26}\ \text{cm}^{-3}\ \text{s}^{-1}$$

For $\tau = 2\ 10^7$ yr,

$$q_{p,IC}\ (>100\ \text{MeV}) = f_e\ 2.2\ 10^{-27}\ \text{cm}^{-3}\ \text{s}^{-1}$$

The scheme for calculation of the contributions from secondary electrons is shown in table 5.1b. The ambient proton spectrum at the Galactic centre, n(E), is approximated to the same spectral shape as the local spectrum, j(E), which is given in equation 2.12. The factor by

Table 5.1

Scheme for calculation of the gamma ray emissivity from primary electron and secondary electron interactions in thick targets.

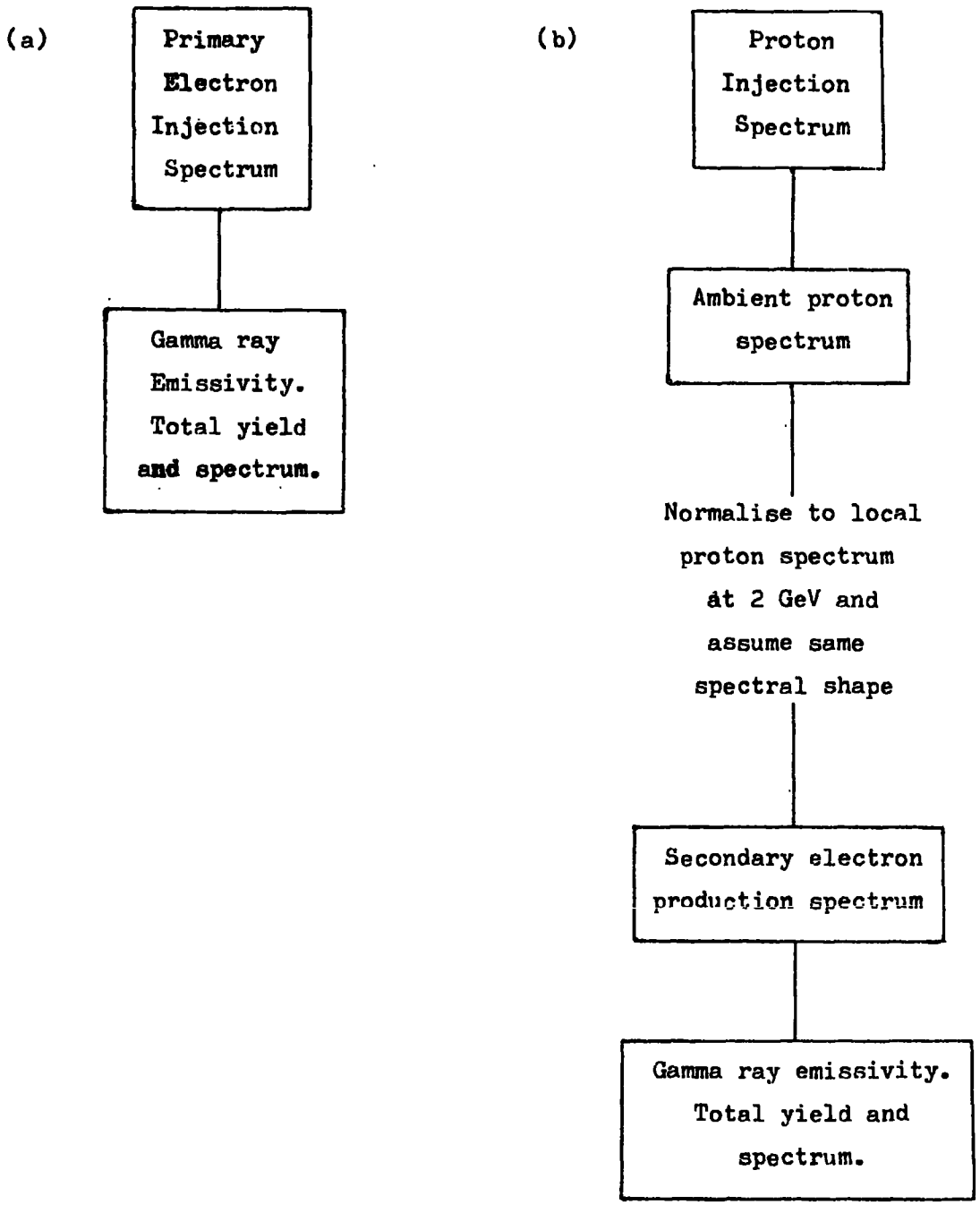

which j(E) must be multiplied to give n(E) is found by comparing j(E) at about 2 GeV with n(E) as calculated in the previous Chapter and shown in figure 4.7. This gives:

$$n(E) \approx j(E)\ f\ 125\ n_{He}/(\lambda\, n_H) \qquad (5.22)$$

Here f is the factor by which the local proton injection rate is multiplied to get that at the Galactic centre (as distinct from the corresponding factor for electrons, f_e). The production spectra of secondary electrons and positrons for j(E) is taken from Ramaty (1974). The appropriate spectra for the Galactic centre are found using 5.22. Here n_H cancels, leaving the secondary electron production a function only of f, n_{He} and λ. The bremsstrahlung and inverse Compton gamma ray emissivities are calculated using 5.7 and 5.14, and the results shown in figures 5.1 and 5.2 (labelled (b) and (d) respectively). In order to compare with the results from primary electron interactions it is assumed in plotting these graphs that $f_e = f$, i.e. the local electron to proton ratio is the source ratio at the Galactic centre. The contribution from neutral pion decay gamma rays, as calculated in the previous Chapter, is also shown along with the total from all processes.

The emissivity of gamma rays above 100 MeV from secondary electron bremsstrahlung is:

$$q_{s,b}\ (>100\ \text{MeV}) = f\ 2.42\ 10^{-24}\ n_{He}/\lambda\ \text{cm}^{-3}\ \text{s}^{-1}$$

For a local cosmic ray lifetime of $2.5\ 10^6$ yr this gives:

$$q_{s,b}\ (>100\ \text{MeV}) = f\ 6.1\ 10^{-25}\ \text{cm}^{-3}\ \text{s}^{-1}$$

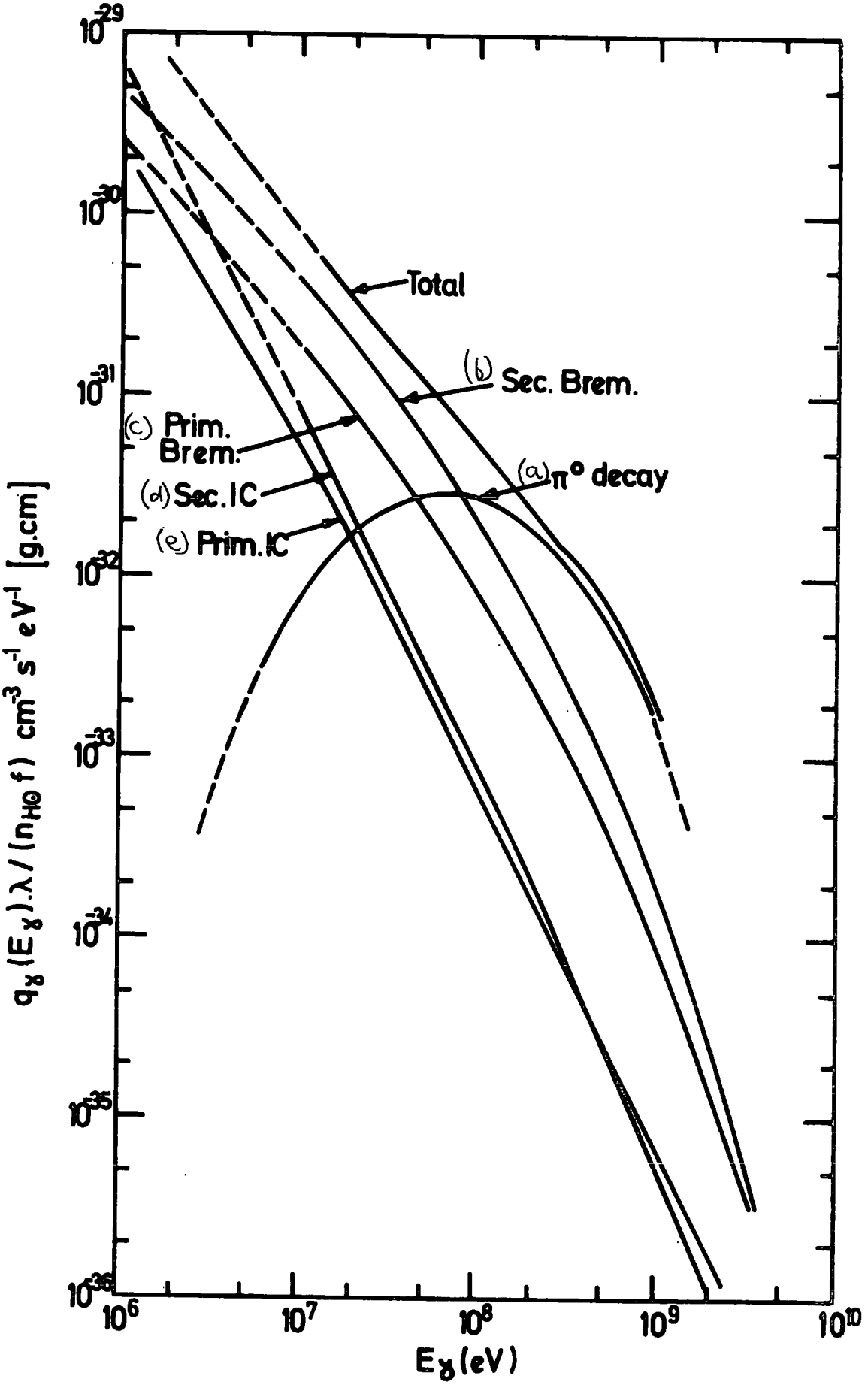

Figure 5.1 Differential gamma ray emissivity spectra for the Galactic centre, in terms of the parameters λ, $n_{H\odot}$ and f, defined in the text. Results are for f_e=f.

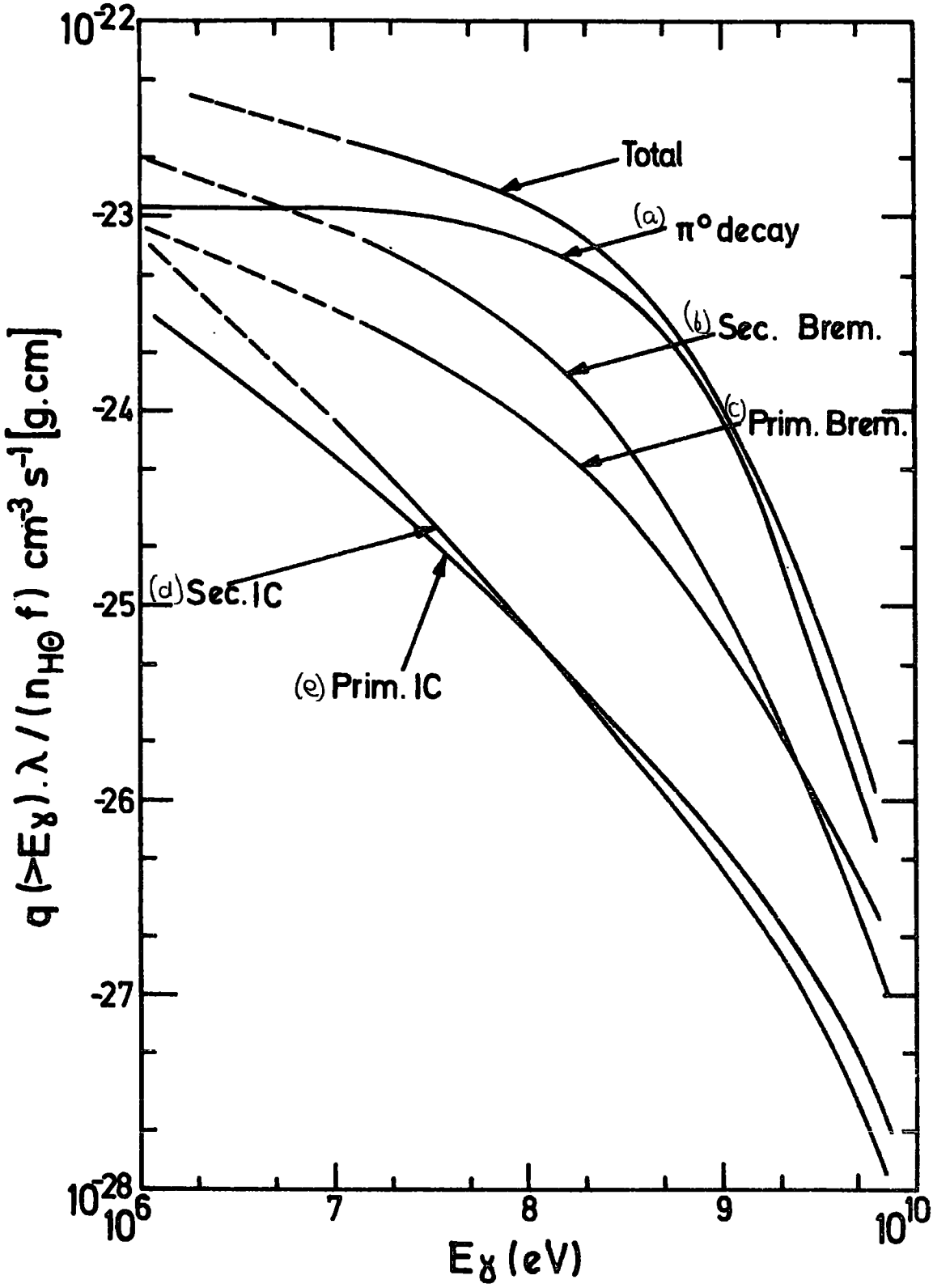

Figure 5.2 Integral gamma ray emissivity spectra for the Galactic centre, in terms of the parameters λ, n_{He} and f, defined in the text. Results are for $f_e = f$.

whereas for $\tau = 2\ 10^7$ yr:

$$q_{s,b}\ (>100\ \text{MeV}) = f\ 7.6\ 10^{-26}\ \text{cm}^{-3}\ \text{s}^{-1}$$

The corresponding contribution from secondary electrons undergoing inverse Compton scattering is:

$$q_{s,IC}\ (>100\ \text{MeV}) = f\ 7.2\ 10^{-26}\ n_{He}/\lambda\ \text{cm}^{-3}\ \text{s}^{-1}$$

For $\tau = 2.5\ 10^6$ yr

$$q_{s,IC}\ (>100\ \text{MeV}) = f\ 1.8\ 10^{-26}\ \text{cm}^{-3}\ \text{s}^{-1}$$

For $\tau = 2\ 10^7$ yr

$$q_{s,IC}\ (>100\ \text{MeV}) = f\ 2.2\ 10^{-27}\ \text{cm}^{-3}\ \text{s}^{-1}$$

5.2 EVIDENCE FOR GALACTIC ORIGIN FOR THE GAMMA RAY PROGENITORS

The trapping of the cosmic rays until they lose all their energy gives the maximum gamma ray emissivity for a given particle injection rate. Comparison of the calculation of the gamma ray flux from the Galactic centre with the observed flux will therefore give a value for f which represents a lower limit to the actual ratio of the Galactic centre to local primary cosmic ray production rate. For evidence that cosmic rays are of Galactic origin, f must be greater than the relative particle lifetime for the local and Galactic centre region.

Since the proton to electron source ratio at the Galactic centre is unknown, the local ratio is adopted, i.e. $f = f_e$. In the future, from a good observation of the spectral shape of the gamma ray flux, it may be possible to determine the source ratio by resolving the percentage

contributions from the various production processes. From figures 5.1 and 5.2 it is seen that the majority of the emissivity is contributed by the protons through neutral pion decay or the interaction of produced secondary electrons. Thus, as long as $f_e \leq f$, the comparison with observations yields information only on f, and the actual value of f_e is not important. However, the case in which only primary electron sources are enhanced, i.e. $f_e \gg f$, is also discussed below.

The flux from the Galactic centre region is proportional to the cosmic ray trapping volume, V (likely values for which are given in section 4.2), but independent of the mass of gas. Firstly, if the particles are trapped within a 300 pc radius:

$$V_1 = 2\ 10^7\ pc^3$$

Secondaly, if particles are confined only inside the ring,

$$V_2 = 10^7\ pc^3$$

The total emissivity above 100 MeV, from the calculations in section 4.5 and 5.1, is, for $\tau = 2.5\ 10^6$ yr,

$$q_1\ (>100\ MeV) = 2.8\ 10^{-24}\ f\ cm^{-3}\ s^{-1}$$

For $\tau = 2\ 10^7$ yr,

$$q_2\ (>100\ MeV) = 3.5\ 10^{-25}\ f\ cm^{-3}\ s^{-1}$$

The error on each of these values is about 20% due to the uncertainty in the nuclear physics for the calculation of the neutral pion decay emissivity. The balance of the values for w_{ph}, n_H and H will only affect the smaller electron contribution (see section 5.1).

The flux from a volume V (cm^3) a distance d (cm) away is:

$$I\ (>100\ MeV) = \frac{q\ (>100\ MeV)}{4\ \pi\ d^2}\ V\ cm^{-2}\ s^{-1} \qquad (5.23)$$

The distance to the Galactic centre is assumed to be 10 kpc. The maximum flux is derived using V_1 and q_1:

$$I_{max}\ (>100\ MeV) = 1.34\ 10^{-7}\ f\ cm^{-2}\ s^{-1}$$

The minimum flux is for V_2 and q_2:

$$I_{min}\ (>100\ MeV) = 8.4\ 10^{-9}\ f\ cm^{-2}\ s^{-1}$$

The SAS-2 measured flux from within 2.6 kpc of the Galactic centre was found to be $6.7\ 10^{-6}\ cm^{-2}\ s^{-1}$ (see section 4.1). From the discussion in section 4.2 it is likely that all the flux originates within 300 pc of the centre. Under this assumption, the observed width of the central peak, which is greater than expected, is due to the angular resolution of the SAS-2 detector.

Using I_{max},

$$f_{min} = 50$$

whereas for I_{min},

$$f_{max} = 800$$

The results show an enhancement of injection of protons at the Galactic centre which is greater than the amount of decrease of cosmic ray lifetime over that locally (≈ 10 for $\tau = 2.5\ 10^6$ yr), thus ruling out extragalactic origin for the particles. However, it should be emphasised

that ratification of the high Galactic centre gamma ray peak from the COS-B experiment is awaited.

The range for f includes the possibility that:

$$f(\underline{r}) \propto n_H(\underline{r})$$

This would be consistent with the models of Bignami and Fichtel (1974) and others (see Table 3.1) in which:

$$n_H \propto n_{CR}$$

If $f_e > 10$ f only the primary electron interactions contribute to the flux. From section 5.1, for $\tau = 2.5\ 10^6$ yr,

$$q\ (>100\ \text{MeV}) = 2.6\ 10^{-25}\ f_e\ \text{cm}^{-3}\ \text{s}^{-1}$$

For $\tau = 2\ 10^7$ yr,

$$q\ (>100\ \text{MeV}) = 3.2\ 10^{-26}\ f_e\ \text{cm}^{-3}\ \text{s}^{-1}$$

Using equation 5.23 and comparing with the observed flux gives:

$$540 < f_e < 8800$$

The required enhancement of electron sources is therefore very large. Nothing can be deduced from this about whether the protons are of Galactic or extragalactic origin, (primary electrons are already known to originate in the Galaxy - see section 4.3.1). The consequence of such a high electron injection concerning synchrotron emission is discussed in the next section, where it is found that consistency with observation occurs as long as the magnetic field is not much higher than the local value. The possibility that the Galactic centre gamma ray flux is due to a high

primary electron source density, without necessarily requiring cosmic ray protons to be of Galactic origin, cannot therefore be excluded. Support for an electron origin for the gamma rays comes from the steep gamma ray spectrum suggested by the very recently reported gamma ray measurements (see Appendix A, section A.5). If $f \approx f_e$ we have found:

$$50 < f < 800$$

The range is large but includes all present uncertainties except possible doubt concerning the observed flux which has yet to be ratified by another experiment. If the cosmic rays are not trapped the value of f may be larger. However the gamma ray production region would now not be confined to the ring, inside which the particle sources occur, and inverse Compton gamma rays would be produced in the non-gas filled region between 300 pc and 2.6 kpc. The results suggest a model in which the source and average gas densities are proportional. This favours Galactic models in which, for the less dense regions where total energy loss does not occur, $n_H \propto n_{CR}$.

5.3 SYNCHROTRON EMISSION FROM THE GALACTIC CENTRE

5.3.1. The observations

The Galactic centre can be observed at radio frequencies with good resolution. Several discrete sources are seen and detailed structure has been recorded particularly for the two which are best known, Sgr A and Sgr B2. The nucleus of Sgr A marks the Galactic centre. It is a nonthermal source with complex structure. In contrast, Sgr B2 is a thermal source emitting several hydrogen recombination lines characteristic of an HII region. In addition to the sources, an extended background

of several degrees is seen at 408 MHz and 85 MHz. Its absence in high frequency surveys (e.g. that of Kapitzky and Dent (1974) at 15.5 GHz) indicates that it is of nonthermal origin.

The extended background, which fits well the region inside the molecular hydrogen ring, was first seen in the survey at 85 MHz of Mills (1956), (see also Hill et al., 1959), where the beamsize was 50 min. of arc. Using a differential frequency scaling law, $\nu^{-2.7}$, the brightness temperature correlates with that found at 408 MHz by Green (1974). The resolution of Green's experiment was less than 3 min. of arc, but unfortunately the only results available are averaged over $\pm$ 3° of Galactic latitude. However, the sources have been removed from the data. The peak is within about 2° of longitude and the intensity from the central region alone is found to be approximately 0.4°K sr. Little (1974), from a survey on the same telescope and at the same frequency as Green presents profiles at $b = 0^\circ$ and $\ell = 0^\circ$ from which the emission from the central region can be found more accurately. We find:

$$I_{obs}\ (408\ \text{MHz}) = 0.3^\circ\text{K sr}$$
$$= 1.4\ 10^{12}\ \text{cm}^{-2}\ \text{s}^{-1}\ \text{eV}^{-1}$$

Using equation 5.23 and assuming ring confinement, i.e. volume V_1,

$$q_{obs}\ (408\ \text{MHz}) = 5.8\ 10^{-5}\ \text{cm}^{-3}\ \text{s}^{-1}\ \text{eV}^{-1}$$

5.3.2. Determination of the Galactic centre magnetic field

For comparison with the above observation, the radio synchrotron emissivity is calculated using equation 5.16, where the primary and secondary injection spectra are as in section 5.1.2. The results, in terms

of the parameters λ, n_{He} and f, for various H between the local value, 3 μG, and that assumed for the Galactic centre in the previous calculations, 44 μG, are shown in figure 5.3. These results show the sum of the secondary and primary electron contributions, assuming $f_e = f$. At 408 MHz the primary electron contribution is typically 0.4 of the total.

The value for f consistent with that found in section 5.2 is required. A confinement volume of 10^7 pc^3 and a local cosmic ray lifetime of 2.5 10^6 yr are chosen for the comparison, (these values are arbitrary). Table 5.2 gives the emissivity at 408 MHz for each of the H values for which results are presented in figure 5.3. The first part of the table is for $f = f_e$ and the second for the case where only the primary electron sources are greatly enhanced at the Galactic centre, i.e. $f_e >> f$. The values for f or f_e required to give consistency with q_{obs} are also shown. Figure 5.4 shows f_e as a function of H for the two conditions. The slope of curve (b), to which primary electrons alone contribute, is slightly flatter than that of (a) due to the flatter production spectrum of primaries than secondaries at energies close to 1 GeV. From equations 5.9 and 5.15 it can be seen that 408 MHz radiation is produced by electrons of about 3 GeV if the magnetic field is 3 μG, or about 0.7 GeV if the field is 44 μG.

Under the selected conditions for τ and V, from section 5.2:

$f = 100$ if $f = f_e$

$f_e = 1080$ if $f_e >> f$

From figure 5.4 the required magnetic fields can be found:

$H = 21\ \mu G$ if $f = f_e$

$H = 7.5\ \mu G$ if $f_e >> f$

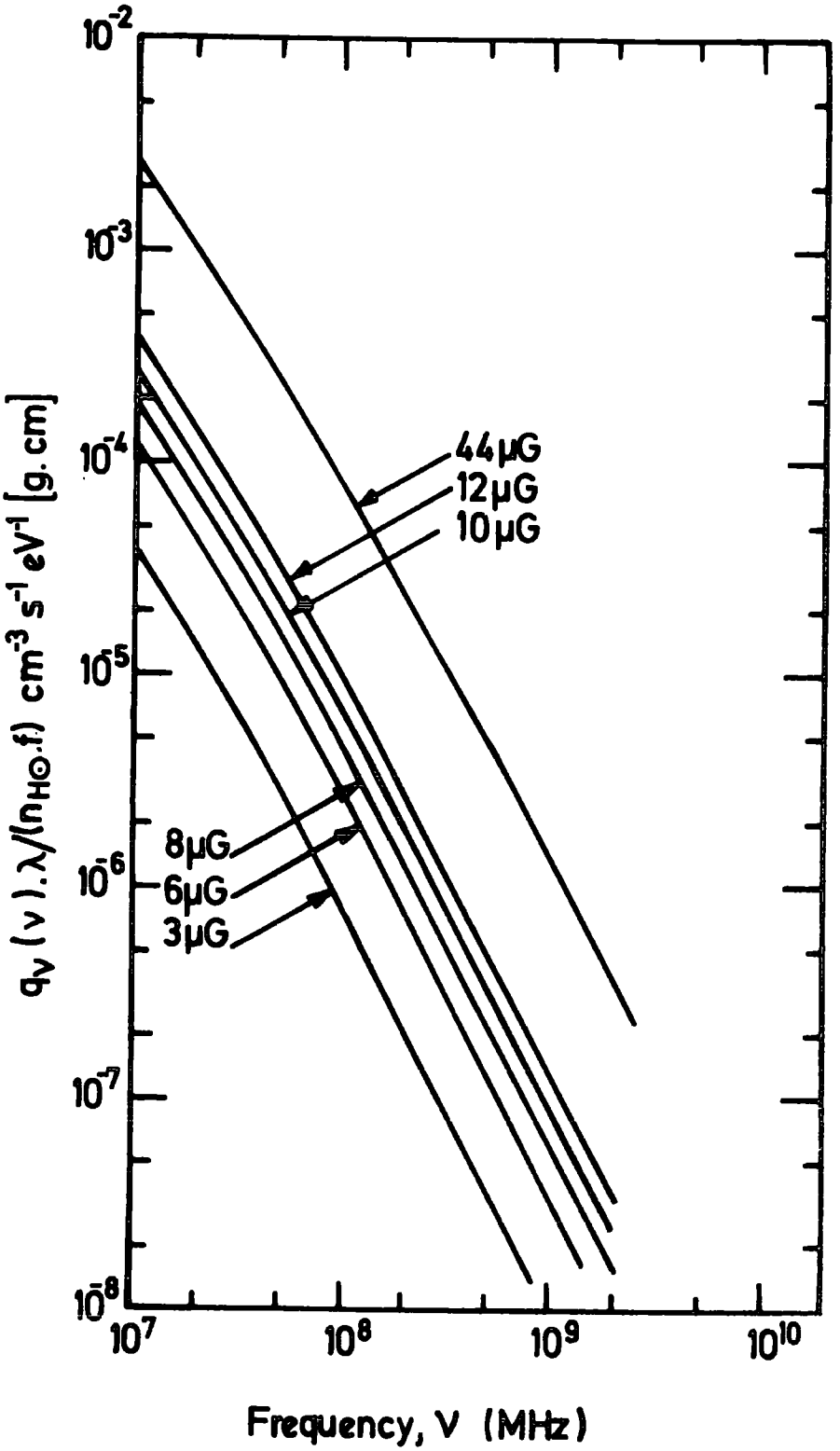

Figure 5.3 The Galactic centre differential radio synchrotron emissivity in terms of the parameters λ, $n_{H\odot}$ and f, defined in the text, for various values of the magnetic field. Results are for f_e=f.

Table 5.2

The 408 MHz Galactic centre emissivity for various values of H (μG), where a local cosmic ray lifetime of 2.5 10^6 yr and trapping volume of 10^7 pc^3 are assumed. Also given is the value for f required to give consistency with the observation q_{obs} (408 MHz) = 5.8 10^{-5} cm^{-3} s^{-1} eV^{-1}.

(a) $f = f_e$

H (μG)	q (cm^{-3} s^{-1} eV^{-1})	f
3	1.3 10^{-8}	4400
6	4.6 10^{-8}	1250
8	8.0 10^{-8}	725
10	1.2 10^{-7}	500
12	1.8 10^{-7}	330
44	1.7 10^{-6}	34

(b) $f_e >> f$

H (μG)	q (cm^{-3} s^{-1} eV^{-1})	f_e
3	5.8 10^{-9}	10000
6	2.0 10^{-8}	2900
8	3.5 10^{-8}	1650
10	4.6 10^{-8}	1260
12	7.0 10^{-8}	830
44	6.0 10^{-7}	97

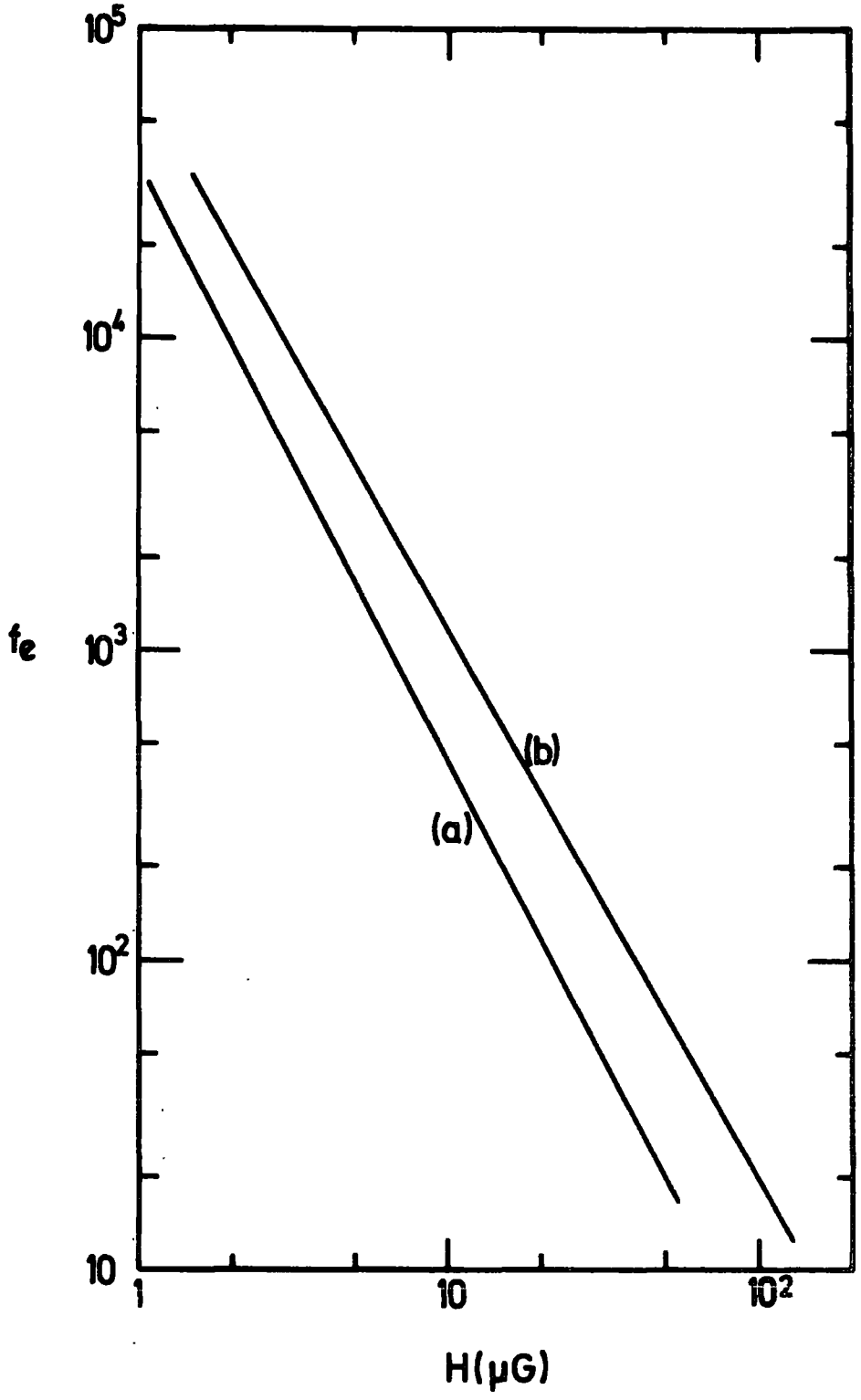

Figure 5.4 f_e as a function of the Galactic centre magnetic field, H. Curve (a) is for $f_e = f$, and curve (b) is for $f_e >> f$. Results are for a local lifetime of 2.5 10^6 yr. and a trapping volume of 10^7 pc^3.

These field values are both lower than 44 μG which occurs for ring confinement under the assumption $n_H \propto H^2$. Taking the average density inside a 300 pc radius without ring confinement (see section 4.2) implies a field of 30 μG which is closer to the calculated values. However, it is not surprising that exact agreement does not occur since the evidence for the relationship $n_H \propto H^2$ is only the similarity of the synchrotron and gamma ray profiles on a Galactic scale. Evidence suggests that the Galactic centre clouds are much younger than the Galaxy. In particular, if the gas forms an expanding ring, its age, from kinematic conditions, is estimated as $2\ 10^6$ yr (Kaifu et al., 1972). Equilibrium may not yet have been established.

A field close to 16 μG is consistent with the argument of Sanders and Wrixon (1973) that a higher pressure than locally, in either magnetic field or cosmic rays is required to support atomic hydrogen clouds seen fairly high above the plane (about 100 pc) at radii of about 300 pc. Whereas the cosmic ray ambient density is only about 14 times the local value (see equation 5.22), the field pressure would be enhanced by the required factor of about 30. This is evidence slightly more in favour of the field value suggested by $f = f_e$.

It should be noted that, if the value of H = 44 μG used in the previous section is an overestimate, it makes negligible difference to f calculated from the gamma ray flux, since synchrotron energy losses are only a small proportion of the total and have only a slight bearing on the amount of energy available for gamma ray production.

Considering $f_e >> f$, it is found that H = 7.5 μG. This is not much higher than the local field value. However, synchrotron emission

observations indicate strong confinement within 300 pc. A high field contrast would be necessary at this boundary which seems unlikely for a low central field.

In conclusion, although the possibility cannot be ruled out that only electron sources are greatly enhanced at the centre, it is probable that $f \approx f_e$. In this case we have found that the cosmic rays must be of Galactic origin. The actual required source enhancement can be calculated to within the accuracy to which the trapping volume and local cosmic ray lifetime are known. At present the lifetime is only known to within a factor of ten. The possibility that the source density is proportional to the gas density is included in the range. To give consistency with synchrotron measurements a field of about 20 μG is required which does not quite satisfy $n_H \propto H^2$. The fact that the synchrotron measurements show enhancement within about 300 pc of the centre provides good support for the original assumption that primary particles produced within this radius are trapped until they lose all their energy. The apparent large width of the gamma ray peak must therefore be due to poor detector resolution.

5.4 GALACTIC CENTRE GAMMA RAY LINES

5.4.1. Introduction

The Rice University observations of gamma ray lines from the Galactic centre are discussed in Appendix A. Table A.6 gives the flux values.

A line close to 0.5 MeV was seen in all three balloon flights. Predating the observations, several authors had calculated the expected intensity of the 0.51 MeV positron annihilation line. The best calculations are by Stecker (1969) and Ramaty et al. (1970), who include the

3-photon positronium annihilation mode in their work. The predictions were about a factor of ten below the observations. After the first two balloon flights, Leventhal (1973) argued that the finite energy resolution of the detector would cause the positron annihilation line to be redshifted from its characteristic energy, 0.51 MeV, to a slightly lower value. This would account for the first two observations being at an energy of about 0.47 MeV, but the argument is inconsistent with the energy recorded for the third flight.

An alternative explanation for the line is given by Fishman and Clayton (1972), who note that ^{7}Li is the most abundant cosmic ray nuclide with an excitation energy below 1 MeV. They therefore attribute the observed line to ^{7}Li nuclear de-excitation at 0.478 MeV. This explanation requires a very high density of low energy cosmic rays which could not be sustained throughout the Galaxy. They calculate that if the line is produced in the Galactic centre region the cosmic ray energy density there must be greater than 100 eV cm^{-3}. This would mean that the low energy cosmic ray pressure is considerably greater than the magnetic field pressure in the region; too great to be consistent with the argument of Sanders and Wrixon (1973) concerning the high latitude atomic hydrogen clouds (see section 5.3.2). Such a high cosmic ray energy density can only be obtained by an additional component below observed energies, for instance a power law spectrum in kinetic energy below 50 MeV. Rygg and Fishman (1973) calculate that as long as such a power law has a steeper negative gradient than 2, the flux from ^{7}Li exceeds that from positron annihilation. However, positrons are produced in two ways. Firstly, with a maximum energy of 1 MeV from beta decay of unstable CNO nuclei, and secondly, at energies of about 35 MeV from charged pion decay. Under

normal conditions the majority of the latter are lost from the Galaxy before annihilation. However, if trapping occurs, 80% will annihilate near rest. (Table II of Stecker, 1969 gives the fraction of positrons annihilating versus lifetime in the Galaxy). Therefore, under the Galactic centre conditions considered in the present work, the positron annihilation flux is expected to exceed that from ^{7}Li de-excitation.

There is the possibility that the 0.5 MeV line is produced along the line of sight rather than at the Galactic centre. This is supported by the fact that for the third balloon flight the detector solid angle was reduced by 0.4, and this proved to be the same factor by which the observed line intensity was lower. However, if the flux is a line of sight phenomenon, the argument of Rygg and Fishman that the line is due to ^{7}Li is expected to hold. There are problems in reconciling the necessary high cosmic ray energy density with observed ionization and light element production rates (see Meneguzzi and Reeves, 1975). A further problem is that it is likely that low energy cosmic rays are excluded from clouds (Solomon and Werner, 1971; Skilling and Strong, 1976, 1977; and others). They would therefore escape from the Galaxy before causing much gamma ray line production or ionization. Under the Galactic centre trapping hypothesis there is no such problem since the particles would be free to lose all their energy, even though the time for this may be longer than for the higher energy particles which could more easily penetrate the clouds.

The observations at 4.6 MeV and 0.9 MeV are almost certainly the nuclear de-excitation of ^{12}C at 4.43 MeV and ^{56}Fe at 0.847 MeV respectively. The emission between 1.2 and 2 MeV is probably due to ^{24}Mg,

^{20}Ne and ^{28}Si. Calculations on relative line strengths are reported by Rygg and Fishman (1973) and Meneguzzi and Reeves (1975), while Lingenfelter and Ramaty (1976b) present detailed work on the ^{12}C line. The cosmic ray spectrum below about 50 MeV, unknown due to solar modulation, is critical to these studies. It seems that, to obtain the measured line intensities, very high cosmic ray energy densities are required, which, as discussed above, presents problems.

In the next subsection the positron annihilation flux for the present Galactic centre model is calculated, in order to check that the observed flux is not exceeded and to find under what conditions the observations can be reproduced. In the final subsection nuclear de-excitation lines are briefly considered.

5.4.2. The 0.51 MeV positron annihilation line

In the following it is assumed that $f_e = f$. Obviously if $f_e >> f$ then the positron production at the Galactic centre will be negligible.

In section 5.2 it was found that:

$$q\ (>100\ \text{MeV}) = 1.1\ 10^{-23}\ f\ n_{He}/\lambda\ \text{cm}^{-3}\ \text{s}^{-1} \qquad (5.24)$$

Using the observed flux of $6.7\ 10^{-6}\ \text{cm}^{-2}\ \text{s}^{-1}$ and a distance for the Galactic centre of 10 kpc, for V in pc^3 equation 5.23 gives:

$$q_{obs}\ (>100\ \text{MeV}) = 2.8\ 10^{-15}/V\ \text{cm}^{-3}\ \text{s}^{-1} \qquad (5.25)$$

Equating 5.24 and 5.25:

$$f = 2.5\ 10^{8}\ \lambda\ /(V\ n_{He}) \qquad (5.26)$$

Substituting for f in equation 5.22:

$$n(E) = j(E)\ 3.1\ 10^{10}/(V\ n_H) \qquad (5.27)$$

The ambient proton spectrum at the Galactic centre is therefore related to the local spectrum by the mass of gas at the Galactic centre alone:

$$n(E) = j(E)\ 7.05\ 10^{8}/M \qquad (5.28)$$

where M is in units of solar mass.

The positron production spectrum both from CNO beta decay and charged pion decay is calculated by Ramaty et al. (1970) for various assumptions about the low energy cosmic ray spectrum. An upper limit to the yield is found for the assumption that the cosmic ray spectrum continues as a power law in kinetic energy of slope -2.5 below the observational limit, with a cutoff at 5 MeV/nucleon. The solar abundance ratios for H:C:N:O have been used in the calculations. Integrating under the positron production spectrum given by Ramaty et al. gives a total yield of 0.898 $g^{-1}\ s^{-1}$.

At the Galactic centre it is assumed that 80% of the positrons annihilate near rest. The percentage may be a little higher for the low energy beta decay positrons. Only $\frac{1}{4}$ of the annihilations contribute to the 0.51 MeV line since the rest will produce a three-photon annihilation continuum (Stecker, 1969). Therefore a factor of $\frac{1}{2}$ is included and we find:

$$q\ (0.51\ \text{MeV}) = \frac{n(E)}{j(E)}\ \frac{1}{2}\ \frac{8}{10}\ 0.898\ g^{-1}\ s^{-1} \qquad (5.29)$$

To find the total yield, equation 5.28 is used and the mass cancels giving:

$$Q\ (0.51\ \text{MeV}) = 5.06\ 10^{41}\ s^{-1}$$

The flux, for d in cm, is given by:

$$I\ (0.51\ \text{MeV}) = \frac{Q\ (0.51\ \text{MeV})}{4\pi d^2}\ \text{cm}^{-2}\ \text{s}^{-1} \qquad (5.30)$$

Therefore,

$$I\ (0.51\ \text{MeV}) = 4.5\ 10^{-5}\ \text{cm}^{-2}\ \text{s}^{-1}$$

This is a factor of 18 to 40 below the observed value. The Galactic centre model therefore does not predict too high a flux and so is not inconsistent with observations. However, if the observed line really is due to positron annihilation, since already an upper limit to the cosmic ray intensity has been used, the only possibility is that the C/H ratio is much higher in the ring. If for example this factor were higher by a factor of ten, we would expect the Galactic centre contribution to definitely dominate that from along the line of sight. Evidence for such an enhancement is put forward by Lingenfelter and Ramaty (1976b) based on the work of D'Odorico et al. (1976) and others. However, the required enhancement in C/H is higher than 10 and so it may be that the hypothesis that the line is due to ^{7}Li de-excitation along the line of sight is more favourable, despite the difficulties mentioned in the introduction. If the C/H ratio is enhanced, it lends support to adopting the lower values for the mass of gas determined from CO measurements (see section 4.2).

It may be that sources of just low energy cosmic rays exist at the Galactic centre, which would not produce particles of high enough energy to give 100 MeV gamma rays. However, there is still a problem of the high energy densities required. No quantitative conclusions on this can be drawn until the nature of the particle sources is known.

5.4.3. Nuclear de-excitation lines

Assuming that low energy cosmic rays can penetrate clouds, the emissivity of lines is proportional to the product of the particle and gas densities. Since this proportionality also roughly applies to gamma rays above 100 MeV assuming they are not mainly of electron origin, we expect:

$$\frac{\text{line flux towards the Galactic centre}}{\text{local line emissivity}} = \frac{\text{100 MeV flux towards the Galactic centre}}{\text{local 100 MeV emissivity}}$$

Considering the ^{12}C line, Haymes et al. (1975) observe a flux of $9.5\ 10^{-4}$ cm^{-2} s^{-1} using a detector of acceptance angle 15° FWHM (see table A.6). Over the same range, from the SAS-2 results of Thompson et al. (1976), a flux of gamma rays above 100 MeV of $2.32\ 10^{-5}$ cm^{-2} s^{-1} is found. Since the local emissivity of gamma rays above 100 MeV is about $1.5\ 10^{-25}$ cm^{-3} s^{-1}, the line emissivity, q_{line}, is:

$$q_{line} = 6.1\ 10^{-24}\ \text{cm}^{-3}\ \text{s}^{-1}$$

However this is over 20 times higher than the maximum allowed by Meneguzzi and Reeves (1975) so as not to exceed ionization and light element production rates. Furthermore, this is only the local emissivity and values even higher would be required towards the Galactic centre. From the calculations of Lingenfelter and Ramaty (1976b), for this line emissivity the local cosmic ray energy density must be at least 60 eV cm^{-3}.

Therefore, from this argument, along with the possibility that low energy cosmic rays are excluded from clouds, it seems that the de-excitation lines must be produced in a localised region of optimum conditions, for example the Galactic centre region itself. Comparing the gamma ray fluxes above 100 MeV, the total in a 15° opening angle is $2.32\ 10^{-5}$ cm^{-2} s^{-1}

whereas that from the Galactic centre region is $6.7\ 10^{-6}$ cm^{-2} s^{-1}. Conditions for line production at the Galactic centre need only to be optimised by a factor of about 10 for domination. This would occur if C/H were increased as suggested in the previous subsection. The Galactic centre will dominate anyway if cosmic ray trapping and eventual cloud penetration occurs whereas exclusion possibly occurs elsewhere.

The flux from the Galactic centre is:

$$I_{line} = \frac{q_{line}\ n_H\ V}{4\pi d^2} \qquad (5.31)$$

where q_{line} is the emissivity in units of H atom^{-1} s^{-1} and the factor n_H V is equal to the number of hydrogen atoms in the ring. Using the observed flux, for M in units of solar mass,

$$q_{line} = \frac{8.98\ 10^{-15}}{M}\ \text{H atom}^{-1}\ \text{s}^{-1}$$

For $5\ 10^7$ $M_\odot$ and allowing for a C/H ratio a factor of ten higher than the local value, the energy density, found by comparison with the calculations of Lingenfelter and Ramaty (1976b), would need to be about 200 eV cm^{-3}. This is probably prohibitively high. Lingenfelter and Ramaty (1976b) postulate that the ^{12}C line is due to de-excitation in the ring, but they use a value for the mass of gas of 10^8-10^9 $M_\odot$ and, with a C/H ratio ten times the local value, require a cosmic ray energy density of 10-10^2 eV cm^{-3}, which is possible. However the likelihood of such a high mass with a large C/H ratio seems remote.

The conclusion is therefore that the evidence is in favour of the lines originating in the Galactic centre region, rather than along the line of sight, due to possible low energy cosmic ray exclusion from

clouds and the low ionization rates for the general interstellar medium now generally observed (see for example Shaver, 1976; Brown, 1973; Barsuhn and Walmsley, 1977). However, unless the Galactic centre mass is underestimated by factors of 10 to 100 it is difficult to predict line intensities as high as those recently observed.

CHAPTER SIX

THE DIFFUSE GAMMA RAY BACKGROUND FLUX

CONTRIBUTION FROM DISCRETE EXTRAGALACTIC SOURCES

6.1 THEORIES FOR THE GAMMA RAY BACKGROUND

Observations of the high latitude gamma ray flux are summarised in Appendix A. See particularly section A.2, figure A.1 and tables A.2 and A.3.

Models for the background flux fit four categories, defined by the production mechanism invoked:

(a) Inverse Compton

Felten and Morrison (1963) suggested that the X-ray and gamma ray background may originate from inverse Compton interactions on intergalactic starlight. After the observation of the 2.7° K background radiation there were several calculations using this as the photon field (Hoyle, 1965; Gould, 1965; Felten, 1965; Fazio et al., 1966; Felten and Morrison, 1966). The consensus was that the emission of electrons from other normal galaxies would have to be higher than seemed likely from the Galaxy, for the intergalactic electron density to reach the required high level. Felten and Morrison (1966) suggested that radio galaxies should give a higher electron output, but, even so, prediction fell short of the observed flux.

Brecher and Morrison (1969) attempted to explain the shape of the spectrum from X-ray to gamma ray energies using an evolutionary model for injection of electrons from normal galaxies, but Cowsik and Kobetich (1972) argue that when some of the approximations are removed from the calculations, only a featureless power law can be produced.

Several authors have estimated, using rather crude models, the likely inverse Compton contribution from electrons in a halo trapping region around the Galaxy (see section 8.1).

(b) Neutral pion decay

Stecker (1969a, 1969b, 1971a) has proposed a model to fit the spectral shape above a few MeV, in which the gamma rays are assumed to originate from neutral pion decay occurring at redshifts of about 70-100. The characteristic peak in the differential gamma ray spectrum at 70 MeV is redshifted to a few MeV and the model is made to fit the apparent "shoulder" in the integral background spectrum at these energies. There are problems associated with this theory, particularly since the spectral "shoulder" now appears less than originally thought. There is also a problem in that large amounts of cosmic ray energy are required at these large redshifts (see Stecker, 1975a).

Probably the most unsatisfactory feature of the theory is that the absolute flux is achieved by normalisation, the free parameter being the maximum redshift for cosmic ray production.

(c) Matter-antimatter annihilation

Stecker et al. (1971) have proposed that the background spectrum is due to matter-antimatter annihilation at large redshifts, arising from the baryon-symmetric big bang cosmology developed by Omnès (1969 and references therein). The spectral shape arises from the absorption window bounded by Compton interactions below about 1 MeV and pair production above about 100 MeV, and the fit is extremely good. Recently the cosmology has been criticised concerning nucleosynthesis and the distortion of the microwave

background, although Stecker (1977) argues that there are in fact no great problems.

The weakness of this model is, as in the previous case, that the spectrum is normalised to the absolute flux.

(d) Repeated inverse Compton scattering and pair production

The gamma ray background theory of Strong et al. (1973a, 1974) is based on the model suggested by Hillas (1968) to explain the observed steepening in the primary cosmic ray spectrum above about $3\ 10^{15}$eV. The requirements are that the cosmic rays above approximately 10^{15}eV are of Universal origin, produced at redshifts back to about 15, and that they lose energy in pair production interactions with the microwave background. On the model of Strong et al., the electron positron pairs then give the background gamma rays by the repetition of the following two processes until the threshold for the latter is reached:

(1) Inverse Compton scattering of the high energy electrons on the microwave background giving high energy gamma rays.

(2) Pair production by interaction of the high energy gamma rays on the microwave background or starlight.

This model is favoured by the fact that absolute values are predicted. However, calculated values lie above the SAS-2 observations by factors of 2-5, although the fit below 10^{7}eV is remarkably good.

6.2 AN APPROACH TO THE BACKGROUND ORIGIN PROBLEM

From above, it is seen that emphasis has been placed on cosmological models for the gamma ray background. They necessarily provide a high degree of isotropy, although until high latitude gamma ray scans are available, 100% isotropy is by no means a certainty.

The main criticism to be levelled at the cosmological models is that, with the exception of the last mentioned, they do not predict absolute flux values. Those models based on fitting the spectral shape suffer problems due to the uncertainty in the flux values at a few MeV.

A different approach is adopted in the present work. Instead of trying to fit a model to the complete background spectrum, certain likely sources of production are considered, the contribution calculated and then compared with the observations. In the following chapters, the inverse Compton flux is calculated for a likely physical model of electron leakage from the Galaxy. Based on this, the electron leakage from other galaxies is estimated and the likely flux from inverse Compton scattering of intergalactic electrons examined.

In this chapter, origin from various categories of extragalactic object is examined. The motivation for the work comes partly from similar studies at X-ray energies. Discrete source contributions to the X-ray background are estimated by Schwartz and Gursky (1973), Boldt (1974) and Rowan-Robinson and Fabian (1975) and others, who have found that, while normal galaxies give a negligible amount, other classes of galaxy provide a higher contribution, although conclusions are that it is unlikely that the total background can have such an origin. However, the X-gamma spectral slope is steeper for the diffuse background than, for example, the Galaxy, and so it may be expected that at gamma ray energies the discrete source contribution is more significant. Unfortunately we are very limited in observations of extragalactic objects in the gamma ray energy regime, and so the analysis is more model dependent than for the X-ray case.

6.3 METHOD OF CALCULATION

Two methods are used to calculate the contribution from a particular class of sources:

Method A

Let each object of a class of sources of number density η per volume $(c/H_o)^3$ (where H_o is the Hubble constant) have a differential luminosity at the present epoch given by $q(E_\gamma) = A\, E_\gamma^{-\alpha}$. In the absence of evolution and absorption, the diffuse background flux, $j(E_\gamma)$, is given by,

$$j(E_\gamma) = \frac{c}{4\pi} \int \eta \left(\frac{H_o}{c}\right)^3 A\, E_\gamma^{-\alpha}\, (1+z)^{-\alpha} (1+z)\, dt \qquad (6.1)$$

but

$$\frac{dz}{dt} = (1+z)^2\, (1+2q_o z)^{\frac{1}{2}}\, H_o \qquad (6.2)$$

where q_o is the deceleration parameter. Since it is now probable that $q_o < 0.5$, it is a good approximation to assume $q_o = 0$ and 6.1 becomes,

$$j(E_\gamma) = \frac{\eta q(E_\gamma)}{4\pi} \left(\frac{H_o}{c}\right)^2 \int_0^\infty (1+z)^{-(\alpha+1)}\, dz \qquad (6.3)$$

For sources contributing to the background flux we expect $\alpha \approx 2$. Therefore evaluation of the integral in 6.3 gives a factor of 1/2 and we have,

$$j(E_\gamma) = \frac{\eta q(E_\gamma)}{8\pi} \left(\frac{H_o}{c}\right)^2 \qquad (6.4)$$

The objects in a particular class exhibit a luminosity distribution, and the integral of luminosity times number per $(c/H_o)^3$ is written $\overline{\eta q(E_\gamma)}$. This quantity can in general be found by assuming that the gamma ray luminosity is proportional to some other property for which the density function for the class of sources is known.

Taking $H_o = 50$ km s^{-1} Mpc^{-1},

$$j(E_\gamma) = 1.3\ 10^{-58}\ \overline{\eta q(E_\gamma)} \qquad (6.5)$$

where $j(E_\gamma)$ is in units of $cm^{-2}\ s^{-1}\ sr^{-1}\ eV^{-1}$ (or $cm^{-2}\ s^{-1}\ sr^{-1}$) and $q(E_\gamma)$ is in $s^{-1}\ eV^{-1}$ (or s^{-1}). Since $\overline{\eta q(E_\gamma)} \propto H_o^{-2}$, $j(E_\gamma)$ is independent of the value adopted for H_o.

Method B

If the gamma ray and radio luminosities of a class of sources are related by $q(E_\gamma) \propto L_R(\nu)$, then the gamma ray background flux, $j(E_\gamma)$, is given by,

$$j(E_\gamma) = \frac{q(E_\gamma)}{L_R(\nu)}\ I_R(\nu) \qquad (6.6)$$

where $I_R(\nu)$ is the radio background attributable to such sources. Unlike Method B, this has the advantage of including evolutionary effects.

Proportionality between radio and gamma ray luminosity is likely since both are produced by cosmic rays of about the same energy. In the Galaxy, for example, the magnetic field is typically of a few microgauss and therefore non-thermal radio emission at a few hundred MHz is produced by electrons of a few GeV. This is approximately the same energy required by protons and electrons for producing gamma rays, by neutral pion decay and bremsstrahlung respectively. Paul et al. (1976), comparing current observations, justify proportionality between the Galactic 150 MHz and gamma ray emissivity.

Using the same notation as in section 2.5, the radio emissivity is roughly proportional to $(n_{ep} + n_{es})\ H^2$, where H is the magnetic field. The main contributions to the gamma ray emissivity are given by equations 2.39 and 2.40. It is unreasonable to expect other galaxies to exhibit large variations in H^2 without roughly corresponding changes in n_H. Therefore, as long as proton sources are distributed between galaxies roughly in proportion to their electron source densities, the assumption of gamma ray and radio proportionality appears well justified.

6.4 THE CONTRIBUTION FROM NORMAL GALAXIES

6.4.1. Calculation using Method A

As yet there are no point source gamma ray observations of normal galaxies. However, the Galaxy itself can be used as the basis for the analysis.

In section 3.4.3, a radial unfolding of the longitude distribution given by Fichtel et al. (1975) enabled the total luminosity of gamma rays above 100 MeV to be found. The value obtained was $q(>100\ \text{MeV}) = 1.3\ 10^{42}\ s^{-1}$. In order to evaluate $\overline{\eta q(>100\ \text{MeV})}$, some indicator of gamma ray luminosity is used, say property P, for which $\overline{\eta P}$ is known. Then,

$$\overline{\eta q(>100\ \text{MeV})} = q_{Gal}\ (>100\ \text{MeV})\ \frac{\overline{\eta P}}{P_{Gal}} \qquad (6.7)$$

One possibility for P is the radio luminosity L_R, and for this, Method B can be used for the analysis (see following section). The other indicators to be examined are optical luminosity, L, since it is likely that the number of cosmic ray sources is related to that of the stars, and neutral hydrogen mass, M_H. It is probable that for neutral pion decay and bremsstrahlung gamma ray production, the best indicator is some function of L and M_H.

(a) Gamma ray emission proportional to optical luminosity

The calculation of the absolute photographic luminosity of the Galaxy, L, is based on data given by Allen (1973). The absolute visual magnitude as seen from the direction of the Galactic pole outside the Galaxy is $M_v = -20.5$. Converting to photographic magnitude gives a value for M_{pg} of approximately -19.66. The corresponding luminosity, L_{max}, is $9.6\ 10^9\ L_\odot$. Calculation of the mean luminosity over all directions, $\bar{L}$,

involves a factor for absorption, and here exp (-0.36 cosec b) (Allen, 1973) is used. A rough estimate for $\bar{L}$ is therefore given by:

$$\bar{L} = \frac{L_{max}}{\exp(-0.36)} \int_0^{\pi/2} \exp(-0.36 \sec \phi) \sin \phi \, d\phi \qquad (6.8)$$

where $\phi = \frac{\pi}{2} - b$

i.e. $\bar{L} \approx 0.6 \, L_{max} = 6 \, 10^9 \, L_\odot$

Luminosity functions given by several authors have been investigated. In each case, the luminosities have been corrected to the photographic range and results scaled to H_o = 50 km s^{-1} Mpc^{-1}. The integral over luminosity of the density function times luminosity, $\overline{\eta L}$, has been found. From Kiang (1961), $\overline{\eta L} = 4.9 \, 10^{19} \, L_\odot \, (c/H_o)^{-3}$, whereas using in addition the absorption correction of Shectman (1973), $3.3 \, 10^{19}$ is found. This latter value agrees well with those from van den Berg (1961) ($3.7 \, 10^{19}$) and Shapiro (1971) ($3.6 \, 10^{19}$), and is used in the present analysis.

Equation 6.7 now yields,

$$\overline{\eta q(>100 \text{ MeV})} = 7.1 \, 10^{51} \, s^{-1} \, (c/H_o)^{-3}$$

i.e. from 6.5

$$j(E_\gamma) = 9.2 \, 10^{-7} \, cm^{-2} \, s^{-1} \, sr^{-1}$$

The high latitude background flux above 100 MeV recorded by Fichtel et al. (1975) is $2 \, 10^{-5}$ cm^{-2} s^{-1} sr^{-1}, and therefore the contribution from normal galaxies is less than 5%.

Recent work by Gott and Turner (1976) suggests that the data, on which the luminosity functions referenced above were based, were biassed by a

large local density enhancement. They find $\overline{\eta L} = 1\ 10^{19}\ L_\odot\ (c/H_o)^{-3}$, which implies an even lower percentage background contribution from normal galaxies, i.e. < 2%.

(b) Gamma ray emission proportional to neutral hydrogen mass

The mean density of HI for galaxies, $\overline{\eta M_H}$, is given by Rowan-Robinson and Fabian (1975) as $9\ 10^{18}\ M_\odot\ (c/H_o)^{-3}$ and the Galactic HI mass as $4\ 10^9\ M_\odot$. Using the value for $q_{Gal}(>100\ MeV)$ given above, equation 6.7 gives,

$$\overline{\eta q(>100\ MeV)} \simeq 3\ 10^{51}\ s^{-1}\ (c/H_o)^{-3}$$

i.e. from 6.5

$$j(E_\gamma) = 4\ 10^{-7}\ cm^{-2}\ s^{-1}\ sr^{-1}$$

This represents 2% of the observed background.

6.4.2. Calculation using Method B

The ratio $q(E_\gamma)/L_R(\nu)$ is found by comparing the intensity of the gamma ray longitude distribution for energies above 100 MeV given by Fichtel et al. (1975) (see figure 3.2), with the corresponding 150 MHz radio measurements of Landecker and Wielebinski (1970). The ratio varies by less than a factor of two with direction in the plane and is consistent with $(1\text{-}2)\ 10^{-7}\ cm^{-2}\ s^{-1}\ sr^{-1}\ K^{-1}$, where the radio measurement is of brightness temperature, T_b.

The contribution to the radio background from normal galaxies is estimated as 4° K at 178 MHz by Longair (1971) and 0.48° K at 408 MHz by Schmidt (1972). Assuming that $T_b \propto \nu^{-2.75}$, corresponding to a differential electron spectrum of slope -2.5, these values give, respectively,

6.4^{o} K and 7.5^{o} K at 150 MHz. From equation 6.6, the gamma ray flux above 100 MeV is given by $j(E_\gamma) = (6.4 - 15)\ 10^{-7}\ cm^{-2}\ s^{-1}\ sr^{-1}$, i.e. between 3% and 7% of the background.

Only about 20% of the diffuse radio background is from normal galaxies. The above estimates of Longair and Schmidt are derived from non-evolutionary models. It is therefore expected that similar results for the gamma ray flux would be obtained using Model A.

6.4.3. Discussion

All the estimates give fairly similar values for the normal galaxy contribution to the gamma ray background, i.e. less than 7% above 100 MeV. This value can be contrasted with 0.5% calculated by Rowan-Robinson and Fabian (1975) for the contribution from normal galaxies to the X-ray background. There is consistency since the differential spectrum of Galactic gamma rays has a slope flatter than -2 (figure 2.3) compared with about -2.4 for the background (figure A.1). It is evident that even if the percentage contribution were higher, the slope of the background could not be matched unless it were assumed that the Galactic cosmic ray slope is uncharacteristic of the average.

Evolution has not been considered. None is apparent in normal galaxy radio emission, unlike the case for the much stronger radio galaxies where probably a combination of luminosity and density evolution is most likely (Schmidt, 1972). However, recently Mattila (1976) has measured the extragalactic background brightness at 4000 $\mathring{A}$ and has found evidence for strong optical luminosity evolution. He has examined the difference in surface brightness between the dark nebula, L134, and its surroundings. A subtraction of the contribution of scattered starlight to the nebula is required, but this is based on a spectral analysis and gives a relatively

small possible error. He finds that the extragalactic background light is about 20 times that expected from non-evolutionary models and given, for example, by Shectman (1973). Although some optical evolution is likely, this factor is surprisingly high, especially since the effect of radio galaxy evolution on the radio background is only a factor of about 4 (see next section). Hopefully, a similar method will soon be used to study other dark nebulae.

This evolution has great significance to the present analysis. From section 6.4.1. it is seen that if optical luminosity alone is an indicator of gamma ray emission, close to 100% of the background may be predicted. However, it is difficult to justify using optical luminosity in preference to either radio luminosity or HI mass as a gamma ray indicator, and therefore, until more data are available, the results remain speculative.

6.5 THE CONTRIBUTION FROM RADIO GALAXIES

6.5.1. The radio background

Longair (1971) estimates that radio galaxies produce a background of 16-19° K at 178 MHz, which gives a total, when normal galaxies are included, of 20-23° K. This is a factor of four larger than obtained without inclusion of cosmological evolution. Evolution is found to have the same effect at 408 MHz, where Schmidt (1972) estimates a background of 1.5° K, giving a total, inclusive of normal galaxies, of 2° K. The present analysis is restricted to use of Method B.

The radio background attributed to radio galaxies, $I_R(\nu)$, can be expressed,

$$I_R(\nu) = 3.08\ 10^{-28}\ T_b\ \nu^2\ W\ m^{-2}\ sr^{-1}\ hz^{-1}$$

where ν is in MHz and T_b is brightness temperature in ^oK.

The above values give,

$$I_R \text{ (178 MHz)} = (1.6 - 1.8)\ 10^{-22} \text{ W m}^{-2} \text{ sr}^{-1} \text{ hz}^{-1}$$

$$I_R \text{ (408 MHz)} = 7.7\ 10^{-23} \text{ W m}^{-2} \text{ sr}^{-1} \text{ hz}^{-1}$$

6.5.2. Calculation assuming similarity to normal galaxies

A rough estimate of the gamma ray background contribution from radio galaxies can be obtained assuming $q(E_\gamma)/L_R(\nu)$ is the same as for normal galaxies (see section 6.4.2). Using equation 6.6, this leads to a flux above 100 MeV of (2-7) 10^{-6} cm^{-2} s^{-1} sr^{-1}, i.e. 10% to 35% of the background.

6.5.3. Result based on M87

At present there are no observations at 100 MeV of gamma rays from radio galaxies. However, an upper limit to the M87 flux of 1.0 10^{-6} cm^{-2} s^{-1} (>100 MeV) has been found by Fichtel et al. (1975). The 178 MHz flux is 970 Jy (see Burbidge, 1970). Using I_R (178 MHz) above,

$$j_\gamma (>100 \text{ MeV}) < 2\ 10^{-5} \text{ cm}^{-2} \text{ sr}^{-1} \text{ s}^{-1}$$

This is just compatible with the observed value.

6.5.4. Result based on Cen A

Observations of gamma rays in the range 1 - 10 MeV from the nearest radio galaxy, Centaurus A, are reported by Hall et al., (1976) (see section A.5 and table A.6). They find line emission at 1.6 MeV and 4.5 MeV, superimposed on a power law continuum of differential slope about -1.9. The 178 MHz flux is about 4800 Jy (see Burbidge, 1970). Assuming Cen A is a typical radio galaxy, using equation 6.6 and I_R (178 MHz) as above, a gamma ray flux $F(E_\gamma)$ cm^{-2} s^{-1} eV^{-1} will give a background from this class of source of,

$$j(E_\gamma) \approx F(E_\gamma) \times 3.6 \text{ cm}^{-2} \text{ s}^{-1} \text{ sr}^{-1} \text{ eV}^{-1}$$

The data points of Hall et al. (1976) have been converted to background flux in this manner and are shown in figure 6.1. The Apollo and SAS-2 background results from figure A.1 are shown for comparison, along with the flux attributed to an extragalactic origin by Fichtel et al. (1977b). The sharp line features will be smoothed to a continuum by the differing redshifts of the sources, and therefore there is evidence that radio galaxies should be a principal contributor to the background in the 1 - 10 MeV range.

The radio emission from Cen A (NGC 5128) comes mainly from large lobes, which extend well beyond the optical image and cover several degrees on the sky. About 1% appears to come from the central nucleus, which is also a source of X-ray and near-infrared radiation. Grindlay et al. (1975) have observed very high energy gamma rays ($\gtrsim$300 GeV) which are from a smaller region than the full radio source. Attributing this emission to the nucleus alone, Grindlay (1975) has modelled the region to fit also the X-ray and infrared measurements. The model comprises component A, which is of angular size $4\ 10^{-4}$ arcsec and magnetic field 2 gauss, and component B, of size $9\ 10^{-3}$ arcsec and field 0.01 gauss. Each region is a strong synchrotron emitter, producing the majority of radiation below 10^5eV, which acts as a photon field for inverse Compton scattering, the major source of the radiation above 10^5eV. The inverse Compton contributions from the A and B components, along with the high energy data point, are shown in figure 6.1, scaled to correspond to the background flux as for the 1 - 10 MeV measurements.

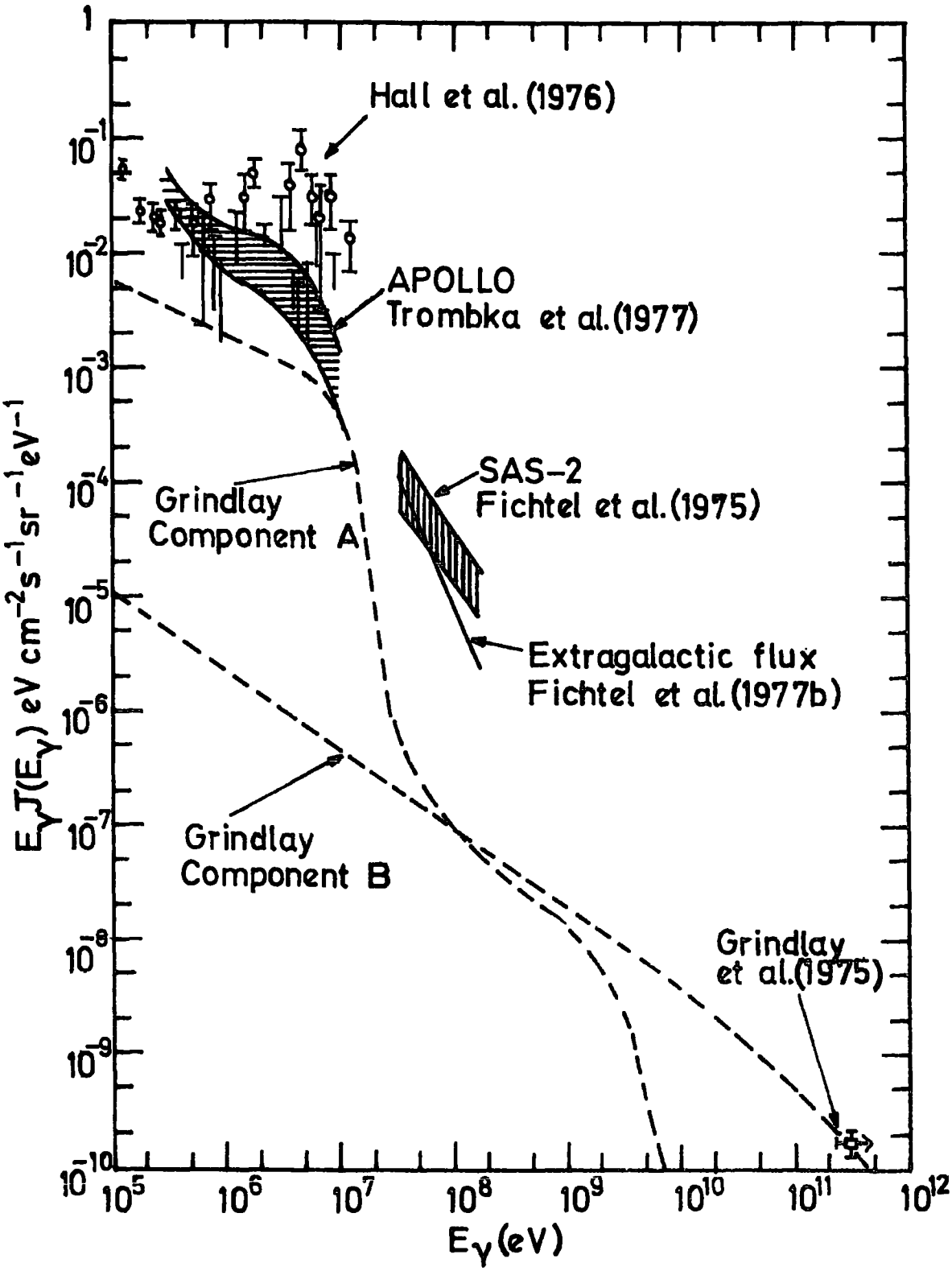

Figure 6.1 The contribution to the diffuse gamma ray background, represented by the SAS-2 and Apollo results, from radio galaxies. The data points, T (upper limits) and ⨽, relate to Cen A, scaled to represent the order of contribution to be expected from radio galaxies. The dashed lines are the two components of the model of Grindlay(1975) for the nucleus of Cen A, similarly scaled. Also shown is the flux attributed to an extra-galactic origin by Fichtel et al.(1977b).

The Grindlay model suggests that the continuum seen by Hall et al. (1976) is also from the nucleus. A certain degree of variability for the nucleus must be invoked for all the measurements to be consistent, and at other observing times the 1 - 10 MeV flux may be as much as a factor of ten lower. However, from figure 6.1 it is evident that this would not significantly affect present conclusions.

A problem with the present analysis is that, if the Grindlay model is correct, the relationship between gamma rays emitted from a central nucleus and radio emission from wide lobes is being expected to be roughly a constant for all radio galaxies. However, Hall et al. (1976) were not able to determine the size of the gamma ray emitting region and the possibility remains that this is of similar extent to the radio or optical regions.

There are unfortunately no Cen A gamma ray observations at 100 MeV. The Grindlay model predicts a very small flux from the nucleus.

6.5.5. Summary

The observations of Cen A, together with an evolutionary model, suggest that radio galaxies can produce the 1 - 10 MeV background flux if the gamma ray and radio luminosities are proportional. There is as yet no evidence for a large contribution at higher energies.

6.6 CONSIDERATION OF OTHER CLASSES OF OBJECT

6.6.1. Clusters of galaxies

Rowan-Robinson and Fabian (1975) estimate a contribution to the 4 keV X-ray background from Abell clusters of 22 - 65% or 5 - 7%, with or without a cosmological evolution factor respectively.

Two processes have been proposed for X-ray production in clusters of galaxies, i.e. inverse Compton and thermal bremsstrahlung. If the former is dominant, significant contribution to the background at gamma ray energies is expected, since the spectrum will be harder than that of the background for an electron spectrum similar to that of the Galaxy. If thermal bremsstrahlung is dominant, the gamma ray contribution from clusters will be negligible.

Spectral resolution of current data is generally not good enough for the production mechanism to be distinguished. Uhuru observations favour a bremsstrahlung spectrum, strongly for Virgo and marginally for Perseus, although either spectra fit observations of Coma (Kellogg et al., 1975). Data from the Copernicus experiment for both Perseus (Fabian et al., 1974) and Centaurus (Mitchell et al., 1975) can be fitted equally well by power law or thermal spectra.

A correlation between the radio and X-ray luminosities of clusters would be suggestive of an inverse Compton X-ray and synchrotron radio flux from the same electron spectrum. Rowan-Robinson and Fabian (1975), using data from 18 Abell clusters, find no general correlation.

Authors of theoretical papers now appear mainly biassed in favour of thermal bremsstrahlung origin. However, further observations are awaited.

6.6.2. Seyfert galaxies

Seyfert galaxies are significant in that they are found by Rowan-Robinson and Fabian (1975) to provide possibly the highest contribution to the X-ray background, i.e. 30 $\pm$ 24% without evolution. Their estimate is based on two observations and two upper limits and has a large error.

Predictions in the gamma ray band are completely model dependent as there are no observations. As for clusters, if the X-ray production

mechanism is inverse Compton then a significant contribution to the gamma ray background is expected. Discussion of one such model is presented elsewhere (Strong et al., 1976). However, the X-ray production mechanism is uncertain and so no useful conclusions are at present possible.

CHAPTER SEVEN

A MODEL FOR THE GALACTIC HALO

7.1 INTRODUCTION

Although inverse Compton scattering is found to be of minor importance for gamma ray production in the Galactic plane, it will dominate in the low gas density region outside the disc. Here gamma rays are expected from scattering of electrons on the 2.7° K blackbody radiation field as well as on starlight and far infrared radiation coming from the Galaxy. The magnitude of the inverse Compton flux depends on the density of electrons in the region, which in turn depends on their method of leakage from the disc.

There has been much debate as to whether or not an electron "halo" exists around the Galaxy. Free electron escape from the disc gives no such feature whereas the currently popular diffusion models do. The potential of a halo for producing gamma rays is great and therefore it is of importance that a realistic model should be investigated. Even if results give less than the observed high latitude flux, such a contribution should be subtracted before considering any remaining isotropic (extragalactic) flux.

Added support for the importance of a halo investigation comes from the very recent realisation that possibly the electron to proton density ratio in the disc is elsewhere higher than observed at the Sun. This is based on two factors:

(a) The steep Galactic gamma ray spectrum recently observed (section A.5) implies that bremsstrahlung relative to neutral

pion production may be higher elsewhere than that calculated locally.

(b) There is a discrepancy in the plane between the observed local electron spectrum and that expected using local magnetic field values and radio data (see section 2.3).

Evidence from non-thermal radio data that a halo to our Galaxy exists is discussed in the next section, and a model for the electron behaviour is developed in the rest of this Chapter.

7.2 EVIDENCE FOR A GALACTIC HALO

7.2.1. Observations of external galaxies

Evidence that an external galaxy similar to our own possesses an electron halo is reported by Sancisi et al. (1974). They have studied NGC 891 which is a nearly edge-on spiral with a disc size similar to that of the Galaxy. Observations at 1415 MHz show a flattened radio synchrotron halo extending beyond the 21cm HI observations to a height, z, of about 5-6 kpc.

At present the only other edge-on Galaxy reported to exhibit a halo is NGC 4631 (Ekers and Sancisi, 1977). This is a late type, slightly irregular galaxy with strong radio emission from its central region, and therefore comparison with the Galaxy may not be appropriate. However, excluding the central 3 kpc, the disc radio emission is similar to that of the Galaxy. The radio halo is non-spherical (flattened in z) as for NGC 891, and it exhibits a radio spectrum which steepens away from the plane.

It is desirable that observations should be made of other edge-on spiral galaxies so that electron propagation models can be tested,

although it should be remembered that use of synchrotron data requires assumptions about the magnetic field to be made.

7.2.2. High latitude radio measurements of the Galaxy

Webster (1975) has shown that low frequency drift scan measurements at various declinations are inconsistent with a constant spectral slope for different high Galactic latitudes. He interprets the results as evidence for a Galactic halo in which the electron spectrum is steeper than that in the disc. In his crude model a spherical halo is uniformly filled with electrons and magnetic field and he calculates limits on the size and emissivity of such a feature.

Bulanov et al. (1976) pointed out that a spatially independent spectral index underestimates the halo emissivity. It is therefore important to use a physical model such as one with electron diffusion. Here energy losses cause the steepening of the spectrum away from the disc.

Many diffusion models have been developed in the past for the Galaxy although the lack of observational constraints on such models, and the fact that large halos around other galaxies were not seen, has led to much doubt and debate. Various geometries have been assumed and the usual approach has been to search for consistency with Galactic radio emission and local lifetimes (see, for example, Dögiel et al. 1975). The conventional idea of a halo has been a large scale structure, perhaps a spherical region with the radius of the Galactic disc. This clearly is not indicated by external galaxies, nor is it the case for a diffusion model with a relatively small diffusion coefficient. Evidence is now in favour of a flattened feature extending to a height of a few kpc.

Strong (1977) has recently developed a method for comparing the results of a diffusion model with drift scan radio data which is independent of the

emission from the disc. He finds consistency with a halo diffusion mean free path, λ, in the range 1 - 17 pc, set by the amount of fall-off of magnetic field towards the anticentre direction in the halo. $\lambda = 1$ pc is for the case in which the halo field is uniform and about 0.2 of that in the disc, causing the FWHM of the 17.5 MHz emission to be about 6 kpc. Recent work of Owens and Jokipii (1977) agrees with a value of λ close to 1 pc.

7.3 A MODEL FOR ELECTRON DIFFUSION FROM THE DISC

7.3.1. Equations for the spatial electron density distribution

There are two extreme approaches to halo diffusion. In the first, the disc and halo are indistinguishable as far as propagation is concerned. This neglects the probable influence of known physical differences between the two regions. In the second approach, that adopted here, the disc is considered to be a containment region out of which the electrons leak. The disc boundary is typically at z between 250 pc and 500 pc, and from the Sun out to these distances the local electron density is assumed.

In the present model, the disc-halo boundary is considered to be almost totally reflecting such that the effect of particles diffusing back into the disc from the halo can be neglected.

The solution to the 3-D diffusion equation for a point source in infinite space with synchrotron and inverse Compton energy losses is given in Appendix B. The insertion of a double-sided totally reflecting plane mirror at the source does not affect the boundary condition there, i.e. $\nabla . n = 0$, and therefore the solution can be used in the present case. The electron density at a distance s away from the source is given by (equation B.23):

$$n(E,s) = \frac{AE^{-\Gamma}}{4Ds\,\pi^{3/2}} \exp(-x)\, x^{\frac{1}{2}} \int_0^{\infty} e^{-xt}\, t^{\Gamma-2}\, (1+t)^{-\Gamma+3/2}\, dt \qquad (7.1)$$

where,

$$x = \frac{bEs^2}{4D} \qquad (7.2)$$

and the energy losses are given by

$$\dot{E} = -\, bE^2 \qquad (7.3)$$

The coefficient of the source function, which is assumed to be a single power law in energy of differential slope $-\Gamma$, is A. D is the diffusion coefficient. In the present model the source region is assumed to be a flat disc of radius R with uniform emission per unit surface area. For z much greater than the Galactic disc thickness, i.e. $z \gtrsim 0.5$ kpc, it is a good approximation to treat the disc as a surface of negligible thickness. The electron density at a position in the halo is therefore a surface integration over point sources in the plane. Figure 7.1 shows the geometry.

We consider a point P(r,z), where r, z are cylindrical polar co-ordinates with an origin at the Galactic centre. All points in the disc at an equal distance, s, from P contribute an amount n(E,s) given by equation 7.1. These sources lie on the circumference of a circle of radius r_1 in the disc.

Writing,

$$n(E, r_1, z) = n(E, s) \qquad (7.4)$$

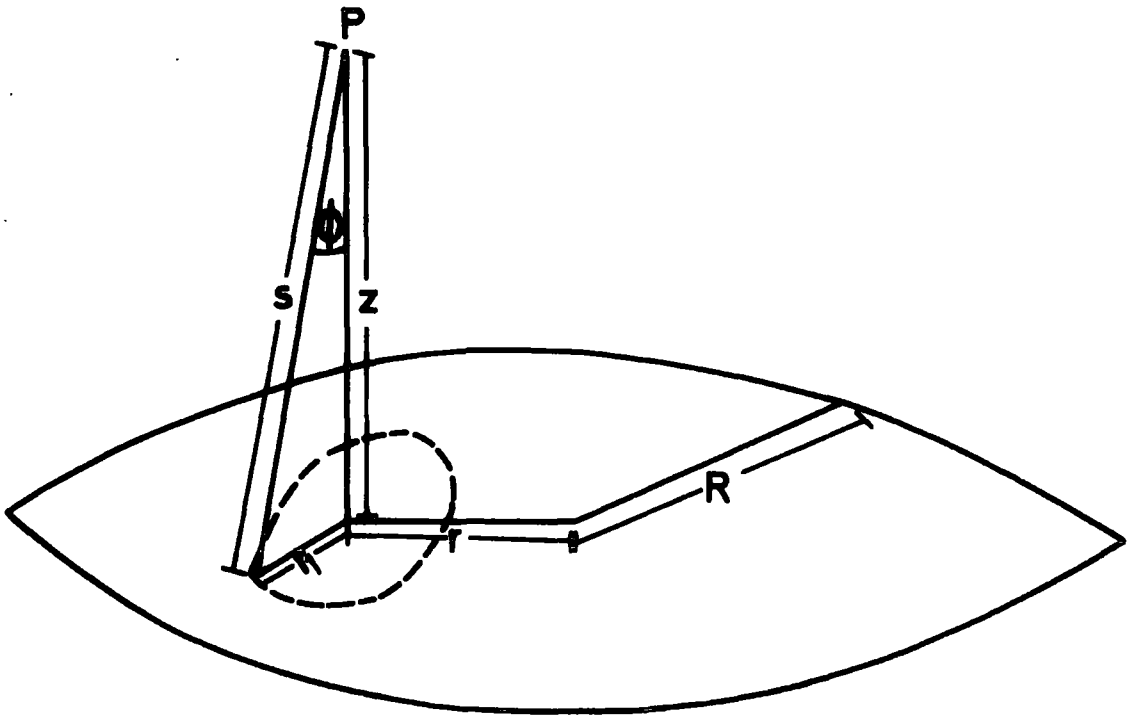

Figure 7.1 The geometry used in the calculation of the electron density as a function of position in the Galactic halo.

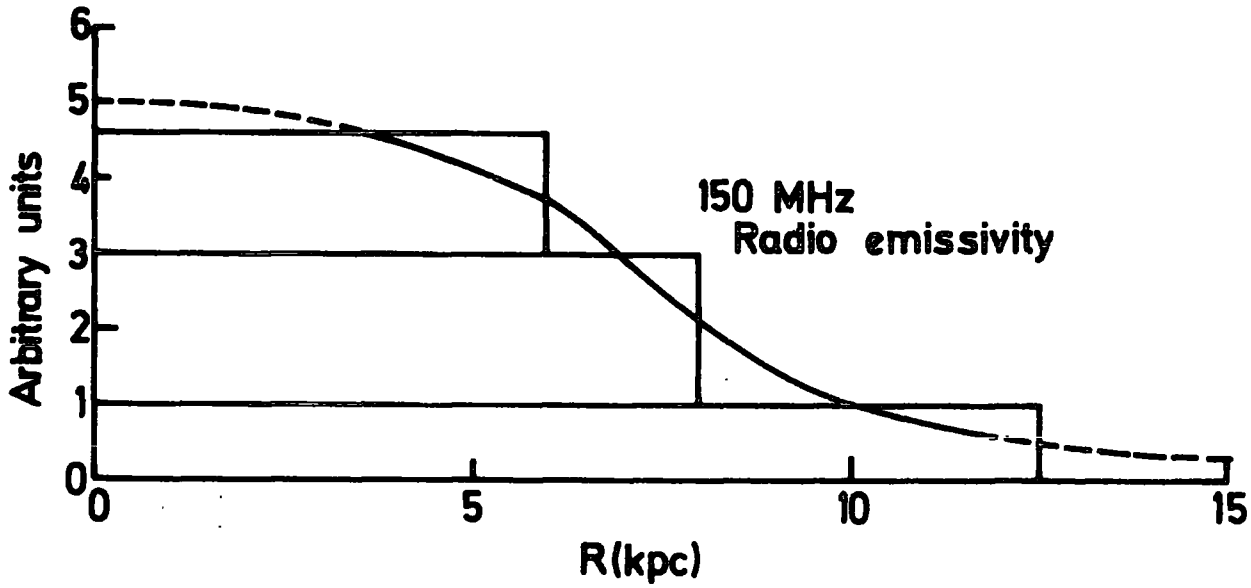

Figure 7.2 150 MHz radio emissivity as a function of Galactic radius (in arbitrary units) from Ilovaisky and Lequeux(1972). The distribution is approximated for Model 2 by three superimposed discs as shown.

the density at P due to the sources is,

$$n(E, r, z, r_1) = 2\, r_1\, \Theta(r_1, r)\, n(E, r_1, z) \tag{7.5}$$

where,

$$\Theta(r_1, r) = \begin{cases} \pi \text{ if } r_1 \leq R-r \\ \cos^{-1}\left[\dfrac{R^2-r^2-r1^2}{2rr_1}\right] \text{ if } r_1 > R-r \end{cases} \tag{7.6}$$

$$(0 < \Theta < \pi)$$

The integral over all possible values of r_1 is given by:

$$n(E, r, z) = \int_{r_{1,min}}^{r_{1,max}} 2r_1\, \Theta(r_1, r)\, n(E, r_1, z)\, dr_1 \tag{7.7}$$

where,

$$r_{1,max} = R + r \tag{7.8}$$

$$r_{1,min} = \begin{cases} r-R & \text{if } r > R \\ 0 & r < R \end{cases} \tag{7.9}$$

As long as the source distribution can be expressed as a function of R (radial symmetry in the disc), the above method can be used where we sum over superimposed discs of radii R_k and relative emissions given by A_k.

7.3.2. The effect on the electron spectral slope

The present model is only applicable if the electron source distribution can be expressed as a power law with a single differential slope, $-\Gamma$.

Consider a point in the plane ($z = 0$). Suppose that the surface is not of radius R but has an infinite radius. In this case the density

of electrons of energy E at any point in the plane is given by the integration of equation B.19 over all r from zero to infinity:

$$n(E) = AE^{-\Gamma} \int_0^{1/bE} d\Theta\, (1-b\Theta E)^{\Gamma-2} \frac{1}{(4D\pi\Theta)^{3/2}} \int_0^{\infty} e^{-r^2/4D\Theta}\, 2\pi r\, dr \qquad (7.10)$$

$$n(E) = AE^{-\Gamma} \int_0^{1/bE} d\Theta\, (1-bE\Theta)^{\Gamma-2} \frac{1}{(4D\pi\Theta)^{3/2}}\, 4D\Theta\pi \qquad (7.11)$$

let $U = bE\Theta$

$$n(E) = AE^{-\Gamma} \int_0^{1} \frac{dU}{bE} (1-U)^{\Gamma-2} (4D\pi)^{-\frac{1}{2}} U^{-\frac{1}{2}} (bE)^{\frac{1}{2}} \qquad (7.12)$$

Therefore,

$$n(E) = AE^{-(\Gamma+\frac{1}{2})} \int_0^{1} dU\, (1-U)^{\Gamma-2} (4D\pi Ub)^{-\frac{1}{2}} \qquad (7.13)$$

Thus in the plane the electron spectrum is steeper by $E^{-\frac{1}{2}}$ than the source spectrum. In the physical situation the plane is not infinite and the steepening, an increasing function of energy, lessens as the disc size decreases and as λ increases. For given parameters, there will be some energy below which the steepening is negligible.

7.4 THE ELECTRON DENSITY AS A FUNCTION OF POSITION IN THE HALO

7.4.1. Parameters for the model

For the physical model and solution of equation 7.7, values for Γ, D, b, A_k and R_k are required.

The disc electrons act as the source for the halo. A spectral slope characteristic of that ambient in the plane must be chosen and, assuming the local value to be typical, $\Gamma = 2.5$ is employed. This is the spectral

slope of local electrons with energies most appropriate for producing gamma rays of about 100 MeV (see equation 2.12).

Calculations have been made for two values of the diffusion mean free path, λ (=3D/c). These are λ = 2 pc and λ = 20 pc, which are values roughly consistent with the range found by Strong (1977) (see section 7.2.2). For the energy losses (equation 7.3), b = 6 10^{-17} GeV^{-1} s^{-1} is taken. In fact b should decrease with distance from the disc (the infrared and starlight energy densities and probably the magnetic field decrease). However the approximation of energy independence for b is valid since it is clear from equation 7.1 that the diffusion coefficient, D, has a greater influence on the solution and this itself is uncertain by a factor of about ten.

Two models for the electron source distribution are taken. For Model 1 there is a uniform injection rate per unit area from a 12.5 kpc radius disc. For Model 2 the injection rate is allowed to increase towards the Galactic centre consistent with the radial unfolding of the 150 MHz radio emissivity given by Ilovaisky and Lequeux (1972). As shown in figure 7.2, the distribution is approximated by 3 superimposed discs.

Obviously it is unphysical to allow a build-up of electron density at the disc-halo boundary. The condition is therefore applied that the local density is also that at R = 10 kpc, z = 500 pc. From the arguments in section 7.3.2 the slope here may be steeper than that of the source spectrum. The energy chosen for the normalisation is 1 GeV since this is approximately the minimum that is of interest in the inverse Compton calculations, electrons of lower energy only contributing to the gamma ray flux below about 10^7eV from scattering on starlight. Figure 7.3 shows

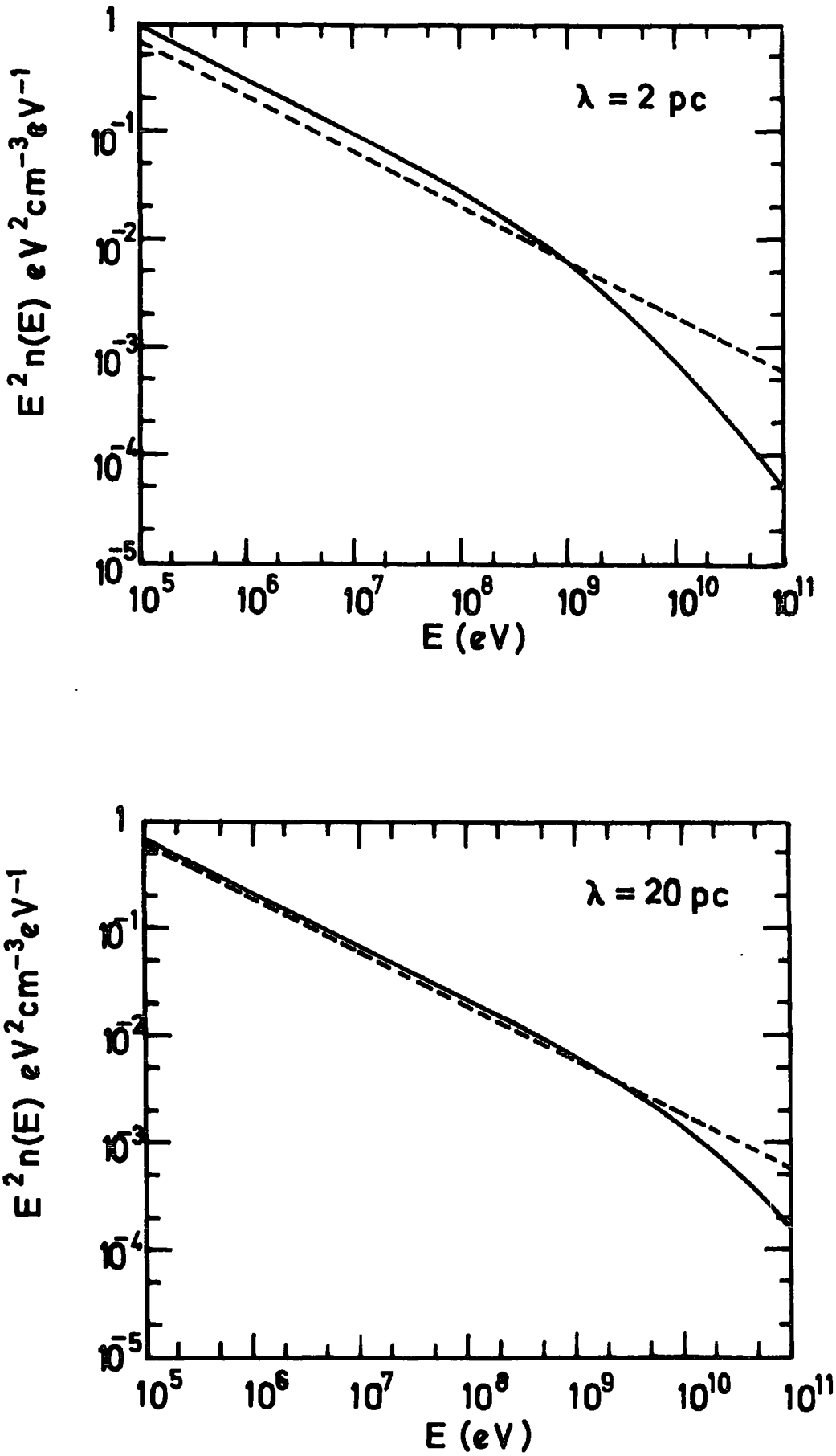

Figure 7.3 Differential electron density spectra (times E^2) for λ=2 pc and λ=20 pc at R=10 kpc, z=500 pc, normalised to the local density at 1 GeV. Results are for Model 1. The dashed lines indicate power laws of differential slope -2·5.

the calculated differential electron density spectra at the normalisation position for Model 1 and λ = 2, 20 pc. Comparison with the source spectrum, a power law of differential slope - 2.5, which takes the local density given by Goldstein et al. (1970) at 1 GeV, shows that normalisation at this energy is reasonably good. The slight build-up of electrons of lower energies in the halo, more apparent for λ = 2 pc as expected, will in fact require preferential leakage back into the disc for equilibrium to be restored.

The normalisation maximises the electron density in the halo relative to that in the disc. However the arguments expressed in section 7.1 support the possibility that we measure a local electron intensity which is less than that elsewhere close to the Sun and so therefore the calculation probably gives realistic electron densities in the halo, rather than upper limits.

The values for A for combinations of Models 1 and 2 with the two values for λ, are given in table 7.1. It is seen that, to maintain the same density at z = 500 pc, the injection rate is higher for the larger λ value since the particles can now get away very much faster.

A rouch check can be made that the calculated values of A are not inconsistent with measured lifetimes of cosmic rays in the disc. This is only approximate since no attempt has been made to model the disc itself where diffusion possibly also occurs but not necessarily with the same mean free path as for the halo. We can however make an order of magnitude check on the parameters needed in the disc for the required leakage over the boundary. The local electron density is written:

$$n_e(E) = \frac{4\pi}{c} j(E) \qquad (7.14)$$

Table 7.1 Values for the coefficient A, where the electron injection rate into the halo per unit surface area is expressed; $A\ E^{-\Gamma}\ cm^{-2}\ s^{-1}\ GeV^{-1}$.

Model 1 consists of a uniform 12.5 kpc radius disc with injection rate coefficient A.

Model 2 consists of a superposition of 3 discs:

(a) Radius 12.5 kpc, injection rate coefficient A.

(b) Radius 8 kpc, injection rate coefficient 2A.

(c) Radius 6 kpc, injection rate coefficient 1.6A.

Also given are values for d/τ derived using equation 7.15.

Electron source distribution	Diffusion mean free path λ(pc)	A	d/τ (pc yr^{-1})	τ(yr) for d = 500 pc
Model 1	2	$4.7\ 10^{-5}$	$7.8\ 10^{-5}$	$6.4\ 10^{6}$
Model 1	20	$3.4\ 10^{-4}$	$5.7\ 10^{-4}$	$8.8\ 10^{5}$
Model 2	2	$2.6\ 10^{-5}$	$4.3\ 10^{-5}$	$1.2\ 10^{7}$
Model 2	20	$1.9\ 10^{-4}$	$3.2\ 10^{-4}$	$1.6\ 10^{6}$

where j(E) is given by equation 2.12. For E = 1 GeV we can write:

$$A \approx \frac{4\pi}{c}\, j(E = 1\ \text{GeV})\, \frac{d}{\tau} \qquad (7.15)$$

where d is the electron disc $\frac{1}{2}$-thickness and τ is the lifetime. Taking a probable value for d of 500 pc, the values for τ are calculated (see table 7.1). Except for Model 1 and λ = 20 pc, which gives a rather low value, the others are consistent with the observed lifetime range (see section 4.4). The value most consistent with recent data is that for Model 2 and λ = 2 pc. This combination is itself more probable than the others since it includes a rise in the electron source density towards the Galactic centre and a mean free path more consistent with work outlined in section 7.2.2.

7.4.2. Derived electron density contour plots for the Halo

Equation 7.7 has been solved using parameters given in the previous section. For illustration, figures 7.4(a-d) show some electron density contour diagrams. In each case the results for λ = 2 pc are shown in the upper hemisphere and those for λ = 20 pc in the lower. Plots for 4 GeV, 40 GeV and 180 GeV are given since these are characteristic of the production of 100 MeV inverse Compton gamma rays on starlight, far infrared and 2.7° K blackbody radiation respectively. Contours are for $z \gtrsim 2$ kpc. The figures give an indication of the "size" of the halo at the various electron energies.

In the following Chapter, calculations of the gamma ray flux using the present diffusion model are presented.

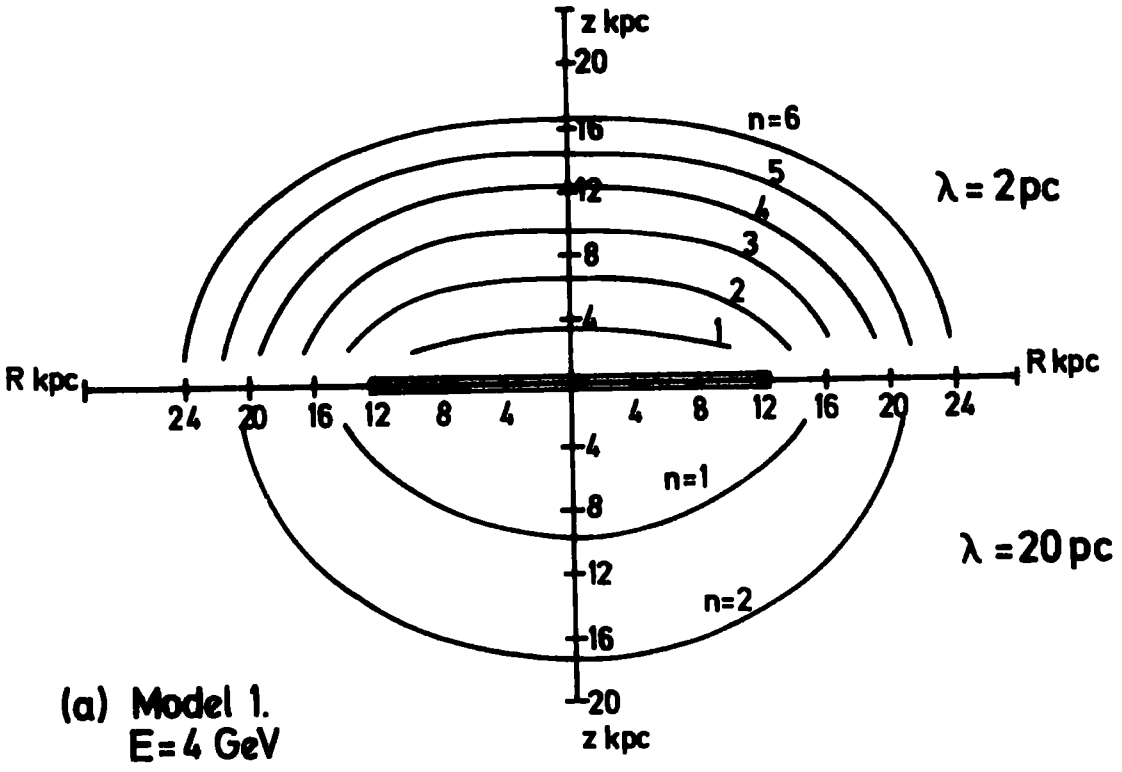

(a) Model 1.
E = 4 GeV

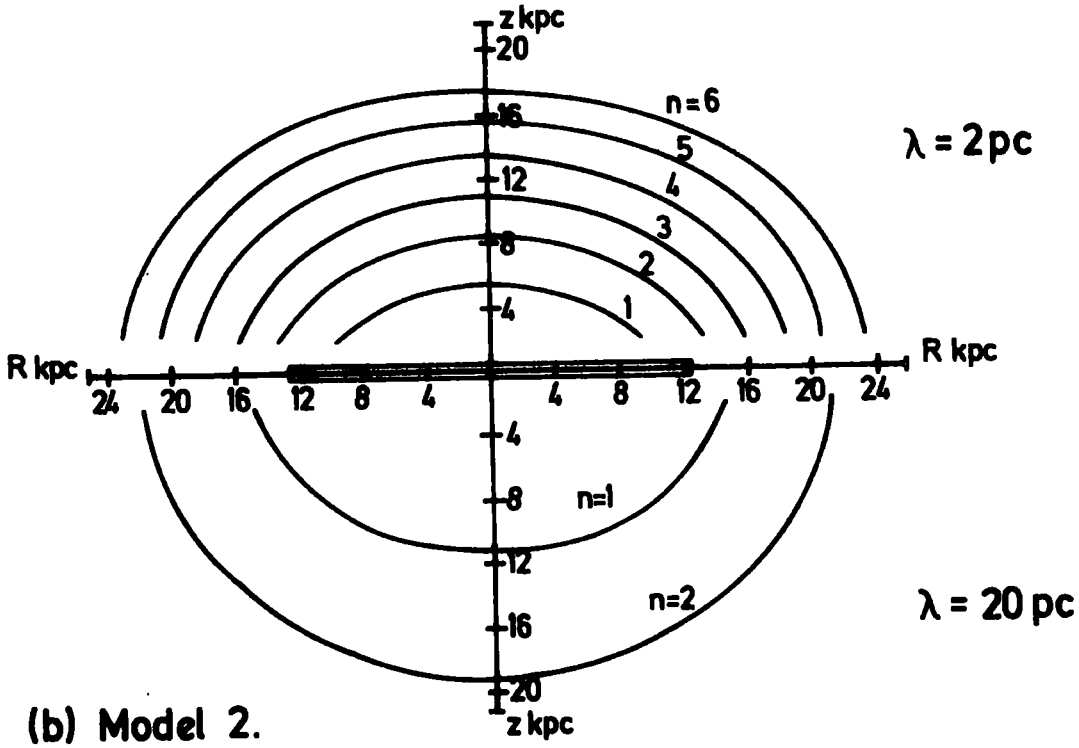

(b) Model 2.
E = 4 GeV

Figure 7.4 Contour plots of electron density for $z \geq 2$ kpc. The nth contour represents $10^{-0.4n}$ times the local density, i.e., consecutive contours represent a change in density of a factor of about 2.51.

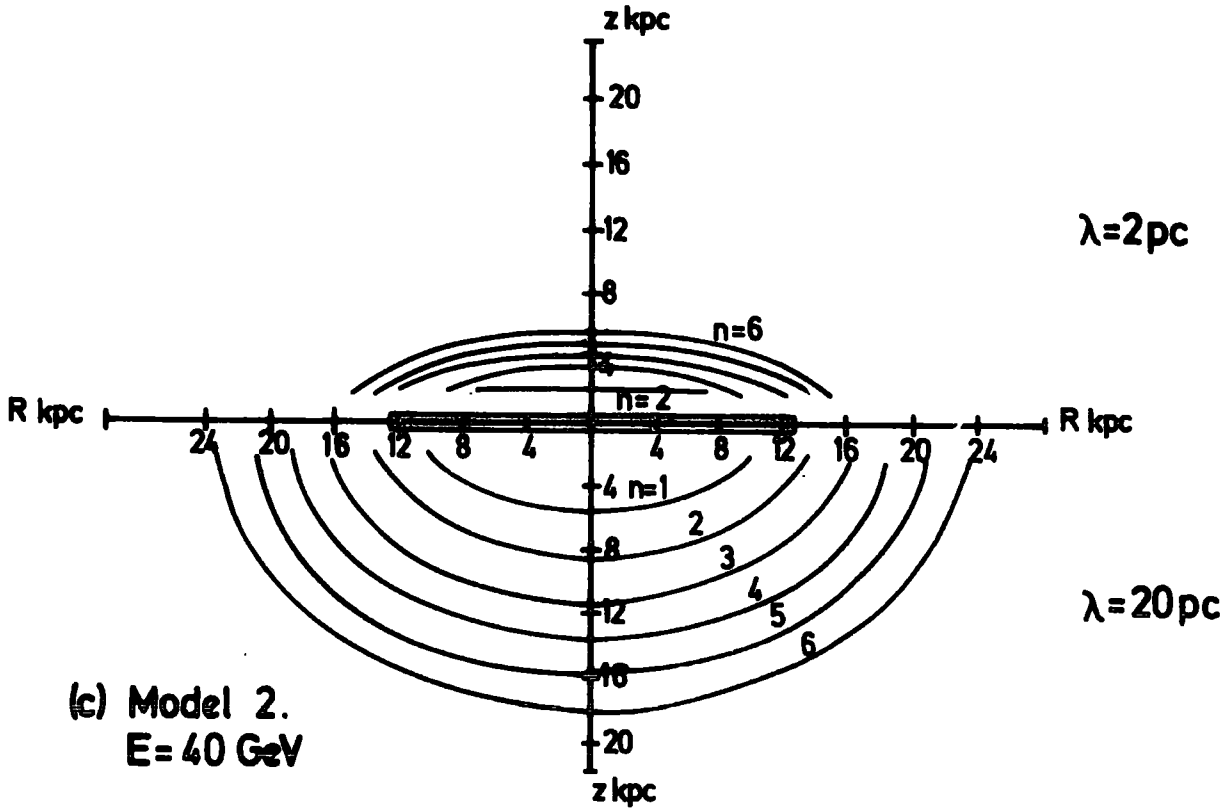

(c) Model 2.
E = 40 GeV

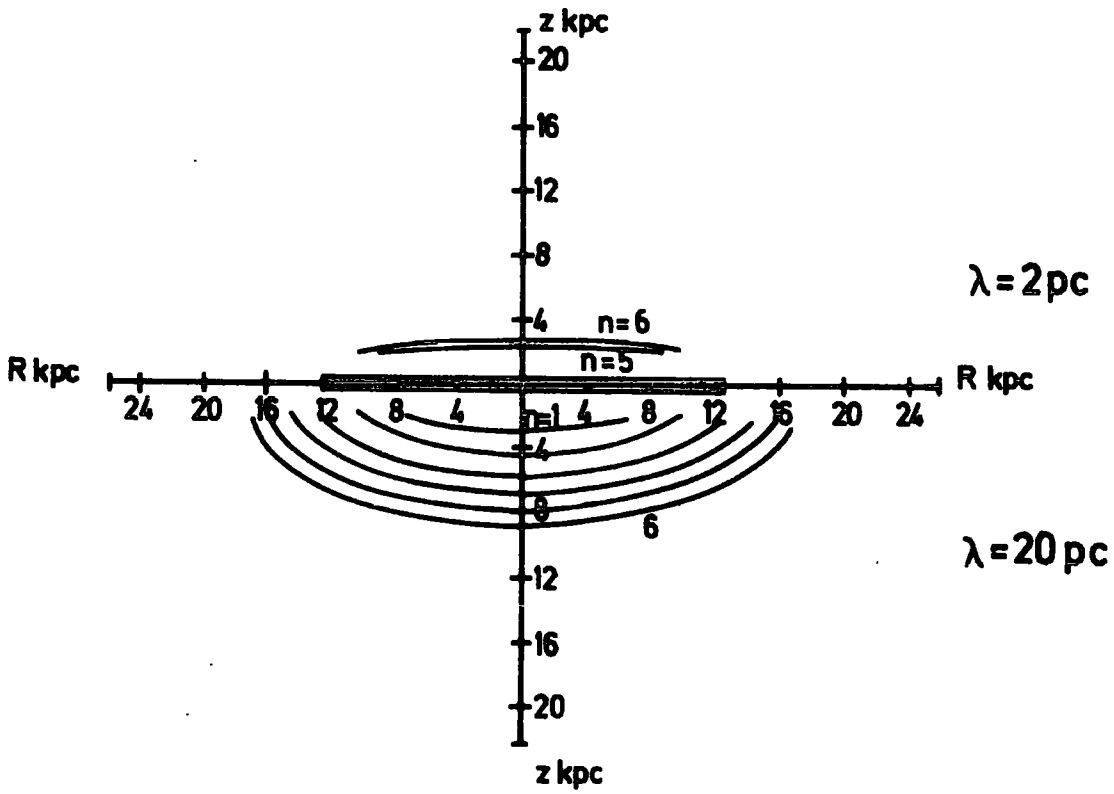

(d) Model 2.
E = 180 GeV

CHAPTER EIGHT

A CALCULATION OF THE GAMMA RAY FLUX FROM INVERSE COMPTON SCATTERING IN THE GALACTIC HALO

8.1 IMPORTANT FEATURES OF THE CALCULATION

In early models for the high latitude inverse Compton gamma ray flux, halos of chosen dimensions were assigned uniform electron intensities. There has been disagreement as to the importance of the mechanism, reflecting differences in the choice of values for halo size and electron density. For example, the first calculations (Felten and Morrison, 1966; Fazio et al., 1966) resulted in a flux below that observed, whereas Bhatia and Tandon (1971), using a higher electron intensity more representative of that observed locally in the disc, found that the 100 MeV high latitude flux could be completely accounted for by inverse Compton interactions. These calculations, although bearing little resemblance to the physical situation, indicate the potentiality of the production mechanism.

The present model is parameterised by the electron diffusion mean free path, which is constrained by the synchrotron measurements but still, unfortunately, uncertain by a factor of ten. The slower the electrons diffuse, the closer to the disc they lose energy, thus causing a steeper gamma ray spectrum.

The test for the model is the predicted anisotropy. Results of high latitude scans in the future should enable the diffusion mean free path and the contribution to the gamma ray flux to be firmly established.

Two important features new to the present calculations are the inclusion of the far infrared photon field, the importance of which has only recently been realised, and consideration of the geometry of the scattering rather than assuming, as has been done in the past, that the starlight is isotropic. After scattering, the gamma ray is beamed in the direction of the electron. Since the starlight and infrared photons are moving away from the plane there is a higher ingredient of head-on collisions than in the isotropic case.

8.2 THE INVERSE COMPTON SCATTERING EQUATIONS

8.2.1. The gamma ray flux

If the photon volume emissivity is $q(E,\underline{s})$ and the electron density is $n(E_e,\underline{x})$, where $\underline{s}$ and $\underline{x}$ are position vectors with respect to the Sun, the differential gamma ray flux from $\underline{x}$, $j(E_\gamma,\underline{x})$ is,

$$j(E_\gamma, \underline{x}) = \frac{1}{16\pi^2} \int dx \iiint d^3(\underline{s}-\underline{x}) \frac{(1-\theta)}{|\underline{s}-\underline{x}|^2} \cdot \int dE_e \; n(E_e, \underline{x}) \int dE \; q(E, \underline{s}) \frac{d\sigma}{dE_\gamma}(E_\gamma, E, \theta, E_e) \tag{8.1}$$

where

$$\theta = \frac{\underline{x} \cdot (\underline{s}-\underline{x})}{|\underline{x}||\underline{s}-\underline{x}|} \tag{8.2}$$

The inverse Compton differential cross section is given by equation 2.24, for $E' = \gamma E(1-\theta)$.

The method of calculation of $n(E_e, \underline{x})$ is given in the previous Chapter.

Equation 8.1 is reduced from a 6-fold to 4-fold integration by use of two approximations. Firstly, using the argument after equation 2.37, a discrete value of photon energy for each of the three photon fields is assumed. Secondly, the volume integration over photon sources is reduced to a surface integration for the cases of infrared and starlight since, as for electrons, at positions in the halo the disc appears to be a surface source.

For the isotropic 2.7° K photon field the gamma ray differential emissivity is given by equation 2.35 and the flux by 2.7 where,

$$j(E_e, \underline{r}) = \frac{c}{4\pi} n(E_e, \underline{r}) \qquad (8.3)$$

In each high latitude direction, the nearest 500 pc along the line of sight is taken to be the disc contribution. This is calculated separately using the local electron intensity and isotropic photon distributions of the local energy density. The adopted local electron spectrum is a power law of differential slope -2.5 (since a single slope is required for the diffusion model), normalised at 1 GeV to the spectrum given in equation 2.12.

8.2.2. The geometrical factor

For illustration of the importance of including the correct geometry, the gamma ray flux for head-on electron-photon collisions is compared with that for an isotropic photon field. Two factors contribute. For head-on collisions, firstly the reaction rate is higher, and secondly, to give a gamma ray of a specific energy, lower energy electrons, of which there is a higher density, are required.

Referring to section 2.4, for head-on collisions $E' = 2\gamma E$. Using the condition $E_\gamma << E_e$ and the definition of X,

$$X = \frac{E_\gamma}{4\gamma^2 E}$$

the cross section from equation 2.24 can be written,

$$\frac{d\sigma}{dX}(E_\gamma, E', E_e) = \frac{3}{2}\sigma_T (1 + 2X^2 - 2X) \tag{8.4}$$

From 2.18 we find,

$$\frac{d\sigma}{dX}(E_\gamma, E, E_e) = 3\sigma_T (1 + 2X^2 - 2X) \tag{8.5}$$

The cross section for an isotropic photon distribution is given by equation 2.26. Comparison of the integrals of equations 8.5 and 2.26 shows that the total reaction rate is doubled for the case of all head-on as opposed to isotropic collisions. From the above equations $\bar{X} = 1/2$, to be compared with the value of 1/3 found for isotropic scattering.

From equation 2.33, the differential gamma ray emissivity is written:

$$q(E_\gamma) \propto \int \frac{d\sigma}{dX}(E_\gamma, E, E_e)\, j(E_e) \frac{dE_e}{dE_\gamma}\, dX \tag{8.6}$$

Consider an electron spectrum which is a single power law of differential slope $-\Gamma$

$$q(E_\gamma) \propto \int_0^1 \frac{d\sigma}{dX}\, X^{(\Gamma-1)/2}\, dX \tag{8.7}$$

For isotropic collisions,

$$q(E_\gamma) \propto 6\sigma_T \left[\frac{1}{\Gamma+1} + \frac{1}{\Gamma+3} - \frac{2}{\Gamma+5} - \frac{4}{(\Gamma+3)^2}\right] \tag{8.8}$$

For head-on collisions,

$$q(E_\gamma) \propto 6\sigma_T \left[\frac{1}{\Gamma+1} + \frac{2}{\Gamma+5} - \frac{2}{\Gamma+3} \right]$$

For example, the emissivity ratio between electron-photon head-on collisions and the isotropic situation is 3 for $\Gamma = 3$ and 2.75 for $\Gamma = 2.5$.

8.3 THE PHOTON SOURCE DISTRIBUTIONS

The parameters used for the three photon distributions are summarised in table 8.1. The 2.7^{o} K blackbody field is isotropic with a photon energy of $6.28\ 10^{-4}$eV and an energy density of 0.25eV cm^{-3}.

In the case of starlight, the source density per unit area of the plane is assumed to follow the mass distribution of Innanen (1973). For normalisation, the mass to light ratio, M/L, is taken as a constant over the disc. This parameter is evaluated in such a way as to compensate for any absorption of the light as it travels through the disc thickness. Values for the integrated starlight flux from high Galactic latitude directions are given by Roach and Megill (1960). Comparing the implied local luminosity per unit area of disc with the local surface mass density gives M/L = 6.54. The total optical luminosity of the Galaxy is found to be $6.3\ 10^{43}$ erg s^{-1}. The value given by Allen (1973) is adopted for the local starlight energy density.

It has only recently been realised that the Galaxy is probably as luminous in far infrared as in optical emission. After reports of large scale CO detection in the Galaxy (see section 3.3.3), Fazio and Stecker (1976) predicted a far infrared emissivity distribution assuming a dust

Table 8.1

The Photon Distributions

	Photon Energy (eV)	Energy Distribution
2.7^{o} K Blackbody	$6.28\ 10^{-4}$	Isotropic. Energy density 0.25eV cm^{-3}.
Starlight	1.4	Mass surface density distribution (Innanen, 1973) with normalisation M/L = 6.54 based on star counts given by Roach and Megill (1960). Local energy density 0.44 eV cm^{-3}, (Allen, 1973).
Far Infrared	$1.2\ 10^{-2}$	H_2 surface density distribution (Gordon and Burton, 1976) with normalisation $2.2\ 10^{-30}$ W/H atom from Ryter and Puget (1977). Local energy density 0.49eV cm^{-3}.

temperature of 10^{o} K. Ryter and Puget (1977) have shown that typical temperatures are higher, about 32^{o} K, and therefore the emissivity is greater. They have compared infrared with molecular hydrogen data for ten Galactic clouds and find an average value for the infrared luminosity per hydrogen atom, L_{IR}^{H}, of $2.2\ 10^{-30}$ Watts H $atom^{-1}$. They find a similar value using the infrared survey of Pipher (1973). Rouan et al. (1977) have reported a slightly higher value for L_{IR}^{H} ($4.2\ 10^{-30}$ W H $atom^{-1}$) derived from infrared measurements in the direction $\ell = 28^{o}$.

In the present calculations the molecular hydrogen surface density distribution of Gordon and Burton (1976) and the value of L_{IR}^{H} given by Ryter and Puget (1977) are used. This gives a total far infrared luminosity for the Galaxy of $7.0\ 10^{43}$ erg s^{-1}, very similar to the value for starlight. The local infrared energy density in the disc is calculated by multiplying the local energy density of starlight by the ratio of the total energy output of the Galaxy in infrared to that in starlight. This method eliminates consideration of absorption of the two wavelengths in the disc. The local infrared energy density is therefore 0.49eV cm^{-3}, slightly higher than the value for starlight.

8.4 THE RESULTANT INVERSE COMPTON GAMMA RAY FLUX

Calculations have been performed for the six directions observed by the SAS-2 satellite (see section A.2). The results for Model 1, λ = 2 pc; Model 2, λ = 2 pc; Model 1, λ = 20 pc, are given in tables 8.2 - 8.4.

The average over the six SAS-2 directions is displayed for the first two sets of results in figures 8.1 and 8.2. Figure 8.3 is an estimate of the results for Model 2, λ = 20 pc based on a study of the calculated

Table 8.2 The inverse Compton flux ($cm^{-2}\ s^{-1}\ sr^{-1}\ eV^{-1}$) for various directions (ℓ , b) and energies. Results are for Model 1 and $\lambda = 2$ pc.

Energy (eV) \ Direction	(0,25)	(0,58)	(19,-23)	(190,-30)	(285,75)	(300,-45)	Average
Starlight photon field							
10^6	$3.3\ 10^{-10}$	$1.3\ 10^{-10}$	$3.0\ 10^{-10}$	$8.9\ 10^{-11}$	$9.8\ 10^{-11}$	$1.3\ 10^{-10}$	$1.8\ 10^{-10}$
$4\ 10^6$	$2.4\ 10^{-11}$	$9.4\ 10^{-12}$	$2.3\ 10^{-11}$	$6.7\ 10^{-12}$	$7.1\ 10^{-12}$	$9.1\ 10^{-12}$	$1.3\ 10^{-11}$
10^7	$4.2\ 10^{-12}$	$1.6\ 10^{-12}$	$3.9\ 10^{-12}$	$1.2\ 10^{-12}$	$1.2\ 10^{-12}$	$1.6\ 10^{-12}$	$2.3\ 10^{-12}$
$4\ 10^7$	$2.7\ 10^{-13}$	$9.6\ 10^{-14}$	$2.4\ 10^{-13}$	$8.0\ 10^{-14}$	$7.7\ 10^{-14}$	$9.8\ 10^{-14}$	$1.4\ 10^{-13}$
10^8	$3.9\ 10^{-14}$	$1.5\ 10^{-14}$	$3.6\ 10^{-14}$	$1.3\ 10^{-14}$	$1.2\ 10^{-14}$	$1.5\ 10^{-14}$	$2.2\ 10^{-14}$
$4\ 10^8$	$2.0\ 10^{-15}$	$8.1\ 10^{-16}$	$2.0\ 10^{-15}$	$8.5\ 10^{-16}$	$7.2\ 10^{-16}$	$8.9\ 10^{-16}$	$1.2\ 10^{-15}$
Infrared photon field							
10^6	$4.2\ 10^{-10}$	$1.4\ 10^{-10}$	$3.8\ 10^{-10}$	$1.4\ 10^{-10}$	$1.2\ 10^{-10}$	$1.5\ 10^{-10}$	$2.2\ 10^{-10}$
$4\ 10^6$	$2.3\ 10^{-11}$	$8.2\ 10^{-12}$	$2.1\ 10^{-11}$	$9.0\ 10^{-12}$	$7.4\ 10^{-12}$	$9.0\ 10^{-12}$	$1.3\ 10^{-11}$
10^7	$3.2\ 10^{-12}$	$1.3\ 10^{-12}$	$3.0\ 10^{-12}$	$1.5\ 10^{-12}$	$1.2\ 10^{-12}$	$1.4\ 10^{-12}$	$1.9\ 10^{-12}$
$4\ 10^7$	$1.6\ 10^{-13}$	$8.2\ 10^{-14}$	$1.6\ 10^{-13}$	$1.1\ 10^{-13}$	$8.3\ 10^{-14}$	$9.2\ 10^{-14}$	$1.1\ 10^{-13}$
10^8	$2.4\ 10^{-14}$	$1.4\ 10^{-14}$	$2.3\ 10^{-14}$	$1.9\ 10^{-14}$	$1.5\ 10^{-14}$	$1.6\ 10^{-14}$	$1.8\ 10^{-14}$
$4\ 10^8$	$1.4\ 10^{-15}$	$1.1\ 10^{-15}$	$1.4\ 10^{-15}$	$1.4\ 10^{-15}$	$1.1\ 10^{-15}$	$1.2\ 10^{-15}$	$1.2\ 10^{-15}$
2.7°K photon field							
10^6	$1.7\ 10^{-10}$	$9.8\ 10^{-11}$	$1.8\ 10^{-10}$	$1.1\ 10^{-10}$	$8.7\ 10^{-11}$	$1.1\ 10^{-10}$	$1.3\ 10^{-10}$
$4\ 10^6$	$9.2\ 10^{-12}$	$5.9\ 10^{-12}$	$9.7\ 10^{-12}$	$6.9\ 10^{-12}$	$5.5\ 10^{-12}$	$6.6\ 10^{-12}$	$7.3\ 10^{-12}$
10^7	$1.4\ 10^{-12}$	$9.9\ 10^{-13}$	$1.5\ 10^{-12}$	$1.2\ 10^{-12}$	$9.4\ 10^{-13}$	$1.1\ 10^{-12}$	$1.2\ 10^{-12}$
$4\ 10^7$	$9.1\ 10^{-14}$	$7.3\ 10^{-14}$	$9.4\ 10^{-14}$	$8.4\ 10^{-14}$	$7.1\ 10^{-14}$	$7.7\ 10^{-14}$	$8.2\ 10^{-14}$
10^8	$1.6\ 10^{-14}$	$1.4\ 10^{-14}$	$1.6\ 10^{-14}$	$1.5\ 10^{-14}$	$1.3\ 10^{-14}$	$1.4\ 10^{-14}$	$1.5\ 10^{-14}$
$4\ 10^8$	$1.2\ 10^{-15}$	$1.1\ 10^{-15}$	$1.3\ 10^{-15}$	$1.2\ 10^{-15}$	$1.1\ 10^{-15}$	$1.2\ 10^{-15}$	$1.2\ 10^{-15}$

Table 8.3 The inverse Compton flux ($cm^{-2}\ s^{-1}\ sr^{-1}\ eV^{-1}$) for various directions (ℓ , b) and energies. Results are for Model 2 and $\lambda = 2$ pc.

Energy (eV) \ Direction	(0,25)	(0,58)	(19,-23)	(190,-30)	(285,75)	(300,-45)	Average
Starlight photon field							
10^6	$4.6\ 10^{-10}$	$1.6\ 10^{-10}$	$4.1\ 10^{-10}$	$9.6\ 10^{-11}$	$1.1\ 10^{-10}$	$1.5\ 10^{-10}$	$2.3\ 10^{-10}$
$4\ 10^6$	$3.6\ 10^{-11}$	$1.2\ 10^{-11}$	$3.2\ 10^{-11}$	$7.0\ 10^{-12}$	$8.3\ 10^{-12}$	$1.1\ 10^{-11}$	$1.8\ 10^{-11}$
10^7	$6.2\ 10^{-12}$	$2.0\ 10^{-12}$	$5.6\ 10^{-12}$	$1.2\ 10^{-12}$	$1.4\ 10^{-12}$	$1.9\ 10^{-12}$	$3.1\ 10^{-12}$
$4\ 10^7$	$4.2\ 10^{-13}$	$1.3\ 10^{-13}$	$3.6\ 10^{-13}$	$7.8\ 10^{-14}$	$8.8\ 10^{-14}$	$1.2\ 10^{-13}$	$2.0\ 10^{-13}$
10^8	$6.5\ 10^{-14}$	$1.9\ 10^{-14}$	$5.8\ 10^{-14}$	$1.2\ 10^{-14}$	$1.3\ 10^{-14}$	$1.8\ 10^{-14}$	$3.1\ 10^{-14}$
$4\ 10^8$	$3.6\ 10^{-15}$	$1.0\ 10^{-15}$	$3.3\ 10^{-15}$	$7.4\ 10^{-16}$	$7.6\ 10^{-16}$	$1.0\ 10^{-15}$	$1.7\ 10^{-15}$
Infrared photon field							
10^6	$6.0\ 10^{-10}$	$1.7\ 10^{-10}$	$5.4\ 10^{-10}$	$1.2\ 10^{-10}$	$1.2\ 10^{-10}$	$1.6\ 10^{-10}$	$2.8\ 10^{-10}$
$4\ 10^6$	$3.4\ 10^{-11}$	$9.2\ 10^{-12}$	$3.1\ 10^{-11}$	$7.5\ 10^{-12}$	$7.2\ 10^{-12}$	$9.2\ 10^{-12}$	$1.6\ 10^{-11}$
10^7	$4.8\ 10^{-12}$	$1.4\ 10^{-12}$	$4.4\ 10^{-12}$	$1.2\ 10^{-12}$	$1.1\ 10^{-12}$	$1.4\ 10^{-12}$	$2.4\ 10^{-12}$
$4\ 10^7$	$2.3\ 10^{-13}$	$8.2\ 10^{-14}$	$2.2\ 10^{-13}$	$8.8\ 10^{-14}$	$7.7\ 10^{-14}$	$8.7\ 10^{-14}$	$1.3\ 10^{-13}$
10^8	$3.1\ 10^{-14}$	$1.4\ 10^{-14}$	$3.0\ 10^{-14}$	$1.6\ 10^{-14}$	$1.4\ 10^{-14}$	$1.5\ 10^{-14}$	$2.0\ 10^{-14}$
$4\ 10^8$	$1.6\ 10^{-15}$	$1.1\ 10^{-15}$	$1.6\ 10^{-15}$	$1.2\ 10^{-15}$	$1.1\ 10^{-15}$	$1.1\ 10^{-15}$	$1.3\ 10^{-15}$
2.7°K photon field							
10^6	$2.7\ 10^{-10}$	$1.0\ 10^{-10}$	$2.9\ 10^{-10}$	$8.2\ 10^{-11}$	$8.4\ 10^{-11}$	$1.1\ 10^{-10}$	$1.6\ 10^{-10}$
$4\ 10^6$	$1.3\ 10^{-11}$	$6.2\ 10^{-12}$	$1.4\ 10^{-11}$	$5.5\ 10^{-12}$	$5.2\ 10^{-12}$	$6.5\ 10^{-12}$	$8.4\ 10^{-12}$
10^7	$1.8\ 10^{-12}$	$1.0\ 10^{-12}$	$1.9\ 10^{-12}$	$9.8\ 10^{-13}$	$9.2\ 10^{-13}$	$1.0\ 10^{-12}$	$1.3\ 10^{-12}$
$4\ 10^7$	$1.0\ 10^{-13}$	$7.2\ 10^{-14}$	$1.1\ 10^{-13}$	$7.5\ 10^{-14}$	$7.0\ 10^{-14}$	$7.4\ 10^{-14}$	$8.4\ 10^{-14}$
10^8	$1.7\ 10^{-14}$	$1.4\ 10^{-14}$	$1.8\ 10^{-14}$	$1.4\ 10^{-14}$	$1.3\ 10^{-14}$	$1.4\ 10^{-14}$	$1.5\ 10^{-14}$
$4\ 10^8$	$1.3\ 10^{-15}$	$1.1\ 10^{-15}$	$1.3\ 10^{-15}$	$1.2\ 10^{-15}$	$1.1\ 10^{-15}$	$1.2\ 10^{-15}$	$1.2\ 10^{-15}$

Table 8.4 The inverse Compton flux (cm^{-2} s^{-1} sr^{-1} eV^{-1}) for various directions (ℓ , b) and energies. Results are for Model 1 and $\lambda = 20$ pc.

Energy (eV) \ Direction	(0,25)	(0,58)	(19,-23)	(190,-30)	(285,75)	(300,-45)	Average
Starlight photon field							
10^6	$3.4\ 10^{-10}$	$1.5\ 10^{-10}$	$3.1\ 10^{-10}$	$9.3\ 10^{-11}$	$1.1\ 10^{-10}$	$1.4\ 10^{-10}$	$1.9\ 10^{-10}$
$4\ 10^6$	$2.9\ 10^{-11}$	$1.2\ 10^{-11}$	$2.6\ 10^{-11}$	$8.0\ 10^{-12}$	$9.2\ 10^{-12}$	$1.2\ 10^{-11}$	$1.6\ 10^{-11}$
10^7	$5.5\ 10^{-12}$	$2.4\ 10^{-12}$	$5.1\ 10^{-12}$	$1.5\ 10^{-12}$	$1.8\ 10^{-12}$	$2.3\ 10^{-12}$	$3.1\ 10^{-12}$
$4\ 10^7$	$4.3\ 10^{-13}$	$1.9\ 10^{-13}$	$4.0\ 10^{-13}$	$1.2\ 10^{-13}$	$1.4\ 10^{-13}$	$1.8\ 10^{-13}$	$2.4\ 10^{-13}$
10^8	$7.7\ 10^{-14}$	$3.2\ 10^{-14}$	$7.3\ 10^{-14}$	$2.2\ 10^{-14}$	$2.4\ 10^{-14}$	$3.1\ 10^{-14}$	$4.3\ 10^{-14}$
$4\ 10^8$	$5.6\ 10^{-15}$	$2.3\ 10^{-15}$	$5.2\ 10^{-15}$	$1.6\ 10^{-15}$	$1.7\ 10^{-15}$	$2.2\ 10^{-15}$	$3.1\ 10^{-15}$
Infrared photon field							
10^6	$6.8\ 10^{-10}$	$3.1\ 10^{-10}$	$6.5\ 10^{-10}$	$2.6\ 10^{-10}$	$2.4\ 10^{-10}$	$3.1\ 10^{-10}$	$4.1\ 10^{-10}$
$4\ 10^6$	$4.9\ 10^{-11}$	$2.2\ 10^{-11}$	$4.7\ 10^{-11}$	$1.9\ 10^{-11}$	$1.7\ 10^{-11}$	$2.2\ 10^{-11}$	$2.9\ 10^{-11}$
10^7	$8.2\ 10^{-12}$	$3.6\ 10^{-12}$	$7.9\ 10^{-12}$	$3.2\ 10^{-12}$	$2.8\ 10^{-12}$	$3.7\ 10^{-12}$	$4.9\ 10^{-12}$
$4\ 10^7$	$5.2\ 10^{-13}$	$2.2\ 10^{-13}$	$5.0\ 10^{-13}$	$2.1\ 10^{-13}$	$1.9\ 10^{-13}$	$2.3\ 10^{-13}$	$3.1\ 10^{-13}$
10^8	$7.9\ 10^{-14}$	$3.5\ 10^{-14}$	$7.7\ 10^{-14}$	$3.6\ 10^{-14}$	$3.0\ 10^{-14}$	$3.7\ 10^{-14}$	$4.9\ 10^{-14}$
$4\ 10^8$	$4.1\ 10^{-15}$	$2.1\ 10^{-15}$	$4.3\ 10^{-15}$	$2.4\ 10^{-15}$	$2.0\ 10^{-15}$	$2.3\ 10^{-15}$	$2.9\ 10^{-15}$
2.7°K photon field							
10^6	$7.2\ 10^{-10}$	$3.9\ 10^{-10}$	$7.4\ 10^{-10}$	$2.6\ 10^{-10}$	$3.0\ 10^{-10}$	$4.1\ 10^{-10}$	$4.7\ 10^{-10}$
$4\ 10^6$	$4.1\ 10^{-11}$	$2.1\ 10^{-11}$	$4.2\ 10^{-11}$	$1.6\ 10^{-11}$	$1.7\ 10^{-11}$	$2.3\ 10^{-11}$	$2.7\ 10^{-11}$
10^7	$5.9\ 10^{-12}$	$3.1\ 10^{-12}$	$6.2\ 10^{-12}$	$2.6\ 10^{-12}$	$2.5\ 10^{-12}$	$3.4\ 10^{-12}$	$4.0\ 10^{-12}$
$4\ 10^7$	$3.0\ 10^{-13}$	$1.7\ 10^{-13}$	$3.2\ 10^{-13}$	$1.6\ 10^{-13}$	$1.5\ 10^{-13}$	$1.9\ 10^{-13}$	$2.2\ 10^{-13}$
10^8	$4.3\ 10^{-14}$	$2.6\ 10^{-14}$	$4.5\ 10^{-14}$	$2.7\ 10^{-14}$	$2.3\ 10^{-14}$	$2.9\ 10^{-14}$	$3.2\ 10^{-14}$
$4\ 10^8$	$2.4\ 10^{-15}$	$1.7\ 10^{-15}$	$2.5\ 10^{-15}$	$1.9\ 10^{-15}$	$1.6\ 10^{-15}$	$1.8\ 10^{-15}$	$2.0\ 10^{-15}$

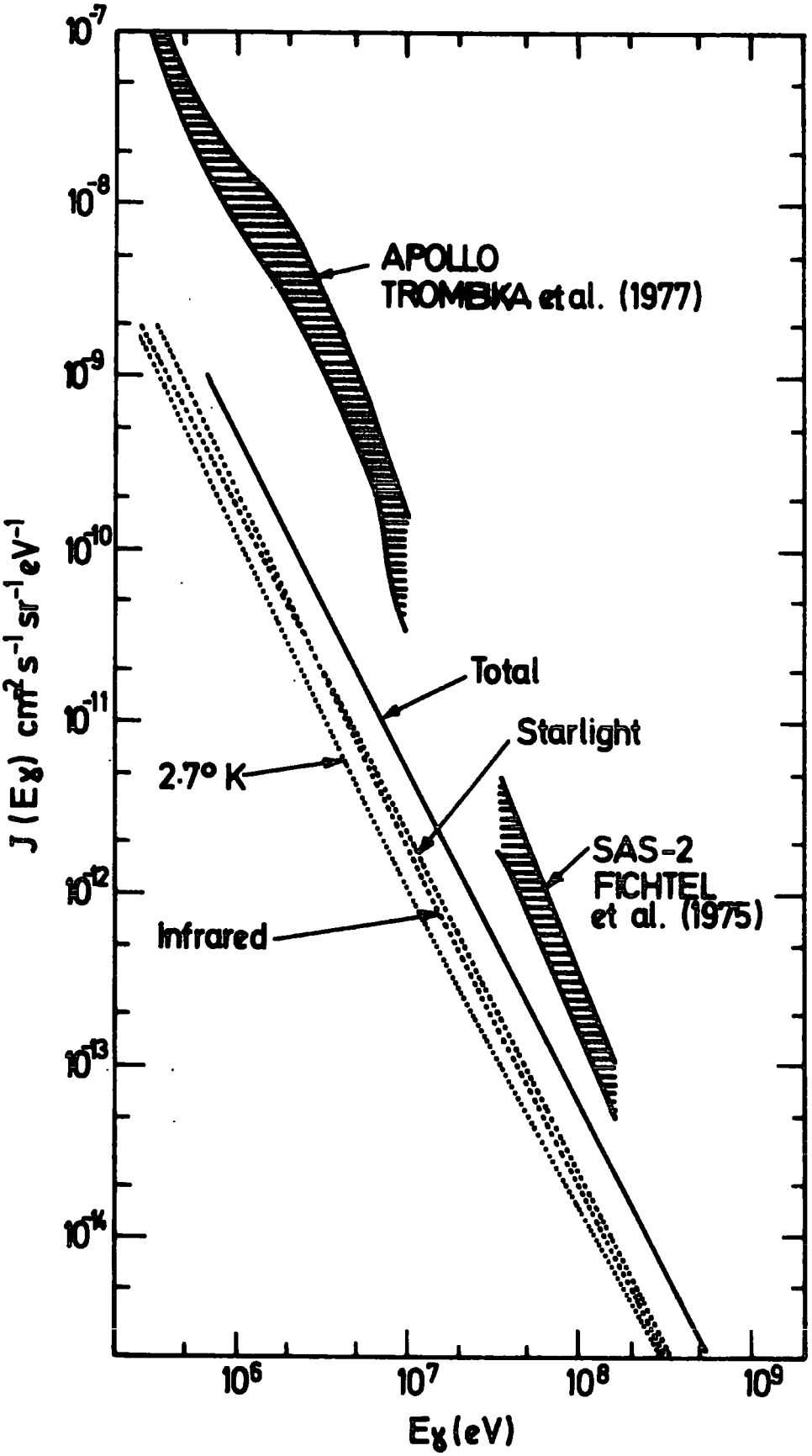

Figure 8.1 The inverse Compton flux for λ=2 pc and Model 1 (uniform electron source distribution) averaged over the six directions given in the text.

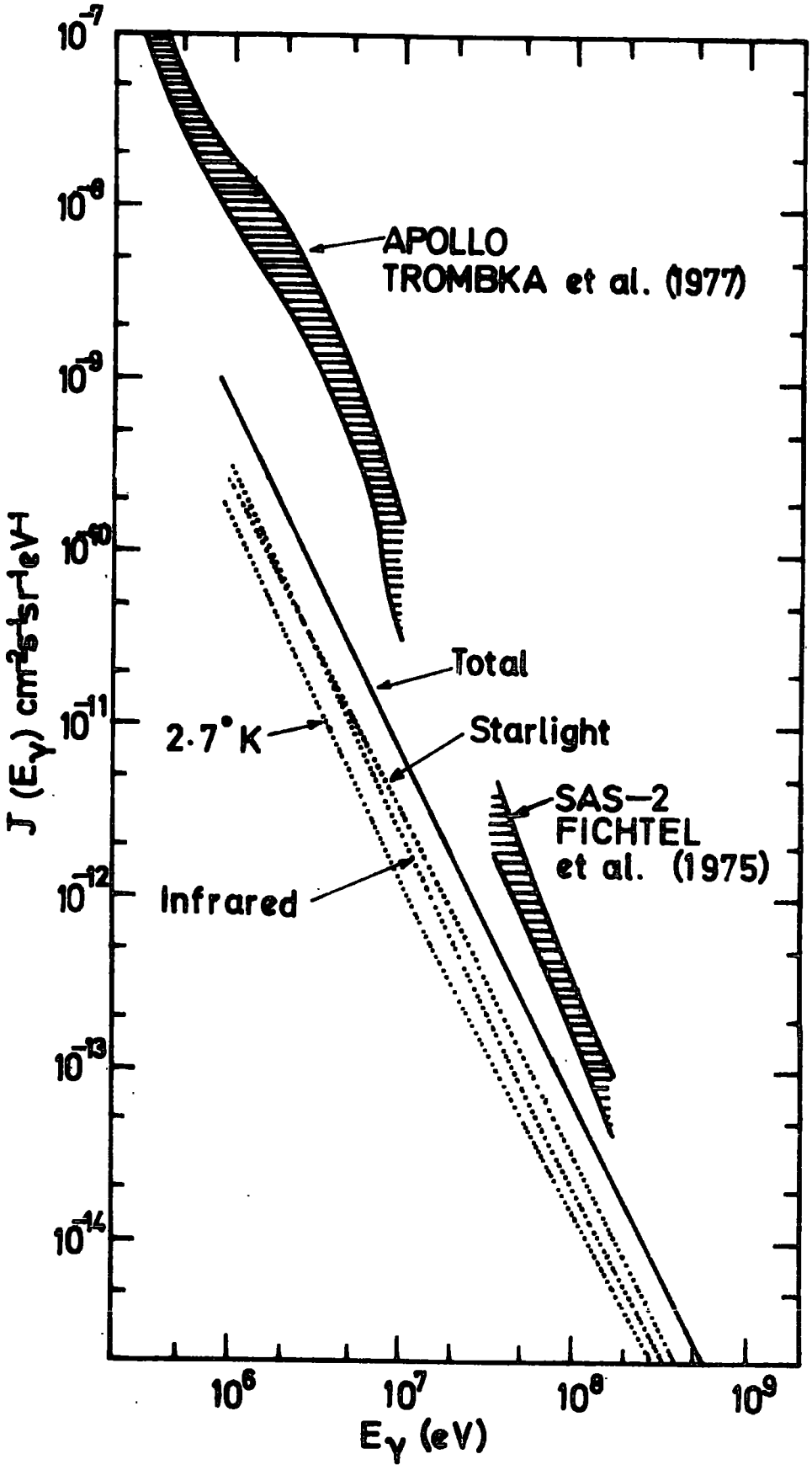

Figure 8.2 The inverse Compton flux for λ=2 pc and Model 2 (electron source distribution increasing towards the Galactic centre) averaged over the six directions given in the text.

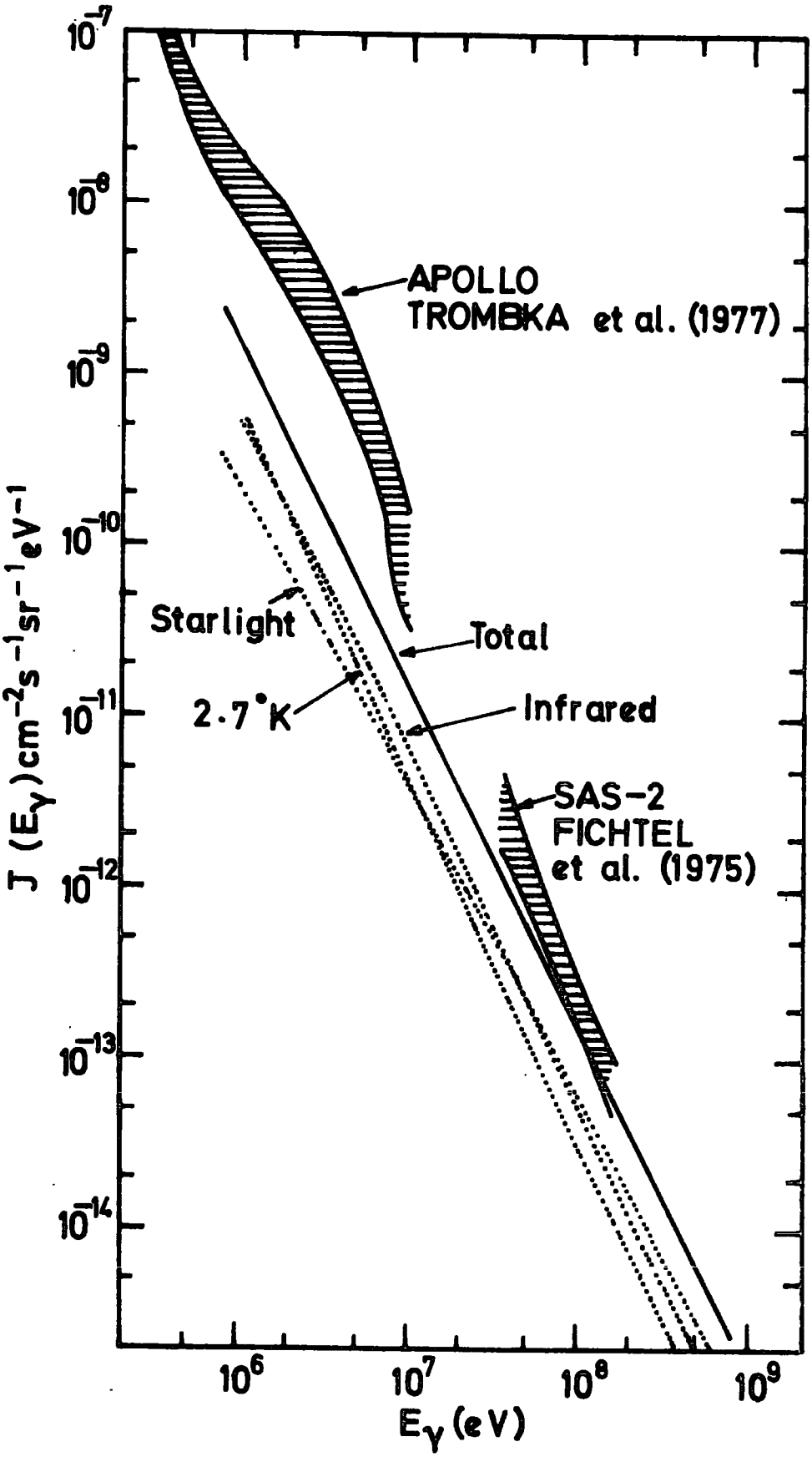

Figure 8.3 The inverse Compton flux for λ=20 pc and Model 2 (electron source distribution increasing towards the Galactic centre) averaged over the six directions given in the text.

values. In each of the figures, the only experimental data shown are those from the Apollo missions and SAS-2, which are representative of the best observations at present available. A more complete summary of observations is given in figure A.1.

For each photon field the contribution from the closest 500 pc, found separately assuming isotropic conditions and the local electron density, is shown in figure 8.4. This corresponds to the disc contribution. No steepening of the disc electron spectrum above 10 GeV has been included which means that the 2.7° K contribution above 10^7eV may be a slight over-estimate. This is of negligible importance since the disc flux is small compared with the observations.

When comparing the results for the different combinations of electron distribution and λ, it is important to consider the difference in characteristic energy of the electrons producing gamma rays of a certain energy on the three photon fields (see section 7.4.2), and remember that the lowest energy electrons can travel furthest without significant energy loss. Consequently, the distance to which we see electron sources is larger at lower energies.

The influence of a gradient in electron density is seen from a study of figures 8.1 and 8.2. As expected, there is very little change in the 2.7° K and infrared contributions compared with that from starlight.

It was shown in section 2.4 that an electron spectrum of differential slope $-\Gamma$ gives an inverse Compton differential gamma ray spectrum of slope $-(\Gamma+1)/2$. This is the situation in the disc. From equation 5.12 it is seen that in the case of total electron energy loss, the differential inverse Compton gamma ray spectrum is of slope $-(\Gamma+2)/2$. This is the

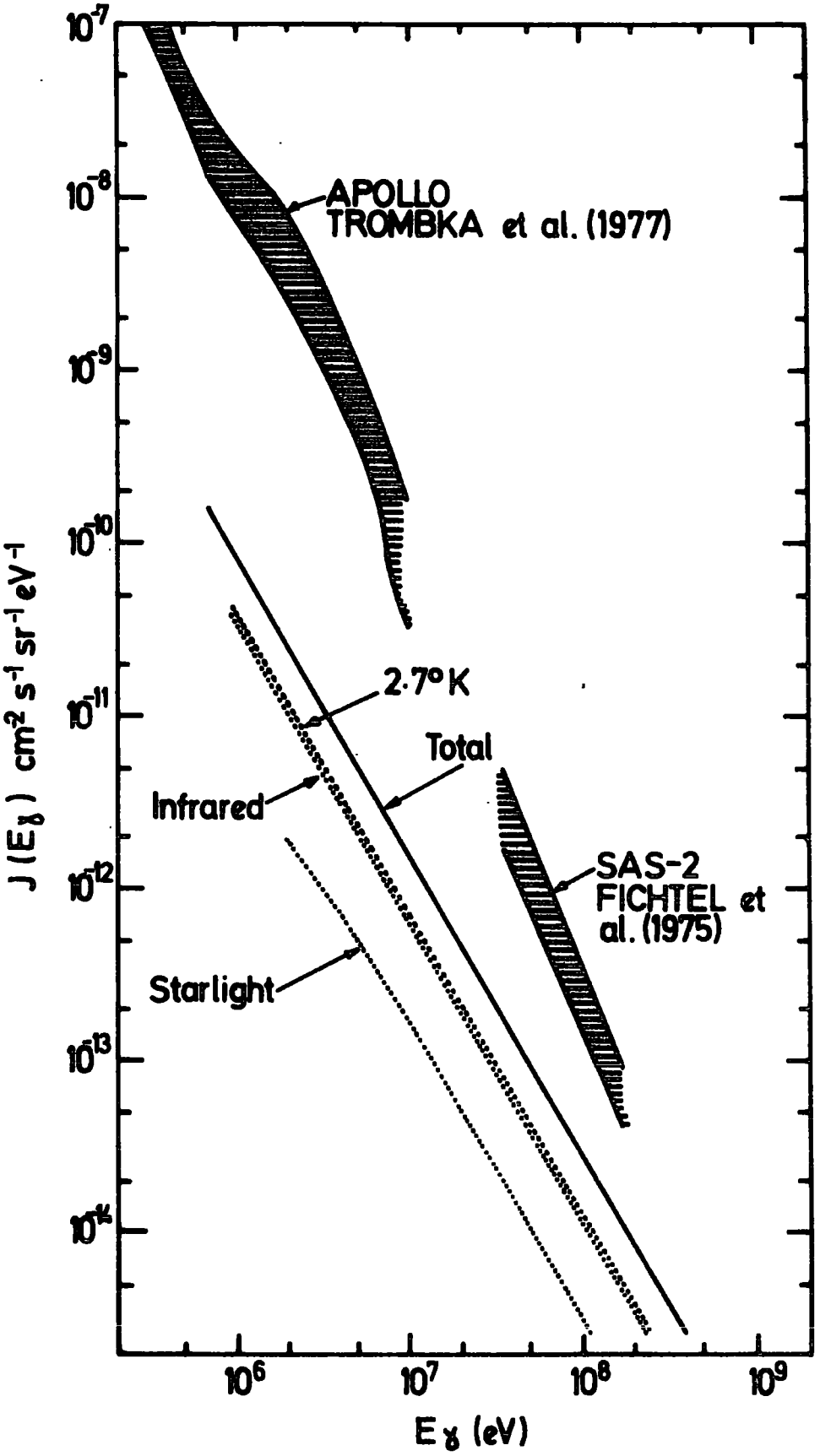

Figure 8.4 The inverse Compton flux contribution from distances $\lesssim 500$ pc.

expected slope for the halo flux if measured at a point in space away from the Galaxy. The slope measured at the Earth is expected to take an intermediate value, biassed by the rate of electron energy loss at close halo distances. Therefore the 2.7^{o} K spectrum should be the steepest of the three photon field contributions, and this is seen in the figures. It does not reach the maximum of -2.25, ($\Gamma = 2.5$), but is approximately -2.15 for $\lambda = 20$ pc. For the case where λ is 2 pc, the percentage of 2.7^{o} K contribution which is from the disc is higher than for $\lambda = 20$ pc, and is particularly noticable as a flattening in the spectral slope above 10^{7}eV.

When λ is increased from 2 pc to 20 pc it is seen that the relative increase in the 2.7^{o} K and infrared contributions is greater than that from starlight. The total spectrum here is marginally steeper than for $\lambda = 2$ pc, but in all three figures (8.1 - 8.3) the total has a slope between -1.9 and -2.

The predicted slope is therefore less than the value of about -2.4 consistent with observation. Therefore it seems unlikely that a halo model for the Galaxy can be used to explain all the high latitude gamma rays. However, the contribution is significant, particularly at 100 MeV where for $\lambda = 20$ pc the flux is consistent with 100% of the observation, and for $\lambda = 2$ pc (probably the more physical value) we have about 40%.

8.5 THE PREDICTED ANISOTROPY

The anisotropy at a particular energy can be expressed as the ratio between the flux in a Galactic centre direction $\ell = 0^{o}$, $b = 25^{o}$ (f_{c}) and that in an anticentre direction $\ell = 190^{o}$, $b = -30^{o}$ (f_{ac}). Values are given in table 8.5. The results in tables 8.2 - 8.4 allow four other directions to be studied. The anisotropy decreases with increasing energy

Table 8.5

Predicted anisotropies, f_c/f_{ac}. The directions of the fluxes f_c and f_{ac} are $\ell = 0^\circ$, $b = 25^\circ$ and $\ell = 190^\circ$, $b = -30^\circ$ respectively.

Gamma ray energy (eV)	f_c/f_{ac}		
	Model 1 λ = 2 pc	Model 2 λ = 2 pc	Model 1 λ = 20 pc
10^6	2.8	4.5	2.8
$4\ 10^6$	2.5	4.1	2.8
10^7	2.3	3.7	2.7
$4\ 10^7$	1.9	3.1	2.6
10^8	1.7	2.7	2.3
$4\ 10^8$	1.3	2.1	2.0

and decreasing λ, which is as expected since the halo becomes gradually more disc-like.

In time it should be possible to place limits on the halo contribution from the level of anisotropy in the observations. A further discussion, in relation to the balance between the contribution from the Galactic halo and implied contributions from halos of external galaxies, is to be found in the following Chapter.

CHAPTER NINE

THE INVERSE COMPTON HALO FLUX FROM EXTERNAL GALAXIES AND THE SUM OF CONTRIBUTIONS TO THE GAMMA RAY BACKGROUND

9.1 INTRODUCTION

If other galaxies exhibit diffusive electron leakage, similar to the Galaxy, they too will have halos. Electrons will exist only in the vicinity of their parent galaxies. In the following, each galaxy is considered to consist of a "disc" and a "halo". The "disc" is the region where cosmic ray particles are confined and where most of the gas and magnetic field are present. The "halo" is the region in which the electrons are undergoing diffusive escape, losing energy mainly by inverse Compton scattering. In the case of large radio galaxies, the term "disc" is probably inappropriate since the large radio lobes usually extend much further than the optical galaxy.

For a disc electron spectrum of differential slope $-\Gamma$ in an external galaxy, the slope of the halo inverse Compton flux is expected to be $-(\Gamma+2)/2$ (see section 8.4). Taking an average for Γ of 2.5 (the value for the Galaxy), the inverse Compton differential slope will be about -2.25, closer to the background slope than the value, -2, found for the Galactic halo.

In Chapter 6, methods were developed for deriving the total flux from a class of objects by relating the gamma ray emission to some other property. These are used here to estimate halo fluxes from normal and radio galaxies. The diffusion mean free path, λ, is taken to be a constant for the sources.

It is expected that increasing λ will cause a decrease in the flux from the Galactic halo relative to that from the halos of other galaxies. Results are calculated for the two values of λ used in Chapters 7 and 8. Finally,

the sum of all the gamma ray background contributions calculated in this thesis is compared with the observed flux.

9.2 THE FLUX FROM HALOS OF NORMAL AND RADIO GALAXIES

When viewed externally, the inverse Compton gamma ray flux from a galaxy halo is the radiation produced through total energy loss of the electrons.

The flux expected from the halo of the Galaxy, when looked at from outside, is to be calculated. Since the halo magnetic field is probably about 0.2 of that of the disc (section 7.2.1), synchrotron electron losses are considered negligible. The inverse Compton losses are on the three photon fields; starlight, far infrared, 2.7° K, whose energy densities are denoted w_1, w_2, w_3 respectively. The electron energy loss rate on each photon field is proportional to the energy density.

Let the gamma ray yields for injected electrons undergoing total energy loss be written $Q_1(E_\gamma)$, $Q_2(E_\gamma)$, $Q_3(E_\gamma)$, for the three photon fields respectively.

Assume the rate of injection of electrons into the halo is given by $P\, E_e^{-\Gamma}$ eV^{-1} s^{-1}.

The average gamma ray energy is related to the electron energy by $E_\gamma = bE_e^2$, where $b = 5.1\ 10^{-12}\ E$ eV^{-1}, and E is the energy of the photon field. The values of b for the three photon fields are denoted b_1, b_2, b_3.

Using equation 5.14,

$$Q_1(E_\gamma) = \frac{1}{2E_\gamma \sqrt{b_1 E_\gamma}} \int_{\sqrt{E_\gamma/b_1}}^{\infty} \left[\frac{w_1}{w_1 + w_2 + w_3}\right] P\, E_e^{-\Gamma}\, dE_e \text{ eV}^{-1} \text{ s}^{-1} \qquad (9.1)$$

Similar expressions can be written for Q_2 and Q_3 giving a total, $Q(E_\gamma)$,

$$Q(E_\gamma) = \frac{P\, E_\gamma^{-(\Gamma+2)/2}}{2(\Gamma-1)} \left[\left(\frac{w_1}{w_1 + w_2 + w_3} \right) b_1^{(\Gamma-2)/2} + \left(\frac{w_2}{w_1 + w_2 + w_3} \right) b_2^{(\Gamma-2)/2} + \left(\frac{w_3}{w_1 + w_2 + w_3} \right) b_3^{(\Gamma-2)/2} \right] \qquad (9.2)$$

Since the halo size is small, the local disc ratios are adopted for the photon field energy densities. Table 8.1 gives these values and also the mean photon energies for calculation of b_1, b_2 and b_3.

Equation 9.2 becomes, for $\Gamma = 2.5$,

$$Q(E_\gamma) = 2.9\ 10^{-4}\ P\ E_\gamma^{-2.25} \quad eV^{-1}\ s^{-1} \qquad (9.3)$$

Or, in the integral form,

$$Q(>E_\gamma) = 2.3\ 10^{-4}\ P\ E_\gamma^{-1.25} \quad s^{-1} \qquad (9.4)$$

Values of P are calculated from the values of A and disc sizes given in table 7.1, and are shown, along with the yield above 100 MeV, in table 9.1.

Using several indicators of gamma ray emission, in section 6.4 it was found that for a Galactic gamma ray yield above 100 MeV of $1.3\ 10^{42}\ s^{-1}$, normal galaxies provide about 4% of the observed background flux. Using proportionality, the corresponding percentages can be calculated for the four values of $Q_\gamma(>100$ MeV) given in table 9.1.

To get a rough estimate of the radio galaxy contribution, it must be assumed that the gamma ray to radio luminosity ratio is the same as for

Table 9.1. Values for the coefficient P, where the electron injection rate into the halo is expressed, $P\ E_e^{-\Gamma}\ eV^{-1}\ s^{-1}$. Also, values for the total gamma ray production rate above 100 MeV.

Electron source distribution	Diffusion mean free path λ (pc)	P	Q_γ (>100 MeV) s^{-1}
Model 1	2	$1.3\ 10^{55}$	$3.0\ 10^{41}$
Model 1	20	$9.4\ 10^{55}$	$2.2\ 10^{42}$
Model 2	2	$1.6\ 10^{55}$	$3.7\ 10^{41}$
Model 2	20	$1.2\ 10^{56}$	$2.7\ 10^{42}$

Table 9.2. Likely contributions to the gamma ray background at 100 MeV.

	Model, λ (pc)	A/A_{max}	Galaxy Disc π^o and Brem	Galaxy Halo	Normal galaxy "discs"	Normal galaxy "halos"	Radio galaxy "discs"	Radio galaxy "halos"	Total
Flux $cm^{-2}s^{-1}sr^{-1}eV^{-1}$	1,2	1	$5.5\ 10^{-14}$	$5.5\ 10^{-14}$	$9.6\ 10^{-15}$	$2.4\ 10^{-15}$	$3.8\ 10^{-14}$	$9.6\ 10^{-15}$	$1.7\ 10^{-13}$
	1,20	0.68	$5.5\ 10^{-14}$	$8.2\ 10^{-14}$	$9.6\ 10^{-15}$	$1.1\ 10^{-14}$	$3.8\ 10^{-14}$	$4.3\ 10^{-14}$	$2.4\ 10^{-13}$
	2,2	1	$5.5\ 10^{-14}$	$6.6\ 10^{-14}$	$9.6\ 10^{-15}$	$2.6\ 10^{-15}$	$3.8\ 10^{-14}$	$1.0\ 10^{-14}$	$1.8\ 10^{-13}$
	2,20	0.54	$5.5\ 10^{-14}$	$8.6\ 10^{-14}$	$9.6\ 10^{-15}$	$1.0\ 10^{-14}$	$3.8\ 10^{-14}$	$4.1\ 10^{-14}$	$2.4\ 10^{-13}$
% of SAS-2 observation	1,2	1	23	23	4	1	16	4	71
	1,20	0.68	23	34	4	5	16	18	100
	2,2	1	23	27	4	1	16	4	75
	2,20	0.54	23	36	4	4	16	17	100

normal galaxies. In this case, from section 6.5 it is seen that the background contribution is about four times that from normal galaxies, i.e. 16% of the observed flux.

More data are awaited before attempts made to include other types of galaxy, such as Seyferts.

9.3 SUM OF THE CONTRIBUTIONS TO THE GAMMA RAY BACKGROUND

9.3.1. Predictions

The contributions to the high latitude gamma ray flux to be considered are the neutral pion decay and bremsstrahlung radiation from the Galactic disc, the inverse Compton flux from the Galactic halo, and the emission from discs and halos of external normal and radio galaxies.

(a) Gamma ray emission from the Galactic disc

The local gamma ray emissivity, which is mainly from neutral pion decay and bremsstrahlung, is calculated in Chapter 2. The total differential emissivity at 100 MeV is $1.1\ 10^{-33}$ H atom^{-1} s^{-1} eV^{-1}. Schlickeiser and Thielheim (1976) have investigated the column density of atomic and molecular hydrogen averaged over the directions appropriate to the SAS-2 results, and find a value of $6.4\ 10^{20}$ H atoms cm^{-2}. These values give a differential gamma ray flux of $5.5\ 10^{-14}$ cm^{-2} s^{-1} sr^{-1} eV^{-1}.

Although the recent gamma ray results, summarised in section A.5, indicate that elsewhere in the Galaxy the electron to proton ratio may be different from that locally, causing a variation in the relative contributions from neutral pion decay and bremsstrahlung, it is not unreasonable to assume that, at high latitudes in the disc, the local emissivity per atom and resultant spectrum hold.

(b) Gamma ray emission from the discs of normal and radio galaxies

The SAS-2 differential background flux at 100 MeV is $2.4\ 10^{-13}$ cm^{-2} s^{-1} sr^{-1} eV^{-1}. Assuming the disc spectra of galaxies are reasonably similar to those of the diffuse background, so that the percentage contribution to the integral background flux at 100 MeV is the same as that to the differential, 4% of this value will be produced by discs of normal galaxies and 16% by discs of radio galaxies (see section 9.2), i.e. $9.6\ 10^{-15}$ cm^{-2} s^{-1} sr^{-1} eV^{-1} and $3.8\ 10^{-14}$ cm^{-2} s^{-1} sr^{-1} eV^{-1} respectively.

The total contribution at 100 MeV from the Galactic disc, and those of other galaxies, is therefore about $1\ 10^{-13}$ cm^{-2} s^{-1} sr^{-1} eV^{-1}.

(c) Inverse Compton gamma ray emission from galactic halos

For each of the models in Chapter 8, the Galactic halo flux was normalised by calculating an appropriate value for A under the assumption that the electron density just across the boundary in the halo was that of the disc. This value of A, A_{max}, is an upper limit. Here, A is constrained by the condition that the total predicted 100 MeV flux must not exceed that observed i.e. the flux from the Galactic halo plus the halos of other galaxies must not be greater than that so far unaccounted for; $1.4\ 10^{-13}$ cm^{-2} s^{-1} sr^{-1} eV^{-1}.

Table 9.2 shows results for the four combinations of electron distribution and diffusion mean free path used previously. The Galactic halo contributions are taken from Chapter 8 and those from the halos of normal and radio galaxies are as described in section 9.2. The disc contributions from (a) and (b) above are also given in table 9.2. It is found that for $\lambda = 2$ pc, the total SAS-2 100 MeV observation cannot be obtained even for $A = A_{max}$, whereas for $\lambda = 20$ pc, $A < A_{max}$ is required.

9.3.2. Comparison with observations

(a) The differential spectrum

Figures 9.1 and 9.2 show predictions for the Model 2 electron distribution and for values of λ of 2 pc and 20 pc respectively, with the SAS-2 and Apollo observations for comparison. It is assumed that the shapes of the locally observed electron and proton spectra are typical of the Galaxy and all normal and radio galaxies. The spectral shapes of the gamma ray contributions are as follows:

Galactic disc The spectral shape is calculated in Chapter 2, for which the integral is shown in figure 2.3.

Extragalactic discs It is assumed that electron dominated gamma ray emission is typical elsewhere in the Galactic disc. When viewed externally, the Galactic disc probably exhibits a gamma ray differential spectrum of slope approximately -1.8, and this slope is taken for the extragalactic disc flux.

Galactic halo Spectral shapes are as shown in figures 8.2 and 8.3.

Extragalactic halos The differential slope is -2.25, as reasoned in section 9.1.

The figures show that in each case, although the fit to observations is poor, the total contribution is significant. The Galactic halo contribution is in both cases dominant, at least above 10^7eV, and therefore the total spectrum is too flat to agree with observed data.

(b) The latitude distribution

The recent analysis of the SAS-2 latitude distribution by Fichtel et al. (1977b), mentioned in section A.5, is now examined and related to the

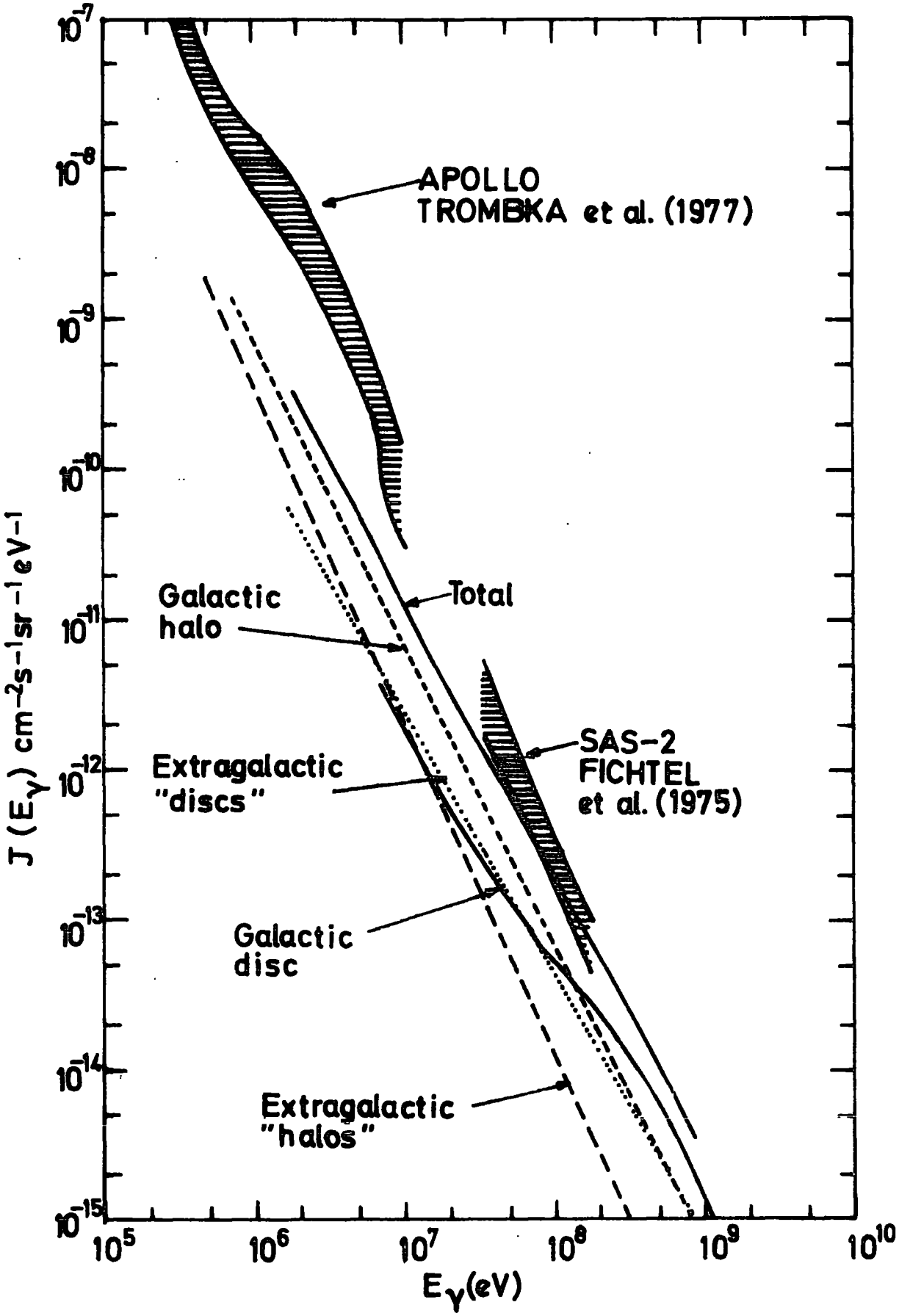

Figure 9.1 Contributions to the gamma ray background and their total, for a diffusion mean free path in the halos of all galaxies of 2 pc. The SAS-2 and Apollo observations are shown for comparison.

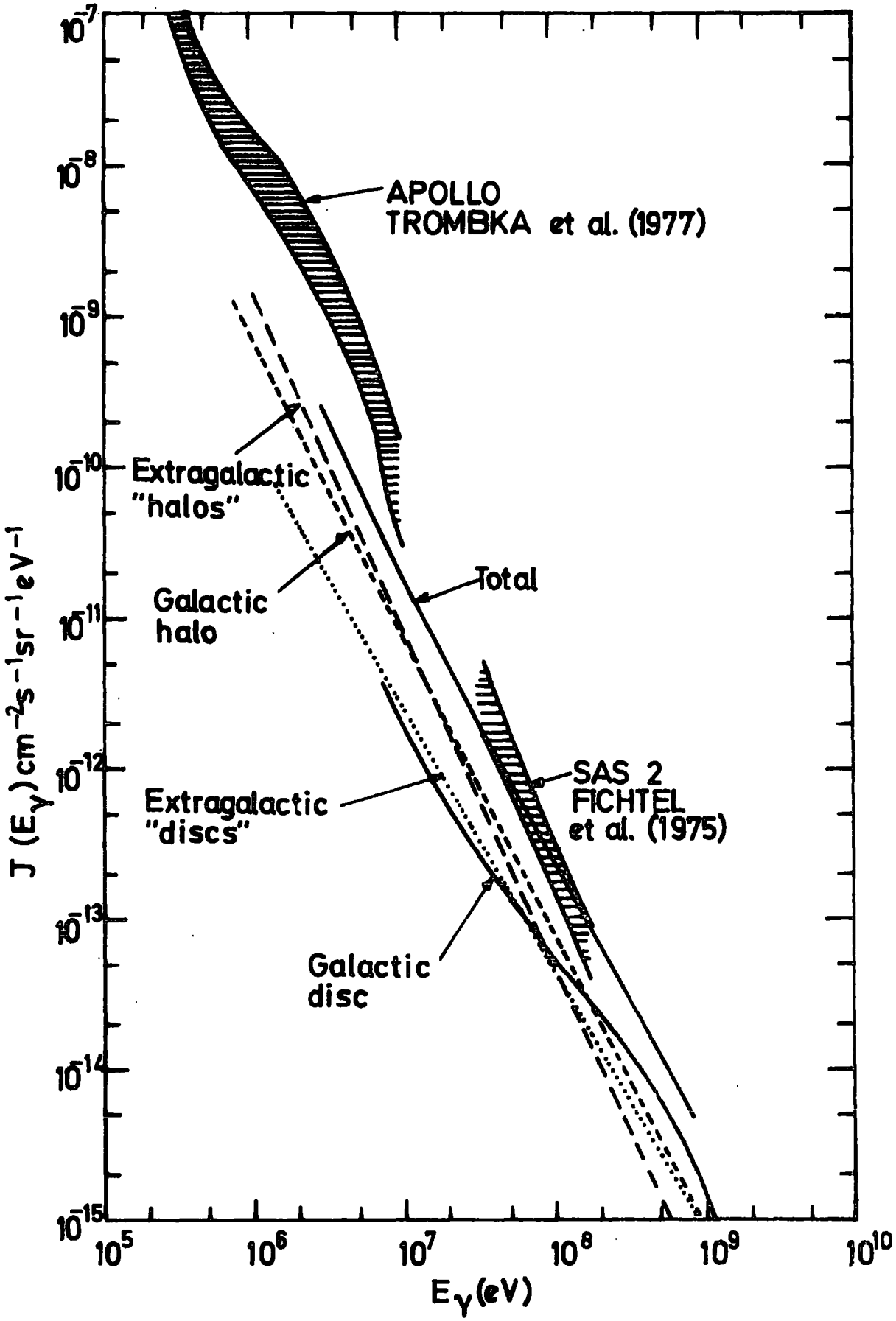

Figure 9.2 Contributions to the gamma ray background and their total, for a diffusion mean free path in the halos of all galaxies of 20 pc. The SAS-2 and Apollo observations are shown for comparison.

present calculations.

Fichtel et al. find that the flux above 100 MeV, integrated over all latitudes, can be expressed,

$$I_\gamma (>100 \text{ MeV}) = 0.42\ 10^{-5} + \frac{1.22\ 10^{-5}}{\sin b} \quad \text{cm}^{-2}\ \text{s}^{-1}\ \text{sr}^{-1} \qquad (9.5)$$

The first term is an isotropic component and the second is the contribution from the disc, considered to be a uniform flat slab. Using the directions averaged by Schlickeiser and Thielheim (1976) in their estimate of the hydrogen column density, the disc contribution from equation 9.5 is $1.5\ 10^{-5}$ cm^{-2} s^{-1} sr^{-1}. However, when the disc contribution is calculated as in section 9.3.1, using the local emissivity and a gas column density of $6.4\ 10^{20}$ H atoms cm^{-2}, the flux is only $9.7\ 10^{-6}$ cm^{-2} s^{-1} sr^{-1}. It is unlikely that at high latitudes the emissivity per H atom is greater than locally. Therefore, it is a likely hypothesis that the deficit is the inverse Compton flux from a flattened halo, which, in structure, is more disc-like than isotropic. This supports the work of Chapter 8. It is significant that this deficit (the halo contribution) is slightly more than the isotropic flux, and therefore consistent with present predictions.

The two component background model of Fichtel et al. is not appropriate for detailed comparison with the present work, in which three components, one of which is neither a flat disc or isotropic in nature, contribute.

9.3.3. Discussion

The aim of the present work was to assess likely contributions to the high latitude gamma ray flux from the Galaxy and discrete extragalactic sources. The total has been found to be a significant proportion of the

observed flux, therefore casting doubt on such cosmological models as are normalised to fit the entire measured spectrum in magnitude and shape. It is unlikely that the Galactic contribution has been overestimated and therefore any residual, when present predictions are subtracted from the observed flux, is of extragalactic origin.

The situation can be described by a three component model consisting of a flat disc, a non-spherical Galactic halo and an isotropic background. High latitude gamma ray scans are needed so that contributions from the various components, required to give a fit to observations, can be unravelled. The Galactic halo provides the anisotropy. Since this contribution is only about 1/3 of the observed flux (at 100 MeV), the anisotropies of table 8.5 are reduced.

For the sources considered here to provide contributions to the observed flux, a steeper spectrum is needed and, in the case of the more likely diffusion mean free path, 2 pc, a higher total flux. It is unlikely that the Galactic disc contribution at 100 MeV has been underestimated, since otherwise more cosmic rays close to the Sun at high latitudes would be required. The spectral shape is possibly in doubt since it is observed by the COS-B satellite to be steeper in all directions in the plane than calculations suggest for the locality of the Sun (see section A.5). The Galactic halo contribution is also probably not underestimated since values for A close to, or equal to, A_{max} are chosen. The spectral shape is in little doubt.

The greatest uncertainty is in the assessment of contributions from extragalactic discs and halos. The relationship of the gamma ray yield from a particular object to that from the complete class is very model dependent, and the choice of property for the indicator of gamma ray emission

is uncertain. For normal galaxies, all indicators give similar results. For radio, galaxies the only property used is the radio emission, and as yet there is no good check.

Data on pages 113 and 114 of Ginzburg and Syrovatskii (1964) give a mean value for the radio index, α, of 0.8 for each of 16 normal galaxies and 9 radio galaxies ($I_\nu \propto \nu^{-\alpha}$ W m^{-2} Hz^{-1}). On pages 195-203 of Lang (1974), spectral indecies for 141 radio galaxies are given. The distribution is shown in figure 9,3, where the spread in values can be seen. The mean is 0.77. Assuming, as is implicit here, that these indecies are appropriate to electrons not undergoing total energy loss, electron spectra similar in slope to that of the Galaxy are implied.

The spectral shape of the extragalactic halo contribution is the closest to that of the observations. The magnitude of this component contribution is the most approximate and is open to considerable doubt, especially for radio galaxies which are obviously so dissimilar in structure to the Galaxy. To increase the halo contribution, the values of λ for other galaxies must be greater than that of the Galaxy or the inverse Compton energy loss must be preferentially on the highest energy photon field. For example, the yield calculated for the Galactic halo is a factor of 2 higher if all energy loss is on starlight in place of the assumed 3-field mixture. However, for radio galaxies, the large radio lobes often extend much further than the optical galaxy, and therefore most inverse Compton loss is expected on the 2.7°K radiation.

In conclusion, it has been shown that a large percentage of the high latitude flux probably emanates from the Galaxy and discrete extragalactic sources. Without modification to adopted parameters, the spectral fit is not good. Radio galaxies possibly give the 1-10 MeV flux. It is unlikely that one mechanism is responsible for the complete observed spectrum.

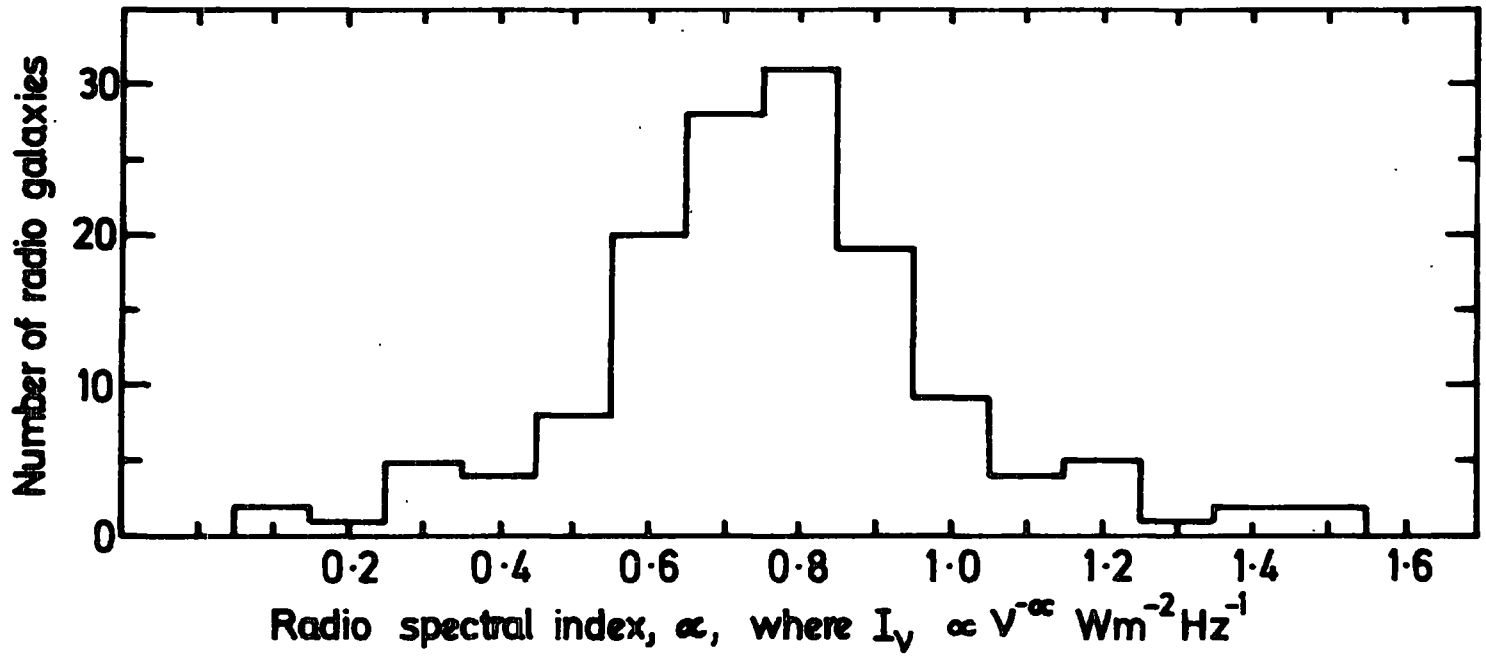

Figure 9.3 The distribution of radio spectral index, using a binsize 0.1, for 141 radio galaxies, from the compilation of Lang(1974).

APPENDIX A

Summary of Gamma Ray Observations

A.1 Introduction

The first cosmic gamma rays were not detected until the early 1960's. Their observation awaited high-altitude balloon, rocket and satellite technology since, like X-rays, they are absorbed by the atmosphere. The low flux necessitates the use of highly efficient detectors.

All experiments require coincidence shielding to discriminate against charged particles, the intensity of which is several orders of magnitude above that of the cosmic gamma rays. Balloon flight observations require correction for the flux of secondary gamma rays produced by cosmic ray cascades in the atmosphere, a fact which in general establishes the superiority of the spacecraft measurements. The usual method of correction involves extrapolating a functional form for the gamma ray intensity versus atmospheric depth.

Gamma rays cannot be detected directly and therefore must be converted into charged particles in a high Z material, usually lead or tungsten. Between 1 and 10 MeV the dominant interaction is Compton scattering, whereas above 10 MeV the cross section for pair production is greater. At low energies, scintillation counters, usually in conjunction with a Cerenkov detector, are most commonly used, whereas above about 10 MeV, spark chambers and nuclear emulsions, which provide a three dimensional "picture" of the event, can be employed.

The disadvantage of scintillators is that they provide poor angular resulution and are usually omnidirectional, although the addition

of a Cerenkov counter will discriminate against gamma rays travelling in an upward direction. This restricts their use to measurement of the diffuse background, although results will be contaminated by gamma rays from the Galaxy and no indication of the level of possible anisotropy is available. Limited angular resolution is achieved by Schonfelder et al. (1975) with their double Compton telescope which measures energy losses in, and time of flight between, two separated scintillators. The advantage of using scintillators is that they are small and light. The most commonly used crystal is thallium-doped sodium iodide.

At higher energies, detectors designed to measure pair production achieve good angular resolution. Nuclear emulsions have been successfully employed and they have the advantage of acting as both convertor and detector. However, they must of course be recovered which limits their use to balloon experiments.

The most popular detector for gamma rays above 10 MeV has been the spark chamber. In most experiments it is triggered by a scintillation-Cerenkov system and the convertor is usually in thin plates placed between the modules of the spark chamber. The angular resolution achieved is generally of the order of a few degrees.

The Galaxy is found to be resolved above the background only at high energies. For example, Schonfelder and Lichti (1974) at 10 MeV, using the double Compton telescope, do not claim significant enhancement from the Galactic disc. However, above about 30 MeV, the spark chamber experiments see clearly the disc and structure within. In the following two sections, the diffuse background and Galactic emission measurements are summarised. A brief review of current gamma ray line measurements is to

be found in A.4. Discrete sources are not in the field of the present work, but a list of those published prior to May 1977 from the SAS-2 and COS-B experiments is given in table A.5.

A.2. The Diffuse Background

Probably the first cosmic gamma ray experiment was that of Hulsizer and Rossi (1949) using a balloon-bourne ionization chamber. In the 1950's and early 1960's there were experiments using cloud chambers, Geiger counters and finally scintillation counters. These experiments placed upper limits to the percentage of the cosmic ray flux due to gamma rays. The first positive identification of cosmic gamma rays was probably from scintillators on board the Ranger 3 and 5 moonprobes (Arnold et al., 1962; Metzger et al., 1964). A flux above 100 MeV was confirmed soon afterwards from the Explorer 11 and OSO-3 spacecraft (Kraushaar and Clark, 1962; Kraushaar et al., 1965; Kraushaar et al., 1972). From the latter came the first reports of an enhanced flux from the Galactic disc (above 100 MeV) and the first longitude distribution of gamma rays.

Experiments carried by balloons and spacecraft, from those on board the Ranger spacecraft to date, are tabulated in tables A.1 and A.2 respectively. The measurements are plotted in figure A.1. Many of the results are upper limits due to the uncertainty in charged particle corrections, and, in the case of balloon experiments, the secondary atmospheric gamma ray flux.

Above 30 MeV the observations are mainly from spacecraft experiments. Only those using high resolution detectors measure the true high latitude flux, not contaminated by much disc emission. To date there has been no experimental search for anisotropy. The only experiment to sample several

TABLE A.1. Experiments recording the gamma ray background using balloon-bourne detectors, tabulated in chronological order.

Reference	Energy (MeV)	Date	Location	Float Altitude g cm^{-2}	Detector	Angular Resolution (FWHM)
Kuo et al. (1973) Case-Western	10	Aug. 1968	Palestine, Texas	3	Spark chamber	
Vedrenne et al. (1971) Toulouse	0.7-4.5	March 1969 Oct. 1969 May 1970	Guiana France U.S.S.R.	4 3.5 4	Stilbene Scintillator. 2.5 cm x 2.5 cm. 28 pulse height channels.	Omnidirectional.
Mayer-Hasselwander et al. (1972) Herterich et al. (1973) Max-Plank, Munich.	>20	June 1970 July 1971		2.2 1.7	Spark chamber	
Daniel et al. (1972) Tata	0.1-8.5	Nov. 1971	Hyderabad, India	4.7	NaI(Tl) scintillator 7.5 cm x 7.5 cm	Omnidirectional.
Share et al. (1974a) N.R.L., Washington.	10-200	Dec. 1971	Parana, Argentina.	2.5	Spark chamber, Emulsion.	About $1\frac{1}{2}^{o}$
Hopper et al. (1973) Case-Western Melbourne	>30	Nov. 1972 Dec. 1972	Longreach, Australia. "	1.5-5	30 gap Spark chamber	

TABLE A.1 (Cont.)

Agrinier et al. (1973) France Italy Brazil	>20	March 1973 3 flights	France Brazil Brazil	2 2.3 5.5	12 gap Spark Chamber	
Schonfelder and Lichti (1974) Schonfelder et al. (1975) Max-Planck, Munich	1.5-10	Feb. 1973 July 1974	Palestine, Texas " "	2.45 2.55	Double Compton Telescope	40°
Tanaka (1974) Nagoya, Japan.	0.1-7.5	April 1974	Hyderabad, India	4.3	NaI(Tl) Scintillator 7.5 cm x 7.5 cm. Active shield of NaI(Tl) and CsI(Tl)	40°

TABLE A.2. Spacecraft experiments recording the gamma ray background. Low energy experiments, followed by those in the higher energy regime, are tabulated in chronological order.

Reference	Energy (MeV)	Date	Spacecraft	Detector	Angular Resolution (FWHM)	Duration
Arnold et al. (1962) Metzger et al. (1964)	0.7-4.4		Ranger 3 Ranger 5	CsI(Tl) and plastic scintillators. 32 pulse height channels.	Omnidirectional	About 1 hour.
Golenetskii et al. (1971) Leningrad	0.3-3.7	Dec. 1966 June 1967	Cosmos 135 Cosmos 163	NaI(Tl) scintillator. 4 cm x 4 cm. 64 pulse height channels.	Omnidirectional	Few months.
Vette et al. (1970) GSFC San Diego.	0.25-6	April-June 1967	ERS-18	NaI(Tl) scintillator 6 pulse height channels	Omnidirectional	About 3 months.
Mazets et al. (1975) Leningrad.	0.028-4.1	Dec. 1971	Cosmos 461	NaI(Tl) scintillator 7 cm x 7 cm. No particle shield.	Omnidirectional	
Trombka et al. (1977, and references therein) GSFC JPL San Diego.	0.3-27		Apollo 15,16,17 Apollo Soyuz	NaI(Tl) scintillator 7 cm x 7 cm	Omnidirectional	

TABLE A.2 (Cont.)

Damle et al. (1976) Tata	0.2-24	April 1975	Aryabhata	CSI(T1) scintillator 12.5 cm x 1.3 cm 64 pulse height channels	Omnidirectional	About 3 days
Kraushaar and Clark (1962) Kraushaar et al. (1965) MIT.	>100	1961	Explorer 11	CsI and NaI sandwich. Çerenkov detector.		7 months. 141 days useful data
Kraushaar et al. (1972) MIT	>100	March 1967 -July 1968	OSO-3	CsI and plastic scintillator convertors. NaI(T1) and Lucite Cerenkov detectors.	About 24°	16 months (621 true events)
Valentine et al. (1970) Rochester, New York.	>100	March 1967 -July 1968	OSO-3	Plastic scintillators. Pb convertor. Lucite Cerenkov detector.	About 40°	
Galper et al. (1973) Moscow.	>100	Jan. 1969	Cosmos 264	5 gap spark chamber		
Bratolyubova-Tsulukidze et al. (1970) Moscow	50-1500		Cosmos 208 Proton 2	Scintillation counter. Cerenkov detector		Proton 2 -25 hours
Fichtel et al. (1975) GSFC	35-200	Nov. 1972 -June 1973	SAS-2	32 gap spark chamber	2°-4°	7 months (8000 true events

FIGURE A.1. Measurements of the diffuse gamma ray background.

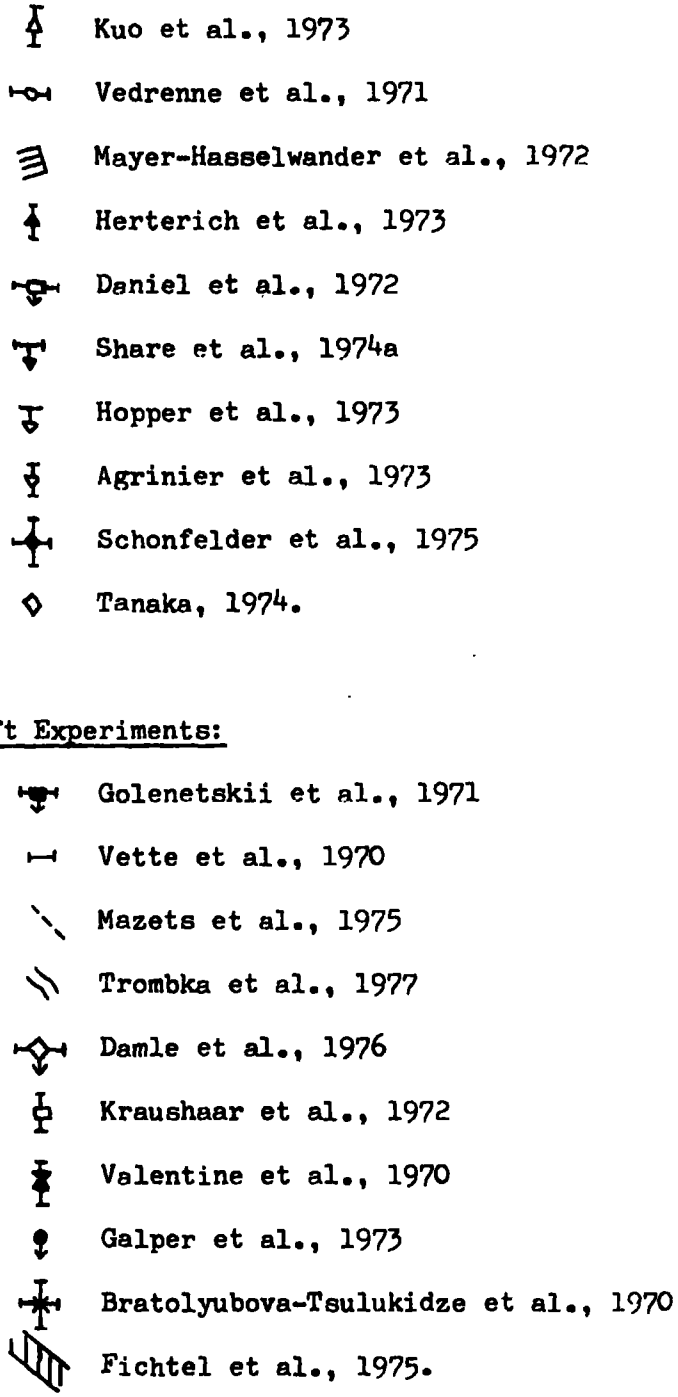

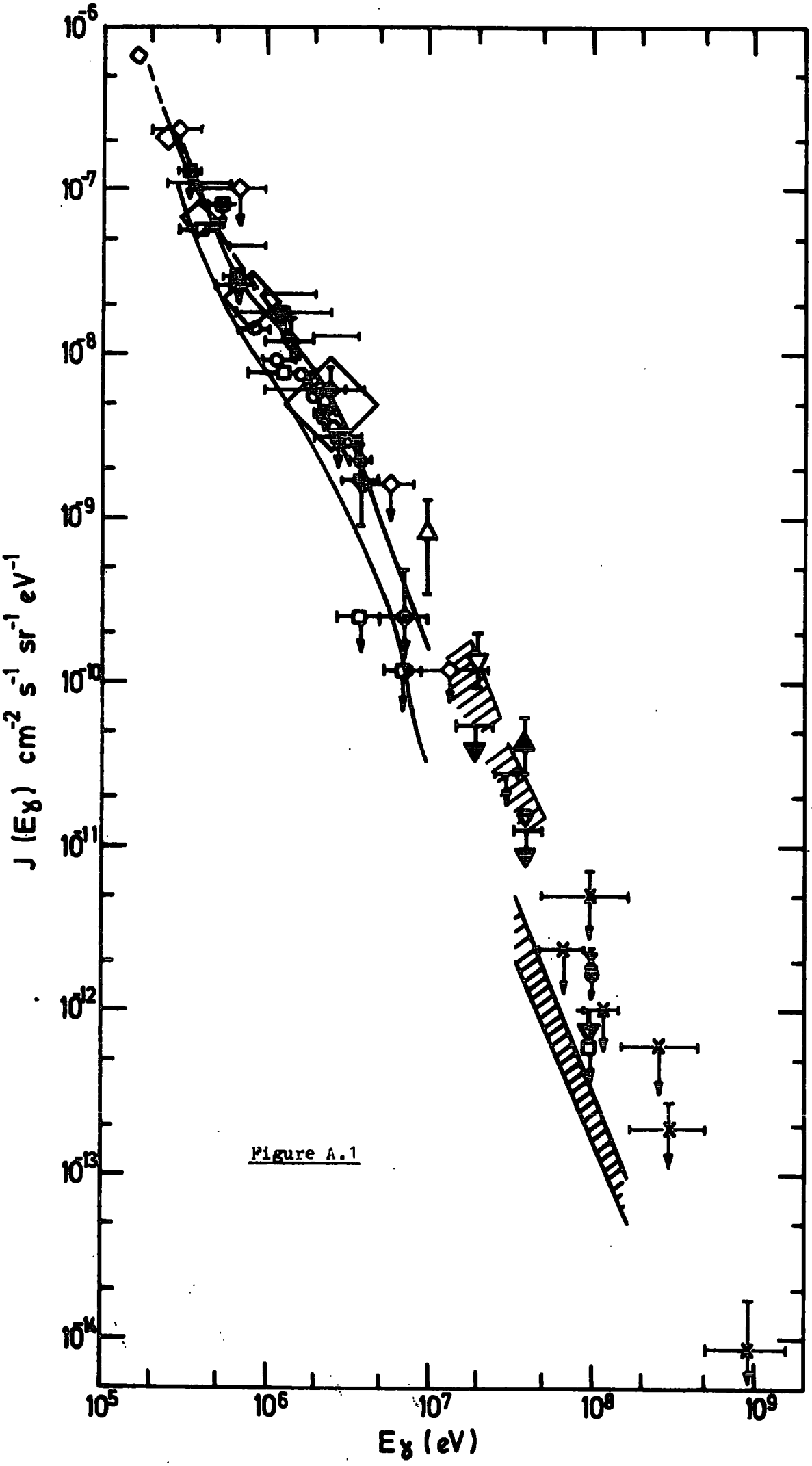
10^{-6}
10^{-7}
10^{-8}
10^{-9}
10^{-10}
10^{-11}
10^{-12}
10^{-13}
10^{-14}
$J(E_\gamma)$ cm^{-2} s^{-1} sr^{-1} eV^{-1}
10^5
10^6
10^7
10^8
10^9
E_γ (eV)

Figure A.1

high latitude directions is that of Fichtel et al. (1975). These data, from the SAS-2 satellite, are the best available at present. The average flux for the following six directions is presented: $\ell = 0^\circ$, $b = 25^\circ$; $\ell = 0^\circ$, $b = 58^\circ$; $\ell = 19^\circ$, $b = -23^\circ$; $\ell = 190^\circ$, $b = -30^\circ$; $\ell = 285^\circ$, $b = 75^\circ$; $\ell = 300^\circ$, $b = -45^\circ$. Unfortunately, due to the small number of events, the flux values for the individual directions are not given. The average integral flux above 100 MeV was found to be (1.93 ± 0.26) 10^{-5} cm^{-2} s^{-1} sr^{-1} and the spectrum was found to be consistent with a steep power law of differential exponent 2.4 ± 0.2 over the energy range where measurements were made: 35 - 200 MeV. It is hoped that, in time, high latitude scans from the COS-B satellite (see Bennett et al., 1976) will be forthcoming.

Below 10 MeV all the experiments, except those of Schonfelder and Lichti (1974), Schonfelder et al. (1975) and Tanaka (1974), are omni-directional. Inspection of figure A.1 shows an apparent enhancement between 1 and 10 MeV over a power law extrapolation from higher energies. However, the validity of this feature is a subject of debate. Most balloon experiments (Daniel et al., 1972 is a notable exception) show the "shoulder". The early spacecraft measurements of Vette et al. (1970) strongly indicate such a flattening of the spectral slope, but only flux upper limits are reported for most other spacecraft experiments. The initial results published from the Apollo missions favoured a "shoulder", but with the latest corrections they are consistent with virtually no enhancement (Trombka et al., 1977). The corrections necessary for non-cosmic gamma ray events ensure that the flux values are more likely over-estimated than underestimated. Therefore, although there is slight

evidence for a "shoulder", results are probably consistent with a power law of differential slope 2.3 - 2.4 between 1 and 200 MeV.

A.3. The Galactic Flux

Except for the low energy line observations in the direction of the Galactic centre (see next section), the Galactic disc is only resolved above the background at energies higher than about 10 MeV. A compilation of balloon bourne experiments recording the Galactic centre flux is given in table A.3. Most employ spark chambers together with, in some cases, nuclear emulsions. The integral flux values, for the longitude and latitude acceptance region given in the table, are shown in figure 3.1 and discussed in section 3.2.

The only satellites to carry experiments designed to survey the Galactic plane are OSO-3, SAS-2 and COS-B. From the last of these only provisional results have so far been published (Bennett et al., 1976). The details of the experiments are given in table A.4.

The early OSO-3 experiment used a scintillator-Cerenkov detector system. A limited angular resolution of about 24° FWHM was achieved. The first Galactic longitude distribution for high energy gamma rays (above 100 MeV) was produced and found to display a broad maximum for $|\ell| < 30^{\circ}$.

The best current results are from the SAS-2 experiment (Fichtel et al., 1975). The fluxes measured are generally lower than those from OSO-3, but are within experimental error when allowance is made for the poor resolution of the earlier detector. The results exhibit the same general feature i.e. an enhanced intensity for $|\ell| < 30^{\circ}$, $|b| < 10^{\circ}$. The data have been presented as longitude distributions integrated over $\pm 10^{\circ}$ of latitude. These are shown in figures 3.2 and 3.3 for longitude

TABLE A.3. Balloon experiments recording the gamma ray flux from the Galactic centre, tabulated in chronological order.

Reference	Energy (MeV)	Date	Location	Float Altitude g cm^{-2}	Detector	Angular Resolution	Galactic Centre Acceptance (where plotted)	Background Also
Kniffen and Fichtel (1970) Fichtel et al. (1972) GSFC	>50	Oct. 1969	Mildura, Australia	2.9	32 gap spark chamber		$-6^\circ < b < 6^\circ$ $-39^\circ < \ell < 24^\circ$	
Frye et al. (1971) Frye et al. (1974) Case-Western Melbourne	>100	Feb. 1969 Feb. 1969 Nov. 1969 Nov. 1972 Dec. 1972	Parkes, Australia " Longreach, Australia " "	2.86 2.96 2.97 1.37 1.38	Spark chamber	1.6°	$-3.5^\circ < b < 3.5^\circ$ $-30^\circ < \ell < 30^\circ$	
Dahlbacka et al. (1973) Minnesota.	>100	March 1970	Mildura, Australia	2.8	Nuclear Emulsion and spark chamber	1.5°	$-6^\circ < b < 6^\circ$	
Bennett et al. (1972) IC, London.	200-10000	Jan. 1971 Feb. 1971	Lusaka, Zambia "	4.1 11	Spark chamber	6°-10°	$-9^\circ < b < 9^\circ$ $-20^\circ < \ell < 50^\circ$	
Browning et al. (1972a) Southampton	>100	Sept. 1971	Palestine, Texas	4.5	70 gap spark chamber		$-3^\circ < b < 3^\circ$ $5^\circ < \ell < 30^\circ$	

TABLE A.3 (Cont.)

Helmken and Hoffman (1973) Smithsonian.	>10	Nov. 1971 Dec. 1971	Parana, Argentina " "	3.2 2.8	Conversion scintillator and gas Cerenkov detector.	25° FWHM at 20 MeV		
Share et al. (1974b) Samini et al. (1974) NRL, Washington	10-200	Dec. 1971	Parana, Argentina	2.5	Spark chamber and nuclear emulsion	1.5°	$-15^\circ < b < 15^\circ$ $-30^\circ < \ell < 30^\circ$	✓
Sood et al. (1974, 1975) IC, London	200-8000	Nov. 1973	Longreach, Australia	3.3-6.5	4 gap spark chamber	1°-5°	$-4^\circ < b < 4^\circ$ $-30^\circ < \ell < 30^\circ$	

TABLE A.4. Spacecraft experiments recording the gamma ray flux from the Galactic centre, tabulated in chronological order.

Reference	Energy (MeV)	Date	Spacecraft	Detector	Angular Resolution	Galactic Centre Acceptance (where plotted)	Duration	Background Also
Clark et al. (1968) Kraushaar et al. (1972) MIT	>100	March 1967 –July 1968	OSO-3	CsI and plastic scintillator convertors. Na(Tl) and Lucite Cerenkov detectors.	About 24°	$-15^\circ < b < 15^\circ$ $-30^\circ < \ell < 30^\circ$	16 months	✓
Fichtel et al. (1975) GSFC	35 - 200	Nov. 1972 –June 1973	SAS-2	32 gap spark chamber.	2° - 4°	$-10^\circ < b < 10^\circ$ $-30^\circ < \ell < 30^\circ$	7 months	✓
Bennett et al. (1976) Caravane collaboration.	70 - 2000	Aug. 1975 to date	COS-B	16 gap spark chamber.	About 3°			

TABLE A.5. Discrete sources from SAS-2 and COS-B published prior to May 1977.

Object	Position ($\sim \pm 1^\circ$)	Distance	Reference	Total Flux cm^{-2} s^{-1}	Pulsed Flux cm^{-2} s^{-1}
Crab Nebula and Pulsar NP-0532	$\ell = 184.6^\circ$ $b = -5.8^\circ$	2 kpc	Thompson et al. (1977) SAS-2	$(3.7 \pm 0.8)\ 10^{-6}$ >100 MeV	$(2.9 \pm 0.5)\ 10^{-6}$ >100 MeV
			Bennett et al. (1977a) COS-B	$(5.0 \pm 1.3)\ 10^{-6}$ >70 MeV	>35% total
Vela remnant and Pulsar PSR 0833-45	$\ell = 263.4^\circ$ $b = -2.8^\circ$	$\leq$470 pc	Thompson et al. (1975) SAS-2	$(6.3 \pm 1.1)\ 10^{-6}$ >100 MeV Value now corrected up by a factor of about 2 to agree with COS-B. See Fichtel et al. (1977a).	About 70% total
			Bennett et al. (1976) COS-B	$(1\text{-}3)\ 10^{-5}$ >100 MeV	$1.0\ 10^{-5}$ >100 MeV
	$\ell = 195^\circ$ $b = 5^\circ$		Thompson et al. (1977) SAS-2	$(4.3 \pm 0.9)\ 10^{-6}$ >100 MeV Possibly 59s period.	

TABLE A.5. (Cont.)

	$\ell = 195^\circ$ $b = 5^\circ$		Bennett et al. (1977a) COS-B	$(3.8 \pm 1.0)\ 10^{-6}$ >70 MeV	
	$\ell = 177^\circ$ $b = -7^\circ$		Bennett et al. (1977a) COS-B	$(2.1 \pm 0.6)\ 10^{-6}$ >70 MeV	
	$\ell = 190^\circ$ $b = 0^\circ$		Bennett et al. (1977a) COS-B	$(3.4 \pm 0.9)\ 10^{-6}$ >70 MeV	
CYG-X3	$\ell = 80^\circ$ $b = 1^\circ$	10 kpc	Lamb et al. (1977) SAS-2	$(4.4 \pm 1.1)\ 10^{-6}$ >100 MeV 4.8 hr periodicity	
PSR 1747-46	$\ell = 345^\circ$ $b = -10.2^\circ$	740 pc	Thompson et al. (1976b) SAS-2	$(1.6 \pm 0.6)\ 10^{-6}$ >100 MeV	$(6.5 \pm 3.3)\ 10^{-7}$ >100 MeV
PSR 1818-04	$\ell = 25.5^\circ$ $b = 4.7^\circ$	3.2 kpc	Hartman et al. (1976) SAS-2		$(2.0 \pm 0.5)\ 10^{-6}$ >35 MeV

binwidths of 5° and $2\frac{1}{2}^{\circ}$ respectively (see also section 3.4.1). Fichtel et al. (1975) have also presented latitude distributions towards both the Galactic centre and anticentre. The SAS-2 experiment was designed to search for sources in the plane, particularly those correlating with known supernova remnants and radio pulsars. Sources claimed are few in number (see table A.5), but many upper limits have been obtained (Fichtel et al., 1975; Ogelman et al., 1976).

The COS-B experiment has already reported fluxes for the Crab and Vela supernova remnants, and these, together with fluxes from other sources found up to May 1977, are given in table A.5.

There have been reports of sources from balloon-bourne experiments. The Southampton University group (Browning et al., 1972b; McKechnie et al., 1976) find several sources in the Cygnus and Cassiopeia regions. In addition, many balloon experiments have observed the Crab (see references given by Bennett et al., 1976).

A.4. Gamma Ray Lines

Gamma ray lines have been observed from the large solar flares of August 4th and 7th, 1972, by Chupp et al. (1973) using a NaI(Tl) scintillator on board the OSO-7 spacecraft. Recently,a possible observation of the positron annihilation line from the Crab was reported by Leventhal et al. (1977) who used a Ge(Li) detector which provides much better energy resolution (less than 1% at 0.5 MeV compared with about 12% for NaI crystals). Relevant to the present work are the observations of lines from the Galactic centre and Centaurus A. The currently reported lines all lie between 0.4 and 5 MeV and are listed in table A.6.

The problems involved in searching for small peaks on a low background flux are immense. Unfortunately all the present measurements have

TABLE A.6. Gamma ray lines from the Galactic centre and Cen A measured by the Rice University group.

Reference	Date	Angular Resolution FWHM	Direction	Energy	Background Flux, photons cm^{-2} s^{-1} kev^{-1}	Line Energy (MeV)	Line Flux, Photons cm^{-2} s^{-1}
Johnson et al. (1972)	Nov. 25 1970	24°	Galactic Centre	23-930 kev	$(10.5\pm2.2)\ E^{-(2.37\pm0.05)}$	0.473 ± 0.03	$(1.8\pm0.5)\ 10^{-3}$
Johnson and Haymes (1973)	Nov. 20 1971	24°	Galactic Centre	30 keV-2.4 MeV	Combined result of 1970 and 1971 flights: $(14.7\pm3.3)\ E^{-(2.42\pm0.05)}$	Combined result: 0.476 ± 0.024	$(1.8\pm0.5)\ 10^{-3}$
Haymes et al. (1975)	April 2 1975	15°	Galactic Centre	0.02-12.27 MeV	For 0.05-0.8 MeV: $(40.7\pm12.5)\ E^{-(2.78\pm0.06)}$	0.53 ± 0.04	$(8.0\pm2.3)\ 10^{-4}$
						0.9 ± 0.1	$(3.7\pm3.1)\ 10^{-4}$
						1.2-2.0 (probably sum of several lines)	$(2.6\pm0.6)\ 10^{-3}$
						4.6 ± 0.1	$(9.5\pm2.7)\ 10^{-4}$
Hall et al. (1976)	April 2 1975	15°	Cen A	0.033-12.25 MeV	$(0.86\pm0.08)\ E^{-(1.9\pm0.1)}$	1.68 ± 0.02	$(2.6\pm1.0)\ 10^{-3}$
						4.5 ± 0.1	$(9.9\pm3.0)\ 10^{-4}$

been made by one group at Rice University and verification by other groups using different techniques is desirable.

The measurements result from three balloon flights. In each case the detector was a NaI(Tl) crystal with collimators also of NaI(Tl) giving an acceptance cone of about 24° FWHM for the first two flights and about 15° FWHM for the third. The background was observed each time by alternately looking towards and away from the source for 10 minute intervals. The zenith angle was kept constant and the detector rotated in azimuth to a point 180° away. Due to the large acceptance angle of the telescope, for some of the time the source would not be completely removed from the field of view during the background measurements. The energy resolution is about 12% at 0.5 MeV.

The results for the Galactic centre from the three flights show consistency. The first two give evidence for a line at about 0.47 MeV. However, the intensity of this line found in the third flight is about 0.4 times the first value, the same factor by which the solid angle is reduced. This supports the suggestion that the gamma rays are produced along the line of sight rather than exclusively at the Galactic centre. Lines at 0.9 and 4.6 MeV were also recorded during the third flight, with a general enhancement between 1.2 and 2 MeV probably due to the sum of several lines.

The third balloon flight also recorded the continuum background and two probable lines from the radio galaxy Centaurus A.

Gamma ray line astronomy is still in its infancy. Since some lines are seen, it is likely that many more are above the threshold for observation. Recently, much work has concentrated on the development of Ge(Li) detectors which, with their superior energy resolution, are so necessary

for gamma ray line astronomy.

Much work has already been done in the theoretical field, predicting relative line strengths (see, Rygg and Fishman, 1973; Meneguzzi and Reeves, 1975; Lingenfelter and Ramaty, 1976a; Lingenfelter and Ramaty, 1976b and references therein). Lines are expected after cosmic ray interactions with gas and dust. The emission includes wide lines (few 100 keV) from cosmic ray de-excitation, and narrow lines (less than 10 keV) from grains. The most commonly expected are those of width about 100 keV from the de-excitation of gas nuclei. Electron-positron annihilation produces a line of about 0.511 MeV (see the calculations of Stecker, 1969; Ramaty et al., 1970). Gamma ray lines have the potential of a useful probe to study the origin and propagation of cosmic rays. Development of a kind of "spectroscopy" using observations and predicted intensities of the various lines is a challenge for the future.

A.5. Very Recent Measurements

Since A.1 - A.4 were written new data have been reported from both SAS-2 and COS-B (12th Eslab Symposium, Frascati, May, 1977). The results are summarised below.

Fichtel et al. (1977a) present a slightly revised version of the SAS-2 distribution of gamma rays above 100 MeV in $2\frac{1}{2}^{\circ}$ bins of longitude and integrated over $\pm 10^{\circ}$ of latitude. The distribution shows the same features as that previously published by Thompson et al. (1976) (see figure 3.3) and in particular there are no changes in the data important to the present work, i.e. the flux in the Galactic centre peak, and the pattern of the distribution for longitudes 30° - 60° on which some of the

arguments in Chapter 3 are based. The most important change is the flux ascribed to Vela, which has been increased by about a factor of 2 and is consistent with the COS-B measurement. No sources in addition to those given in Table A.5 are reported by SAS-2.

Fichtel et al. (1977a) present the first SAS-2 longitude distribution integrated over a latitude range of $\pm 5^{\circ}$. The shape is similar to that for the broader latitude range, which is as expected since most of the radiation is concentrated in the plane. In particular, the Galactic centre peak is estimated to contain the same flux as in the wider distribution. In the same paper, a longitude distribution for the energy range 35-100 MeV is presented for $|b| < 10^{\circ}$. Although the Galactic centre enhancement is still prominant, fewer features are generally noticable. This is due to the fact that the detector angular resolution is less good at these energies and the distribution itself is for longitude binwidths of 5°. Unfortunately, no Galactic energy spectra are presented in the paper.

Fichtel et al. (1977b) report on the SAS-2 high latitude flux. Latitude distributions are presented, (a) integrated over $|\ell| \gtrsim 60^{\circ}$-$90^{\circ}$, (b) integrated over remaining longitudes. Unfortunately anisotropy information is lost in such a data presentation but presumably statistics are too poor for conclusions to be reached. The authors calculate a best fit to their data for a two component model consisting of a uniform flat disc plus an isotropic background. Taking the integral over all lontitudes, they find:

$$q_{\gamma} \ (>100 \text{ MeV}) = 0.42 \ 10^{-5} + \frac{1.22 \ 10^{-5}}{\sin b} \ \text{cm}^{-2} \ \text{sr}^{-1} \ \text{s}^{-1}$$

A status report on the COS-B experiment was presented at the Frascati symposium. From a study of four regions of the sky, 40° wide in longitude and 30° wide in latitude, 11 point sources have been found in addition to the Crab and Vela pulsars (Hermsen et al., 1977). All as yet are unidentified. The Cygnus region is among those studied so far and no source is seen to be compatible in position and period with Cyg X-3 reported by SAS-2. However, the source 195 + 4 is confirmed and consistency with a 59s period is found (Masnou et al. 1977). The remaining sources are not compatible with known radio pulsars. The COS-B data indicate that sources constitute a significant amount of the overall Galactic gamma ray emission (some may be interstellar clouds).

The first COS-B longitude profile is presented by Bennett et al. (1977b) although much of the analysis is incomplete. The average flux for $|l| < 30^{\circ}$ agrees with the SAS-2 value. Energy spectra for four directions in the plane, each integrated over 30° of longitude, are presented. The spectra for the four directions are indistinguishable from each other, but are significantly steeper than expected from pure neutral pion decay, and are consistent with pure bremsstrahlung. The best fit appears to be for a mixture, but with bremsstrahlung a significantly higher relative contribution than found in Chapter 2 using locally observed electron and proton intensities. This is evidence for the electron to proton density ratio being higher than that locally, elsewhere in the Galaxy.

APPENDIX B

Solution of the Diffusion Equation for a Point Source

The normal steady state 3-D diffusion equation with energy losses and an energy independent diffusion coefficient, D, can be written:

$$-D\ \nabla^2 n + \frac{d}{dE}(n\dot{E}) = q(E, \underline{r}) \tag{B.1}$$

(Ginzburg and Syrovatskii, 1964). In the equation, $n(E, \underline{r})$ represents the number of electrons per unit volume at $\underline{r}$ with energy E, and $q(E, \underline{r})$ is the source function. Solutions of equation B.1 may be found for many source models (see e.g. Gratton, 1972). In the following, a derivation of the form for a point source, used in Chapter 7, is given:

B.1 can be written:

$$-D\ \nabla^2 (n\dot{E}) + \dot{E}\frac{d}{dE}(n\dot{E}) = \dot{E}(E)\ q\ (E, \underline{r}) \tag{B.2}$$

Using the following definitions:

$$\phi = n\dot{E} \tag{B.3}$$

$$\Theta = \int_{E_o}^{E} \frac{dE'}{\dot{E}(E')}, \quad \text{where} \begin{cases} E_o > E \\ \Theta > 0 \end{cases} \tag{B.4}$$

the Green function $G(\Theta, \underline{r}, \underline{r}_o)$ is the solution to:

$$-\nabla^2 G + \frac{1}{D}\frac{dG}{d\Theta} = \delta(\Theta)\ \ \delta(\underline{r}-\underline{r}_o) \tag{B.5}$$

The general solution to B.2. is therefore given by,

$$n(E, \underline{r}) = \iint d^3 r_o\, d\Theta\ \ G(\underline{r},\ \underline{r}_o, \Theta)\ \ q(E_o, \underline{r}_o)\frac{\dot{E}(E_o)}{\dot{E}(E)} \tag{B.6}$$

The solution to equation B.5 is found, for example, in Morse and Feshback (1953).

Introducing the Fourier transform (assuming infinite space) and letting $\underline{r}_o$ be the zero vector:

$$G(\underline{r}, \Theta) = \frac{1}{(2\pi)^3} \int_{-\infty}^{\infty} e^{i\underline{k}\cdot\underline{r}}\, g(\underline{k}, \Theta)\, d^3k \qquad (B.7)$$

Substituting B.7 into B.5 gives:

$$\frac{1}{(2\pi)^3} \int e^{i\underline{k}\cdot\underline{r}} \left(k^2 g + \frac{1}{D}\frac{dg}{d\Theta} \right) d^3k = \delta(\Theta) \frac{1}{(2\pi)^3} \int e^{i\underline{k}\cdot\underline{r}}\, d^3k \qquad (B.8)$$

This gives,

$$k^2 g + \frac{1}{D}\frac{dg}{d\Theta} = \delta(\Theta) \qquad (B.9)$$

$$g(\underline{k},\Theta) = e^{-k^2 D\Theta} \qquad (B.10)$$

Substituting B.10 into B.7

$$G(\underline{r}, \Theta) = \frac{1}{(2\pi)^3} \int_{-\infty}^{\infty} e^{i\underline{k}\cdot\underline{r}}\, e^{-k^2 D\Theta}\, d^3k \qquad (B.11)$$

$$G(\underline{r}, \Theta) = \frac{1}{(2\pi)^3} \int_{-\infty}^{\infty} \left(e^{ik_x x - k_x^2 D\Theta}\, dk_x \right) \left(e^{ik_y y - k_y^2 D\Theta}\, dk_y \right) \left(e^{ik_z z - k_z^2 D\Theta}\, dk_z \right) \qquad (B.12)$$

consider $\int_{-\infty}^{\infty} e^{ik_x x - k_x^2 D\Theta}\, dk_x$

$$ik_x x - k_x^2 D\Theta = -\left(k_x (D\Theta)^{\frac{1}{2}} - \frac{ix}{2(D\Theta)^{\frac{1}{2}}} \right)^2 - \left(\frac{x^2}{4D\Theta} \right)$$

$$= -D\Theta w^2 - \frac{x^2}{4D\Theta}$$

where $W = k_x - \frac{ix}{2D\theta}$

$$\int_{-\infty}^{\infty} e^{ik_x x - k_x^2 D\theta}\, dk_x = \int_{-\infty}^{\infty} e^{-D\theta W^2}\, e^{-x^2/4D\theta}\, dW$$
$$= e^{-x^2/4D\theta}\, \sqrt{\pi/D\theta}$$

Treating the integrals over the y and z coordinates similarly, gives,

$$G(\underline{r}, \theta) = e^{-r^2/4D\theta}\, \frac{1}{(4\pi\theta D)^{3/2}} \qquad (B.13)$$

The solution of $n(E, \underline{r})$ for a point source at the origin of the coordinate system can be expressed, using B.6, as,

$$n(E, \underline{r}) = \int_0^{\theta_{max}} d\theta\, q(E_o)\, \frac{\dot{E}(E_o)}{\dot{E}(E)}\, e^{-r^2/4D\theta}\, \frac{1}{(4D\pi\theta)^{3/2}} \qquad (B.14)$$

Let the source function be a power law of slope Γ, such that

$$q(E_o)\, dE_o = A\, E_o^{-\Gamma}\, dE_o \qquad (B.15)$$

If the energy losses are by synchrotron radiation and inverse Compton scattering they are of the form:

$$\dot{E} = -bE^2 \qquad (B.16)$$

Using B.4

$$\theta = (E_o - E)/bE\, E_o \qquad (B.17)$$

θ_{max} is for the case $E_o >> E$, i.e.

$$\theta_{max} = \frac{1}{bE} \qquad (B.18)$$

Using B.15, B.16, B.17 and B.18 in B.14 gives,

$$n(E, \underline{r}) = A\, E^{-\Gamma} \int_0^{1/bE} d\Theta (1-b\Theta E)^{\Gamma-2}\; e^{-r^2/4D\Theta}\; \frac{1}{(4D\pi\Theta)^{3/2}} \qquad (B.19)$$

let $u = bE\Theta$

$$n(E, \underline{r}) = A\, E^{-\Gamma} \int_0^1 \frac{du}{bE} (1-u)^{\Gamma-2} \left(\frac{bE}{4\pi Du}\right)^{3/2} \exp\left(-\frac{r^2 bE}{4Du}\right) \qquad (B.20)$$

Defining

$$x = \frac{bEr^2}{4D} \qquad (B.21)$$

$$n(E, \underline{r}) = A\, E^{-\Gamma} \int_0^1 \frac{du}{bE} (1-u)^{\Gamma-2} \left(\frac{x}{\pi u r^2}\right)^{3/2} \exp\left(-\frac{x}{u}\right) \qquad (B.22)$$

let $t = (1/u)-1$

$$n(E, \underline{r}) = \frac{A\, E^{-\Gamma}}{4Dr\pi^{3/2}} \exp(-x)\, x^{\frac{1}{2}} \int_0^\infty e^{-xt}\; t^{\Gamma-2}\, (1+t)^{-(\Gamma-(3/2))}\, dt \qquad (B.23)$$

Equation B.23, where x is defined in B.21, is therefore the solution for the electron density at $\underline{r}$ due to a point source at the origin. This convenient form for the solution enables the integral to be solved for a range of x and interpolation to be used for the required values.

The solution is sometimes written,

$$n(E, \underline{r}) = \frac{A\, E^{-\Gamma}}{4Dr\pi^{3/2}} \exp(-x)\, x^{\frac{1}{2}}\; \Gamma(\Gamma-1)\; U(\Gamma-1, {}^{3}/_{2}, x) \qquad (B.24)$$

where $U(\Gamma-1, {}^{3}/_{2}, x)$ is the confluent hypergeometric function of the second kind.

REFERENCES

Agrinier, B., Forichon, M., Laray, J.P., Parlier, B., Montmerle, T., Boella, G., Maraschi, L., Sacco, B., Scarsi, L., Da Costa, J.M., Palmeria, R., 1973, Proc. 13th Int. Cosmic Ray Conf., Denver, 1, 8.

Allaby, J.V., Binon, F., Diddens, A.N., Duteil, P., Klovning, A., Meunier, R., Peigneux, J.P., Sacharidis, E.J., Schlupmann, K., Spighel, M., Stroot, J.P., Thorndike, A.M. and Wetherell, A.M., 1970, CERN Report 70-12, Nuclear Physics Division.

Allen, C.W., 1973, "Astrophysical Quantities", London: Athlone Press.

Arnold, J.R., Metzger, A.E., Anderson, E.C., Van Dilla, M.A., 1962, J. Geophys. Res., 67, 4878.

Baker, P.L. and Burton, W.B., 1975, Astrophys. J., 198, 281.

Bania, T.M., 1977, Astrophys. J., in the press.

Barsuhn, J. and Walmsley, C.M., 1977, Astron. Astrophys., 54, 345.

Bennett, K., Penango, P., Rochester, G.K., Sanderson, T.R. and Sood, R.K., 1972, Nature, 238, 31.

Bennett, K. et al. (The Caravane Collaboration), 1976, in "The Structure and Content of the Galaxy and Galactic Gamma Rays", NASA CP-002, (Washington: U.S. Govt. Printing Office), 24.

Bennett, K. et al. (The Caravane Collaboration), 1977a, Astron. Astrophys., 56, 461.

Bennett, K. et al., (The Caravane Collaboration), 1977b, Proc. 12th Eslab Symposium, "Recent Advances in Gamma Ray Astronomy", ESA SP-124.

Bhatia, V.B. and Tandon, J.N., 1971, Astrophys. Lett., 8, 99.

Bignami, G.F. and Fichtel, C.E., 1974, Astrophys. J. Lett., 189, L65.

Bignami, G.F., Fichtel, C.E., Kniffen, D.A. and Thompson, D.J., 1975, Astrophys. J., 199, 54.

Bignami, G.F. and Piccinotti, G., 1977, Astron. Astrophys., in the press.

Blair, I.M., Taylor, A.E., Chapman, W.S., Kalmus, P.I.P., Litt, J., Miller, M.C., Scott, D.B., Sherman, H.J., Astbury, A. and Walker, T.G., 1966, Phys. Rev. Lett., 17, 789.

Blumenthal, G.R. and Gould, R.J., 1970, Rev. Mod. Phys., 42, 237.

Boggild, H., Dahl-Jensen, E., Dahl-Jensen, I., Hansen, K.H., Hopper, J.E., Lohse, E.R., Mortensen, B. and Moller, R., 1975, Nucl. Phys., B91, 365.

Boldt, E., 1974, "High Energy Particles and Quanta in Astrophysics", ed. F.B. McDonald and C.E. Fichtel, MIT Press, 368.

Bracci, E., Droulez, J.P., Flaminio, E., Hansen, J.D. and Morrison, D.R.O., 1973, CERN Report 73-1, High Energy Group.

Bratolyubova-Tsulukidze, L.I., Grigorov, N.L., Kalinkin, L.F., Melioransky, A.S., Pryakhin, E.A., Savenko, I.A., Yufarkin, V. Ya., 1970, Acta Phys., 29, Suppl. 1, 123.

Brecher, K. and Morrison, P., 1969, Phys. Rev. Lett., 23, 802.

Brown, R.L., 1973, Astrophys. J., 184, 693.

Browning, R., Ramsden, D. and Wright, R.J., 1972a, Nature, 238, 138.

Browning, R., Ramsden, D. and Wright, R.J., 1972b, Nature Phys. Sci., 235, 128.

Bulanov, S.V., Syrovatskii, C.I. and Dogiel, V.A., 1976, Astrophys. Space Sci., 44, 255.

Burbidge, G.R., 1970, Ann. Rev. Astron. Astrophys., 8, 369.

Burton, W.B., 1971, Astron. Astrophys., 10, 76.

Burton, W.B., 1974, in "Galactic and Extragalactic Radio Astronomy", eds. G.K. Verschuur and K.I. Kellermann, New York: Springer, 82.

Burton, W.B., 1976a, Ann. Rev. Astron. Astrophys., 14, 277.

Burton, W.B., 1976b, in "The Structure and Content of the Galaxy and Galactic Gamma Rays", NASA CP-002 (Washington: U.S. Govt. Printing Office), 177.

Burton, W.B., Gordon, M.A., Bania, T.M. and Lockman, F.J., 1975, Astrophys. J., 202, 30.

Burton, W.B. and Gordon, M.A., 1976, Astrophys. J. Lett, 207, L189.

Burton, W.B. and Gordon, M.A., 1977, Astron. Astrophys., in the press.

Carruthers, G.R., 1970, Astrophys. J. Lett., 161, L81.

Cavallo, G. and Gould, R.J., 1971, Il Nuovo Cimento, 2B, 77.

Chupp, E.L., Forrest, D.J., Higbie, P.R., Suri, A.N., Tsai, C. and Dunphy, P.P., 1973, Nature, 241, 333.

Clark, G.W., Garmire, G.P. and Kraushaar, W.L., 1968. Astrophys. J. Lett., 153, L203.

Cohen, R.J., 1975, Mon. Not. R. astr. Soc., 171, 659.

Cohen, R.J. and Davies, R.D., 1976, Mon. Not. R. astr. Soc., 175, 1.

Comstock, G.M., Hsieh, K.C. and Simpson, J.A., 1972, Astrophys. J., 173, 691.

Cowsik, R. and Kobetich, E.J., 1972, Astrophys. J., 177, 585.

Cummings, A.C., Stone, E.C. and Vogt, R.E., 1973, Proc. 13th Int. Cosmic Ray Conf., Denver, 1, 340.

Dahlbacka, G.H., Freier, P.S. and Waddington, C.J., 1973, Astrophys. J., 180, 371.

Damle, S.V., Daniel, R.R. and Lavakare, P.J., 1976, Pramana, 7, 355.

Daniel, R.R., Joseph, G. and Lavakare, P.J., 1972, Astrophys. Space Sci., 18, 462.

Daugherty, J.K., Hartman, R.C. and Schmidt, P.J., 1975, Astrophys. J., 198, 493.

Diddens, A.N. and Schlupmann, K., 1972, Landolt-Bornstein, New Series, Group 1, 6, 53.

Dilworth, C., Maraschi, L. and Perola, G.C., 1974, Astron. Astrophys., 33, 43.

Dodds, D., 1977, Unpublished Ph.D. thesis, University of Durham, U.K.

Dodds, D., Strong, A.W., Wolfendale, A.W. and Wdowczyk, J., 1974, Nature, 250, 716.

Dodds, D., Strong, A.W., Wolfendale, A.W. and Wdowczyk, J., 1975a, J. Phys. A., 8, 624.

Dodds, D., Strong, A.W. and Wolfendale, A.W., 1975b, Mon. Not. R. astr. Soc., 171, 569.

Dodds, D., Wolfendale, A.W. and Wdowczyk, J., 1976, Mon. Not. R. astr. Soc., 176, 345.

D'Odorico, S., Peimbert, M. and Sabbadin, F., 1976, Astron. Astrophys., 47, 341.

Dogiel, V.A., Bulanov, S.V. and Syrovatskii, S.I., 1975, Proc. 14th Int. Cosmic Ray Conf., Munich, 2, 700.

Ekers, R.D. and Sancisi, R., 1977, Astron. Astrophys., 54, 973.

Fabian, A.C., Zarnecki, J.C., Culhane, J.L., Hawkins, F.J., Peacock, A., Pounds, K.A. and Parkinson, J.H., 1974, Astrophys. J. Lett, 189, L59.

Fazio, G.G., Stecker, F.W. and Wright, J.P., 1966, Astrophys. J., 144, 611.

Fazio, G.G. and Stecker, F.W., 1976, Astrophys. J. Lett., 207, L49.

Felten, J.E., 1965, Phys. Rev. Lett., 15, 1003.

Felten, J.E. and Morrison, P., 1963, Phys. Rev. Lett., 10, 453.

Felten, J.E. and Morrison, P., 1966, Astrophys. J., 146, 686.

Fichtel, C.E., Hartman, R.C., Kniffen, D.A. and Sommer, M., 1972, Astrophys. J., 171, 31.

Fichtel, C.E., Hartman, R.C., Kniffen, D.A., Thompson, D.J., Bignami, G.F., Ogelman, H., Ozel, M.F. and Tumer, T., 1975, Astrophys. J., 198, 163.

Fichtel, C.E., Kniffen, D.A., Thompson, D.J., Bignami, G.F. and Cheung, C.Y., 1976, Astrophys. J., 208, 211.

Fichtel, C.E., Kniffen, D.A. and Thompson, D.J., 1977a, Proc. 12th Eslab Symposium, "Recent Advances in Gamma Ray Astronomy", ESA SP-124.

Fichtel, C.E., Kniffen, D.A., Hartman, R.C., Thompson, D.J., Ogelman, H., Ozel, M. and Tumer, T., 1977b, Proc. 12th Eslab Symposium, "Recent Advances in Gamma Ray Astronomy", ESA SP-124.

Fishman, G.J. and Clayton, D.D., 1972, Astrophys. J., 178, 337.

Fisk, L.A., 1974, in "High Energy Particles and Quanta in Astrophysics", ed. F.B. McDonald and C.E. Fichtel, MIT Press, 170.

Frye, G.M., Albats, P.A., Zych, A.D., Staib, J.A., Hopper, V.D., Rawlinson, W.R. and Thomas, J.A., 1971, Nature, 231, 372.

Frye, G.M., Albats, P., Thomson, G.B., Hopper, V.D., Mace, O.B., Thomas, J.A. and Staib, J.A., 1974, Proc. 9th Eslab Symposium, "The Context and Status of Gamma Ray Astronomy", ESRO SP-106.

Fuchs, B., Schlickeiser, R. and Theilheim, K.O., 1976, Astrophys. J., 206, 589.

Galper, A.M., Kirillov-Ugryumov, V.G., Luchkov, B.I. and Ozerov, Y.V., 1973, Proc. 13th Int. Cosmic Ray Conf., Denver, 1, 450.

Garcia-Munoz, M., Mason, G.M. and Simpson, J.A., 1975, Astrophys. J. Lett., 201, L141.

Giler, M., Wdowczyk, J. and Wolfendale, A.W., 1977, J. Phys. A., 10, 843.

Ginzburg, V.L., 1969, "Elementary Processes for Cosmic Ray Astrophysics", Gordon and Breach Inc., New York.

Ginzburg, V.L., 1972, Nature Phys. Sci., 239, 8.

Ginzburg, V.L. and Syrovatskii, S.I., 1964, "The Origin of Cosmic Rays", Pergamon Press.

Goldstein, M.L., Ramaty, R. and Fisk, L.A., 1970, Phys. Rev. Lett., 24, 1193.

Golenetskii, S.V., Mazets, E.P., Ilinskii, V.N., Aptekar, R.L., Dredov, M.M., Guruyan, Yu. A., Panov, V.N., 1971, Astrophys. Lett., 9, 69.

Gordon, M.A. and Burton, W.B., 1976, Astrophys. J., 208, 346.

Gott, J.R. and Turner, E.L., 1976, Astrophys. J., 209, 1.

Gould, R.J., 1965, Phys. Rev. Lett., 15, 511.

Gratton, L., 1972, Astrophys. Space Sci., 16, 81.

Green, A.J., 1974, Astron. Astrophys. Suppl., 18, 267.

Grindlay, J.E., 1975, Astrophys. J., 199, 49.

Grindlay, J.E., Helmken, H.F., Hanbury Brown, R., Davis, J. and Allen, L.R., 1975, Astrophys. J. Lett., 197, L9.

Hagen. F.A., Fisher, A.J. and Ormes, J.R., 1976, Astrophys. J., 212, 262.

Hall, R.D. Meegan, C.A., Walraven, G.D., Djuth, F.T. and Haymes, R.C., 1976, Astrophys. J., 210, 631.

Hartman, R.C., Fichtel, C.E., Kniffen, D.A., Lamb, R.C., Thompson, D.J., Bignami, G.F., Ogelman, H., Ozel, M. and Tumer, T., 1976, in "The Structure and Content of the Galaxy and Galactic Gamma Rays", NASA CP-002 (Washington: U.S. Govt. Printing Office,), 12.

Haymes, R.C., Walraven, G.D., Meegan, C.A., Hall, R.D., Djuth, F.T. and Shelton, D.H., 1975, Astrophys. J., 201, 593.

Heiles, C., 1971, Ann. Rev. Astron. Astrophys., 9, 293.

Heitler, W., 1954, "The Quantum Theory of Radiation", Oxford Univ. Press.

Helmken, H. and Hoffman, J., 1973, Nature Phys. Sci., 243, 6.

Hermsen, W. et al. (The Caravane Collaboration), 1977, Proc. 12th Eslab Symposium, "Recent Advances in Gamma Ray Astronomy", ESA SP-124.

Herterich, W., Pinkau, K., Rothermel, H. and Sommer, M., 1973, Proc. 13th Int. Cosmic Ray Conf., Denver, 1, 21.

Hill, E.R., Slee, O.B. and Mills, B.Y., 1959, Austral. J. Phys., 11, 530.

Hillas, A.M., 1968, Can. J. Phys., 46, S623.

Hoffmann, W.F., Frederick, C.L. and Emery, R.J., 1971, Astrophys. J. Lett., 164, L23.

Hollenbach, D.J., Werner, M.W. and Salpeter, E.E., 1971, Astrophys. J., 163, 165.

Hopper, V.D., Mace, O.B., Thomas, J.A., Albats, P., Frye, G.B., Thompson, G.B., and Staib, J.A., 1973, Astrophys. J. Lett., 186, L55.

Hoyle, F., 1965, Phys. Rev. Lett., 15, 131.

Hulsizer, R. and Rossi, B.B., 1949, Phys. Rev., 73, 1402.

Ilovaisky, S.A. and Lequeux, J., 1972, Astron. Astrophys., 20, 347.

Innanen, K.A., 1973, Astrophys. Space Sci., 22, 393.

Jenkins, E.B., 1976, in "The Structure and Content of the Galaxy and Galactic Gamma Rays", NASA CP-002, (Washington: U.S. Govt. Printing Office), 239.

Johnson, W.N., Harnden, F.R. and Haymes, R.C., 1972, Astrophys. J. Lett., 172, L1.

Johnson, W.N. and Haymes, R.C., 1973, Astrophys. J., 184, 103.

Kaifu, N., Kato, T. and Iguchi, T., 1972, Nature, 238, 105.

Kaifu, N., Morris, M., Palmer, P. and Zuckerman, B., 1975, Astrophys. J., 201, 98.

Kapitzky, J.E. and Dent, W.A., 1974, Astrophys. J., 188, 27.

Kellogg, E., Baldwin, J.R. and Koch, D., 1975, Astrophys. J., 199, 299.

Kerr, F.J., 1967, in IAU Symposium 31, ed. H. van Woerden, Academic Press, 239.

Kiang, T.D., 1961, Mon. Not. R. astr. Soc., 122, 263.

Kniffen, D.A. and Fichtel, C.E., 1970, Astrophys. J. Lett., 161, L157.

Kniffen, D.A., Hartman, R.C., Thompson, D.J. and Fichtel, C.E., 1973, Astrophys. J. Lett., 186, L105.

Kniffen, D.A., Fichtel, C.E. and Thompson, D.J., 1977, Astrophys. J., 215, 765.

Knowles, S.H. and Cheung, A.C., 1971, Astrophys. J. Lett., 164, L19.

Koch, H.W. and Motz, J.W., 1959, Rev. Mod. Phys., 31, 920.

Kraushaar, W.L. and Clark, G.W., 1962, Phys. Rev. Lett., 8, 106.

Kraushaar, W.L., Clark, G.W., Garmire, G.P., Helmken, H., Higbie, P. and Agogino, M., 1965, Astrophys. J., 141, 845.

Kraushaar, W.L., Clark, G.W., Garmire, G.P., Borken, R., Higbie, P., Leong, C. and Thorsos, T., 1972, Astrophys. J., 177, 341.

Kuo, F., Frye, G.M. and Zych, A.D., 1973, Astrophys. J. Lett., 186, L51.

Lamb, R.C., Fichtel, C.E., Hartman, R.C., Kniffen, D.A. and Thompson, D.J., 1977, Astrophys. J. Lett., 212, L63.

Landecker, T.L. and Wielebinski, R., 1970, Aust. J. Phys., Astrophys. Suppl., 16, 1.

Lang, K.R., 1974, "Astrophysical Formulae", Springer-Verlag.

Leung, C.M. and Liszt, H.S., 1976, Astrophys. J., 208, 732.

Leventhal, M., 1973, Astrophys. J. Lett., 183, L147.

Leventhal, M., MacCallum, C.J. and Watts, A.C., 1977, Nature, 266, 696.

Levy, D.J. and Goldsmith, D.W., 1972, Astrophys. J., 177, 643.

Lin, C.C. and Shu, F.H., 1967, in "Radio Astronomy and the Galactic System", ed. H. van Woerden, Academic Press, 313.

Lin, C.C., Yuan, C. and Shu, F.H., 1969, Astrophys. J., 155, 721.

Lingenfelter, R.E. and Ramaty, R., 1976a, Astrophys. J. Lett., 211, L19.

Lingelfelter, R.E. and Ramaty, R., 1976b, in "The Structure and Content of the Galaxy and Galactic Gamma Rays," NASA CP-002, (Washington: U.S. Govt. Printing Office), 264.

Liszt, H.S., Sanders, R.H. and Burton, W.B., 1975, Astrophys. J., 198, 537.

Liszt, H.S., Burton, W.B., Sanders, R.H. and Scoville, N.Z., 1977, Astrophys. J., 213, 38.

Little, A.G., 1974, in "Galactic Radio Astronomy", IAU 60, ed. F.J. Kerr and S.C. Simonson, 491.

Longair, M.S., 1971, Rep. Prog. Phys., 34, 1125.

Masnou, J.L. et al. (The Caravane Collaboration), 1977, Proc. 12th Eslab Symposium, "Recent Advances in Gamma Ray Astronomy, ESA SP-124.

Mattila, K., 1976, Astron. Astrophys., 47, 77.

Mayer-Hasselwander, H.A., Pfefferman, E., Pinkau, K., Rothermel, H. and Sommer, M., 1972, Astrophys. J. Lett., 175, L23.

Mazets, E.P., Golenetskii, S.V., Il'inskii, V.N., Gur'yan, Yu. A., Kharitonova, T.V., 1975, Astrophys. Space Sci., 33, 347.

McGee, R.X., 1970, Australian J. Phys., 23, 541.

McKechnie, S.P., Mount, K.E. and Ramsden, D., 1976, Astrophys. J. Lett., 207, L151.

Meneguzzi, M. and Reeves, H., 1975, Astron. Astrophys., 40, 91.

Metzger, A.E., Anderson, E.C., Van Dilla, M.A. and Arnold, J.R., 1964, Nature, 204, 766.

Meyer, P., 1975, in "Origin of Cosmic Rays", eds. J.L. Osborne and A.W. Wolfendale, D. Reidel, 233.

Mills, B.Y., 1956, The Observatory, 76, 65.

Mitchell, R.J., Charles, P.A., Culhane, J.L., Davison, P.J.N. and Fabian, A.C., 1975, Astrophys. J. Lett., 200, L5.

Morrison, P., 1958, Il Nuovo Cimento, 7, 858.

Morse, P.M. and Feshback, H., 1953, "Methods of Theoretical Physics," McGraw-Hill, 857.

O'Dell, F.W., Shapiro, M.M., Silberberg, R. and Tsao, C.H., 1975, Proc. 14th Int. Cosmic Ray Conf., Munich, 2, 526.

Ogelman, H., Fichtel, C.E., Kniffen, D.A. and Thompson, D.J., 1976, Astrophys. J., 209, 584.

Omnès, R., 1969, Phys. Rev. Lett., 23, 38.

Orth, C.D. and Buffington, A., 1976, Astrophys. J., 206, 312.

Owens, A.J. and Jokipii, J.R., 1977, Astrophys. J., 215, 677.

Paul, J., Cassé, M. and Cesarsky, C.J., 1974, Proc. 9th Eslab Symposium, "The Context and Status of Gamma Ray Astronomy", ESRO SP-106, 249.

Paul, J., Cassé, M. and Cesarsky, C.J., 1976, Astrophys. J., 207, 62.

Phillips, T.G., Jefferts, K.B. and Wannier, P.G., 1973, Astrophys. J. Lett., 186, L19.

Piccinotti, G. and Bignami, G.F., 1976, Astron. Astrophys., 52, 69.

Pipher, J.L., 1973, in "Interstellar Dust and Related Topics", IAU Symp. 52, eds. J.M. Greenberg and H.C. Van De Hulst, D. Reidel, 559.

Plambeck, R.L., Williams, D.R.W. and Goldsmith, P.F., 1977, Astrophys. J. Lett. 213, L41.

Puget, J.L. and Stecker, F.W., 1974, Astrophys. J., 191, 323.

Puget, J.L., Ryter, C., Serra, G. and Bignami, G., 1975, Proc. 14th Int. Cosmic Ray Conf., Munich, 1, 52.

Puget, J.L., Ryter, C., Serra, G. and Bignami, G., 1976, Astron. Astrophys., 50, 247.

Ramaty, R., 1974, in "High Energy Particles and Quanta in Astrophysics", eds. F.B. McDonald and C.E. Fichtel, MIT Press, 122.

Ramaty, R., Stecker, F.W. and Misra, D., 1970, J. Geophys. Res., 75, 1141.

Roach, F.E. and Megill, L.R., 1960, Astrophys. J., 133, 228.

Roberts, W.W., 1976, in "The Structure and Content of the Galaxy and Galactic Gamma Rays", NASA CP-002, (Washington: U.S. Govt. Printing Office), 128.

Robinson, B.J. and McGee, R.X., 1970, Australian J. Phys., 23, 405.

Rouan, D., Lena, P.J., Puget, J.L., de Boer, K.S. and Wijnbergen, J.J., 1977, Astrophys. J. Lett., 213, L35.

Rougoor, G.W. and Oort, J.H., 1960, Proc. of the National Academy of Sciences, 46, 1.

Rowan-Robinson, M. and Fabian, A.C., 1975, Mon. Not. R. astr. Soc., 170, 199.

Rygg, T.A. and Fishman, G.J., 1973, Proc. 13th Int. Cosmic Ray Conf., Denver, 1, 472.

Ryter, C.E. and Puget, J.L., 1977, Astrophys. J., 215, 775.

Samimi, J., Share, G.H. and Kinzer, R.L., 1974, Proc. 9th Eslab Symposium, "The Context and Status of Gamma Ray Astronomy", ESRO SP-106, 211.

Sancisi, R., Allen, R.J. and Van Albada, T.S., 1974, Proc. CNRS Int. Colloquium on Spiral Galaxies, Bures-sur-Yvette, France.

Sanders, R.H. and Lowinger, T., 1972, Astron. J., 77, 292.

Sanders, R.H. and Wrixon, G.T., 1973, Astron. Astrophys., 26, 365.

Sanders, R.H. and Wrixon, G.T., 1974, Astron. Astrophys., 33, 9.

Schlickeiser, R. and Thielheim, K.O., 1974a, Astron. Astrophys., 34, 167.

Schlickeiser, R. and Thielheim, K.O., 1974b, Phys. Lett., 53B, 369.

Schlickeiser, R. and Thielheim, K.O., 1976, Nature, 261, 478.

Schmidt, M., 1972, Astrophys. J., 176, 289.

Schonfelder, V. and Lichti, G., 1974, Astrophys. J. Lett., 191, L1.

Schonfelder, V., Lichti, G. and Moyano, C., 1975, Nature, 257, 375.

Schwartz, D. and Gursky, H., 1973, in "Gamma Ray Astrophysics", NASA SP-339 (Washington: U.S. Govt. Printing Office).

Scoville, N.Z., 1972, Astrophys. J. Lett., 175, L127.

Scoville, N.Z. and Solomon, P.M., 1973, Astrophys. J., 180, 55.

Scoville, N.Z. and Solomon, P.M., 1974, Astrophys. J. Lett., 187, L67.

Scoville, N.Z., Solomon, P.M. and Jefferts, K.B., 1974, Astrophys. J. Lett., 187, L63.

Scoville, N.Z. and Solomon, P.M., 1975, Astrophys. J. Lett., 199, L105.

Scoville, N.Z., Solomon, P.M. and Sanders, D.B., 1976, in "The Structure and Content of the Galaxy and Galactic Gamma Rays," NASA CP-002 (Washington: U.S. Govt. Printing Office), 163.

Setti, G. and Woltjer, L., 1971, Astrophysical Lett., 8, 125.

Shane, W.W., 1972, Astron. Astrophys., 16, 118.

Shapiro, S., 1971, Astron. J., 76, 291.

Share, G.H., Kinzer, R.L. and Seeman, N., 1974a, Astrophys. J., 187, 511.

Share, G.H., Kinzer, R.L. and Seeman, N., 1974b, Astrophys. J., 187, 45.

Shaver, P.A., 1976, Astron. Astrophys., 49, 149.

Shectman, S.A., 1973, Astrophys. J., 179, 681.

Shukla, P.G. and Paul, J., 1976, Astrophys. J., 208, 893.

Simonson, S.C., 1976, Astron. Astrophys., 46, 261.

Simonson, S.C. and Mader, G.L., 1973, Astron. Astrophys., 27, 337.

Skilling, J. and Strong, A.W., 1976, Astron. Astrophys., 53, 253.

Skilling, J. and Strong, A.W., 1977, Proc. 12th Eslab Symposium, "Recent Advances in Gamma Ray Astronomy", ESA SP-124.

Smith, A.M., 1973, Astrophys, J. Lett., 179, L11.

Soifer, B.T. and Houck, J.P., 1973, Astrophys. J., 186, 169.

Solomon, P.M. and Wickramasinghe, N.C., 1969, Astrophys. J., 158, 449.

Solomon, P.M. and Werner, M.W., 1971, Astrophys. J., 165, 41.

Solomon, P.M., Scoville, N.Z., Jefferts, K.B., Penzias, A.A. and Wilson, R.W., 1972, Astrophys. J., 178, 125.

Solomon, P.M. and Stecker, F.W., 1974, Proc. 9th Eslab Symposium, "The Context and Status of Gamma Ray Astronomy", ESRO SP-106, 253.

Sood, R.K., Bennett, K., Clayton, P.G. and Rochester, G.K., 1974, Proc. 9th Eslab Symposium, "The Context and Status of Gamma Ray Astronomy", ESRO SP-106, 217.

Sood, R.K., Bennett, K., Clayton, P.G. and Rochester, G.K., 1975, Proc. 14th Int. Cosmic Ray Conf., Munich, 1, 35.

Spitzer, L., Drake, J.F., Jenkins, E.B., Morton, D.C., Rogerson, J.B. and York, D.G., 1973, Astrophys, J. Lett., 181, L116.

Spitzer, L. and Jenkins, E.B., 1975, Ann. Rev. Astron. Astrophys., 13, 133.

Stecker, F.W., 1969, Astrophys. Space Sci., 3, 579.

Stecker, F.W., 1969a, Astrophys. J., 157, 507.

Stecker, F.W., 1969b, Nature, 224, 870.

Stecker, F.W., 1970, Astrophys. Space Sci., 6, 377.

Stecker, F.W., 1971, "Cosmic Gamma Rays", Mono Book Corp., Baltimore, Maryland.

Stecker, F.W., 1971a, Nature, 229, 105.

Stecker, F.W., 1973, Astrophys. J., 185, 499.

Stecker, F.W., 1975, Phys. Rev. Lett., 35, 188.

Stecker, F.W., 1975a, "Origin of Cosmic Rays", ed. J.L. Osborne and A.W. Wolfendale, Reidel, 267.

Stecker, F.W., 1977, Proc. 12th Eslab Symp., "Recent Advances in Gamma Ray Astronomy", ESA SP-124.

Stecker, F.W., 1977a, Astrophys. J., 212, 60.

Stecker, F.W., Morgan, D.L. and Bredekamp, J.H., 1971, Phys. Rev. Lett, 27, 1469.

Stecker, F.W., Solomon, P.M., Scoville, N.Z. and Ryter, C.E., 1975, Proc. 14th Int. Cosmic Ray Conf., Munich, 1, 46.

Strong, A.W., 1975, J. Phys. A., 8, 617.

Strong, A.W., 1977, Mon. Not. R. astr. Soc., Vol. 181, in the press.

Strong, A.W., Wdowczyk, J. and Wolfendale, A.W., 1973, in "Gamma Ray Astrophysics", NASA SP-339, (Washington: U.S. Govt. Printing Office), 259.

Strong, A.W., Wolfendale, A.W. and Wdowczyk, J., 1973a, Nature, 241, 109.

Strong, A.W., Wdowczyk, J. and Wolfendale, A.W., 1974, J. Phys. A., 7, 120.

Strong, A.W., Wolfendale, A.W. and Worrall, D.M., 1976, Mon. Not. R. astr. Soc., 175, 23P.

Strong, A.W., Wolfendale, A.W. and Dahanayake, C., 1977, Mon. Not. R. astr. Soc., 179, 69P.

Tanaka, Y., 1974, Proc. 9th Eslab Symposium, "The Content and Status of Gamma Ray Astronomy", ESRO SP-106, 117.

Thielheim, K.O. and Langhoff, W., 1968, J. Phys. A., 1, 694.

Thompson, D.J., Fichtel, C.E., Kniffen, D.A. and Ogelman, H.B., 1975, Astrophys. J. Lett., 200, L79.

Thompson, D.J., Fichtel, C.E., Hartman, R.C., Kniffen, D.A., Bignami, G.F., Lamb, R.C., Ogelman, H., Ozel, M.E. and Tumer, T., 1976, in "The Structure and Content of the Galaxy and Galactic Gamma Rays," NASA CP-002, 1.

Thompson, D.J., Fichtel, C.E., Kniffen, D.A., Lamb, R.C. and Ogelman, H.B., 1976b, Astrophysical Lett., 17, 173.

Thompson, D.J., Fichtel, C.E., Hartman, R.C., Kniffen, D.A. and Lamb, R.C., 1977, Astrophys. J., 213, 252.

Trimble, V., 1975, Rev. Mod. Phys., 47, 877.

Trombka, J.I., Dyer, C.S., Evans, L.G., Bielefeld, M.J., Seltzer, S.M. and Metzger, A.E., 1977, Astrophys. J., 212, 925.

Valentine, D., Kaplon, M.F. and Badhwar, G., 1970, Acta Phys., 29, Suppl. 1, 101.

van den Bergh, S., 1961, Zs. f. Ap., 53, 19.

van der Kruit, P.C., 1970, Astron. Astrophys., 4, 462.

van der Kruit, P.C., 1971, Astron. Astrophys., 13, 405.

Vedrenne, G.E., Albernhe, F., Martin, I. and Talon, R., 1971, Astron. Astrophys., 15, 50.

Vette, J.I., Gruber, D., Matteson, J.L. and Peterson, L.E., 1970, Astrophys. J. Lett., 160, L161.

Wannier, P.G., Penzias, A.A., Wilson, R.W. and Linke, R.A., 1976, Astrophys. J., 204, 26.

Webster, A., 1975, Mon. Not. R. astr. Soc., 171, 243.

Westerhout, G., 1973, "Maryland-Green Bank Galactic 21 cm line Survey", Baltimore, Maryland, 3rd ed.

Wrixon, G.T. and Sanders, R.H., 1973, Astron. Astrophys., Suppl. 11, 339.

A C K N O W L E D G E M E N T S

The Science Research Council is thanked for the provision of a Research Studentship during the period of this work.

I wish to thank Professor A.W. Wolfendale, F.R.S., for making available the facilities of the Physics Department of the University of Durham and, as my supervisor, for his enthusiastic guidance and encouragement.

It is also a pleasure to thank Dr. A.W. Strong for advice, encouragement and many helpful discussions.

Dr. J.L. Osborne and other members of the Durham Physics Department with whom I have been in conversation on various aspects of this work are thanked.

I wish to acknowledge helpful discussions with Drs. C. Cesarsky and M. Cassé during a two-week visit to Centre d'Etudes Nucléaires de Saclay.

The facilities provided by the Durham University Computer Unit are gratefully acknowledged.

Finally, I wish to thank Mrs. V.A. Gold for her care in typing this thesis, and Mrs. A. Gregory for her extremely good drawing of the diagrams.